Metal supported on carbon based materials for adsorptive desulphurisation of fuels

by

LIBERTY LUNGISANI MGUNI

submitted in accordance with the requirements
for the degree of

DOCTOR OF PHILOSOPHY

at the

UNIVERSITY OF SOUTH AFRICA

SUPERVISOR: Prof Y YAO

(SEPTEMBER 2021)

DECLARATION

I declare that this dissertation is my work. It is being submitted for the degree of Doctor of Philosophy Science, Engineering and Technology to the University of South Africa, Johannesburg. No portion of this work referred to in this thesis has been submitted in support of an application for another degree or qualification of this or any other university or another institute of learning.

19 Sepetember 2021

Signature of Candidate **Day** **Month** **Year**

ABSTRACT

The transport industry is one of the biggest contributors to air pollution, with the major air pollutants being CO_x, NO_x, and SO_x. SO_x is produced by the combustion of the organic sulphur compound found in fuels, e.g. thiophene, mercaptan and sulfides. Adsorptive desulphurization with novel adsorbents was investigated at ambient conditions in this study, to find an economically viable and effective alternative method of removing sulphur from diesel fuel.

First, a review of adsorbent improvement strategies was done, including their effects on thermodynamics, kinetics and equilibrium adsorption isotherms, as well as the screening of the most promising adsorbent. Activated carbon (AC) was the most promising adsorbent, based on the figure of merit (FoM), while metal-organic frameworks (MOFs) were the most active. There is no consensus on the parameters that have the most influence on adsorption activity, and machine learning presents an opportunity to investigate this phenomenon. In this work, three regression techniques were used in research: linear regression; multiple regression; random forest. The findings suggest that adsorbent properties (metal ion, metal properties, surface area and pore volume) need the most attention in order to improve adsorbent activity.

The first experimental work done was to screen a number of commercial adsorbents using both model and conventional diesel. AC showed good activity with both model diesel and conventional diesel. For the first time, the sulphur adsorption order for conventional diesel produced in South Africa was reported on, with decreasing order of: 4-MDBT>> 4,6-DMDBT~4 E,6-MDBT~2,4,6-TMDBT~1,4,6-TMDBT. The study also investigated the effect of different supports and Lewis acid metals, and the analysis indicated that AC and NiO were the most promising. The high activity level of NiO was attributed to it having the lowest acidity level, based on the ionic-covalent parameter.

MOFs are an emerging class of porous materials that are constructed from metal-containing nodes and organic linkers. They have the potential to be easily manipulated to synthesize an adsorbent with unique properties. In this study, Ni-doped MOFs (Ni-BDC) and the composites of AC@Ni-BDC were synthesized in the presence of formic acid, which has evidenced three effects, namely: i) accelerating MOF synthesis; ii) modulating crystallite size; iii) controlling crystallinity. The experimental results showed that modulated synthesis of Ni-based MOFs using formic acid improved the overall adsorptive activity of MOF almost twofold. The adsorption activity of the composite towards thiophene (TH) was the average of the two materials (i.e. AC and Ni-BDC), while the activity doubled for dibenzothiophene (DBT) and 4, 6-dimethyldibenzothiophene (4, 6 DMDBT) with respect to the expected average. The improved activity was attributed to enhanced pore structure, crystallinity and synergistic effects that produce stronger acidic sites. Finally, the synthesized composite has the potential to remove the sulphur compounds in a broad spectrum.

Keywords: Adsorptive desulphurization, Diesel fuels, activated carbon, metal-organic frameworks, machine learning

ACKNOWLEDGEMENTS

The author of this thesis would like to take this opportunity to express his heartfelt gratitude to all the people who gave the much-needed support to make this project a success.

Special mention goes to the following: My supervisors at IDEAS Prof Yali Yao, Prof Xinying Liu, Prof Diane Hildebrandt, Dr Andrew Ndhlovu and the department as a whole. I also want to thank Jianwei Ren from CSIR, for accommodating me at their facilities and for the support and insights that he shared.

I am indebted to technicians at IDEAS namely Humphry, Dolly, Mandla and Rabelani for their patience and assistance with the equipment and analysis. And also a special thanks goes to all Nanows staff for their support with most of the characterisation analysis.

I am thankful to all postgraduate students in IDEAS for their help, assistance and destressing sessions. Special thanks to my lab partners Thandeka, Tsepiso and Thuli for moral support and all the help they provided during my study. To my mum, father and late brother (Sehlelo) thank you for your support in all forms and encouragement.

I am grateful to UNISA/IDEAS for funding my research and above all, I thank God for his guidance, protection and patience with me.

LIST OF PUBLICATIONS AND PRESENTATIONS

Presentations

1) Liberty L Mguni, Yali Yao, Xinying Liu and Diane Hildebrandt. Effect of loading Cr_2O_3 on alumina on low sulphur conventional diesel desulphurization. Catalysis Society of South Africa (CATSA), Pilanesberg, North-West (19-22th Nov 2017).

2) Liberty L Mguni, Yali Yao, Thulisile Nkomzwayo, Xinying Liu, and Diane Hildebrandt Desulphurization of diesel fuels using metal oxide loaded activated charcoal and alumina. National University of Lesotho International Science and Technology Innovation Conference and Expo (NULISTICE): 23 – 26 January 2018, Maseru, Lesotho

3) Liberty L Mguni, Yali Yao, Xinying Liu and Diane Hildebrandt. Effect of support on NiO activity on adsorption desulphurization of model diesel. Catalysis Society of South Africa (CATSA), Waterberg, Limpopo (11-14th Nov 2018)

4) Liberty L Mguni, Yali Yao, Jianwei Ren, Xinying Liu and Diane Hildebrandt. Modulated synthesized Ni-doped MOF-5 with improved adsorptive desulphurization activity. Catalysis Society of South Africa (CATSA), Club Mykonos, Langebaan, Cape Town (10-13th Nov 2019

Publications:

1) Mguni, L.L., Yao, Y., Liu, X., Yuan, Z. and Hildebrandt, D. "Ultra-deep desulphurization of both model and commercial diesel fuels by adsorption method." *Journal of Environmental Chemical Engineering*, (2019) p.102957.

2) Mguni, Liberty L., Yali Yao, Thulisile Nkomzwayo, Xinying Liu, Diane Hildebrandt, and David Glasser. "Desulphurization of diesel fuels using intermediate Lewis acids loaded on activated charcoal and alumina." *Chemical Engineering Communications* (2018): 1-9.

3) Liberty L. Mguni, Yali Yao, Jianwei Ren, Xinying Liu, and Diane Hildebrandt. "Modulated Synthesis of a Novel Nickel-Based Metal-Organic Framework Composite Material for the Adsorptive Desulphurization of Liquid Fuels" *Industrial & Engineering Chemistry Research* 2021 60 (30), 10997-11008. DOI: 10.1021/acs.iecr.1c01082

4) Liberty L. Mguni, Yali Yao, Jianwei Ren, Xinying Liu, Diane Hildebrandt, Modulated synthesized Ni-based MOF with improved adsorptive desulfurization activity, Journal of Cleaner Production, 2021, 323, 129196, doi.org/10.1016/j.jclepro.2021.129196.

5) Liberty L. Mguni, Andrew Ndhlovu, Yali Yao, Jianwei Ren, Xinying Liu, and Diane Hildebrandt. "Insight into adsorptive desulphurization by zeolites: A machine learning exploration", Submitted for Publication

6) Liberty L. Mguni and Yali Yao. "Effect of support on selected Lewis acid metal oxide", Submitted for Publication

7) Liberty L Mguni, James Fox, Yali Yao. "Effect of adsorption improvement strategies on thermodynamics, kinetics and equilibrium isotherms of adsorptive desulphurization: A review (In preparation)

TABLE OF CONTENTS

LIST OF FIGURES

LIST OF TABLES

LIST OF ABBREVIATIONS AND SYMBOLS

Abbreviation/acronym/symbol	Full form/definition (units)
AC	Activated carbon
ADS	Adsorptive desulphurization
BDC	1,4-benzenedicarboxylate
BET	Brunauer–Emmett–Teller
DBT	Dibenzothiophene
DMF	N,N-Dimethylformamide
4,6 DMDBT	4,6-Dimethyldibenzothiophene
FID	Flame ionization detector
FTIR	Fourier-transform infrared spectroscopy
FoM	Figure of merit
HDS	Hydrodesulphurization
GC	Gas chromatography
MOFs	Metal organic frameworks
MOF-5/ IRMOF-1	Metal-organic framework (MOF) formed from Zn_4O nodes with 1,4-benzodicarboxylic acid struts between the nodes
MOF-5(Ni)	MOF-5 doped with nickel
MOF-5(xNi/Zn)	MOF-5 composed of x % nickel and (1-x) % Zn
MOF-5 x eq	MOF-5 synthesized by modulator x molar equivalent with respect to metal ion
MOF-5(Ni) x eq	MOF-5 based on nickel synthesized by modulator x molar equivalent with respect to metal ion
PFPD	Pulsed Flame Photometric Detector
SEM	Scanning electron microscope
TCD	Thermal Conductivity Detector
TH	Thiophene
TPD-pyridine	Pyridine temperature-programmed desorption
XRD	X-Ray Diffraction Analysis
XPS	X-ray photoelectron spectroscopy

1. INTRODUCTION

1.1 Introduction

In a concerted effort to protect the earth from the harmful effects of toxic emissions, especially those of industrial origin, international agencies are introducing increasingly stringent regulations regarding the amount of sulphur allowed in fuels such as gasoline and diesel. Another reason for fuel producers attempting to reduce the sulphur content is that it affects fuel cell applications and catalytic converters. This topic has, therefore, become a priority for researchers and engineers in this field.

Hydrodesulphurization (HDS) is the main technology used by industries to remove sulphur from liquid fuels. HDS is effective in the removal of aliphatic S in liquid fuels. Because of the stringent regulations - i.e. less than 10 ppm in some countries - there is a need to remove unreactive chemical species like benzothiophene (BT), 4-methyl-dibenzothiophene (4-MDBT), 4,6-dimethyl-dibenzothiophene (4,6-DMDBT) and 1-methylnaphanelene (Hernandez-Maldonado and Yang, 2004; Jeevanandam et al., 2005; Muzic et al., 2008). Removing these sulphur compounds using HDS results in a significant escalation in cost, because of the need to work with hydrogen at an elevated temperature under high pressure (Jeevanandam et al., 2005; Xuemin et al., 2008).

Because HDS requires hydrogen and high pressure, it is not suitable for small scale industrial applications. Therefore alternative desulphurization approaches have been developed recently. Table 1.1 presents the advantages and disadvantages of technologies that have been used to remove sulphur compounds from liquid fuels. Among these, adsorptive desulphurization (ADS) represents a great opportunity, because the technology can remove sulphur at ambient conditions, it is relatively low cost and it removes highly substituted dibenzothiophene. However, a myriad of challenges associated with this technology still has to be overcome.

ADS is a relatively new approach compared to the well-established HDS technology. Hence, there is very little data available on research done using real liquid fuels, with most work done using model fuel to mimic real fuels (Lee, 2020). A crucial factor in ADS is selecting the adsorbent (Jha et al., 2019), the efficiency of the adsorbent is highly dependent on sorbent properties. To the best of our knowledge, no reported work has elucidated the relative importance of these sorbent properties, which is why adsorbent design remains an art that involves trial and error.

Furthermore, there are still many opportunities to synthesize new adsorbents or improve the adsorption capacity and selectivity of existing adsorbents. Finally, there is little understanding of the structure-function relationship between adsorbent properties, and adsorption capacity and selectivity (Crandall et al., 2019).

Table 1.1: Advantages and disadvantages of various technologies for liquid fuel desulphurization

Technology	Advantage	Disadvantage
Hydrodesulphurization	Widely used	high temperature 400°C
	Well-studied	High-pressure (20MPa)
	Effectively removes thiols	low for alkylated-DBT
Noble catalyst- high cost		
Biodesulphurization	Mild conditions	Slow degradation
	Simple conditions	Challenge of suitable biocatalyst
Solvent extraction	Mild conditions	Poor solvent recovery
	Limited suitable solvents	Low yield
Oxidative desulphurization	Improved extraction polar	Difficult in oxidant selection Unwanted side reactions
Adsorption	Ambient conditions	Poor selectivity
	Reusability	Low adsorption capacity
	Environmental-friendly	

This study aimed to remove sulphur from diesel fuel using ADS. Choosing an appropriate material is highly challenging and often involves trial and error. However, some reports indicate that machine learning (ML) and computational methods can be used to improve this exercise (Sahu et al., 2019; Zhu et al., 2019; Lin et al., 2020). In this work, ML was used to identify factors with a strong influence on the adsorption activity of adsorbents. Activity/selectivity can be improved by controling the features of the adsorbent.

The characteristics of sulphur compounds can be changed by oxidation to make them more polar, and therefore probably easier to remove from non-polar diesel, while the features of the

adsorbent can be changed by adsorbent surface modification. Adsorption is a surface phenomenon; hence, in this work, most strategies employed were to improve the activity of highly porous adsorbents. The adsorbents used are activated carbon (AC) and metal-organic frameworks (MOF) and these were tested using both model diesel and conventional diesel. AC has been used as an adsorbent in the past and it has been reported to offer a porous structure with a high surface area and high pore volume (Yu et al., 2009; Al. Swat et al., 2017; Moreira et al., 2017). AC is naturally hydrophobic/ less polar but the sulphur compounds that have to be removed have a net S charge and a dipole moment, which means that AC has weak adsorption activity in desulphurization. Therefore, various improvement strategies have been employed, such as: treating the AC with acid (Saleh and Danmaliki, 2016; Shah et al., 2017); nitrogen doping (Seredych et al., 2010; Shi et al., 2015); metal loading (Ania and Bandosz, 2006; Mguni et al., 2019); bimetallic loading (Danmaliki and Saleh, 2017; Saleh, 2018). However, in general, AC: shows high activity for high molecular weight (MW) sulphur compounds and low activity for low MW sulphur compounds and has few structural possibilities (Bu et al., 2011).

Metal-organic frameworks (MOFs) are a new class of porous adsorbents that offer more straightforward structural engineering and infinite structural possibilities (Greer et al., 2016; Abdelhameed et al., 2017; Kampouraki et al., 2019; Ullah et al., 2019). In contrast to AC, they offer good activity with low MW sulphur compounds. Most of the research work done with MOFs has focused on improving adsorption activity by metal loading (Aslam et al., 2017), pore size adjustment (Sun et al., 2012), metal ion exchange (Huanhuan Li et al., 2012; Khan and Jhung, 2013; Wang et al., 2015) and ligand functionalising (Shi et al., 2011). One of the major challenges with MOFs is that they are sensitive to moisture.

This work focused on systematically screening potential supports and metals using model and conventional fuels. This process was assisted by first understanding the parameters that have a strong influence on adsorption capacity using ML. Once the most promising support and metal were identified, they were used to synthesize a novel metal doped Ni-MOF materials and support-MOF composites that could adsorb sulphur compounds over a broad MW range. The MOF and composite were synthesized using a modulator, in order to improve their resistance to moisture, and control crystallinity and crystallite size.

1.2 Research Objectives

The main aim of this study was to identify strategies that could be used to improve the activity of porous materials such as activated carbon and Ni-based MOF for adsorptive desulphurization. MOFs were selected because of their tuneable pore structure, while AC was used because of facile synthesis and the low cost. Although AC has been reported as being used for adsorption, most of the studies were done using model diesel. In this work, we report for the first time on the desulphurization of commercial diesel fuel from South Africa, as well as on novel Ni-BDC MOF material and AC@Ni-BDC composite. The latter were synthesized using a modulated synthesis of the most promising metal and support, based on the screening done in this work, i.e. Ni and AC.

Modulated synthesis has been reported to: improve the crystallinity of the material; vary the crystal size of the MOFs; improve ease of handling; and decrease reaction time and the degree of aggregation (Wiβmann et al., 2012). In this work, modulated synthesis enabled us to vary the crystallite and crystallinity of the Ni-based MOF adsorbent. Therefore, this report also explains the effect of crystallite size and crystallinity on adsorption activity, which will contribute to better understanding the structure-function relationship between adsorbent properties and adsorption capacity.

The specific objectives of this work are:

- To investigate what variables have the biggest effect on adsorption using ML (The analysis was carried out on zeolites, because of the better characterisation data compared to other adsorption materials).
- To screen porous material for potential adsorptive desulphurization when using both model diesel and conventional diesel.
- To modify activated carbon using intermediate Lewis acids and investigate their desulphurization activity.
- To analyse the effect of support on the most active intermediate Lewis acid (NiO) on ADS activity.
- To synthesize a novel MOF based on the most active intermediate Lewis acid (Ni) and analyse its ADS activity.
- To synthesize a novel composite of AC and MOF with a nickel base and investigate its ADS activity.

1.3 Thesis Outline

The thesis is composed of ten chapters. The current chapter introduced the aim and the structure of the thesis. Chapters 2-9 were prepared as papers for publication in journals. The short introductions of Chapters 2-10 are as follows:

Chapter 2: This chapter looks at the improvement strategies described in the literature. It focuses on the effects of these strategies on kinetics, thermodynamics and adsorption isotherms. Finally, a comparison of adsorbents activity is provided, based on the partition coefficient and figure of merit (FoM).

Chapter 3: The chapter outlines the experimental techniques used in this work. Adsorbent synthesis and batch adsorption experiment procedures are detailed. The chapter also outlines the characterisation methods used for adsorbents and the fuel analysis techniques.

Chapter 4: This chapter explains which adsorption parameters have a strong influence on the adsorption activity of adsorbents. The analysis was done using ML, to be specific random forest and linear regression were used.

Chapter 5: Details are provided of the screening done of commercial adsorbents using a model and conventional diesel, with the selectivity and activity of the catalyst having been analysed.

Chapter 6: This chapter deals with the effect of adding Lewis acid-metal oxides to AC was investigated using both model diesel and conventional diesel.

Chapter 7: This chapter explains the effect of the support on the most active Lewis acid-metal oxide. This was investigated using model diesel and conventional diesel.

Chapter 8: This chapter details the novel synthesis method used to produce MOF based on nickel. The effect of crystallinity and crystallite size on adsorption activity and selectivity were investigated.

Chapter 9: This chapter deals with a novel composite based on MOF based nickel and AC that was produced to improve AC activity, since MOF based on nickel showed a higher affinity for sulphur than AC, but poor pore structure. In contrast, AC had an excellent pore structure.

Chapter 10: It gives the overall conclusions and perspectives.

References

Abdelhameed, R.M., Emam, H.E., Rocha, J., Silva, A.M.S., 2017. Cu-BTC metal-organic framework natural fabric composites for fuel purification. Fuel Processing Technology 159, 306–312. https://doi.org/10.1016/j.fuproc.2017.02.001

Al. Swat, A.A., Saleh, T.A., Ganiyu, S.A., Siddiqui, M.N., Alhooshani, K.R., 2017. Preparation of activated carbon, zinc oxide and nickel oxide composites for potential application in the desulphurization of model diesel fuels. Journal of Analytical and Applied Pyrolysis 128, 246–256. https://doi.org/10.1016/j.jaap.2017.10.004

Ania, C.O., Bandosz, T.J., 2006. Metal-loaded polystyrene-based activated carbons as dibenzothiophene removal media via reactive adsorption. Carbon 44, 2404–2412. https://doi.org/10.1016/j.carbon.2006.05.016

Aslam, S., Subhan, F., Yan, Z., Etim, U.J., Zeng, J., 2017. Dispersion of nickel nanoparticles in the cages of metal-organic framework: An efficient sorbent for adsorptive removal of thiophene. Chemical Engineering Journal 315, 469–480. https://doi.org/10.1016/j.cej.2017.01.047

Bu, J., Loh, G., Gwie, C.G., Dewiyanti, S., Tasrif, M., Borgna, A., 2011. Desulphurization of diesel fuels by selective adsorption on activated carbons: Competitive adsorption of polycyclic aromatic sulphur heterocycles and polycyclic aromatic hydrocarbons. Chemical Engineering Journal 166, 207–217. https://doi.org/10.1016/j.cej.2010.10.063

Crandall, B.S., Zhang, J., Stavila, V., Allendorf, M.D., Li, Z., 2019. Desulphurization of Liquid Hydrocarbon Fuels with Microporous and Mesoporous Materials: Metal-Organic Frameworks, Zeolites, and Mesoporous Silicas. Ind. Eng. Chem. Res. 58, 19322–19352. https://doi.org/10.1021/acs.iecr.9b03183

Danmaliki, G.I., Saleh, T.A., 2017. Effects of bimetallic Ce/Fe nanoparticles on the desulphurization of thiophenes using activated carbon. Chemical Engineering Journal 307, 914–927. https://doi.org/10.1016/j.cej.2016.08.143

Greer, H.F., Liu, Y., Greenaway, A., Wright, P.A., Zhou, W., 2016. Synthesis and formation mechanism of textured MOF-5. Crystal Growth & Design 16, 2104–2111.

Hernandez-Maldonado, A.J., Yang, R.T., 2004. New sorbents for desulphurization of diesel fuels via ?-complexation. AIChE Journal 50, 791–801. https://doi.org/10.1002/aic.10074

Jeevanandam, P., Klabunde, K.J., Tetzler, S.H., 2005. Adsorption of thiophenes out of hydrocarbons using metal impregnated nanocrystalline aluminum oxide. Microporous and Mesoporous Materials 79, 101–110. https://doi.org/10.1016/j.micromeso.2004.10.029

Jha, D., Haider, M.B., Kumar, R., Byamba-Ochir, N., Shim, W.G., Marriyappan Sivagnanam, B., Moon, H., 2019. Enhanced Adsorptive Desulphurization Using Mongolian Anthracite-Based Activated Carbon. ACS Omega 4, 20844–20853. https://doi.org/10.1021/acsomega.9b03432

Kampouraki, Z.-C., Giannakoudakis, D.A., Nair, V., Hosseini-Bandegharaei, A., Colmenares, J.C., Deliyanni, E.A., 2019. Metal-Organic Frameworks as Desulphurization Adsorbents of DBT and 4,6-DMDBT from Fuels. Molecules 24, 4525. https://doi.org/10.3390/molecules24244525

Khan, N.A., Jhung, S.H., 2013. Effect of central metal ions of analogous metal-organic frameworks on the adsorptive removal of benzothiophene from a model fuel. Journal of Hazardous Materials 260, 1050–1056. https://doi.org/10.1016/j.jhazmat.2013.06.076

Lee, K., 2020. Liquid Phase Adsorptive Desulphurization using Modified Zeolites for Transportation and Fuel Cell Applications 197.

Li, Huanhuan, Shi, W., Zhao, K., Li, Han, Bing, Y., Cheng, P., 2012. Enhanced Hydrostability in Ni-doped MOF-5. Inorg. Chem. 51, 9200–9207. https://doi.org/10.1021/ic3002898

Lin, S., Wang, Y., Zhao, Y., Pericchi, L.R., Hernández-Maldonado, A.J., Chen, Z., 2020. Machine-learning-assisted screening of pure-silica zeolites for effective removal of linear siloxanes and derivatives. Journal of Materials Chemistry A 8, 3228–3237.

Mguni, L.L., Yao, Y., Nkomzwayo, T., Liu, X., Hildebrandt, D., Glasser, D., 2019. Desulphurization of diesel fuels using intermediate Lewis acids loaded on activated charcoal and alumina. Chemical Engineering Communications 206, 572–580. https://doi.org/10.1080/00986445.2018.1511983

Moreira, A.M., Brandão, H.L., Hackbarth, F.V., Maass, D., Ulson de Souza, A.A., Guelli U. de Souza, S.M.A., 2017. Adsorptive desulphurization of heavy naphthenic oil: Equilibrium and kinetic studies. Chemical Engineering Science 172, 23–31. https://doi.org/10.1016/j.ces.2017.06.010

Muzic, M., Sertic-Bionda, K., Gomzi, Z., 2008. Kinetic and Statistical Studies of Adsorptive Desulphurization of Diesel Fuel on Commercial Activated Carbons. Chemical Engineering & Technology 31, 355–364. https://doi.org/10.1002/ceat.200700341

Sahu, H., Yang, F., Ye, X., Ma, J., Fang, W., Ma, H., 2019. Designing promising molecules for organic solar cells via machine learning assisted virtual screening. Journal of Materials Chemistry A 7, 17480–17488.

Saleh, T.A., 2018. Simultaneous adsorptive desulphurization of diesel fuel over bimetallic nanoparticles loaded on activated carbon. Journal of Cleaner Production 172, 2123–2132. https://doi.org/10.1016/j.jclepro.2017.11.208

Saleh, T.A., Danmaliki, G.I., 2016. Influence of acidic and basic treatments of activated carbon derived from waste rubber tires on adsorptive desulphurization of thiophenes. Journal of the Taiwan Institute of Chemical Engineers 60, 460–468. https://doi.org/10.1016/j.jtice.2015.11.008

Seredych, M., Hulicova-Jurcakova, D., Bandosz, T.J., 2010. Effect of the Incorporation of Nitrogen to a Carbon Matrix on the Selectivity and Capacity for Adsorption of Dibenzothiophenes from Model Diesel Fuel. Langmuir 26, 227–233. https://doi.org/10.1021/la902059y

Shah, S.S., Ahmad, I., Ahmad, W., Ishaq, M., Khan, H., 2017. Deep Desulphurization Study of Liquid Fuels Using Acid Treated Activated Charcoal as Adsorbent. Energy Fuels 7.

Shi, F., Hammoud, M., Thompson, L.T., 2011. Selective adsorption of dibenzothiophene by functionalized metal organic framework sorbents. Applied Catalysis B: Environmental 103, 261–265. https://doi.org/10.1016/j.apcatb.2010.07.016

Shi, Y., Liu, G., Wang, L., Zhang, X., 2015. Efficient adsorptive removal of dibenzothiophene from model fuel over heteroatom-doped porous carbons by carbonization of an organic salt. Chemical Engineering Journal 259, 771–778. https://doi.org/10.1016/j.cej.2014.08.054

Sun, L.-B., Li, J.-R., Park, J., Zhou, H.-C., 2012. Cooperative template-directed assembly of mesoporous metal–organic frameworks. Journal of the American Chemical Society 134, 126–129.

Ullah, L., Zhao, G., Hedin, N., Ding, X., Zhang, S., Yao, X., Nie, Y., Zhang, Y., 2019. Highly efficient adsorption of benzothiophene from model fuel on a metal-organic framework modified with dodeca-tungstophosphoric acid. Chemical Engineering Journal 362, 30–40. https://doi.org/10.1016/j.cej.2018.12.141

Wang, T., Li, X., Dai, W., Fang, Y., Huang, H., 2015. Enhanced adsorption of dibenzothiophene with zinc/copper-based metal–organic frameworks. J. Mater. Chem. A 3, 21044–21050. https://doi.org/10.1039/C5TA05204A

Wiβmann, G., Schaate, A., Lilienthal, S., Bremer, I., Schneider, A.M., Behrens, P., 2012. Modulated synthesis of Zr-fumarate MOF. Microporous and Mesoporous Materials 152, 64–70.

Xuemin, C., Yufeng, H., Jiguang, L., Qianqing, L., Wenjia, Y., 2008. Desulphurization of Diesel Fuel by Extraction with [BF4] based Ionic Liquids. Chinese Journal of Chemical Engineering 16, 881–884.

Yu, M., Li, Z., Ji, Q., Wang, S., Su, D., Lin, Y.S., 2009. Effect of thermal oxidation of activated carbon surface on its adsorption towards dibenzothiophene. Chemical Engineering Journal 148, 242–247.

Zhu, X., Wang, X., Ok, Y.S., 2019. The application of machine learning methods for prediction of metal sorption onto biochars. Journal of Hazardous Materials 378, 120727. https://doi.org/10.1016/j.jhazmat.2019.06.004

2. LITERATURE REVIEW

This work was prepared as a review paper entitled: **Effect of adsorption improvement strategies on thermodynamics, kinetics and equilibrium isotherms of adsorptive desulphurization: A review**

Summary

Desulphurization from the gas phase is a comparatively simple endeavour, for which many commercial technologies already exist; however, desulphurization technologies that can remove sulphur from the liquid phase are needed. Due to relatively mild operating conditions, adsorption is considered the most promising route for liquid phase desulphurization. This document provides a discussion of various types of adsorbent material on the basis of thermodynamics, kinetics and equilibrium isotherms. Activated carbon (AC) is a highly versatile adsorbent material because of its ease-of-use and desirable physical and chemical properties. Based on the figure of merit (FoM) parameter, AC is the most promising adsorbent. However, if the technical barriers for synthesizing metal-organic frameworks (MOFs), such as cost, do not prove prohibitive, the cobalt-based metal-organic framework, $[Co_6(oba)_6(CH3O)_4(O)_2]n{\cdot}3DMF$ (TMU-11) appears to be an extremely promising alternative, due to its high adsorptive activity. Finally, adsorption of solvent by adsorbent is desirable to improve activity for an entropy-driven adsorption reaction.

Keywords: adsorption desulphurization; thermodynamics; kinetics; adsorption isotherms; figure of merit

2.1 Introduction

The transport industry is one of the biggest contributors to sulphur oxide (SO_X) gas emissions. These emissions are caused by the oxidation of sulphur impurities in the fuel, which is converted into SO_X during combustion and then emitted into the environment, where they cause environmental problems such as acid rain (Labana et al., 2005). The most direct solution to the problem of SO_X emissions is to remove the sulphur impurities from the fuel before combustion in engines, which has led to numerous nations legislating lower allowable sulphur quantities in both diesel and gasoline (UNEP, 2015; Williams and Minjares, 2016).

Sulphur can be removed easily, from the gas phase, when producing synthetic fuels and hydrocarbons using the amine wash process. Proprietary technologies, such as Rectisol and Selexol, have ensured that this part of desulphurization is understood fairly well (Nexant, Inc., 2011; Sadegh-Vaziri et al., 2015). However, research opportunities still exist in terms of removing sulphur from the liquid phase. This could potentially be used to improve fuel quality during oil refining and in locations where the application of expensive commercial technologies may not be viable (such as in developing economies). The focus of this thesis will be on discussing the research that has been done on the liquid phase desulphurization of fuels and hydrocarbons.

Desulphurization from the liquid phase is a complicated process, as the sulphur is chemically bonded within hydrocarbon molecules. The goal is to remove the sulphur and to simultaneously avoid compromising the properties of the fuel itself. Desulphurization is conventionally carried out by a process of hydro desulphurization (HDS) (Hensen, 2000; Bhatia and Sharma, 2010; Sikarwar et al., 2019), whereby sulphur impurities are catalytically converted into hydrogen sulphide via reaction with hydrogen. For example, propanethiol can be hydrogenated into propane and hydrogen sulphide, which results in a saturated hydrocarbon that can be combusted without SO_X emissions. The formula is provided in equation 2.1:

$$C_3H_8S + H_2 \rightarrow C_3H_8 + H_2S \qquad (2.1)$$

HDS has proven effective in the desulphurization of straight-chain molecules but has been found to be less effective with cyclo- molecules (Betiha et al., 2018). The various derivatives of benzothiophene have proven to be particularly resistant to hydrogenation by the HDS process (Hernandez-Maldonado and Yang, 2004; Jeevanandam et al., 2005; Muzic et al., 2008).

For this reason, other technologies are used to complement HDS, for example: adsorption, solvent extraction, biodesulphurization, oxidative desulphurization and liquid ions. A detailed analysis of these technologies has been given in numerous publications (Labana et al., 2005; Abro et al., 2014; Ahmed and Jhung, 2016; Lee and Valla, 2019). While the purpose of desulphurization is to ameliorate the environmental impact of emissions, the impact of pollution on the environment is not measured solely by SO_X emissions. Other important considerations include energy use and carbon emissions. For these reasons, adsorption desulphurization has been suggested as the most promising supplement to HDS, because the process can be carried out at ambient conditions (Lee and Valla, 2019), which addresses SO_X, carbon and energy concerns at the same time.

The effectiveness of any adsorption technology is affected by porosity, surface area and favourable adsorption sites of the adsorbents. The challenge in the adsorption of sulphur compounds in liquid fuel is the presence of polycyclic aromatic hydrocarbons (PAHs) and heterocyclic nitrogen-containing compounds (HNCs). While these compounds do not contain sulphur themselves, they have a structure similar to compounds that do contain sulphur. (See Figure 2.1.) This causes difficulties with the selective separation of sulphur from these compounds, which is then further exacerbated by the similar electronic properties of these compounds. (See Table 2.1.) These issues, combined with the need to reduce sulphur to ppb levels, makes for a difficult separation process.

Several selective separation methods can be applied in adsorption, including: molecular sieving; kinetic effect based on the molecular diffusion effect; adsorbate-adsorbent interactions (also known as the thermodynamic effect; quantum effect (Worch, 2012; Fakhraei Ghazvini et al., 2021). The properties that can be used for selective separation of sulphur are net S charge, dipole moment (slightly higher) and the logarithm of the separation equilibrium constant (log K_{ow}). Furthermore, a comparison of sulphur and nitrogen compound properties suggests that sulphur and nitrogen compounds can both be removed simultaneously. Therefore, adsorbate-adsorbent interaction manipulation has the greatest potential for improving adsorbent activity. Hence, most research has focused on improving adsorbent-adsorbate interaction.

The improvement strategies for adsorptive desulphurization adsorbent are well documented in a number of reviews (Bagheri et al., 2017; Tan et al., 2018; Lee and Valla, 2019; Saha et al., 2020). To the best of our knowledge, there is limited literature that summarizes and compares the effect of these strategies on both the kinetics and thermodynamics of desulphurization.

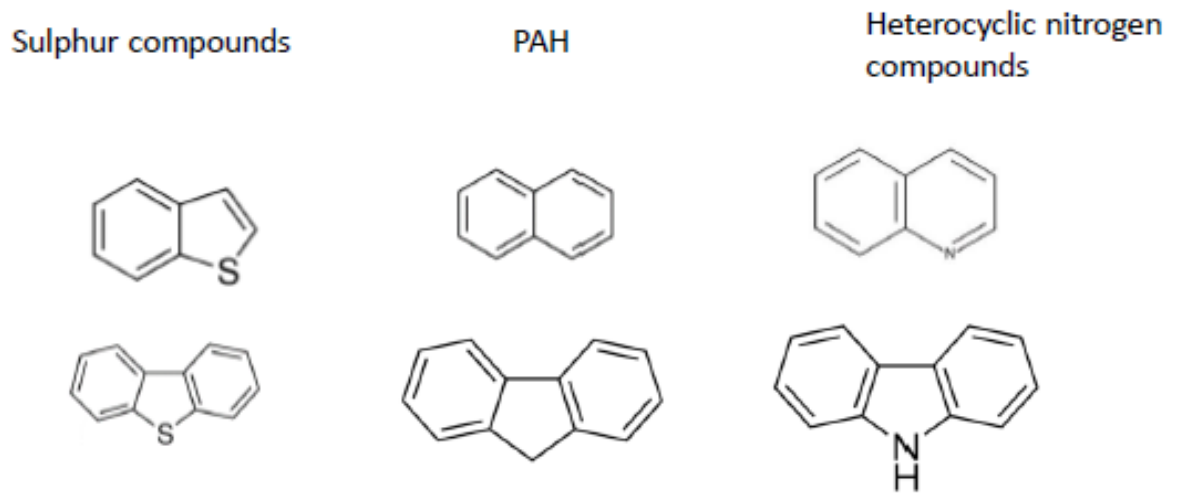

Figure 2.1: Similarity in the chemical structures of sulphur compounds, PAH and heterocyclic nitrogen compounds.

Most of the experimental work reported in the literature (Danmaliki and Saleh, 2017; Lu et al., 2017; Shah et al., 2017; Saleh et al., 2018; Shah et al., 2018) has focused on what effect these strategies have on adsorption capacity and selectivity, and the researchers then did kinetic, thermodynamic and equilibrium isotherm analysis on the most active adsorbents. This practice represents a challenge in analysing the effects of kinetics, thermodynamics and equilibrium isotherms on adsorbent improvement strategies. The comparison of work reported by different researchers will be limited to systems with similar adsorption conditions: adsorbent loading, temperature and initial sulphur compound concentration. This work analyses information obtained by comparing adsorbents before and after the implementation of an improvement strategy, and also discusses the effect of process parameters. A suggested direction that research on adsorptive desulphurization should take, based on the analysis results, is also provided.

Table 2.1: Property polarisability of diesel and gasoline sulphur compounds (Kim et al., 2006; Bu et al., 2011; Xiao et al., 2012; Li et al., 2015)

Properties				
Compound	**kinetic diameter**	**net S/N charge**	**Dipole (D)**	**logKow**
Thiophene	0.56×0.77	0.023	0.51	1.81
BT	0.65×0.89	0.261	0.79	3.12
DBT	0.65×0.91	0.242	0.79	4.38
4,6DMDBT	0.78×1.23	0.239	0.748	
PAH				
Naphthalene	0.74×0.92	-	0	3.3
Fluorene	0.75×1.14	-	0.28	4.18
Anthracene	0.75×1.14	-	0	4.45
Phenanthrene	0.80×1.18	-	0.55	4.46
heterocyclic nitrogen compounds				
Indole		-0.449	1.8442	2.14
Quinoline		-0.699	2.1038	2.03
Carbazole		-0.705	1.6665	3.72
Acridine		-0.72	1.9243	3.4

2.1.1 Adsorption desulphurization mechanisms

Adsorption of sulphur compounds may proceed via physical or chemical adsorption. Physical adsorption is based on weak van der Waals forces and weak electrostatic forces while chemical adsorption involves electron transfer leading to the formation of bonds between adsorbate and adsorbent. The economic viability of an adsorbent depends on selectivity and adsorption capacity. The challenge with the two adsorption modes i.e. physical and chemical adsorption is that physical adsorption has a high capacity because of the ability to form multiple layers but has poor selectivity while chemical adsorption has good selectivity but reduced adsorption capacity because of monolayer adsorption. Other characteristics of physical and chemical adsorption are presented in Table 2.2.

Table 2.2: Properties of physical and chemical adsorption (Murzin and Salami, 2005)

Physical	**Chemical**
weak Van der Waals forces	Chemical bond formation
Favoured at low temperature	Favoured at high temperature
Activation energy is not required	Activation energy required
Low enthalpy of adsorption (5-10 kJ/mol)	High enthalpy of adsorption (30-70 kJ/mol)

In principle, the adsorption mechanism detects the kinetic, thermodynamic and equilibrium isotherms. This necessitates a very brief discussion on adsorption mechanisms, but readers are referred to detailed reviews on the subject (Hernández‐Maldonado and Yang, 2004; Khan et al., 2013; Khan and Jhung, 2017; Lee and Valla, 2019).

Adsorption mechanisms for activated carbon

AC and other carbonous materials are some of the most studied adsorbents because of their stability, good mechanical strength and good pore structure (Svinterikos et al., 2019). AC is naturally hydrophobic / less polar, but the sulphur compounds that have to be removed have a net S charge and a dipole moment, which gives AC weak adsorption activity for desulphurization. However, the advantages of AC still make it worth pursuing as an adsorbent. Improvement strategies such as acid treating the AC (Saleh and Danmaliki, 2016; Shah et al., 2017), nitrogen doping (Seredych et al., 2010; Shi et al., 2015) metal loading (Ania and Bandosz, 2006; Mguni et al., 2019) and bimetallic loading (Danmaliki and Saleh, 2017; Saleh, 2018) have been employed to improve the activity of AC. All these strategies aim at improving / increasing / introducing functional groups on the AC surface. The adsorption for carbon material has been attributed to π-π stacking while the addition of metal or bimetals has been suggested to lead to π- complexation. These adsorption modes are summarised in Figure 2.2 and their adsorption isotherms are indicated. The adsorption mechanism of three carbon materials are presented, namely: reduced graphene oxide (rGO); carbon black−graphene composite (CB-G); nickel impregnated graphene (Ni-G). Adsorption isotherms for rGO and CB-G were best fitted with the Langmuir isotherm, indicating uniform adsorption sites, while, the isotherms for Ni-G were best fitted with the Freundlich isotherm at lower DBT concentrations and the Langmuir isotherm at higher DBT concentrations.

This type of correlation suggests that the adsorption process starts at Ni-sites on the adsorbents and then continues by adsorption on the uniform graphitic surface (Sedaghat et al., 2019).

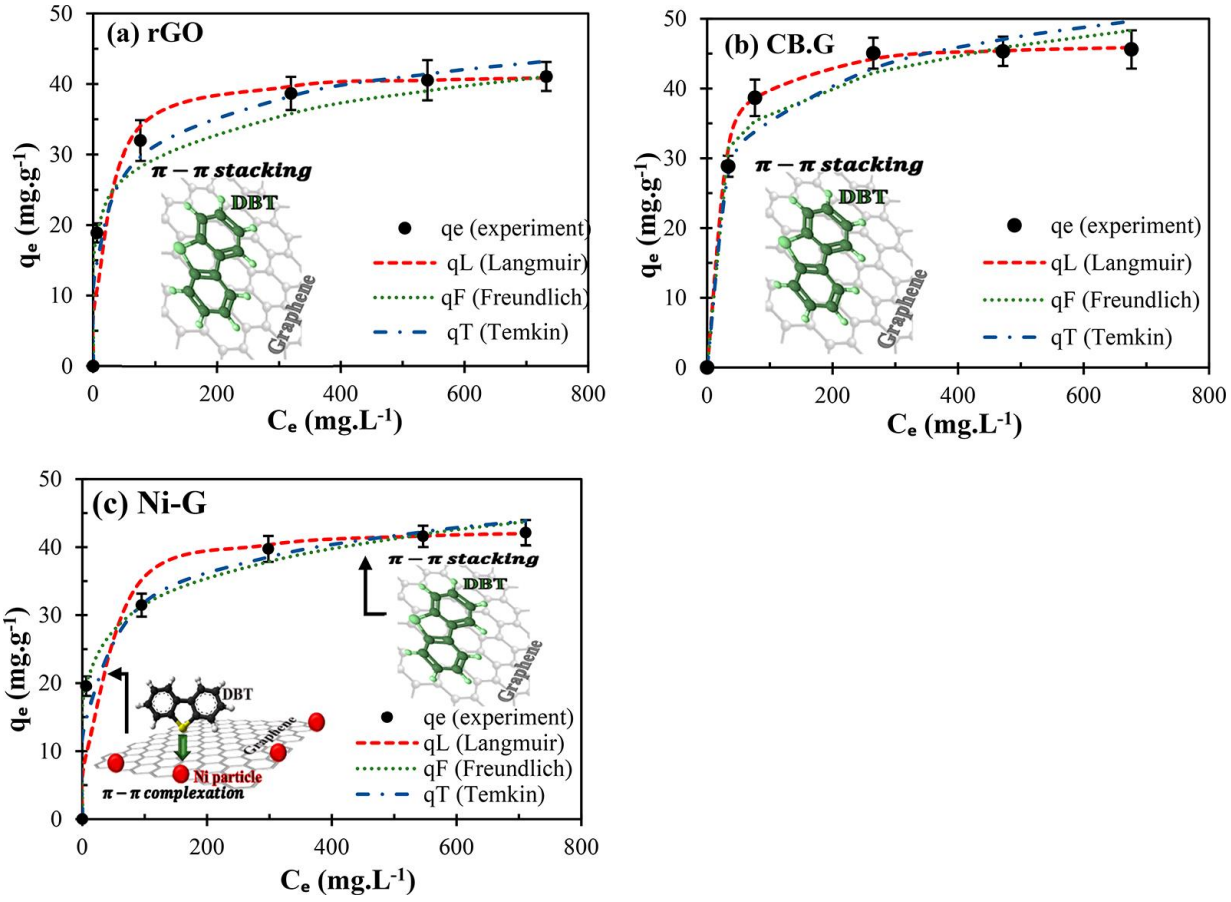

Figure 2.2: Adsorption mechanisms of graphene and Ni loaded graphene for: (a) reduced graphene oxide (rGO); (b) carbon black−graphene composite (CB.G); (c) Ni loaded graphene (Ni-G). q_e refers to equilibrium loading; qL refers to Langmuir equilibrium is; qF Freundlich equilibrium isotherm; qT refers to Temkin equilibrium isotherm. Adsorption conditions: DBT adsorption in batch mode at 25 °C: Reprinted (adapted) with permission from Sedaghat et al. (2019). Copyright 2019 American Chemical Society.

Adsorption mechanisms for zeolites

Zeolites are another common adsorbent that possesses an excellent ordered structure (Muzic et al., 2010). Zeolites are alumina-silicates, with their properties being determined by the Si/Al ratio. A low Si/Al ratio produces acidic adsorbents that are ideal for sulphur adsorption and metal ion exchange. The strategies that have been used to improve these adsorbents are metal ion exchange, controlling the Si/Al ratio, controlling the pore structure, and producing bimetallic zeolites. Bimetallic zeolites have been reported to have a synergistic effect because of electron transfer between π-bonding metal and σ bonding for high valence metal (Song et al., 2013).

There are three widely reported adsorption mechanisms: hydrogen bonding -for HY zeolites facilitated by Bronsted acid sites (Liao et al., 2019); π-complexation interaction for transitional metals- with empty 4s orbitals and full 3d orbitals commonly reported including: CuY (Ma and Yang, 2007; Song et al., 2016); AgY (Xue et al., 2005); NiY (Wang et al., 2009) and ZnY (Hernández-Maldonado et al., 2005); metal-sulphur bond via σ-bond- this has been reported for high valence metals, i.e. CeY (Hernández-Maldonado and Yang, 2004) and LaY (Tian et al., 2006). The π-complexation and direct σ-bonding interactions are presented in Figure 2.3.

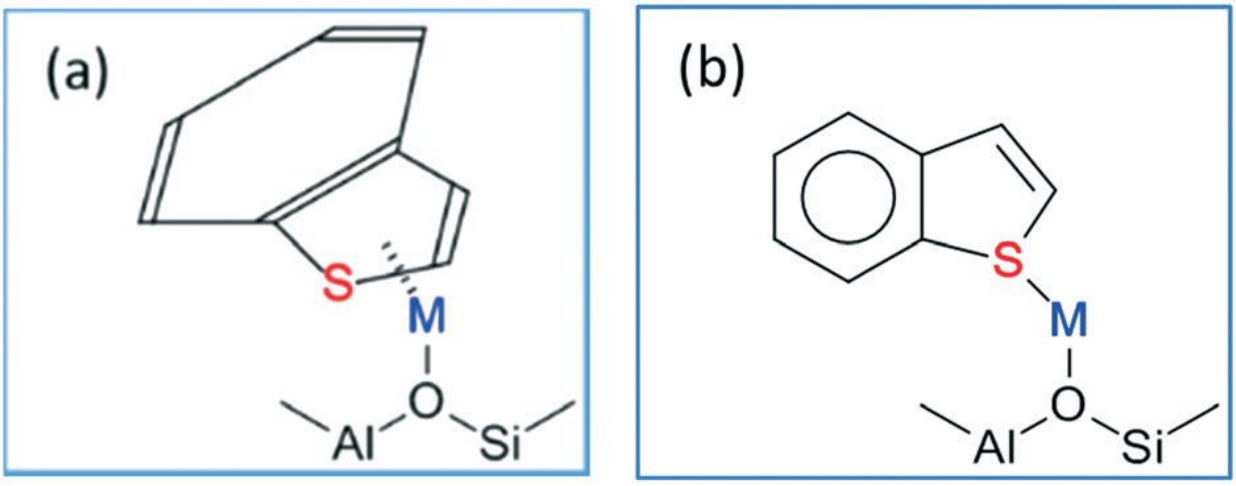

Figure 2.3: Adsorption configurations: a) π-complexation; b) direct σ-bonding interaction. Reprinted (adapted) with permission from Lee and Valla (2019). Copyright 2019 Royal Society of Chemistry.

Adsorption mechanisms for Metal-organic frameworks

The tunable structures of metal-organic frameworks (MOFs) are a desirable property for adsorptive desulphurization. They have been reported to show superior adsorption properties relative to other adsorbents. Adsorption improvement strategies include metal loading (Aslam et al., 2017), pore size adjustment (Sun et al., 2012), metal ion exchange (Huanhuan Li et al., 2012) (Khan and Jhung, 2013; Wang et al., 2015) and ligand functionalising (Shi et al., 2011). It has been suggested that functionality is more important in MOFs than surface area and pore volume. MOFs have several possible adsorption mechanisms, depending on the central metal ion, the organic framework and its functionalisation. MOFs may adsorb via π-complexing if the metal ion is a transitional metal, and this has been reported for Zn, Ni and Cu. Coordinately unsaturated sites (unsaturated metals) have been reported to have a higher capacity for sulphur and π-π bonding has been reported, due to the contribution of aromatic compounds on the organic framework (Ahmed and Jhung, 2016). The primary adsorption mechanisms that have been reported for MOFs are presented in Figure 2.4.

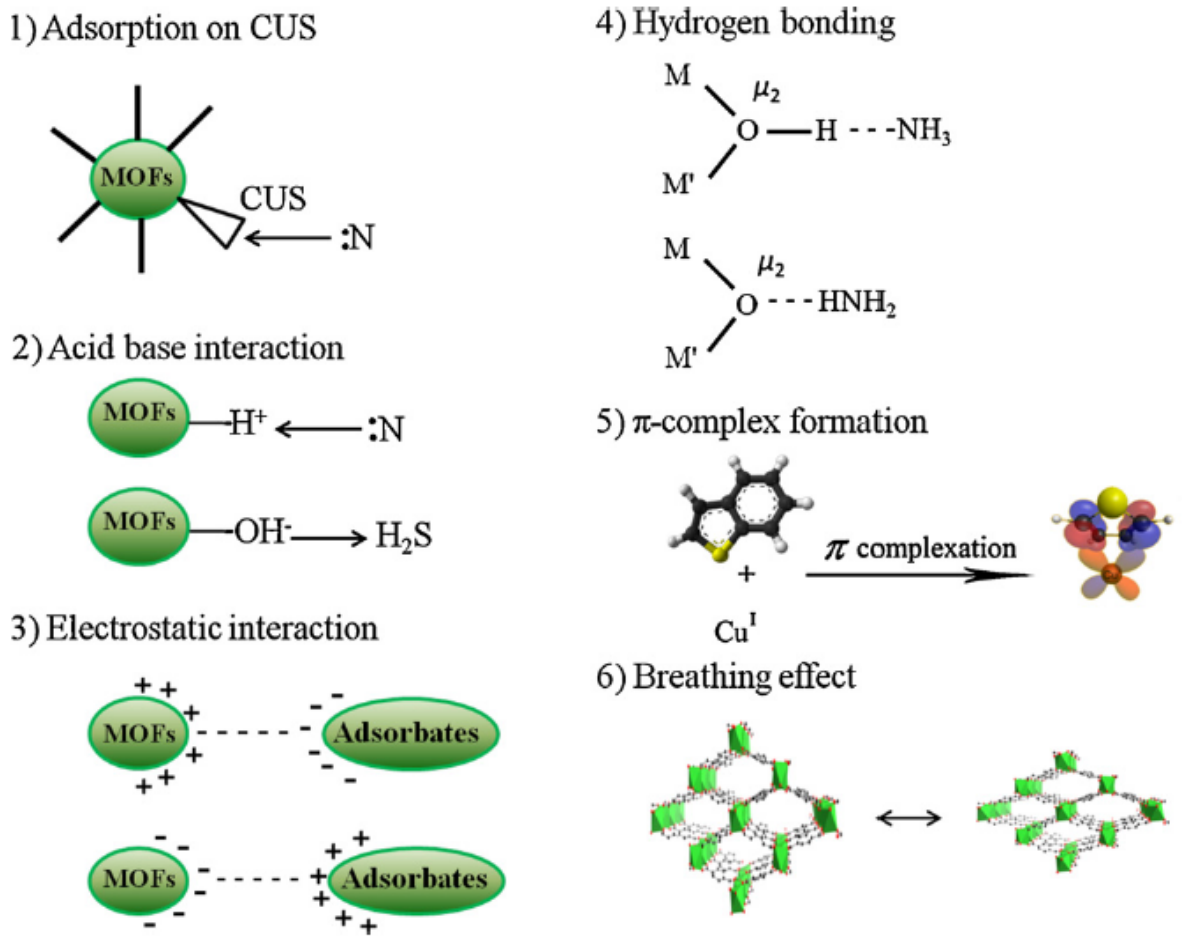

Figure 2.4: Adsorption mechanisms for MOFs. Reprinted with permission from Khan et al. (2013). Copyright 2013 with permission from Elsevier.

2.2 Thermodynamics of adsorption

Adsorption thermodynamics is usually analysed by using the classical relationship between the changes in Gibbs free energy (ΔG), enthalpy (ΔH) and entropy (ΔS), as per equation 2.2.

$$lnK_d = \frac{-\Delta G_0}{RT} = \frac{\Delta S_0}{R} - \frac{\Delta H_0}{R}\frac{1}{T} \qquad (2.2)$$

Where: K_d is the equilibrium constant; ΔG_0 is the change in Gibbs free energy; ΔH_0 is the change in enthalpy energy; ΔS_0 is the change in entropy; R- is the gas constant.

ΔG_0 provides information about the spontaneity of the adsorption process, while ΔH_0 quantifies and gives the direction to which heat is being transported during the adsorption process. If the process is exothermic, it liberates energy; if the process is endothermic, it adsorbs heat. ΔH is also useful for identifying the type of adsorption (i.e. physical adsorption, where: ΔH is between 2.1 and 20.9 kJ/mol; chemisorption is between 30 and 70 kJ/mol (Tadashi, 2011). ΔS (entropy change) indicates if the randomness increases (positive value) or decreases (negative value) during adsorption. A discussion on the correct way to calculate K_d and ΔG is not provided in this chapter, as it has been discussed in many other reviews (Ghosal and Gupta, 2017; Kopinke et al., 2018).

2.2.1 Carbonous Material

Table 2.3, provides a summary of the thermodynamic properties of highly porous adsorbents and how these properties are affected by various types of adsorption activity improvement strategies. As stated earlier, one of the most studied materials for adsorptive desulphurization is AC. AC comes from different sources, including coal (Saha et al., 2016), wood (Wen et al., 2010b) (Ahmed and Ahmaruzzaman, 2015), sewage sludge (Aribike et al., 2019) and waste tires (Saleh and Danmaliki, 2016a and 2016b).

Table 2.3a shows that ΔH, ΔG and ΔS ranges from -169 to 55.38 kJ/mol, -12.59 to 6.9 kJ/mol and -5.2 to 79.4 J/mol, respectively. The difference in enthalpies may be attributed to differences in the contaminates of the AC source material. An analysis of the work done by Thaligari showed that adding Zn (Thaligari et al., 2016) and Ni (Thaligari et al., 2018) to AC led to a decrease in ΔH, ΔG and ΔS. Positive ΔH indicates an endothermic process that suggests a combination of a chemical process and a physical process. ΔH is affected by the formation of the sulphur-adsorbent bond (exothermic) and desorption of the adsorbed solvent (endothermic). This is consistent with the hydrophobic nature of AC, so the adsorption of the nonpolar solvent is expected. These effects are summarised in Figure 2.5.

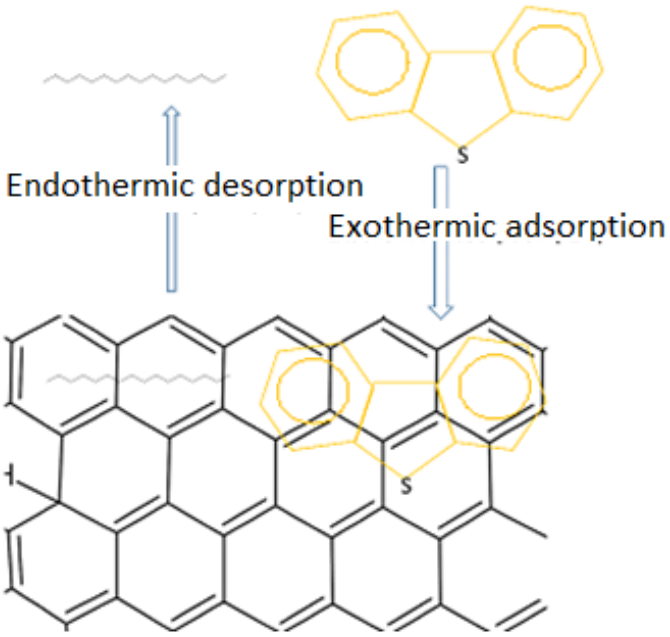

Figure 2.5: Endothermic adsorption of DBT on AC

The high ΔS for AC is due to high solvent desorption from the adsorbent, whilst DBT is adsorbing. The high positive ΔH is also based on the assumption that high solvent desorption energy is not fully offset by the adsorption energy of DBT. The ΔH and ΔS data for Zn/AC indicates poor selectivity for sulphur compounds or higher affinity for solvents relative to Ni/AC. The adsorption capacity was observed to improve with addition of metals in this order Zn/AC< Ni/AC.

Olajire et al. (2017) modified AC from brewer's spent grain using Ag via wet impregnation. The Ag nanoparticles (AgNPs) were synthesized from cobwebs ($AgNPs^{cw}$) and the Cola nitida plant ($AgNPs^{kp}$). The thermodynamic properties did not change much for $AgNPs^{kp}$/AC and AC; however, a slight increase in ΔH and ΔS was observed for $AgNPs^{cw}$ and AC. This suggests a slight decrease in solvent adsorption and hence a lower ΔS and ΔH. The adsorption capacity increased in this order: AC (33.1 mg/g)< $AgNPs^{kp}$ (63.1 mg/g)< $AgNPs^{cw}$ (71.9 mg/g).

Jha et al. (2019) synthesized Mongolian anthracite-based AC via physical treatment. They varied the mass ratio of the activation reagent (KOH) to anthracite to produce PMAC1/3 and PMAC1/4. PMAC 1/3 (84.56 mg/g) showed high adsorption capacity compared to PMAC1/4 (74.25 mg/g). This higher activity for PMAC1/3 was attributed to a higher micropore volume (66.4 %) compared to PMAC1/4 (42.2 %) and a comparable pore diameter to DBT size, which leads to high adsorption capacity. Consistent with the adsorption data, the thermodynamic data showed that adsorption of PMCA1/3 was most favourable.

This was driven by enthalpy since both ΔS figures were negative and ΔH was -14.89 and -0.036 for PMAC1/3 and PMAC1/4, respectively.

Sedaghat et al. (2019) synthesized 3D hydrothermal graphenic adsorbents and investigated the thermodynamic properties of reduced graphene oxide (rGO) and carbon black−graphene composite (CB-G). Adsorbent rGO and CB-G both had a negative ΔS (−210.51 J/mol and −162.85 J/mol), which suggests a decrease in randomness that is attributed to a decrease in the degree of freedom of DBT as it adsorbs to adsorbents. Enthalpy of adsorption of -69.01 kJ/mol and -50.42 kJ/mol for rGO and CB-G, respectively, suggests chemical bonding for bonded adsorbates. Consistent with the exothermic nature of adsorption, ΔG for both adsorbents was observed to decrease with temperature. Since the ΔS is negative, the process is driven by enthalpy, and the ΔG and ΔH values suggest that adsorption is more favourable for rGO. However, rGO has a slightly lower adsorption capacity compared to CB-G (see Table 2.3). The higher CB-G adsorption capacity is attributed to CB packing in the adsorbent structure.

Patil et al. (2014) reported on the activity of SHIRASAGI GH2x 4/6 and SHIRASAGI SRCx 4/6. The ΔH of adsorption was negative for GH2x and positive for SRCx, which suggests an exothermic and an endothermic nature, respectively. The higher activity of SRCx was attributed to a narrow pore distribution and a high Si content. Jha et al. (2020) reported on the adsorption activity of graphene nanoplatelets. The process was enthalpy driven, and the adsorption capacity of sulphur compounds increased with molecular weight. A similar trend in the |-ΔH| was reported.

2.2.2 Metal Oxides

Kumar et al. (2011a) reported on zirconia, with the improvement strategies employed being drying, calcination and sulfonation. (See Table 2.3b.) Negative values for ΔH and ΔS were observed to decrease in this order: dried zirconia>calcined zirconia>sulfonated zirconia. The lowest values of ΔH and ΔS were recorded for dried zirconia, which suggests a strong adsorbent-DBT bond and low solvent desorption. This could be attributed to polar hydroxyl groups on the adsorbent surface - hence low solvent adsorption.

There was a drop in |ΔH| and |ΔS| with the calcination and sulfonation treatment methods. The drop might suggest a weaker adsorbent-DBT bond and/or an increase in solvent desorption during adsorption, as indicated by a decrease in |ΔS|.

The weakening of adsorption bonds is a positive phenomenon - if it does not affect adsorption kinetics and capacity- since it translates into easier regeneration. There was a slight increase in adsorption capacity in this order: dried zirconia<calcined zirconia<sulfonated zirconia. This suggests that treatment results in an increase in the available adsorption sites, in that order. This adsorption order cannot be explained by thermodynamics, which suggests that, in this case, the adsorption capacity was not controlled by thermodynamics.

2.2.3 Clays

Ishaq et al. (2017) used bentonite without treatment (UB), acid-treated (AAB) and loaded with magnetite (MNLB). Acid treatment led to a slight drop in ΔH (38.0 kJ/mol) and an increase in ΔS (149.8 kJ/mol), which suggests increased solvent adsorption. However, the addition of magnetite led to a decrease in both ΔS (122.6 kJ/mol) and ΔH (27.4 kJ/mol). (See Table 2.3c.) A decrease in ΔS and ΔH suggests lower solvent adsorption and/or an increase in adsorbate-DBT bond strength. Even though the driving force for adsorption was entropy, MNLB showed high spontaneity, based on ΔG. The amount of sulphur adsorbed increased with treatment in the order UB< MNLB < AAB, which is consistent with entropy being the driving force

2.2.4 MOFs

The thermodynamics data reported for the most active adsorbent (TMU-11) is 81.85 kJ/mol and 334.13 J/mol for ΔH and ΔS, respectively (Bagheri et al., 2017). (See Table 2.3 d.) A high ΔH and ΔS suggest high solvent adsorption. Hence entropy was the driving force for the adsorption investigation done in this research study.

Khan et al. (2011) investigated the effect of different metals on MIL-53/47. MIL-53 (Al) and MIL-53(Cr) had similar ΔH and ΔS. However, MIL-47 had a higher ΔH (29.6 kJ/mol) and a high ΔS (143.9 J/mol). As stated earlier, a positive ΔH suggests both physical and chemical adsorption. A high ΔS and ΔH suggest higher solvent desorption. Khan et al. (2011) also pointed out that spontaneity (-ΔG) in their system was attributed to entropy. They also noted that adsorption capacity increased with an increase in ΔS and -ΔG.

2.2.5 Zeolites

The effects of changing the sulphur compound (for example, from TP to BT) have been reported in work carried out by the team lead by Song (2016b). They reported that adsorption capacity increased with molecular weight, which was attributed to improved electron density. With an increase in molecular weight, ΔH decreased from -19.5 kJ/mol to -26.1 kJ/mol for TP and BT, respectively. (See Table 2.3e.) For both molecules, ΔG decreased with temperature, which is consistent with the exothermic nature of this adsorption. The spontaneity (ΔG) of adsorption was consistent with enthalpy being the driving force.

2.2.6 Thermodynamic summary and recommendation

Based on the reported thermodynamics, adsorption may be driven by enthalpy or entropy. The adsorption of the solvent may be desirable to promote adsorption via entropy. The most active adsorbent material (TMU 11) is driven by the highest observed ΔS, as indicated in Table 2.3 However, the adsorption energy should not be too high, as this could make regeneration difficult.

Table 2.3: Thermodynamic data for adsorbent on adsorptive desulphurization

a) Thermodynamic data for carbonous material in adsorptive desulphurization

Adsorbents	**Adsorbate**	**Temp (K)**	**Conditions**	**Q (mg/g)**	**ΔG^0 (kJ/mol)**	**ΔH^0 kJ/mol**	**ΔS^0 J/mol**	**Reference**
Zn/AC	DBT	293	m = 30 g/L C_0 = 54 – 551mg/L	16.704	-4.21	4.89	3.0	Thaligari et al., 2016
		303		20.928	-4.90			
		313		30.784	-5.14			
Ni/AC	DBT	288	C_0=50-800mg/L m =20 mg/l	17.60	-4.39	2.04	10.00	Thaligari et al., 2018
		303		59.20	-4.52			
		318		37.76	-4.64			
AC-Bewers	DBT	308	200 mg/L, m = 0.3 g	33.1	-34.8	23.75	190	Olajire et al., 2017
		318			-36.7			
		328			-38.6			
AgNPskp/AC	DBT	308		63.3	-34.6	23.89	190	
		318			-36.5			
		328			-38.4			
AgNPscw/AC	DBT	308		71.9	-33.9	21.54	180	
		318			-35.7			
		328			-37.5			
PMAC1/3	DBT	313	500 ppm, m = 1.25-20 mg/L	25.69	-4.24	-14.89	-24.76	Jha et al., 2019
		323			-3.27			
		333			-2.88			
		343			-2.19			
PMAC1/4	DBT	313		23.55	-3.317	-0.037	-0.065	
		323			-2.907			
		333			-2.372			
		343			-2.269			
r-GO	DBT	288	100 – 100 mg/L m = 2.5 g/L	41.8	-7.09	-79.01	-210.5	Sedaghat et al., 2019
		298			-5.12			
		313			-3.43			
CB-GO	DBT	288		46.9	-4.54	-50.42	-162.8	Sedaghat et al., 2019
		298			-0.58			

		313			0.96			
Carbon GH2x	TP	303	450 mg/L m = 5- 50 mg/L	5.474	-10.71	-169.07	-522	Patil et al., 2014
		313			-5.48			
		323			-0.25			
Carbon SRCx	TP	303		20.174	-3.33	55.38	0.914	
		313			-5.27			
Graphene nanoplatelets	DBT	313	500 ppm m = 1.25- 20 g/L	181.6	−1.302	−8.75	−24	Jha et al., 2020
		323			−1.241			
		333			−0.849			
	2-MT	313		268.5	−0.868	−4.16	-11	
		323			−0.824			
		333			−0.779			
	T	313		360.10	−0.558	−3.15	-8	
		323			−0.497			
		333			−0.346			

b) Thermodynamic data for metal oxides in adsorptive desulphurization

Adsorbents	**Adsorbate**	**Temp (K)**	**Conditions**	**Q (mg/g)**	**ΔG^0 (kJ/mol)**	**ΔH^0 kJ/mol**	**ΔS^0 J/mol**	**References**
Dried zirconia	DBT	303	C_0 =30-1000mg/l, m=10g/l	48.3	-10.36	-165.3	-509.9	Kumar et al., 2011
		308			-9.15			
		313			-5.36			
Calcined zirconia	DBT	303		50.1	-10.66	-125.5	-379.4	
		308			-8.30			
		313			-7.20			
Sulfated zirconia	DBT	303		51.3	-10.91	-96.7	-284.1	
		308			-8.88			
		313			-7.70			
		333			-10.8			
		313			-1.682			
		323			-1.285			

c) Thermodynamic data for clays, MOFs and zeolite materials in adsorptive desulphurization

Adsorbents	**Adsorbate**	**Temp (K)**	**Conditions**	**Q (mg/g)**	**ΔG^0 (kJ/mol)**	**ΔH^0 kJ/mol**	**ΔS^0 J/mol**	**References**
Untreated bentonite	DBT	293	100 mg/L m = 1 g/L	59.9	-3.4	39.6	146.5	Ishaq et al., 2017
		313			-6.3			
		333			-9.1			
Activated bentonite	DBT	293		74.6	-4.6	38.0	149.8	
		313			-8.3			
		333			-10.8			
Fe3O4/bentonite	DBT	293			-7.6			
		313		50.0	-10.6	27.4	122.6	
		333			-12.7			
TMU-11	DBT	298	500 ppm m = 0.6 mg/L	825	-17.72	81.85	334.13	Bagheri et al., 2017
		318			-24.40			
		343			-32.76			
MIL-53(Al)	BT	298	1000 ppm	34.4	-12.8	5.6	61.4	Khan et al., 2011
		308		39.4	-12.9			
		318		40.0	-13.1			
MIL-53(Cr)	BT	298		80.0	-12.9	7.4	69.2	
		308		87.8	-13.6			
		318		96.2	-14.3			
MIL-47	BT	298		215.4	-13.3	29.6	143.9	
		308		219.8	-14.8			
		318		224.7	-16.2			
AgCeY	TP	293		11.45	-2.972	-19.74		Song et al., 2016b
		303		12.544	-2.324			
		313		12.768	-1.682			
		323		13.344	-1.285			
	BT	293	C0=200mg/l, 0.2g/20ml	19.1	-3.286	-26.16		Song et al., 2016b
		303		21.12	-2.734			
		313		22.496	-2.092			
		323		23.168	-0.884			
CuAgY	TP	303		48.95	-3.83	-19.11	-50.43	Lu et al., 2017

		313	C_0=162-770, 02g/25ml	54.08	-3.32			
		323		60.98	-2.82			
Palygorskite	DBT	298	C_0 = 500 mg/g m = 37.5 g/L	1.63	6.02	44.73	47.52	Câmara et al., 2019
		308		3.44	4.00			
		318		6.25	1.84			
$Cu^{I}Ce^{IV}Y$	BT	293	C_o = 99 – 499 mg/L m = 10 g/L	32.58	-19.98	-26.22	-21.4	Song et al., 2014
		303		38.05	-19.66			
		313		39.62	-19.56			

2.3 Kinetics of adsorptive desulphurization

Adsorption kinetics studies investigate the rate at which adsorbents are transferred from bulk fluid to the adsorbent surface. Adsorption kinetics are applied in: i) identifying adsorption mechanisms; ii) quantifying adsorption parameters; iii) designing adsorption columns. It is generally accepted that adsorption proceeds by these steps: i) transport of adsorbate from the bulk to the external surface of the adsorbent; ii) passage through the liquid film; iii) transport through the pore; iv) adsorption on the adsorbent surface. This adsorption process is summarised in Figure 2.6 below.

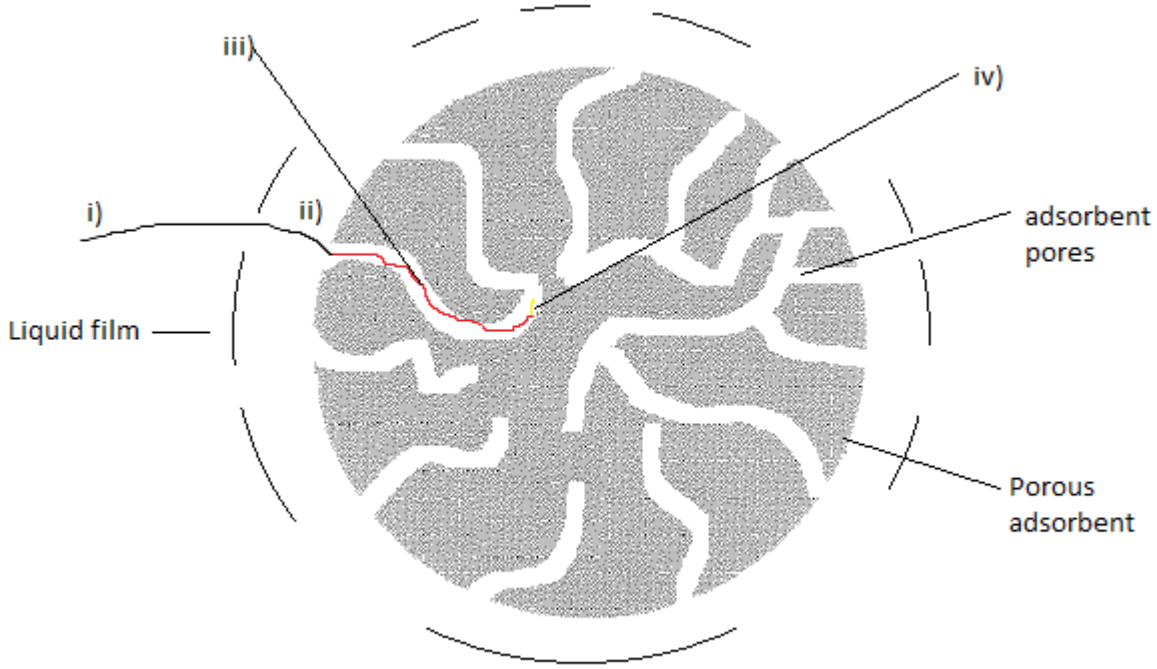

Figure 2.6: Diagram that illustrates the steps in adsorption.

Several kinetic models are used to describe the adsorption of the adsorbate to the adsorbent surface. This thesis will focus on the most commonly used models, i.e. the Lagergren pseudo-first-order and pseudo-second-order models. A weakness of empirical models is that all the steps in the adsorption process are bundled into a single set of parameters, which means they are poorly suited to describing the mechanisms independently of each other (Song et al., 2014; Simonin, 2016; Callura et al., 2019). However, the Lagergren pseudo-first-order and pseudo-second-order kinetics are generally accepted to represent physical and chemical adsorption, respectively (Ho and McKay, 1999; Khan Rao and Khatoon, 2017).

Lagergren pseudo-first-order model

Lagergren (1898) used a first-order rate equation to describe the kinetic process of the liquid-solid phase adsorption, based on equation 2.3.

$$\frac{dq_t}{dt} = k_1(q_e - q_t) \qquad (2.3)$$

Where: q_e and q_t are the adsorption capacity at equilibrium and at a time (t), respectively; k_1 (1/min) is the pseudo-first-order rate constant.

The linearized integral equation is expressed as follows:

$$\log(q_e - q_t) = log_{q_e} - \frac{k_1 t}{2.303} \qquad (2.4)$$

Pseudo-second order model

The primary assumption is that the rate-limiting step may be chemical adsorption. The rate of adsorption is dependent upon the number of divalent sites available on the surface, as per equation 2.5.

$$\frac{dq_t}{dt} = k_2(q_e - q_t)^2 \qquad (2.5)$$

The integrated form is:

$$\frac{t}{q_t} = \frac{1}{k_2 {q_e}^2} + \frac{1}{q_e} \qquad (2.6)$$

Where: q_e and q_t are the adsorption capacity at equilibrium and at a time (t), respectively; k_2 is the pseudo-second-order rate constant.

Elovich model

The Elovich model is applied to chemisorption adsorption. This model helps to predict the mass and surface diffusion, and the activation and deactivation energy of a system. The model assumes that the rate of adsorption of the solute decreases exponentially as the amount of adsorbate solute increases (Wu et al., 2009).

$$\frac{dq_t}{dt} = \alpha exp^{-\beta q} \qquad (2.7)$$

2.3.1 Carbonous material

Both pore structure and the number and type of functional groups have been reported to have a significant effect on adsorption kinetics. The Mongolian anthracite PMAC 1/3 synthesized by Jha et al. (2019) showed high adsorption capacity because of its smaller surface area when compared to PMAC1/4. (See Table 2.4a.) The higher activity of PMAC1/3 was attributed to it having a higher micropore volume (66.4 %) than PMAC1/4 (42.2 %) and a comparable pore diameter of adsorbent to DBT size, which led to high adsorption capacity. However, k_2 for PMAC1/3 was lower than for PMAC1/4, which could be due to the smaller pores of PMAC1/3, which lead to higher pore diffusion resistance.

Patil et al. (2014b) investigated two modified AC materials: SHIRASAGI GH2x 4/6 and SHIRASAGI SRCx 4/6. They reported that surface modification increased sulphur removal, initial adsorption and k_2. They suggested that higher mesopore volume and a high oxygen content influence preferential adsorption on SRCx. They also suggested that the Al/Si ratio affects adsorption capacity and adsorption rate and that Si participates in adsorption – hence the increase in activity with a decrease in the Al/Si ratio.

Wen et al. (2010b) investigated the effect of different sulphur compounds on the adsorption kinetics of AC that was derived from woody material and then treated with H_3PO_4. They reported that the adsorption capacity, k_2 and h were higher for 4,6 DMDBT than for DBT. This could be due to a higher affinity for 4,6DMDBT because of a higher electron density.

The effect of adding intermediate Lewis acids on AC has raised much interest in the field of adsorptive desulphurization. The sulphur compounds that need to be removed are soft Lewis bases; hence their removal is expected to be enhanced by intermediate to soft Lewis acids, based on the "Hard Soft Acid Base" principle. A number of Lewis acid metals have been reported, including Sn (Shah et al., 2016), Ni (Thaligari et al., 2018b), Zn (Thaligari et al., 2016), Co (Mguni et al., 2019), Cu (Saleh, 2018) and Ag (Olajire et al., 2017). Olajire et al. (2017) modified AC using Ag, and reported that the adsorption capacity increased in this order: AC<AgNPskp/AC<AgNPscw/AC. The increase in capacity after adding Ag was due to enhanced adsorption by the Ag-DBT bond, as depicted in Figure 2.7. The initial adsorption rate also increased in that order, which suggests improved adsorbent-DBT affinity. However, the order for k_2 was different, which suggests that after initial fast adsorption, adsorption thereafter depends on the pore structure that dictates the rate at which adsorbates are transported until equilibrium.

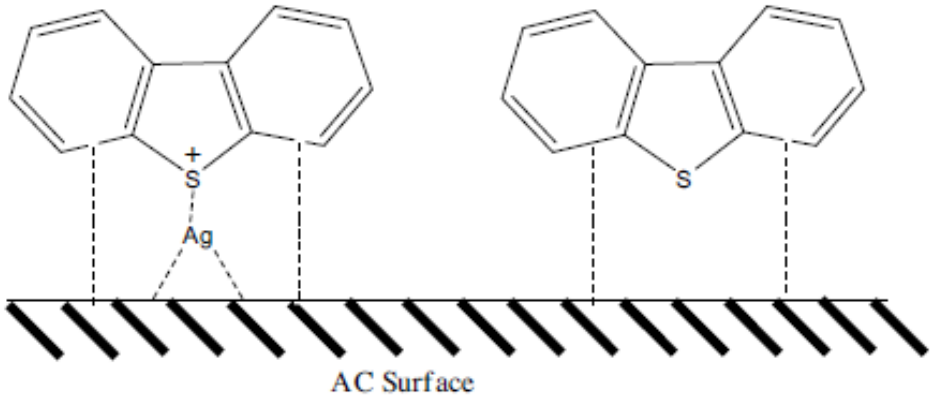

Figure 2.7: Possible interaction of DBT molecules with blank and nano-Ag/AC adsorbents. Reprinted with permission from Olajire et al. (2017). Copyright 2017 with permission from Elsevier.

Ganiyu et al. (2016) investigated the effect of adding alumina onto AC and reported this leads to an increase in activity due to improved surface acidity. However, an increase in alumina loading beyond 2.5 wt% led to more than 50% surface area loss, even though there was an increase in acidity. Initial adsorption rate had a similar trend to that of adsorption capacity (no correlation with k_2).

Nazal et al. (2019) impregnated carbonaceous materials with alumina oxide. The materials used were AC, graphene oxide and carbon nanotubes. They observed that the addition of alumina on CNT and AC led to an increase in DBT adsorption. The increase in the adsorption of DBT using carbon adsorbents loaded with Al_2O_3 is a consequence of the synergetic effect of introducing additional acidic adsorption sites. Alumina introduced unsaturated amphoteric surfaces that act as Bronsted acids and Lewis acids in the environment of the base DBT. The addition of alumina had a negative effect on the adsorption capacity of GO, which was attributed to the agglomeration of the oxide on the GO surface. The adsorption capacity order was as follows: ACAL10-ACAL5>CNTAL5>CNTAL10>GOAL5> GOAL10. It did not correlate with k_2 or with h.

Aribike et al. (2019) reported the effect of temperature on adsorption kinetics of activated sewage sludge. They reported that: the Elovich model best fitted at 25 °C, 35 °C, 45 °C and 50 °C; the first-order model best fitted at 30 °C; the intra-particle model best fitted at 40 °C. These results suggest that the controlling adsorption mechanism depends on temperature.

Sedaghat et al. (2019) investigated three adsorbents, reduced graphite oxide, carbon graphite composite and Ni supported on graphene. They reported that rGO and CB-G experimental data fitted pseudo-second-order kinetics best. This suggests that adsorption was controlled by liquid-solid interaction and that it is also dependent on the DBT concentration. The adsorption rate, k_2 and h were higher for rGO. Ni-G had a correlation coefficient of pseudo-second-order slightly lower than for first-order and concluded that adsorption was based on both diffusion and liquid-solid interaction. The low k_2 for Ni-G was considered to be due to slower adsorption of DBT on graphene after the initial π-complex with Ni and the graphene−DBT interaction. This concurred with the mechanisms observed for adsorption isotherms (Sedaghat et al., 2019).

The adsorption activity of graphene nanoplatelets was observed to follow second-order kinetics. Adsorption capacity increased with an increase in the MW of sulphur compounds, i.e. T < 2MT<DBT, and k_2 followed the same order.

When the analysis was done with a multiple component system the same adsorption order and k_2 order was observed but there was a decrease in activity, which was attributed to competitive adsorption (Jha et al., 2020).

Danmaliki and Saleh (2017) used AC loaded with the bimetals Ce/Fe, and reported that k_2 increased with sulphur molecular weight, i.e. TH<BT<<DBT. The increase in activity could be attributed to an increase in electron density. The adsorption constants k_1 also increased in the same order. Saleh (2018) also reported on CoCu/AC: it interacted with sulphur compounds in the order DBT > MDBT > DMDBT > MBT > BT > thiophene. The higher adsorptive removal of DBTs was attributed to the high level of interaction between the delocalised p-electrons in the DBTs and the CoCu/AC adsorbent.

2.3.2 Metal oxides

Another type of material that has been reported extensively are metal oxides. Kumar et al. (2011b) used zirconia and improvement strategies of drying, calcination and sulphonation. Increasing the temperature led to a decrease in activity and hence a drop in the initial adsorption rate (h), k_2 and Q, which is consistent with the exothermic nature of the reaction. However, the effect of treatment methods had an adsorption order of ZC383≈ZD893<SZC893, while k_2 followed the order ZC383≈ZD893>SZC893. Thermodynamics results suggested that sulphonation might have increased solvent adsorption– hence the low adsorption rate and therefore, a longer period to reach equilibrium. Srivastav and Srivastava (2009b) reported on

the adsorption kinetics of alumina and stated that Q increased with initial DBT concentration, but no trend was observed for k_2 and initial adsorption rate. (See Table 2.4b.)

2.3.3 Clays

Ishaq et al. (2017) used Bentonite treated by acid and loaded with magnetite. The adsorption of DBT was observed to be as per the pseudo-second-order model, which suggests chemisorption. (See Table 2.4c.) Bentonite treatment led to increased adsorption capacity in this order: untreated bentonite>treated by acid>loaded with magnetite (Ishaq et al., 2017). The increase in adsorption capacity was attributed to increased porosity following acid treatment and the rough surface of bentonite loaded with magnetite. However, the adsorption rate constant, k_2, was observed to increase in this order: untreated bentonite<loaded with magnetite< treated by acid. The lower k_2 for bentonite loaded with magnetite might be due to magnetite blocking the pores, and hence a slow transport process.

2.3.4 MOFs

Metal-organic frameworks (MOFs) is a part of a class of materials that have been reported to be very promising for adsorptive desulphurization. MOFs is part of an emerging class of porous materials that are constructed from metal-containing nodes and organic linkers. They are known to have endless structural possibilities and a high surface area. The adsorbent with the highest reported capacity, TUM11, was observed to follow pseudo-second-order kinetics, which suggests that adsorption is chemical in nature (Bagheri et al., 2017). (See Table 2.4.) Khan et al. (2011) investigated the effect of different metals in MIL-47, MIL-53(Al) and MIL-53(Cr). The adsorption capacity was observed to increase in this order: MIL-53(Al) <MIL-53(Cr) <MIL-47. The adsorption data followed the pseudo-second-order, and k_2 was observed to follow the same trend as the adsorption capacity. The difference in activity was attributed to different BT-metal ion interactions, since the adsorbents were isostructural.

Aslam et al. (2017) investigated the effect of loading Ni on MIL-101. Nickel was loaded by impregnation followed by reduction under hydrogen at 300 ^{o}C. The adsorption was observed to follow pseudo-second-order kinetics. The adsorption capacity and k_2 were observed to follow this increasing order: MIL-101<30Ni-MIL-101<10Ni-MIL-101<20Ni-MIL-101. The increase in activity with Ni content was attributed to Ni-thiophene bonds, and the drop at 30Ni-MIL-101 was due to the blockage of pores and agglomeration of Ni characterised by increased crystallite size (from 1.2 nm to >20 nm). The pore-blocking and agglomeration of crystallites were characterised by a drop in the acidity of the adsorbent.

2.3.5 Zeolites

Jiang and Ng (2010) investigated the effect of the initial DBT concentration and temperature on the adsorption kinetics of NaY zeolite. The initial adsorption rate and adsorption capacity were observed to increase with an increase in initial concentration and temperature. The increase in initial concentration led to an increase in the driving force to overcome mass transfer resistance between the liquid and solid phase, while an increase in temperature improved the diffusion rate owing to decreased viscosity of the solution. However, no trend was observed for k_2 for both parameters.

Lu et al. (2017b) investigated the effect of temperature on the adsorption of TH on CuAgY. They observed that adsorption capacity and initial adsorption rate increased with temperature, in contrast to the exothermic nature of the adsorption. K_2 was not significantly affected: it varied between 2.86E-4 and 3.10E-3 relative to an increase in Q from 51.66 to 62.73 mg/g. The increase in activity with temperature may be attributed to an improvement in the diffusion rate.

Song et al. (2016b) used AgCeY and reported on the effect on k_1 and Q of temperature and different sulphur adsorption compounds. Q and k_1 increased with temperature and sulphur molecular size, i.e. from TH to BT. Even though the adsorption reaction was exothermic, the increase in k_1 and Q might be due to reduced diffusion resistance, as discussed earlier. The increase in activity with molecular weight is due to an increase in the electron density of the sulphur compound, and hence an improvement in the adsorbate-adsorbent interaction.

2.3.6 Other adsorbents

Magnetic molecularly imprinted polymer -Fe_3O_4@SiO_2@MIPs was used to investigate the effect of DBT initial concentration on adsorption kinetics (Hui Li et al., 2012). Adsorption capacity increased with initial concentration, while k_2 decreased. The decrease in k_2 might be due to the need for DBT to traverse long pathways after fast initial adsorption.

2.3.7 Kinetics summary and recommendation

Most of the reported research work on adsorptive desulphurization has been observed to fit pseudo-second-order adsorption kinetics. This could be because most of the work analysed the adsorption data until adsorption reached equilibrium. This is because the pseudo-first-order model fits the experimental data well for an initial period of the first reaction step only (Ho and McKay, 1999; Sen Gupta and Bhattacharyya, 2011). From the kinetic results, it can be observed that, generally, a high adsorption capacity does not translate to a faster adsorption rate. However, the initial rate usually improves because of improved adsorbent-adsorbate affinity. The initial adsorption rate is a better parameter to describe adsorbate–adsorbent affinity since adsorption is thereafter determined by mass transfer resistance, as the adsorbate has to transverse a long-distance and face steric repulsion by adsorbed molecules. The overall rate constant is typically not dependent on the adsorption capacity, but the pore structure of the adsorbent. Hence, a good pore structure and adsorbent particle size are paramount for the design of effective adsorbents that minimise the length traversed by the adsorbate, as well as pore obstruction after initial adsorption.

Table 2.4: Adsorption kinetics of sulphur compounds

a) Adsorption kinetics of sulphur compounds by carbonous material									
Adsorbent	**Adsorbate**	**Temp (K)**	**Q (mg/g)**	**First order**		**Second order**			**Reference**
				K_1	**R^2**	**K_2**	**h**	**R^2**	
PMAC 1/4	DBT	303	23.55	0.0262	0.890	0.890	/	0.990	Jha et al., 2019
PMAC 1/3	DBT	303	25.69	0.0179	0.840	0.103	/	0.990	
GH2x4/6	DBT	304	5.475	0.020	0.883	0.012	/	0.994	Patil et al., 2014
SRCx4/6	DBT	304	20.174	0.246	0.897	0.086	/	0.937	
AC	DBT	313	29.211	0.0492	0.9400	0.00561	/	0.992	Wen et al., 2010
AC	4,6DMDBT	313	27.196	0.0751	0.9434	0.00967	/	0.9918	
AC-Brewers	DBT	/	12.6	0.36	0.97	15E-3	/	0.99	Olajire et al., 2017
AgNPskp/AC	DBT	/	24.7	0.34	0.98	7.2E-3	/	0.99	
AgNPscw/AC	DBT	/	29.1	0.35	0.93	7.5E-3	/	1.00	
AC-Al2.5	DBT	RT	8.82	17.96	0.8817	17.96E-3	$8.02*10^{-2}$	0.9999	Ganiyu et al., 2016
AC-Al5.0	DBT	RT	8.68	16.12	0.9174	16.12E-3	$6.56*10^{-2}$	0.9998	
AC-Al7.5	DBT	RT	8.26	17.96	0.9591	17.96E-3	$3.15*10^{-2}$	0.9993	
AC-Al10	DBT	RT	6.99	11.75	0.8372	11.75E-3	$4.5*10^{-3}$	0.9997	
ACAL10	DBT	RT	39.3	/	/	0.015	/	0.9999	Nazal et al., 2019
ACAL5	DBT	RT	39.2	/	/	0.033	/	1.000	
CNTAL10	DBT	RT	23.4	/	/	0.09	/	1.000	

CNTAL5	DBT	RT	25.4	/	/	0.02	/	0.9993	
GOAL10	DBT	RT	9.4	/	/	0.035	/	0.9981	
GOAL5	DBT	RT	16,8	/	/	0.15	/	0.9999	
RGO	DBT	298	41.8	2.95E-2	0.868	6.271E-2	23.98	0.999	Sedaghat et al., 2019
CB-G	DBT	298	46.9	4.10E-3	0.851	4.823E-3	2.382	0.905	
Ni-G	DBT	298	43.3	3.30E-3	0.961	1.868E-3	0.485	0.953	
Graphene nanoplatelets	DBT	/	153.970	0.044	0.860	9.920×10^{-4}	/	0.997	Jha et al., 2020
	2-MT	/	107.250	0.039	0.986	8.792×10^{-4}	/	0.998	
	T	/	119.250	0.042	0.946	5.495×10^{-4}	/	0.993	
Co/Mo/AC	Thiophene	298	2.2	0.0623	0.9898	0.0439	/	0.9694	Saleh et al., 2018
	BT	298	2.32	0.0562	0.9544	0.0345	/	0.9251	
	MBT	298	2.72	0.0620	0.9572	0.0441	/	0.9625	
	DBT	298	3.68	0.0688	0.9486	0.0304	/	0.9556	
	MDBT	298	3.64	0.0792	0.9533	0.0441	/	0.9625	
	DMDBT	298	3.72	0.0736	0.9714	0.0311	/	0.9702	
CoCu/AC	Thiophene	/	1.84	0.0638	0.7825	0.0757	/	0.9827	Saleh, 2018
	BT	/	2.12	0.0683	0.9698	0.0567	/	0.9865	
	MBT	/	2.48	0.0677	0.5789	0.0684	/	0.9885	

	DBT	/	3.52	0.0706	0.9006	0.0437	/	0.9859	
	MDBT	/	3.44	0.0655	0.9471	0.0542	/	0.9929	
	DMDBT	/	3.40	0.0602	0.9211	0.0406	/	0.9876	
b) Adsorption kinetics of sulphur compounds by metal oxides									
Adsorbent	**Adsorbate**	**Temp (K)**	**Q (mg/g)**	**First order**		**Second order**			**Reference**
				K_1	**R^2**	**K_2**	**h**	**R^2**	
Dried zirconia	DBT	303	53.8	0.0042	0.982	8.2E-05	0.298	0.989	Kumar et al., 2011
Dried zirconia	DBT	308	49.7	0.0029	0.983	6.0E-05	0.205	0.987	
Dried zirconia	DBT	313	46.5	0.019	0.981	3.2E-05	0.102	0.986	
Calcined zirconia	DBT	303	56.9	0.0052	0.959	1.0E-04	0.369	0.978	
Calcined zirconia	DBT	308	49.4	0.0027	0.979	6.5E-05	0.200	0.979	
Calcined zirconia	DBT	313	44.0	0.0015	0.960	2.8E-05	0.096	0.967	
Sulfated zirconia	DBT	303	59.9	0.0028	0.985	5.0E-05	0.238	0.986	
Sulfated zirconia	DBT	308	49.7	0.0018	0.980	2.4E-05	0.117	0.983	

Sulfated zirconia	DBT	313	44.2	0.0009	0.960	8.0E-06	0.053	0.963	
c) Adsorption kinetics of sulphur compounds by clays									
				First order		**Second order**			**Reference**
Adsorbent	**Adsorbate**	**Temp (K)**	**Q**	**K_1**	**R^2**	**K_2**	**h**	**R^2**	
Untreated bentonite	DBT	298	59.9	0.032	0.975	0.21	/	0.991	Ishaq et al., 2017
Activated bentonite	DBT	298	74.6	0.036	0.905	0.044	/	0.998	
Fe3O4/bentonite	DBT	298	50	0.034	0.889	102.1	0.023	0.996	
Palygorskite	DBT	298	1.94	0.16	0.8700	0.1200	0.02	0.99	Câmara et al., 2020
d) Adsorption kinetics of sulphur compounds by MOFs									
Adsorbent	**Adsorbate**	**Temp (K)**	**Q (mg/g)**	**First order**		**Second order**			**Reference**
				K_1	**R^2**	**K_2**	**h**	**R^2**	
TMU-11	DBT	333	825	0.075	0.0862	0.00034	/	0.992	Bagheri et al., 2017
MIL-101	Thiophene	/	6.12	0.0196	0.910	0.0083	/	0.967	Khan et al., 2011
10Ni-MIL-101	Thiophene	/	18.16	0.0217	0.941	0.0075	/	0.991	
20Ni-MIL-101	Thiophene	/	21.51	0.0190	0.963	0.0158	/	0.998	
30Ni-MIL-101	Thiophene	/	14.32	0.0217	0.803	0.0084	/	0.976	

MIL-53(Al)	BT	298	34.4	$2.38*10^{-2}$	0.999	/	/	/	Khan et al., 2011
	BT	308	39.4	/	/	/	/	/	
	BT	318	40.0	/	/	/	/	/	
MIL-53(Cr)	BT	298	80.0	2.57*10-2	1.00	/	/	/	
	BT	318	45	2.53*10-2	0.999	/	/	/	
	BT	298	215.4	4.24*10-2	1.00	/	/	/	
MIL-47	BT	308	219.8	4.50*10-2	1.00	/	/	/	
	BT	318	224.7	4.62*10-2	1.00	/	/	/	
AgCeY	TH	40	11.264	0.045	0.999	/	/	/	Song et al., 2016c
	TH	50	11.456	0.054	0.999	/	/	/	
	BT	20	17.056	0.0540	0.999	/	/	/	
	BT	30	18.048	0.058	0.997	/	/	/	
	BT	40	18.784	0.064	0.998	/	/	/	
	BT	50	19.136	0.074	0.999	/	/	/	
NaY	DBT	303	39.04	/	/	2.8E-4	0.4333	0.984	Jiang and Ng, 2010
	DBT	318	41.60	/	/	3.69E-4	0.6387	0.990	
	DBT	333	43.52	/	/	4.41E-4	0.8362	0.981	
Cu-BTC	DBT	298	61.51	/	/	9.6E-5	/	0.999	Matloob et al., 2019
Cu-BTC@ Gr	DBT	298	70.99	/	/	6.8E-5	/	0.99	
e) Adsorption kinetics of sulphur compounds by zeolites									
Adsorbent	**Adsorbate**	**Temp(K)**	**Q (mg/g)**	**First order**		**Second order**			**Reference**
				K_1	**R^2**	**K_2**	**h**	**R^2**	

NaY	DBT	303	39.04	/	/	2.8E-4	0.4333	0.984	Jiang and Ng, 2010
	DBT	318	41.60	/	/	3.69E-4	0.6387	0.990	
	DBT	333	43.52	/	/	4.41E-4	0.8362	0.981	
CuAgY	Thiophene	303	48.95	0.1065	0.9819	0.0028	/	0.9910	Lu et al., 2017
	Thiophene	313	54.08	0.1172	0.9824	0.0030	/	0.9824	
	Thiophene	323	60.98	0.1177	0.9727	0.0027	/	0.9956	
AgCeY	TH	40	11.264	0.045	0.999	/	/	/	Song et al., 2016c
	TH	50	11.456	0.054	0.999	/	/	/	
	BT	20	17.056	0.0540	0.999	/	/	/	
	BT	30	18.048	0.058	0.997	/	/	/	
	BT	40	18.784	0.064	0.998	/	/	/	
	BT	50	19.136	0.074	0.999	/	/	/	
CuICeIVY	BT	273	17.856	0.0496	/	/	/	0.998	Song et al., 2014
	BT	303	18.976	0.0578	/	/	/	0.997	
	BT	313	19.936	0.0674	/	/	/	0.999	
MIL-53(Al)	BT	298	34.4	$2.38*10^{-2}$	0.999	/	/	/	Khan et al., 2011
	BT	308	39.4	/	/	/	/	/	
	BT	318	40.0	/	/	/	/	/	
MIL-53(Cr)	BT	298	80.0	2.57*10-2	1.00	/	/	/	
	BT	318	45	2.53*10-2	0.999	/	/	/	
	BT	298	215.4	4.24*10-2	1.00	/	/	/	
MIL-47	BT	308	219.8	4.50*10-2	1.00	/	/	/	
	BT	318	224.7	4.62*10-2	1.00	/	/	/	

f) Adsorption kinetics of sulphur compounds by other adsorbents									
Adsorbent	**BT** concentration (ppm)	**Temp (K)**	**Q (mg/g)**	**First order**		**Second order**			**Reference**
				K_1	**R^2**	**K_2**	**h**	**R^2**	
Fe3O4@SiO2@MIPs	100	303	9.96	1.34E-2	0.996	3.06E-3	/	0.9998	Hui Li et al., 2012
	200		15.21	1.59E-2	0.996	1.99E-3	/	0.9996	
	300		21.15	1.68E-2	0.996	1.81E-3	/	0.9996	

Where: Q is the adsorption capacity.

2.4 Equilibrium isotherm insights into adsorbent improvement strategies

Equilibrium isotherms relate the adsorbate concentration in the bulk and the adsorbate amount at the interface (Eastoe and Dalton, 2000). They also provide insight into specific adsorbent surface properties and adsorbate-adsorbent affinity (Câmara et al., 2020). A summary of the isotherms reported for desulphurization is provided in Table 2.5.

Langmuir isotherm

The Langmuir adsorption isotherm is one of the most popular adsorption isotherms in use. It is based on the assumptions that maximum adsorption capacity corresponds to the saturated monolayer adsorbent on the adsorbent surface, adsorption takes place at a finite number of uniform sites and there is no interaction among adsorbed species. The Langmuir model is expressed as per the following equation:

$$\frac{C_e}{q_e} = \frac{1}{q_e K_L} + \frac{C_e}{q_{max}} \qquad (2.8)$$

Where: C_e is the concentration of adsorbate at equilibrium (mg/g).

q_e is the equilibrium adsorption capacity (mg/g)

q_{max} is the maximum adsorption loading of adsorbate (mg/g)

K_L is the Langmuir constant that relates to adsorption capacity (mg/g).

Freundlich isotherm

The Freundlich isotherm model is an empirical formula that assumes heterogeneous adsorption due to the diversity of adsorption sites, and the exponential distribution of active sites and their energies. The adsorption equation is given below.

$$\mathrm{Ln}(q) = \ln\left(k_f\right) + \frac{1}{n}\ln\left(C'\right) \qquad (2.9)$$

Where: K_F is adsorption capacity (L/mg); $1/n$ is adsorption intensity.

It also indicates the relative distribution of the energy and the heterogeneity of the adsorbate sites.

Temkin isotherm

Temkin isotherm is an empirical equation that was originally proposed by Slygin and Frumkin (Abdollahi, 2015). Temkin considered the effect of adsorbate/adsorbent interactions on the

adsorption isotherm and proposed that the heat of adsorption of all the molecules in the layer would decrease linearly with coverage. The Temkin isotherm is valid only for an intermediate range of ion concentrations.

$$q_e = \frac{RT}{b}\ln(K_T) + \frac{RT}{b}\ln\ C_e \qquad (2.10)$$

Where: b is the Temkin constant related to the heat of sorption (J/mol); K_T is the Temkin isotherm constant (L/g); R is the gas constant (8.314 J/mol K); T is the absolute temperature (K).

Dubinin–Radushkevich isotherm

The Dubinin–Radushkevich isotherm is generally applied to express the adsorption mechanism with a Gaussian energy distribution onto a heterogeneous surface. The isotherm is an empirical equation for the adsorption of gases/liquids on the mesoporous adsorbents and for adsorption from the liquid phase (Ayawei et al., 2017):

$$lnq_e = lnq_D - B_D(RTln\left(1 + \frac{1}{C_e}\right))^2 \qquad (2.11)$$

Where: B_D is the free energy of adsorption per mole of adsorbate (mol^2/J^2); q_D is the theoretical monolayer saturation capacity. The apparent energy of adsorption from the Dubinin-Radushkevich isotherm, E, can be computed using the relationship, as follows:

$$E = \frac{1}{(2B_D)^{\frac{1}{2}}} \qquad (2.12)$$

Brunauer, Emmett and Teller isotherm

The Brunauer, Emmett and Teller (BET) isotherm was proposed for flat surfaces where there is no limit on the number of layers that can be accommodated on the surface. The surface is assumed to be energetically homogeneous and there is no interaction between the adsorbed molecules. The BET isotherm for liquids is as follows:

$$q_e = q_m \frac{b_s C_e}{(1-b_L C_e)(1-b_L C_e+b_s C_e)} \qquad (2.13)$$

Where: qm (mg/g) is the amount of adsorbate per weight of adsorbent; Ce is the solute equilibrium concentration; bs is the equilibrium constant of adsorption of the first layer; b_L is the equilibrium adsorption-desorption constant for the upper layers of adsorbate on the adsorbent.

Sips isotherm model

Sips isotherm is a combination of the Langmuir and Freundlich isotherms. At low adsorbate concentrations, it reduces to the Freundlich isotherm; at high concentrations, it predicts a monolayer adsorption capacity that is characteristic of the Langmuir isotherm (Foo and Hameed, 2010).

$$q_e = \frac{K_s C_e^{\beta s}}{1 - a_s C_e^{\beta s}} \qquad (2.14)$$

Where: Ks is the Sips isotherm model constant (L/g); βs is the Sips isotherm exponent; as is the Sips isotherm model constant (L/g).

Toth isotherm model

The Toth isotherm model is an empirical equation that was developed to improve Langmuir isotherm fitting. This model is most useful for describing heterogeneous adsorption systems that satisfy both low and high-end boundaries of adsorbate concentration.

$$\frac{q_e}{q_m} = \theta = \frac{K_e C_e}{[1 + (K_L C_3)^n]^{\frac{1}{n}}} \qquad (2.15)$$

Where: K_L is the Toth isotherm constant (mg/g); n is the Toth isotherm constant (mg/g).

Redlich–Peterson isotherm model

The Redlich–Peterson isotherm is a hybrid isotherm that features both Langmuir and Freundlich isotherms, and incorporates three parameters into an empirical equation. It combines elements from both the Langmuir and Freundlich equations; therefore, the mechanism of adsorption is a mix of isotherms and does not follow the ideal monolayer adsorption isotherm.

$$q_e = \frac{AC_e}{1 + BC_e^{\beta}} \qquad (2.16)$$

Where: A is the Redlich-Peterson isotherm constant (L/g); B is the constant (Lm/g); β is the exponent that lies between 0 and 1; Ce is the equilibrium liquid-phase concentration of the adsorbent (mg/l); qe is the equilibrium adsorbate loading on the adsorbent (mg/g).

2.3.1 Carbonous material

The two-electron pairs on the sulphur atom and/or the electrons in the benzene structure act as electron donors to electron acceptors or electron-withdrawing groups on AC (e.g. carboxylic, aldehyde and hydroxyl groups). Most of the work that has been reported for AC fitted Freundlich isotherm (Bu et al., 2011; Saleh and Danmaliki, 2016b; Shah et al., 2018). (See Table 2.5a.) This is consistent with the heterogeneous nature of AC, which has several different contaminants, depending on the source material.

Alhamed and Bamufleh (2009) reported on the effect of varying synthesis conditions on AC adsorption. AC was synthesized from the fruit of the date palm, and the varied conditions were: synthesis temperature (T_{carb}); residence time (θ_{carb}); activator($ZnCl_2$) to AC ratio (R). The data fitted the Freundlich isotherm, which was attributed to a highly heterogeneous AC surface. The GAC samples produced at Tcarb = 700 °C, R = 2.0 and θ_{carb} = 1.0 h (DDS-22) had the highest adsorption capacity (k_f = 2.012 mg S/g dry GAC and n = 2.447). It was concluded that sulphur removal depended mainly on textural properties, such as pore volume and pore size.

Muzic et al. (2010) reported on commercial AC, SRCx and GH2x, with different Si/Al ratios and pore-structures. SRCx exhibited a higher adsorption capacity, and its higher activity was attributed to a higher Si/Al ratio. GH2x and SRCx data fitted the Freundlich isotherm, which was attributed to the heterogeneous nature of the AC surface. The values of separation factor, R_L, were $0<R_L<1$, which indicates favourable adsorption. This was further confirmed with the values of the Freundlich coefficient *n* being larger than one thus indicating physical adsorption.

Wen et al. (2010b) used wood-based AC to determine the effect of temperature on equilibrium isotherms. The Freundlich isotherm described the adsorption of DBT best, which indicates a heterogeneous surface for adsorption. An increase in temperature from 298 to 328 K led to an increase in adsorption capacity from 35.84 mg/g to 50.56 mg/g. However, the increase in temperature led to a decrease in n from 2.421 to 1.657, which suggests a decrease in favourability to adsorb on AC. This is consistent with the exothermic nature of the reaction.

Jha et al. (2020) carried out ADS using graphene nanoplatelets and observed that adsorption of DBT fitted the Langmuir isotherm better, while the adsorption of 2-MT and thiophene fitted the Freundlich isotherm better. This suggests that the surface was homogenous at a 9 Å scale, while it was heterogeneous for a smaller scale of 5 to 7 Å. With the two small-molecule

adsorbates, 2-MT and thiophene, *n* increased while K_f decreased with a decrease in molecular size. The increase in n is consistent with the earlier suggestion that heterogeneity increased with a decrease in molecular scale. A decrease in K_f suggests a decrease in favourability to adsorb, which is in agreement with the adsorption capacity of these two molecules.

Haji and Erkey (2003) used carbon aerogels (CAs) with different pore sizes to investigate the adsorption of DBT. They reported that the Freundlich isotherm was the best fit, which indicates the heterogeneous nature of the adsorbent. CAs with an average pore size of 22 nm had a higher adsorption capacity than CAs with a pore size of 4 nm, which is consistent with a K_F of 0.519 and 0.774, respectively. This was attributed to lower internal mass transfer resistance due to the larger pore diameter. Furthermore, the DBT has a kinetic diameter greater than 4 nm, which suggests there is little surface available for adsorption. The parameter n was 0.444 and 0.447 for CAs 4nm and CAs 22 nm, respectively, which suggests that adsorption favourability for the two adsorbents was similar.

Jha et al. (2019) investigated the effect of varying the chemical activator to the mangolion anthracite ratio. They reported that PMC1/3 absorbent best-fitted SIP, while PMAC1/4 adsorbent fitted dual-site Langmuir. The PMC1/3 adsorption parameters were b = 8.138 and m = 0.390; this suggests heterogeneity of the adsorption sites. PMAC1/4 fitted dual-site Langmuir. This isotherm assumes that the heterogeneous adsorbent is formed by two homogeneous sites with different energetic patches.

Sedaghat et al. (2019) looked at three carbonaceous materials: reduced graphite oxide (rGO), carbon black-graphene (CB-G) and nickel-graphite composite. The adsorption best matched the Langmuir isotherm, which indicates uniform DBT adsorption. This was attributed to π-π stacking of the aromatic groups of DBT on graphene. For Ni-G, adsorption best fitted the Freundlich isotherm at low DBT concentrations and the Langmuir isotherm at high DBT concentrations. It was suggested that this was because adsorption started at specific sites and then proceeded to the uniform graphitic surface. Freundlich fitting indicates that the adsorption energy diminishes exponentially as the adsorbent fills with DBT. CB-G had the highest activity, which was attributed to CB acting as a spacer between the graphene sheets and thus providing more space for DBT adsorption.

Thaligari et al. (2018b) investigated the effect of temperature on the adsorption of DBT on Ni/AC and observed that the experimental data best suited the R-P isotherm. This suggests that adsorption was not ideal, the mechanism is a mixture of Langmuir and Freundlich adsorption. Adsorption capacity increased with temperature and then dropped at 318 K. This increase in capacity was attributed to an increase in the mobility of solute and a decrease in the retarding force on the molecule. Since adsorption is an exothermic process, a further increase in temperature leads to a drop in activity. A similar trend for adsorption capacity was observed for K_L.

Thaligari et al. (2016) did similar work using Zn/AC and reported that activity increased with temperature. This was attributed to increased mobility and reduced retardation forces. The magnitude of K_F shows that the adsorption capacity of Zn-GAC for DBT adsorption increased with an increase in temperature. The data best fitted the R-P and Freundlich isotherms. B for R-P was close to $\beta = [1 - (1/n)]$ than 1 suggesting heterogeneity of adsorbent consistent with Freundlich model.

Olajire et al. (2017) looked at the effect on equilibrium isotherms of loading Ag on AC from brewer's spent grain. The isotherms investigated were Langmuir, Freundlich and Temkin. The data fitted the Freundlich isotherm best, which suggests heterogeneity of the adsorbent. n increased with metal loading, which suggests an increase in heterogeneity, while K_F increased because of an increase in adsorbate loading. An increase in heterogeneity might be due to the introduction of Ag and thus new sites.

Ganiyu et al. (2016) investigated the effect of loading alumina on AC on DBT adsorption. The adsorption capacity decreased in this order: AC-AL2.5>AC-AL5>AC-AL20>AC-AL10>AC. The addition of alumina led to improved activity, which was attributed to the introduction of acid sites. Strangely, the adsorbent with the highest capacity had the least adsorption affinity (K_L), and adsorption was the least favourable (R_L=1.48). Nazal et al. (2019) also reported on the effect of loading alumina on carbonaceous materials. The materials used were AC, carbon nanotube (CNT) and graphite oxide (GO). These were loaded with 5 and 10.9 % alumina and were labelled ACAL10, CNTAL10 and GOAL10, respectively, for 10.9 % loading. The data were fitted to the Freundlich and Langmuir isotherms, and the data best fitted the Freundlich isotherm. This suggested that the adsorbent surface was heterogeneous in nature.

There was no significant change in n, which ranged between 1.2 and 1.9, which suggested no significant change in heterogeneity. K_F increased for the modified adsorbents, with the exception of GOAL, with the increase representing a high adsorption capacity. The increase in adsorption capacity upon loading alumina was attributed to synergetic effects, as discussed earlier.

Danmaliki and Saleh (2017) investigated the effect of different sulphur compounds on adsorption isotherms using a bimetallic system supported on AC (CeFe/AC). The Freundlich isotherm data fit was consistent with the heterogeneous nature of AC. K_F increased with molecular size (thiophene, BT and DBT), which is consistent with adsorption capacity. The increase in adsorption capacity is due to increased electron density with molecular weight and hence better metal-adsorbate bonds. However, n decreased with the increase in molecular weight.

2.4.2 Metal oxides

Kumar et al. (2011b) looked at the effect of improvement strategies on adsorption equilibrium isotherms. The zirconia improvement strategies employed were drying (ZC383), calcination (ZC893) and sulphonation (SZC893). The data fitted the BET isotherm, as indicated in Table 5b, and the adsorption capacity decreased with temperature, which indicates the exothermic nature of adsorption. The adsorption capacity increased in this order: ZD383<ZC893<SZC893, which was attributed to an increase in the active tetragonal phase.

Srivastav and Srivastava (2009b) investigated the effect of temperature on DBT-alumina adsorption isotherms, i.e. Freundlich, Langmuir, Temkin and Redlich-Peterson. The data fitted the Langmuir isotherm, which suggests monolayer adsorption and a homogeneous surface for alumina. This is consistent with the nature of a well-ordered material like alumina. Adsorption capacity and adsorption affinity (K_L) increased with temperature and was attributed to increased mobility of adsorbate and a decrease in the retarding forces acting on the diffusion molecules.

2.4.3 Clays

Câmara et al. (2020) investigated the effect of temperature on DBT adsorption with a hydrated aluminium silicate, palygorskite clay (Pal). Pal was used without treatment, and after being calcined and sulphonated. Untreated Pal showed the highest activity - hence it was used to investigate the effects of varying temperature on adsorption isotherms. Of the four models used, the best data fit was with the Langmuir model – see Table 2.5c. Adsorption capacity and K_L increased with temperature, which showed the endothermic nature of adsorption.

Ishaq et al. (2017) investigated the effect of treatment methods on bentonite adsorption isotherms. The Langmuir model was a better fit than the Freundlich model, similar to Pal. This suggests the homogeneous nature of active sites in clays.

2.4.4 MOFs

The most active adsorbent followed the Langmuir adsorption isotherm in the Bagheri et al. study (2017). Aslam et al. (2017) reported the effect of loading Ni on MIL-100 on adsorption isotherms, with the experimental data fitting the Langmuir isotherm – see Table 2.5d. This is no surprise for a well-ordered mesoporous MOF structure. Loading Ni led to an increase in adsorption capacity to 20Ni-MIL-100; thereafter, a drop was observed, which was attributed to pore blocking. The change in adsorption capacity correlated well with K_L.

2.2.5 Zeolites

Xiaojuan et al. (2018) reported on the effect of temperature on BT adsorption by $CuY^{III}Y$ zeolite. Activity increased with temperature, which they attributed to improved adsorbent-adsorbate affinity. The experimental data fitted the Langmuir isotherm, which is consistent with the well-ordered structure of zeolites. Adsorption affinity decreased with an increase in Q, and the decrease in affinity is consistent with the exothermic nature of adsorption. (See Table 2.5e).

Lu et al. (2017b) investigated the removal of thiophene using CuAgY zeolite, using the Langmuir, Freundlich and SIPs model. The best data fit was with the Sip model, which suggests a combination of the Langmuir and Freundlich isotherms. Adsorption capacity increased with temperature, as explained earlier. Song et al. (2016b) reported on the adsorption of thiophene on AgCeY zeolite, with the data fitting the Langmuir isotherm.

Adsorption capacity improved significantly from 11.20 mg/g to 19.87 mg/g when the sulphur compound was changed from thiophene to BT. This was attributed to increased electron density, as stated earlier. Adsorption capacity also increased with a temperature increase, while K_L dropped. This is consistent with the other work of these authors, in which they used $Cu^{II}Ce^{IV}Y$ zeolite (Song et al., 2014). The drop in K_L was attributed to the exothermic nature of adsorption, as explained earlier. Jiang and Ng (2010) reported on the adsorption of DBT on NaY zeolite: With an increase in temperature, Q increased, while adsorption affinity K_L decreased. The increase in adsorption capacity could be due to improved diffusion, while K_L is a reflection of the exothermic nature of adsorption.

2.4.6 Other adsorbents

Li et al. (2012) investigated DBT adsorption on Fe_3O_4@SiO_2@MIPs. The data fitted the Freundlich isotherm, which indicates that the adsorbent surface area was non-uniform. Adsorption capacity increased with K_F and n increased with temperature, indicating the favourability of adsorption with temperature, which is consistent with the endothermic nature of this process.

Ahmadi et al. (2019) reported on the effect of sulphur compounds and temperature on adsorbate-cobalt modified mesoporous material (CoO-MSU-S) adsorption. The data fitted the Langmuir isotherm, which suggests that CoO-MSU-S has a uniform surface. The adsorption capacity was 22.88 mg/g and 25.64 mg/g for DBT and BT at 313 k, respectively, which suggests that activity increased with a decrease in molecular size. This was consistent with a decrease in adsorption affinity, which indicates a decrease in adsorbate-CoO-MSU-S bond affinity. Lower activity towards DBT was attributed to adsorption via M-S interaction, rather than π-complexation – hence the extra benzene ring in the DBT structure results in a larger molecule and lower bond strength. The adsorption capacity also increased with temperature, which is contrary to the drop in adsorption affinity. The drop in adsorption affinity may be attributed to the exothermic nature of the reaction, while the increase in adsorption capacity is due to improved adsorbate transportation/diffusion.

The work discussed above is based on the adsorption of model fuel. Model fuels are simple synthetic systems used to represent real fuels and are typically composed of a hydrocarbon (e.g. hexadecane) and a sulphur compound (e.g. thiophene). However, Muzic et al. (2008) used three commercial ACs to investigate the adsorption of conventional diesel fuel. Both the Langmuir and Freundlich isotherms were a good fit, with the Freundlich isotherm being slightly more suitable. The adsorption order was C3>G2H>RGM, which is consistent with the separation factor, which was between $0<R_L<1$ and $n>1$. This indicates that adsorption was favourable. An increase in initial diesel sulphur concentration leads to an increase in favourable adsorption because of the improved driving force. Finally, the isotherm data also validated the appropriateness of using diesel as a single component. Marín-Rosas et al., 2010 also did research on diesel fuel and fitted the experimental data of AC, CAC and CAA (produced from different sources) to four isotherms, i.e. BET, SIPs, Freundlich and Langmuir. The data fitted the Freundlich, SIPs and BET models well at high Ce values. The m values for CAC and CAA were 0.634 and 0.606, respectively, which suggests heterogeneity of sites consistent with the Freundlich isotherm. BET fitting at high concentrations is consistent with the expectation that multiple layers occur at high Ce and adsorbate loading. C the parameter for BET for CAA was observed to be 11.2 times that of CAC, which means that the CAA adsorbate had a better affinity for sulphur; this was attributed to the higher pore volume of CAA (0.6 cm^3/g) compared to that of CAC (0.5 cm^3/g).

2.4.7 Adsorption isotherms summary

AC adsorbents have been generally observed to follow the Freundlich adsorption isotherm, because of the physical bonding via π-π bonding that takes place between AC and sulphur compounds. The heterogeneous nature of AC is due to contaminates dependent on the source material. A purer material such as graphene is expected to fit the Langmuir isotherm better because of better π-π stacking with insignificant contaminates. Metal loading on AC has understandably produced an adsorbent with a combination of the Langmuir and Freundlich isotherms or with one of them dominating. Well-ordered materials like metal oxides, zeolite and MOFs generally follow the Langmuir adsorption model.

Table 2.5: Adsorption isotherms for sulphur compounds adsorption

a) Adsorption isotherms for carbonous materials													
Adsorbents	**Adsorbate (initial conc)**	**Temp (K)**	**Langmuir**			**Freundlich**			**BET**				**Reference**
			K_L(I/mg)	**Q_m(mg/g)**	**R^2**	**K_F**	**n**	**R^2**	**K_B**	**$q_{m,B}$**	**C_S**	**R^2**	
AC - date fruit	DBT 5000 ppm	/	0.0197	21.89	0.988	2.012	2.447	0.999	/	/	/	/	Alhamed and Bamufleh, 2009
AC	diesel 27 ppm	313	0.0034	48.928	0.8714	1.744	0.413	0.9046	/	/	/	/	Muzic et al., 2010
Zeolite MS 13X	diesel 27 ppm	313	0.0379	0.4083	0.8001	0.0235	1.4786	0.9343	/	/	/	/	
AC – wood-based with H3PO4 activation	DBT 23µmol/g	313	0.0034	36.8928	0.8935	0.4167	2.421	0.9046	/	/	/	/	Wen et al., 2010
	DBT 23µmol/g	313	0.0015	50.4096	0.8714	0.0612	1.657	0.9623	/	/	/	/	
Graphene nanoplatelets	DBT 500 mg/L	303	0.004	181.650	0.986	3.010	1.61	0.948	/	/	/	/	Jha et al., 2020
	2-MT 500 mg/L	303	0.002	268.500	0.943	0.151	0.835	0.989	/	/	/	/	
	T 500 mg/L	303	4.79×10^{-7}	360.10×10^{-2}	0.955	0.088	0.893	0.995	/	/	/	/	
4 nm CA	DBT	RT	0.00537	11.18	0.882	0.519	0.444	0.953	/	/	/	/	Haji and Erkey, 2003
22 nm CA	DBT	RT	0.00657	15.06	0.921	0.744	0.447	0.971	/	/	/	/	

rGO	DBT 100−1000 mg /L	298	0.057	41.8	0.999	13.864	6.079	0.966	/	/	/	/	Sedaghat et al., 2019
CB-G		298	0.060	46.9	0.999	19.004	6.983	0.853	/	/	/	/	
Ni-G		298	0.045	43.3	0.988	14.621	5.992	0.991	/	/	/	/	
AC brewers	DBT 100, 200, 300, 400, 500 and 600 mg/L	298	3.6E-3	33.1	0.94	0.4E-3	0.4167	0.99	/	/	/	/	Olajire et al., 2017
AgNPskp/AC		298	4.2E-3	63.3	0.92	3.2E-3	0.4762	0.97	/	/	/	/	
AGNPscw/AC		298	4.5E-3	71.9	0.91	4.5E-3	0.4762	0.97	/	/	/	/	
AC – pure	DBT 50–200 ppm	/	0.01195	10.49	0.8782	0.86	2.48	0.7282	/	/	/	/	Ganiyu et al., 2016
AC-Al-2.5		/	0.00338	34.48	0.9989	0.27	1.34	0.9964	/	/	/	/	
AC-Al-5.0		/	0.00452	27.03	0.9962	0.35	1.46	0.9894	/	/	/	/	
AC-Al-7.5		/	0.00628	20.41	0.9936	0.49	1.68	0.9708	/	/	/	/	
AC-Al-10.0		/	0.01279	11.19	0.9187	0.96	2.49	0.796	/	/	/	/	
AC/Ce/Fe	Thiophene 50 ppm	/	0.019	0.33	0.969	6.4E08	4.5	0.999	/	/	/	/	Danmaliki and Saleh, 2017
	BT 50 ppm	/	0.065	2.48	0.958	2.3E05	2.9	0.999	/	/	/	/	
	DBT 50 ppm	/	0.033	3.7	0.985	0.0656	1.6	0.999	/	/	/	/	

b) Adsorption isotherms for metal oxides													
Adsorbents	**Adsorbate (Initial conc)**	**Temp (K)**	**Langmuir**			**Freundlich**			**BET**				**Reference**
			K_L(I/mg)	**Q_m(mg/g)**	**R^2**	**K_F**	**n**	**R^2**	**K_B**	**$q_{m,B}$**	**C_S**	**R^2**	
Zirconia	DBT 30 - 1000 mg/L	308	3.95E-06	12.234	0.990	0.048	0.999	0.990	0.26	352	2604	0.999	Kumar et al., 2011
Dried zirconia		308	9.56E-07	54.969	0.945	0.053	0.999	0.945	0.12	387	1488	0.998	
Calcined zirconia		308	4.20E-07	159.904	0.926	0.067	1.000	0.927	0.08	415	1324	0.993	
Alumina	DBT 100, 200, 500 and 1000 mg/L	303	0.0065	16.07	0.9611	0.3593	1.7695	0.9069	/	/	/	/	Srivastav and Srivastava, 2009
		303	0.0051	21.02	0.9880	0.2520	1.4708	0.9472	/	/	/	/	
		303	0.0109	22.58	0.9915	0.7010	1.8159	0.9915	/	/	/	/	
		303	0.0112	21.25	0.9936	0.7184	1.8678	0.9665	/	/	/	/	
c) Adsorption isotherms for clays													
Adsorbents	**Adsorbate (initial conc)**	**Temp (K)**	**Langmuir**			**Freundlich**			**BET**				**Reference**
			K_L(I/mg)	**Q_m(mg/g)**	**R^2**	**K_F**	**n**	**R^2**	**K_B**	**$q_{m,B}$**	**C_S**	**R^2**	
Untreated bentonite	DBT 100 - 600 mg/L	298	1.6 *10-2	344	0.9978	20.4	1.80	0.9726	/	/	/	/	Ishaq et al., 2017
AAB		298	3.0 · 10-2	367.5	0.9935	22.8	1.95	0.9803	/	/	/	/	
MNLB		298	393	1.2	0.9933	24.9	1.97	0.9759	/	/	/	/	
d) Adsorption isotherms for MOFs													

Adsorbents	**Adsorbate (initial conc)**	**Temp**	**Langmuir**			**Freundlich**			**BET**				**Reference**
		(K)	**K_L(I/mg)**	**Q_m(mg/g)**	**R^2**	**K_F**	**n**	**R^2**	**K_B**	**$q_{m,B}$**	**C_S**	**R^2**	
TMU-11	DBT 0 - 500 ppm	333	0.0945	825	0.999	730.9	26.95	0.9714	/	/	/	/	Bagheri et al., 2017
MIL-101 thiophene	Thiophene 100 - 700 ppmw	303	0.0016	10.475	0.9993	0.0728	1.5092	0,9905	/	/	/	/	Aslam et al., 2017
10Ni-MIL-101		303	0.0033	27.840	0.9904	0.5661	1.8142	0.9632	/	/	/	/	
20Ni-MIL-101		303	0.0093	28.835	0.98882	3.6325	3.3312	0.9859	/	/	/	/	
30Ni-MIL-101		303	0.0011	25.425	0.9909	0.1200	1.3201	0.9891	/	/	/	/	

e) Adsorption isotherms for zeolites

Adsorbents	**Adsorbate (initial conc)**	**Temp**	**Langmuir**			**Freundlich**			**BET**				**Reference**
		(K)	**K_L(I/mg)**	**Q_m(mg/g)**	**R^2**	**K_F**	**n**	**R^2**	**K_B**	**$q_{m,B}$**	**C_S**	**R^2**	
$Cu^{I}Y^{III}$	BT 100, 150, 200, 250, 300, 350, 450, and 500 mg/L	293	3.093	1.86	0.999	/	/	/	/	/	/	/	Xiaojuan et al., 2018
$Cu^{I}Y^{III}$		303	2.708	1.98	0.998	/	/	/	/	/	/	/	
$Cu^{I}Y^{III}$		323	2.087	2.29	0.999	/	/	/	/	/	/	/	

2.5 Comparison of adsorbent performance

A comparison of the performance of six adsorbents was done, i.e.: AC, clay, zeolite, metal oxides, graphene and MOFs. Adsorption capacity is not an objective metric for meaningfully assessing the actual performance of sorbents if adsorbate initial concentrations are different (Al-Wabel et al., 2019). Therefore, the authors compared the activity of different adsorbents using partition coefficient (PC) values. It was observed that metal oxide showed the lowest PC values of about 0-0.02. Low-cost clays and high-cost graphene showed poor activity between 0 and 0.05. MOFs have been reported to be a promising adsorbent of the future, but the high cost is a problem that needs to be overcome. Figure 2.8 shows that the performance of MOFs was lower than the performance of AC (0.5-2.5) and zeolites (0-2.5), except for TMU 11 with a PC value of 82 (not shown in Figure 2.8). Zeolites and AC had a large PC range, which may be attributed to the different source and treatment methods for AC, while for zeolites a wide range of metals may be exchanged ranging from Na to Ag. Zeolite materials based on Cu and Ag show high activity, which may be attributed to the ability of Cu and Ag to form a pi-bond. In addition, the hard-soft acid-base theory indicates that these are the most appropriate metals since sulphur compounds are soft/intermediate bases and these metals are soft acids. Improvement in activity was also observed with AC with the addition of metal.

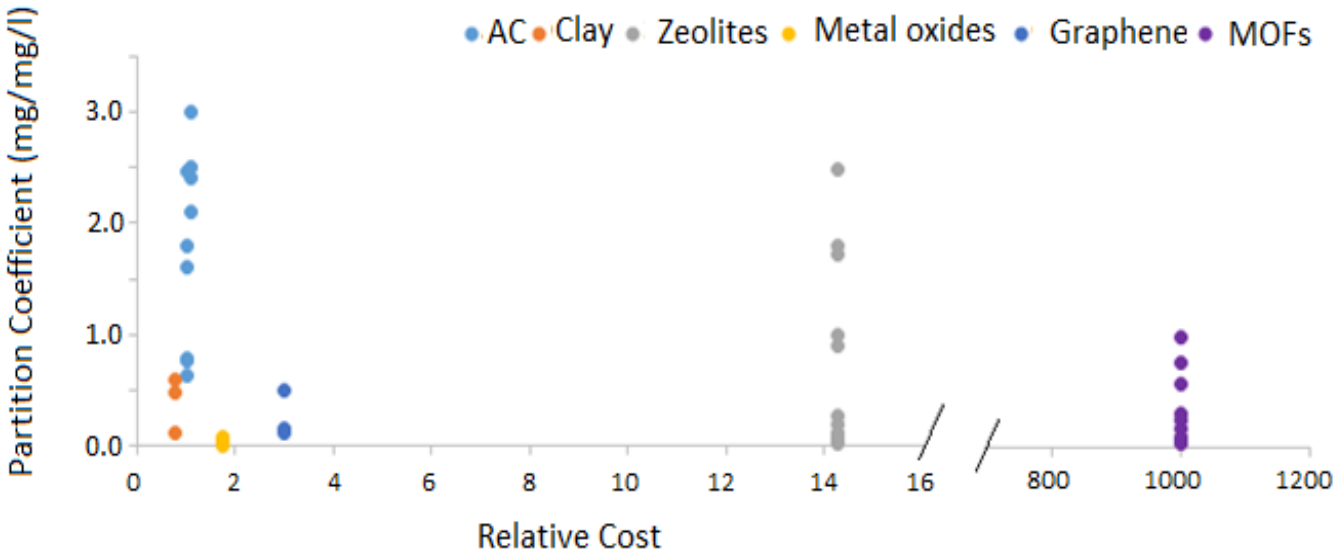

Figure 2.8: Partition coefficient versus relative cost

A figure of merits (FoMs) the most promising adsorbents were analysed, with FoM estimated as follows: FoM = PC/adsorbent cost. The number of times that an adsorbent can be used was not incorporated, because of limited data.

The relative cost for the adsorbents was 1, 1000, 0.8, 10 and 1.45 for AC, MOFs, clays, zeolites and metal oxides, respectively (Khan et al., 2019; Szulejko et al., 2019). AC showed the highest average FoM value and the FoM order of the adsorbent was as follows: AC (0.1396)>> clay (0.0362) > zeolites (0.0045) > MOFs> (0.0012) >metal oxide (0.0002). The MOF with the highest reported adsorption capacity value showed a low FoM value of 0.00586 because of the cost of the MOFs. Even though MOFs exhibit improved performance, the cost is still prohibitive for widespread industrial applications.

2.6 Concluding remarks and perspectives

2.6.1 Concluding remarks

The principal measure for the performance of any desulphurization adsorbent is how well the sulphur compounds are removed from the mixture. The purpose of adsorption research is to improve the activity of adsorbents through modification. This document had collected data on a variety of these modifications and presented an overview of the results. The observations are summarized below

i) From a kinetics viewpoint, most of the reported research on adsorptive desulphurization has indicated that desulphurization follows the pseudo-second-order adsorption model. This may be because most of the work analysed the adsorption data until adsorption reached equilibrium, and the pseudo-first-order model fits the experimental data well for an initial period of the first reaction step only. The initial adsorption rate is a better parameter for describing adsorbate activity and correlates better with adsorption capacity.

ii) From a thermodynamics viewpoint, adsorption may be driven by enthalpy or entropy driving forces. Entropy-driven adsorption suggests that solvent adsorption is probably required for intimate contact between sulphur compound and the adsorbent. Therefore, future work should focus on engineering surfaces that have controlled hydrophobicity.

iii) AC adsorbents have been generally observed to follow the Freundlich adsorption isotherm, which suggests that AC surfaces are heterogeneous in nature.

iv) Metal oxides, zeolite and MOFs generally follow the Langmuir adsorption isotherm.

v) Overall, TMU 11 is the most promising adsorbent, based on its activity and desirable thermodynamic properties. The challenge with MOFs is that they are expensive, with a relative cost 1000 times greater than AC. This is prohibitive and inhibits the use of MOFs in most industrial applications.

vi) When comparing the adsorbents using FoM (activity and cost), AC becomes the most promising adsorbent. Unless the cost of MOFs changes dramatically, it would be most advantageous to continue developing strategies to improve the performance of AC as a topic for further research.

2.6.2 Perspectives

There is a lack of information on the desulphurization of real fuels. As most of the reporting is on model fuels, there is a need to do research on real fuels. The adsorption of sulphur becomes more complex with conventional fuels, as there are many compounds that can potentially compete with sulphur compounds, including monoaromatics, polyaromatics, nitrogen-heterocyclic aromatics and additives. In this multiple-adsorbing system, the adsorbates compete for available adsorption sites on the adsorbent, hence there is lower activity compared to a simple model fuel system. In these complex systems, selectivity becomes an important factor, hence, more work needs to be done using commercial fuels, in order to build a more realistic understanding of the process.

The challenge of competitive adsorption with polyaromatic hydrocarbons may be alleviated by changing the characteristics of sulphur compounds by pre-treatment, e.g. by oxidative desulphurization (ODS). Oxidation of sulphur compounds to corresponding sulfones by catalytic ODS could significantly improve the polarity of the sulphur compounds that could be selectively removed by ADS. Therefore, the configuration of ODS followed by ADS with mild reaction conditions could be a promising process for the deep desulphurization of fuels.

As mentioned earlier, AC is the most promising adsorbent, based on the FoM, while MOFs are the most active. Therefore, more research should be done on reducing the cost of MOFs, including using cheaper and less hazardous solvents like water; searching for alternative ligands; synthesis of composite materials with cheaper materials being used as the support. For example, the composite of AC and MOFs would combine the benefit of cheap AC and highly active MOFs. More work needs to be done in this regard.

Finally, there are many opportunities or strategies yet to be used to improve ADS activity. This presents an opportunity to use computational methods and machine learning to determine variables in adsorbents that have a strong influence on activity and screening through numerous adsorbents to find the most promising ones.

References

Abdollahi, S.B., 2015. A new approach for analysis of adsorption from liquid phase: A critical review. J. Pollut. Eff. Control 03. https://doi.org/10.4172/2375-4397.1000139

Abro, R., Abdeltawab, A.A., Al-Deyab, S.S., Yu, G., Qazi, A.B., Gao, S., Chen, X., 2014. A review of extractive desulphurization of fuel oils using ionic liquids. RSC Adv 4, 35302–35317. https://doi.org/10.1039/C4RA03478C

Ahmadi, M., Mohammadian, M., Khosravi-Nikou, M.R., Baghban, A., 2019. Experimental, kinetic, and thermodynamic studies of adsorptive desulphurization and denitrogenation of model fuels using novel mesoporous materials. J. Hazard. Mater. 374, 129–139. https://doi.org/10.1016/j.jhazmat.2019.04.029

Ahmed, I., Jhung, S.H., 2016. Adsorptive desulphurization and denitrogenation using metal-organic frameworks. J. Hazard. Mater. 301, 259–276.

Ahmed, Md.J.K., Ahmaruzzaman, M., 2015. Adsorptive desulphurization of feed diesel using chemically impregnated coconut coir waste. Int. J. Environ. Sci. Technol. 12, 2847–2856. https://doi.org/10.1007/s13762-014-0654-4

Alhamed, Y.A., Bamufleh, H.S., 2009. Sulphur removal from model diesel fuel using granular activated carbon from dates' stones activated by ZnCl2. Fuel 88, 87–94. https://doi.org/10.1016/j.fuel.2008.07.019

Ania, C.O., Bandosz, T.J., 2006. Metal-loaded polystyrene-based activated carbons as dibenzothiophene removal media via reactive adsorption. Carbon Energy Storage Environ. Prot. 44, 2404–2412. https://doi.org/10.1016/j.carbon.2006.05.016

Aribike, D.S., Usman, M.A., Oloruntoba, M.M., 2019. Adsorptive desulphurization of diesel using activated sewage sludge: Kinetics, equilibrium and thermodynamics studies. Appl. Petrochem. Res. https://doi.org/10.1007/s13203-019-00239-2

Aslam, S., Subhan, F., Yan, Z., Etim, U.J., Zeng, J., 2017. Dispersion of nickel nanoparticles in the cages of metal-organic framework: An efficient sorbent for adsorptive removal of thiophene. Chem. Eng. J. 315, 469–480. https://doi.org/10.1016/j.cej.2017.01.047

Ayawei, N., Ebelegi, A.N., Wankasi, D., 2017. Modelling and interpretation of adsorption isotherms. J. Chem. 2017, 1–11. https://doi.org/10.1155/2017/3039817

Bagheri, M., Masoomi, M.Y., Morsali, A., 2017. High organic sulphur removal performance of a cobalt-based metal-organic framework. J. Hazard. Mater. 331, 142–149. https://doi.org/10.1016/j.jhazmat.2017.02.037

Betiha, M.A., Rabie, A.M., Ahmed, H.S., Abdelrahman, A.A., El-Shahat, M.F., 2018. Oxidative desulphurization using graphene and its composites for fuel containing thiophene and its derivatives: An update review. Egypt. J. Pet. 27, 715–730. https://doi.org/10.1016/j.ejpe.2017.10.006

Bhatia, S., Sharma, D.K., 2010. Biodesulphurization of dibenzothiophene, its alkylated derivatives and crude oil by a newly isolated strain Pantoea agglomerans D23W3. Biochem. Eng. J. 50, 104–109. https://doi.org/10.1016/j.bej.2010.04.001

Bu, J., Loh, G., Gwie, C.G., Dewiyanti, S., Tasrif, M., Borgna, A., 2011. Desulphurization of diesel fuels by selective adsorption on activated carbons: Competitive adsorption of polycyclic aromatic sulphur heterocycles and polycyclic aromatic hydrocarbons. Chem. Eng. J. 166, 207–217. https://doi.org/10.1016/j.cej.2010.10.063

Callura, J.C., Perkins, K.M., Baltrus, J.P., Washburn, N.R., Dzombak, D.A., Karamalidis, A.K., 2019. Adsorption kinetics, thermodynamics, and isotherm studies for functionalized lanthanide-chelating resins. J. Colloid Interface Sci. 557, 465–477. https://doi.org/10.1016/j.jcis.2019.08.097

Câmara, A.B., Sales, R.V., Bertolino, L.C., Furlanetto, R.P., Rodríguez-Castellón, E., De Carvalho, L.S., 2019. Novel application for palygorskite clay mineral: A kinetic and thermodynamic assessment of diesel fuel desulphurization. Adsorption 1–16.

Câmara, A.B.F., Sales, R.V., Bertolino, L.C., Furlanetto, R.P.P., Rodríguez-Castellón, E., De Carvalho, L.S., 2020. Novel application for palygorskite clay mineral: A kinetic and thermodynamic assessment of diesel fuel desulphurization. Adsorption 26, 267–282. https://doi.org/10.1007/s10450-019-00144-z

Danmaliki, G.I., Saleh, T.A., 2017. Effects of bimetallic Ce/Fe nanoparticles on the desulphurization of thiophenes using activated carbon. Chem. Eng. J. 307, 914–927. https://doi.org/10.1016/j.cej.2016.08.143

Eastoe, J., Dalton, J., 2000. Dynamic surface tension and adsorption mechanisms of surfactants at the air-water interface. Adv. Colloid Interface Sci. 85, 103–144.

Fakhraei Ghazvini, M., Vahedi, M., Najafi Nobar, S., Sabouri, F., 2021. Investigation of the MOF adsorbents and the gas adsorptive separation mechanisms. J. Environ. Chem. Eng. 9, 104790. https://doi.org/10.1016/j.jece.2020.104790

Foo, K.Y., Hameed, B.H., 2010. Insights into the modeling of adsorption isotherm systems. Chem. Eng. J. 156, 2–10. https://doi.org/10.1016/j.cej.2009.09.013

Ganiyu, S.A., Alhooshani, K., Sulaiman, K.O., Qamaruddin, M., Bakare, I.A., Tanimu, A., Saleh, T.A., 2016. Influence of aluminium impregnation on activated carbon for enhanced desulphurization of DBT at ambient temperature: Role of surface acidity and textural properties. Chem. Eng. J. 303, 489–500. https://doi.org/10.1016/j.cej.2016.06.005

Ghosal, P.S., Gupta, A.K., 2017. Determination of thermodynamic parameters from Langmuir isotherm constant-revisited. J. Mol. Liq. 225, 137–146. https://doi.org/10.1016/j.molliq.2016.11.058

Haji, S., Erkey, C., 2003. Removal of dibenzothiophene from model diesel by adsorption on carbon aerogels for fuel cell applications. Ind. Eng. Chem. Res. 42, 6933–6937. https://doi.org/10.1021/ie030518m

Hensen, E.J.M., 2000. Hydrodesulphurization catalysis and mechanism of supported transition metal sulfides. Eindhoven University of Technology.

Hernández-Maldonado, A.J., Yang, F.H., Qi, G., Yang, R.T., 2005. Desulphurization of transportation fuels by π-complexation sorbents: Cu(I)-, Ni(II)-, and Zn(II)-zeolites. Fuel Process. PEM Fuel Cells Adv. Cataysts Adsorbents Electrocatalysts 56, 111–126. https://doi.org/10.1016/j.apcatb.2004.06.023

Hernandez-Maldonado, A.J., Yang, R.T., 2004. New sorbents for desulphurization of diesel fuels via ?-complexation. AIChE J. 50, 791–801. https://doi.org/10.1002/aic.10074

Hernández‐Maldonado, A.J., Yang, R.T., 2004. Desulphurization of transportation fuels by adsorption. Catal. Rev. 46, 111–150. https://doi.org/10.1081/CR-200032697

Hernández-Maldonado, A.J., Yang, R.T., 2004. Desulphurization of diesel fuels via π-complexation with nickel(II)-exchanged X- and Y-zeolites. Ind. Eng. Chem. Res. 43, 1081–1089. https://doi.org/10.1021/ie034206v

Ho, Y.S., McKay, G., 1999. Pseudo-second order model for sorption processes. Process Biochem. 34, 451–465. https://doi.org/10.1016/S0032-9592(98)00112-5

Ishaq, M., Sultan, S., Ahmad, I., Ullah, H., Yaseen, M., Amir, A., 2017. Adsorptive desulphurization of model oil using untreated, acid-activated and magnetite nanoparticle loaded bentonite as adsorbent. J. Saudi Chem. Soc. 21, 143–151.

Jeevanandam, P., Klabunde, K.J., Tetzler, S.H., 2005. Adsorption of thiophenes out of hydrocarbons using metal impregnated nanocrystalline aluminium oxide. Microporous Mesoporous Mater. 79, 101–110. https://doi.org/10.1016/j.micromeso.2004.10.029

Jha, D., Haider, M.B., Kumar, R., Byamba-Ochir, N., Shim, W.G., Marriyappan Sivagnanam, B., Moon, H., 2019. Enhanced adsorptive desulphurization using Mongolian anthracite-based activated carbon. ACS Omega 4, 20844–20853. https://doi.org/10.1021/acsomega.9b03432

Jha, D., Haider, M.B., Kumar, R., Shim, W.G., Marriyappan Sivagnanam, B., 2020. Batch and continuous adsorptive desulphurization of model diesel fuels using graphene nanoplatelets. J. Chem. Eng. Data 65, 2120–2132. https://doi.org/10.1021/acs.jced.9b01204

Jiang, J., Ng, F.T.T., 2010. Production of low sulphur diesel fuel via adsorption: An equilibrium and kinetic study on the adsorption of dibenzothiophene onto NaY zeolite. Adsorption 16, 549–558. https://doi.org/10.1007/s10450-010-9259-5

Khan, A., Szulejko, J.E., Kim, K-H., Sammadar, P., Lee, S.S., Yang, X., Ok, Y.S., 2019. A comparison of figure of merit (FoM) for various materials in adsorptive removal of benzene under ambient temperature and pressure. Environ. Res. 168, 96–108. https://doi.org/10.1016/j.envres.2018.09.019

Khan, N.A., Hasan, Z., Jhung, S.H., 2013. Adsorptive removal of hazardous materials using metal-organic frameworks (MOFs): A review. J. Hazard. Mater. 244–245, 444–456. https://doi.org/10.1016/j.jhazmat.2012.11.011

Khan, N.A., Jhung, S.H., 2017. Adsorptive removal and separation of chemicals with metal-organic frameworks: Contribution of π-complexation. J. Hazard. Mater. 325, 198–213. https://doi.org/10.1016/j.jhazmat.2016.11.070

Khan, N.A., Jhung, S.H., 2013. Effect of central metal ions of analogous metal-organic frameworks on the adsorptive removal of benzothiophene from a model fuel. J. Hazard. Mater. 260, 1050–1056. https://doi.org/10.1016/j.jhazmat.2013.06.076

Khan, N.A., Jun, J.W., Jeong, J.H., Jhung, S.H., 2011. Remarkable adsorptive performance of a metal-organic framework, vanadium-benzenedicarboxylate (MIL-47), for benzothiophene. Chem Commun 47, 1306–1308. https://doi.org/10.1039/C0CC04759G

Khan Rao, R.A., Khatoon, A., 2017. Aluminate treated Casuarina equisetifolia leaves as potential adsorbent for sequestering Cu(II), Pb(II) and Ni(II) from aqueous solution. J. Clean. Prod. 165, 1280–1295. https://doi.org/10.1016/j.jclepro.2017.07.160

Kim, J.H., Ma, X., Zhou, A., Song, C., 2006. Ultra-deep desulphurization and denitrogenation of diesel fuel by selective adsorption over three different adsorbents: A study on adsorptive selectivity and mechanism. Catal. Today 111, 74–83.

Kopinke, F-D., Georgi, A., Goss, K-U., 2018. Comment on "Mistakes and inconsistencies regarding adsorption of contaminants from aqueous solution: A critical review, published by Tran et al. [Water Research 120, 2017, 88–116]." Water Res. 129, 520–521. https://doi.org/10.1016/j.watres.2017.09.055

Kumar, S., Srivastava, V.C., Badoni, R.P., 2011. Studies on adsorptive desulphurization by zirconia-based adsorbents. Fuel 90, 3209–3216. https://doi.org/10.1016/j.fuel.2011.06.029

Labana, L., Pandey, G., Jain, R.K., 2005. Desulphurization of dibenzothiophene and diesel oils by bacteria. Lett. Appl. Microbiol. 40, 159–163.

Lee, K.X., Valla, J.A., 2019. Adsorptive desulphurization of liquid hydrocarbons using zeolite-based sorbents: A comprehensive review. React. Chem. Eng. 4, 1357–1386. https://doi.org/10.1039/C9RE00036D

Li, Hui, Xu, W., Wang, N., Ma, X., Niu, D., Jiang, B., Liu, L., Huang, W., Yang, W., Zhou, Z., 2012. Synthesis of magnetic molecularly imprinted polymer particles for selective adsorption and separation of dibenzothiophene. Microchim. Acta 179, 123–130. https://doi.org/10.1007/s00604-012-0873-7

Li, Huanhuan, Shi, W., Zhao, K., Li, Han, Bing, Y., Cheng, P., 2012. Enhanced hydrostability in Ni-doped MOF-5. Inorg. Chem. 51, 9200–9207. https://doi.org/10.1021/ic3002898

Li, Y-X., Jiang, W-J., Tan, P., Liu, X-Q., Zhang, D-Y., Sun, L-B., 2015. What matters to the adsorptive desulphurization performance of metal-organic frameworks? J. Phys. Chem. C 119, 21969–21977. https://doi.org/10.1021/acs.jpcc.5b07546

Liao, J., Zhang, Y., Fan, L., Chang, L., Bao, W., 2019. Insight into the acid sites over modified NaY zeolite and their adsorption mechanisms for thiophene and benzene. Ind. Eng. Chem. Res. 58, 4572–4580. https://doi.org/10.1021/acs.iecr.8b05046

Lu, Y., Wang, R., Nan, Y., Liu, F., Yang, X., 2017. Removal of sulphur from model gasoline by CuAgY zeolite: Equilibrium, thermodynamics and kinetics. RSC Adv. 7, 51528–51537.

Ma, L., Yang, R.T., 2007. Selective adsorption of sulphur compounds: Isotherms, heats, and relationship between adsorption from vapor and liquid solution. Ind. Eng. Chem. Res. 46, 2760–2768. https://doi.org/10.1021/ie0700516

Marín-Rosas, C., Ramírez-Verduzco, L.F., Murrieta-Guevara, F.R., Hernández-Tapia, G., Rodríguez-Otal, L.M., 2010. Desulphurization of low sulphur diesel by adsorption using activated carbon: Adsorption isotherms. Ind. Eng. Chem. Res. 49, 4372–4376. https://doi.org/10.1021/ie901756b

Mguni, L.L., Yao, Y., Nkomzwayo, T., Liu, X., Hildebrandt, D., Glasser, D., 2019. Desulphurization of diesel fuels using intermediate Lewis acids loaded on activated charcoal and alumina. Chem. Eng. Commun. 206, 572–580. https://doi.org/10.1080/00986445.2018.1511983

Murzin, D., Salmi, T., 2005. Chapter 2 - Catalysis, in: Murzin, D., Salmi, T. (Eds.), Catalytic Kinetics. Elsevier Science, Amsterdam, pp. 27–72. https://doi.org/10.1016/B978-044451605-3/50002-2

Muzic, M., Sertic-Bionda, K., Gomzi, Z., 2008. Kinetic and statistical studies of adsorptive desulphurization of diesel fuel on commercial activated carbons. Chem. Eng. Technol. 31, 355–364. https://doi.org/10.1002/ceat.200700341

Muzic, M., Sertic-Bionda, K., Gomzi, Z., Podolski, S., Telen, S., 2010. Study of diesel fuel desulphurization by adsorption. Chem. Eng. Res. Des. 88, 487–495. https://doi.org/10.1016/j.cherd.2009.08.016

Nazal, M.K., Khaled, M., Atieh, M.A., Aljundi, I.H., Oweimreen, G.A., Abulkibash, A.M., 2019. The nature and kinetics of the adsorption of dibenzothiophene in model diesel fuel on carbonaceous materials loaded with aluminum oxide particles. Arab. J. Chem. 12, 3678–3691. https://doi.org/10.1016/j.arabjc.2015.12.003

Nexant, Inc., 2011. Survey and Down-Selection of Acid Gas Removal Systems for the Thermochemical Conversion of Biomass to Ethanol with a Detailed Analysis of an MDEA System (No. NREL/SR-5100-50482, 1013266). National Renewable Energy Laboratory (NREL), Golden, CO., San Francisco, California. https://doi.org/10.2172/1013266

Olajire, A.A., Abidemi, J.J., Lateef, A., Benson, N.U., 2017. Adsorptive desulphurization of model oil by Ag nanoparticles-modified activated carbon prepared from brewer's spent grains. J. Environ. Chem. Eng. 5, 147–159. https://doi.org/10.1016/j.jece.2016.11.033

Patil, S.V., Sorokhaibam, L.G., Bhandari, V.M., Killedar, D.J., Ranade, V.V., 2014. Investigating role of sulphur specific carbon adsorbents in deep desulphurization. J. Environ. Chem. Eng. 2, 1495–1505.

Sadegh-Vaziri, R., Amovic, M., Ljunggren, R., Engvall, K., 2015. A medium-scale 50 MW fuel biomass gasification based Bio-SNG plant: A developed gas cleaning process. Energies 8, 5287–5302. https://doi.org/10.3390/en8065287

Saha, B., Singh, A., Sengupta, S., 2016. Study and optimization of adsorption of sulphur compounds present in fuel. RSC Adv. 6, 76434–76447. https://doi.org/10.1039/C6RA16367J

Saha, B., Vedachalam, S., Dalai, A.K., 2021. Review on recent advances in adsorptive desulphurization. Fuel Process. Technol. 214, 106685. https://doi.org/10.1016/j.fuproc.2020.106685

Saleh, T.A., 2018. Simultaneous adsorptive desulphurization of diesel fuel over bimetallic nanoparticles loaded on activated carbon. J. Clean. Prod. 172, 2123–2132. https://doi.org/10.1016/j.jclepro.2017.11.208

Saleh, T.A., Al-Hammadi, S.A., Tanimu, A., Alhooshani, K., 2018. Ultra-deep adsorptive desulphurization of fuels on cobalt and molybdenum nanoparticles loaded on activated carbon derived from waste rubber. J. Colloid Interface Sci. 513, 779–787. https://doi.org/10.1016/j.jcis.2017.11.076

Saleh, T.A., Danmaliki, G.I., 2016a. Influence of acidic and basic treatments of activated carbon derived from waste rubber tires on adsorptive desulphurization of thiophenes. J. Taiwan Inst. Chem. Eng. 60, 460–468. https://doi.org/10.1016/j.jtice.2015.11.008

Saleh, T.A., Danmaliki, G.I., 2016b. Adsorptive desulphurization of dibenzothiophene from fuels by rubber tyres-derived carbons: Kinetics and isotherms evaluation. Process Saf. Environ. Prot. 102, 9–19. https://doi.org/10.1016/j.psep.2016.02.005

Sedaghat, S., Ahadian, M.M., Jafarian, M., Hatamie, S., 2019. Model fuel deep desulphurization using modified 3D graphenic adsorbents: Isotherm, kinetic, and thermodynamic study. Ind. Eng. Chem. Res. 58, 10341–10351. https://doi.org/10.1021/acs.iecr.9b00250

Sen Gupta, S., Bhattacharyya, K.G., 2011. Kinetics of adsorption of metal ions on inorganic materials: A review. Adv. Colloid Interface Sci. 162, 39–58. https://doi.org/10.1016/j.cis.2010.12.004

Seredych, M., Hulicova-Jurcakova, D., Bandosz, T.J., 2010. Effect of the incorporation of nitrogen to a carbon matrix on the selectivity and capacity for adsorption of dibenzothiophenes from model diesel fuel. Langmuir 26, 227–233. https://doi.org/10.1021/la902059y

Shah, S.S., Ahmad, I., Ahmad, W., 2016. Adsorptive desulphurization study of liquid fuels using Tin (Sn) impregnated activated charcoal. J. Hazard. Mater. 304, 205–213. https://doi.org/10.1016/j.jhazmat.2015.10.046

Shah, S.S., Ahmad, I., Ahmad, W., Ishaq, M., Gul, K., Khan, R., Khan, H., 2018. Study on adsorptive capability of acid activated charcoal for desulphurization of model and commercial fuel oil samples. J. Environ. Chem. Eng. 6, 4037–4043. https://doi.org/10.1016/j.jece.2018.06.008

Shah, S.S., Ahmad, I., Ahmad, W., Ishaq, M., Khan, H., 2017. Deep desulphurization study of liquid fuels using acid treated activated charcoal as adsorbent. Energy Fuels 31, 7867–7873. https://doi.org/10.1021/acs.energyfuels.7b00914

Shi, F., Hammoud, M., Thompson, L.T., 2011. Selective adsorption of dibenzothiophene by functionalized metal organic framework sorbents. Appl. Catal. B Environ. 103, 261–265. https://doi.org/10.1016/j.apcatb.2010.07.016

Shi, Y., Liu, G., Wang, L., Zhang, X., 2015. Efficient adsorptive removal of dibenzothiophene from model fuel over heteroatom-doped porous carbons by carbonization of an organic salt. Chem. Eng. J. 259, 771–778. https://doi.org/10.1016/j.cej.2014.08.054

Sikarwar, P., Gosu, V., Subbaramaiah, V., 2019. An overview of conventional and alternative technologies for the production of ultra-low-sulphur fuels. Rev. Chem. Eng. 35, 669–705.

Simonin, J-P., 2016. On the comparison of pseudo-first order and pseudo-second order rate laws in the modeling of adsorption kinetics. Chem. Eng. J. 300, 254–263. https://doi.org/10.1016/j.cej.2016.04.079

Song, H., Chang, Y., Song, H., 2016a. Deep adsorptive desulphurization over Cu, Ce bimetal ion-exchanged Y-typed molecule sieve. Adsorption 22, 139–150. https://doi.org/10.1007/s10450-015-9731-3

Song, H., Chang, Y., Wan, X., Dai, M., Song, H., Jin, Z., 2014. Equilibrium, kinetic, and thermodynamic studies on adsorptive desulphurization onto CuICeIVY zeolite. Ind. Eng. Chem. Res. 53, 5701–5708.

Song, Hua, Wan, X., Dai, M., Zhang, J., Li, F., Song, Hualin, 2013. Deep desulphurization of model gasoline by selective adsorption over Cu–Ce bimetal ion-exchanged Y zeolite. Fuel Process. Technol. 116, 52–62. https://doi.org/10.1016/j.fuproc.2013.04.017

Song, H., Yang, G., Song, H-L., Cui, X., Li, F., Yuan, D., 2016b. Kinetic and thermodynamic studies on adsorption of thiophene and benzothiophene onto AgCeY Zeolite. J. Taiwan Inst. Chem. Eng. 63, 125–132.

Srivastav, A., Srivastava, V.C., 2009. Adsorptive desulphurization by activated alumina. J. Hazard. Mater. 170, 1133–1140. https://doi.org/10.1016/j.jhazmat.2009.05.088

Sun, L-B., Li, J-R., Park, J., Zhou, H-C., 2012. Cooperative template-directed assembly of mesoporous metal–organic frameworks. J. Am. Chem. Soc. 134, 126–129.

Svinterikos, E., Zuburtikudis, I., Al-Marzouqi, M., 2019. Carbon nanomaterials for the adsorptive desulphurization of fuels. J. Nanotechnol. 2019, 1–13. https://doi.org/10.1155/2019/2809867

Szulejko, J.E., Kim, K-H., Parise, J., 2019. Seeking the most powerful and practical real-world sorbents for gaseous benzene as a representative volatile organic compound based on performance metrics. Sep. Purif. Technol. 212, 980–985. https://doi.org/10.1016/j.seppur.2018.11.001

Tadashi, M., 2011. Thermodynamics. IntechOpen.

Tan, P., Jiang, Y., Sun, L-B., Liu, X-Q., AlBahily, K., Ravon, U., Vinu, A., 2018. Design and fabrication of nanoporous adsorbents for the removal of aromatic sulphur compounds. J. Mater. Chem. A 6, 23978–24012. https://doi.org/10.1039/C8TA09184F

Thaligari, S.K., Gupta, S., Srivastava, V.C., Prasad, B., 2018. Adsorptive desulphurization and denitrogenation by nickel impregnated activated carbon. Indian J. Chem. Technol. 25, 522–530.

Thaligari, S.K., Srivastava, V.C., Prasad, B., 2016. Adsorptive desulphurization by zinc-impregnated activated carbon: Characterization, kinetics, isotherms, and thermodynamic modeling. Clean Technol. Environ. Policy 18, 1021–1030. https://doi.org/10.1007/s10098-015-1090-y

Tian, F., Wu, W., Jiang, Z., Liang, C., Yang, Y., Ying, P., Sun, X., Cai, T., Li, C., 2006. The study of thiophene adsorption onto La (III)-exchanged zeolite NaY by FT-IR spectroscopy. J. Colloid Interface Sci. 301, 395–401.

UNEP, 2015. Diesel sulphur levels. Middle East, North Africa & West Asia Diesel Sulphur Matrix. UNEP.

Wang, J., Xu, F., Xie, W., Mei, Z., Zhang, Q., Cai, J., Cai, W., 2009. The enhanced adsorption of dibenzothiophene onto cerium/nickel-exchanged zeolite Y. J. Hazard. Mater. 163, 538–543. https://doi.org/10.1016/j.jhazmat.2008.07.027

Wang, T., Li, X., Dai, W., Fang, Y., Huang, H., 2015. Enhanced adsorption of dibenzothiophene with zinc/copper-based metal–organic frameworks. J. Mater. Chem. A 3, 21044–21050. https://doi.org/10.1039/C5TA05204A

Wen, J., Han, X., Lin, H., Zheng, Y., Chu, W., 2010. A critical study on the adsorption of heterocyclic sulphur and nitrogen compounds by activated carbon: Equilibrium, kinetics and thermodynamics. Chem. Eng. J. 164, 29–36. https://doi.org/10.1016/j.cej.2010.07.068

Williams, M., Minjares, R., 2016. A technical summary of Euro 6/VI vehicle emission standards. The International Council on Clean Transport.

Worch, E., 2012. Adsorption technology in water treatment. De Gruyter. https://doi.org/10.1515/9783110240238

Wu, F.-C., Tseng, R.-L., Juang, R.-S., 2009. Characteristics of Elovich equation used for the analysis of adsorption kinetics in dye-chitosan systems. Chem. Eng. J. 150, 366–373. https://doi.org/10.1016/j.cej.2009.01.014

Xiao, J., Song, C., Ma, X., Li, Z., 2012. Effects of aromatics, diesel additives, nitrogen compounds, and moisture on adsorptive desulphurization of diesel fuel over activated carbon. Ind. Eng. Chem. Res. 51, 3436–3443. https://doi.org/10.1021/ie202440t

Xiaojuan, L., Hua, S., Youxin, C., 2018.Study of Isothermal Equilibrium, Kinetics and Thermodynamics of adsorptive desulphurization on synthesized $Cu^{I}Y^{III}Y$ Zeolite. *中国炼油与石油化工(英文版)*, (2018 年 02), pp.24-33.

Xue, M., Chitrakar, R., Sakane, K., Hirotsu, T., Ooi, K., Yoshimura, Y., Feng, Q., Sumida, N., 2005. Selective adsorption of thiophene and 1-benzothiophene on metal-ion-exchanged zeolites in

organic medium. J. Colloid Interface Sci. 285, 487–492. https://doi.org/10.1016/j.jcis.2004.12.031

3. METHODOLOGY AND EXPERIMENTAL DESIGN

3.1 Introduction

The literature review indicated that both MOFs and AC are promising adsorbents. ML was used to further understand the features that need to be optimised. Linear regression and random forest analysis were done, with full details of these methods given in Chapter 4. The experimental work started with a screen of the commonly used adsorbents, namely: activated carbons, molecular sieves, MOFs and metal oxide materials. The analysis indicated that AC and MOFs were the most promising options, with AC favouring high molecular organic sulphur compounds; MOFs favouring adsorption of smaller organic sulphur compounds, because of the smaller pore windows. This analysis culminated in the synthesis of MOF@AC composites, and the synthesized adsorbents were tested on both model diesel and real diesel.

The general experimental procedures and the equipment used are provided below, while a detailed account of the test work is presented in the chapters that follow. Chapters 4 to 9 have been prepared for submission as papers for future publication or have been published as journal articles. Details of the experimental procedures are provided in those chapters and a small degree of repetition will be observed.

3.2 Materials and Chemicals

3.2.1 Gas

All the gases used in this study were supplied by AFROX (African Oxygen) Ltd. Nitrogen was used as the carrier gas, hydrogen was used as the fuel, whilst air was the oxidant for the gas chromatogram.

3.2.2 Chemicals

The chemicals used were: 1,4-benzenedicarboxylic acid (H_2BDC) (98 %); N,N-dimethylformamide (DMF, 99.8 %); formic acid (85 %); zinc (II) nitrate hexahydrate ($Zn(NO_3)_2 \cdot 6H_2O$) and nickel (II) nitrate hexahydrate ($Ni(NO_3)_2 \cdot 6H_2O$) (97 %); hexadecane (98 %); thiophene (98 %); dibenzothiophene DBT (98 %); 4,6 dimethyl benzothiophene (98 %). Hexadecane (99 %) and toluene (99.5 %) were ALL obtained from Sigma Aldrich. Copper (II) nitrate trihydrate (>98 %) and cobalt (II) nitrate hexahydrate (99 %) were purchased from Merck. Commercial diesel was bought from a garage in Johannesburg, South Africa.

3.2.3 Adsorbents

The adsorbents used in this work (AC, titania (TiO_2), alumina (Al_2O_3), silica (SiO_2) and molecular sieves 13X and 5A) were also obtained from Sigma Aldrich. The activated carbon T103 and T104 (T103 and T104) were obtained from Tongxing Chemical Co. Ltd, Henan Province, China. Other adsorbents used were: AC/support loaded with metal oxides produced via incipient impregnation; MOF-5; Ni-BDC; Ni-BDC@AC composite.

3.3 Experimental Set-up

Adsorption experiments were carried out using a batch and a fixed bed reactor. The setups are shown in Figure 3.1 below. The parameters that were investigated included: type of adsorbent; dosage of adsorbent; adsorption time; initial diesel concentration; adsorption temperature; diesel pumping rate.

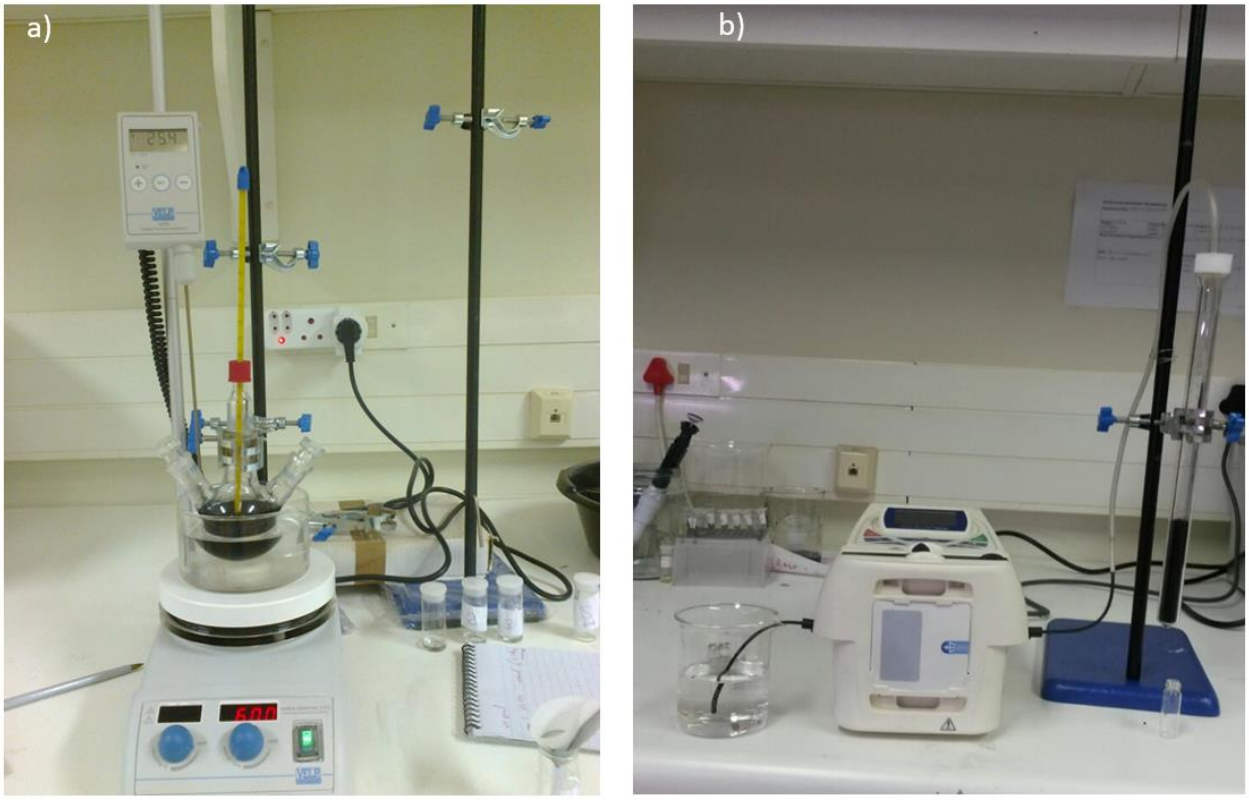

Figure 3.1: Two reactors used in this research: a) Batch reactor; b) Fixed bed reactor

3.4 Adsorbent synthesis

The adsorbents were synthesized to improve the activity and selectivity of the adsorbents. The synthesis methods used are presented in sections 3.4.1 to 3.4.4.

3.4.1 Loading metal oxide on the support

Supports AC, TiO_2, Al_2O_3 and SiO_2 were loaded via incipient impregnation with aqueous solutions of different d- transitional metal nitrate salts. The support loaded with metal nitrate was then dried by evaporation at 110 ^oC overnight and then calcined at 400 ^oC for 4 h in nitrogen and air for AC and other supports respectively. More details regarding the preparation of the materials are provided in Chapters 5 to 7.

3.4.2 Modulated synthesis of MOF-5/Ni-BDC

MOF-5 was synthesized using the solvothermal treatment method (Li et al., 1999). The modification made to this method was adding Ni and formic acid as a modulator. The aim of the modulation was to improve crystallinity and control the crystallite size of the adsorbent. More details regarding the preparation of the materials are provided in Chapters 8 and 9.

3.4.3 Modulated synthesis of Ni-BDC@AC

A Ni-BDC@AC composite sample was prepared by carrying out Ni-BDC synthesis in the presence of AC. This work investigated the effect on the modulator in the presence of AC for the first time. More details regarding the preparation of the materials are provided in Chapter 9.

3.5 Diesel analysis

Samples taken during the adsorption experiments were analyzed using a 7890B Agilent Gas Chromatograph (GC) with two detectors: a Flame Ionization Detector (FID) and a Pulsed Flame Photometric Detector (PFPD). A J&W DB-1 GC capillary column (30 m length, 0.32 mm internal diameter, and 0.25 μm film thickness) was used to separate the components in the diesel fuel. The temperature of the detectors was set to 300 °C. For the model diesel analysis, the oven temperature was initially maintained at 50 °C for 0.5 min, then increased at a rate of 10 °C/min to 280 °C, and then held at 280 °C for 5 min; for the commercial diesel analysis, the ramping rate of the oven temperature was changed from 10 °C/min to 5 °C/min in order to have a good separation of the sulphur compounds, while the other settings remained the same as that for the model diesel analysis. Nitrogen gas was used as a gas carrier at a flow rate of 1.2 mL/min. After the separation of each component in the diesel by the GC capillary column, the

sulphur substances were detected and quantified using the PFPD detector. Figure 3.2 shows the sulphur component analysis when using GC-PFPD with both model diesel and commercial diesel.

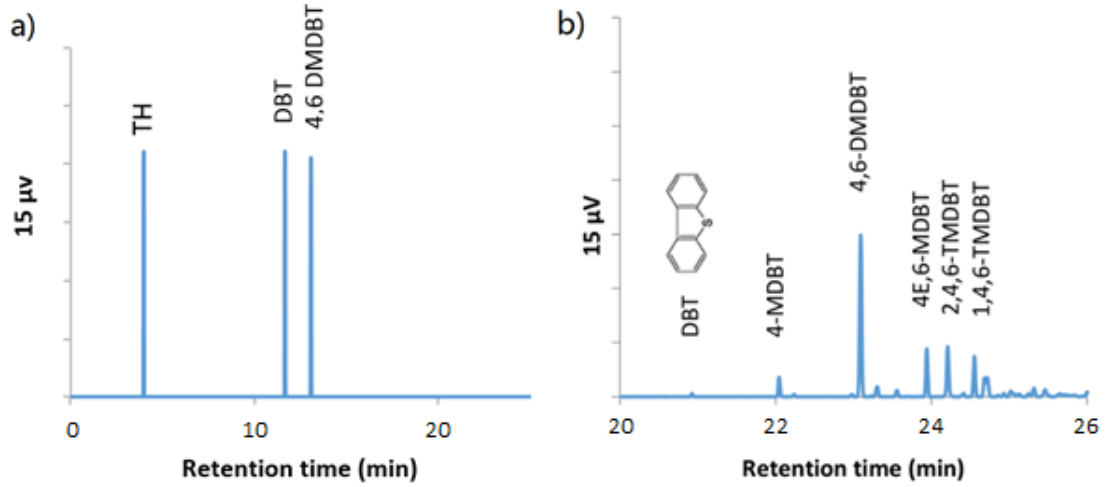

Figure 3.2: Diesel chromatogram from GC-PFPD for: a) model diesel; b) commercial diesel.

Quantification of the major sulphur compounds was carried out using a normalization method (Safa et al., 2017), with the concentration of each sulphur compound being determined using the following equation (3.1):

$$C_{s,i} = C_{s,ref} \frac{{A_i}^{0.5}}{{A_{ref}}^{0.5}} \qquad (3.1)$$

Where: $C_{S,\,ref}$ is the sulphur concentration in the reference sample; A_i is the peak area that corresponds to the sulphur compound to be measured - i; A_{ref} is the area of the reference peak in the GC-PFPD chromatograms. The relative error for analysis of the sulphur compounds was less than 6 %.

References

Li, H., Eddaoudi, M., O'Keeffe, M., Yaghi, O.M., 1999. Design and synthesis of an exceptionally stable and highly porous metal-organic framework. Nature 402, 276.

Safa, M.A., Al-Shamary, T., Al-Majren, R., Bouresli, R., Ma, X., 2017. Reactivities of various alkyl dibenzothiophenes in oxidative desulphurization of middle distillate with cumene hydroperoxide. Energy & fuels 31, 7464–7470.

4. INSIGHT INTO ADSORPTIVE DESULPHURIZATION BY ZEOLITES: A MACHINE LEARNING EXPLORATION

This work has been submitted to the journal of Energy & Fuel. Part of this work will be presented at the following conference:

31st INTERNATIONAL CATSA CONFERENCE – VIRTUAL 7th -10th NOVEMBER, 2021

Summary

Adsorptive desulphurization (ADS) has received great attention because of its potential due to mild conditions required to remove sulphur thus addressing SO_X, carbon and energy concerns at the same time. A number of properties have been reported to determine the adsorption activity of zeolites in ADS. However, there is no consensus on the parameters with a dominating influence - hence adsorbent synthesis design has remained an art. Machine learning (ML) has gained popularity as a powerful tool for understanding the catalytic mechanism and providing insight into catalytic design. In this study, regression techniques - linear regression and random forests (RF) regression - were used to explore the process of ADS by zeolites. The relative importance of adsorbent properties, process parameters and optimum variables for ADS were investigated, using zeolites data gathered from the literature. The results showed that relationships between ADS variables and adsorption activity were non-linear in nature, and require more complicated models to avoid violation of linear regression assumptions. Multiple linear regression and RF analysis yielded coefficients of determination (R^2) of 0.88 and 0.93, respectively. Initial adsorbate concentration (C_0) showed the highest relative importance of the variables, followed by zeolite properties (metal ion, mesoporous volume, pore size, Si/Al ratio and surface area) for ADS activity. These findings suggest that for improvement of ADS activity more attention should be given to modification of the adsorbent properties. Furthermore, this work demonstrates the utility of ML and literature survey data as an inexpensive alternative to experimentation when doing research to obtain mechanistic insight into the complex process of ADS.

Keywords: adsorption desulphurization; zeolites; adsorbent properties; regression; machine learning

4.1 Introduction

Removing sulphur from liquid fuels has become a great problem all around the world. Combustion of sulphur in a fuel engine produces SO_X gases that react with moisture to produce smog and acid rain, which exacerbates other environmental challenges (Wang et al., 2005). However, environmental impact is not measured solely by SO_X emissions, as energy usage and carbon emissions are also important considerations, among others. There are a number of technologies that show potential for removing sulphur, one of which is adsorptive desulphurization (ADS). It has received a good deal of attention because of its potential when using mild conditions to remove sulphur, which addresses SO_X, carbon and energy concerns at the same time. Several adsorbents have been reported, including metal-organic framework materials, activated carbon, metal oxides, clays and zeolites (Tan et al., 2018). These have shown varying success, costs and selectivity; (Szulejko et al., 2019; Ganiyu and Lateef, 2021). Here, we focus on zeolites that have been widely studied, owing to their high specific surface area, large exchangeable cation sites and promising activity (Shi et al., 2012).

Zeolites are aluminosilicate materials that occur naturally or are manufactured synthetically. They may be modified in many ways to improve their adsorption capacity and can be tuned over a wide range of acidity and basicity of hydrophilicity and hydrophobicity, and many cations can be introduced by ion exchange (Jacobs et al., 2001). Several properties have been reported to determine the adsorption activity of zeolites. However, there is no consensus on the parameters that have the most dominating effect. This lack of consensus could be because of the different operating conditions and/or zeolite properties hence-the rate-limiting property/condition varies. Song et al., (2016) reported that the activity of AgCeY is dependent on the Si/Al ratio. The activity increased with an increase in the Si/Al ratio and this was attributed to an increase in Lewis acid sites. Contrarily, Mahmoudi, (2016) reported: an

increase in activity with a decrease in Si/Al ratio; the optimum ratio was 4.05, and a further decrease led to the collapse of the zeolite structure, and hence a decrease in activity. Activity has also been reported to depend on the adsorbing metal, with many researchers reporting high activity using Ag, Cu and good selectivity when using Ce and La (Xiao et al., 2008; Shi et al., 2012). In addition, doping of zeolites with alkali metal-K has been reported to improve reducibility (Velu et al., 2005). Bi-metallics have also been used to take advantage of pi-bonding metals high adsorption capacity and Ce direct bonding, and hence high selectivity (Velu et al., 2003). The adsorbent pore structure has been reported to affect adsorption activity. Tian et al., 2012 reported that the formation of mesopores on beta zeolite improved the desulphurization performance for DBT with a larger molecular diameter.

The adsorption activity has also been reported to depend on the sulphur compound being removed. Zhou, et al., (2006) reported that adsorbate adsorption depended on π-complexation interaction with the adsorbent and the geometric structures. They reported that the selectivity of adsorption followed the order BT > TP > DBT > 4,6-DMDBT > benzene, which is consistent with the bond order obtained using the natural bond orbital (NBO) analysis method. Ma and Yang, 2007 also showed that larger sulphur compounds such as DBT exhibit higher adsorption energies.

The individual relationships between the properties of zeolites and adsorption capacity during desulphurization have been examined and are largely understood (Dehghan and Anbia, 2017). However, the relative importance and interaction of zeolite properties on adsorption are poorly understood and, to the best of our knowledge, they have not been explicitly studied. Machine learning (ML) is a type of artificial intelligence (AI) whereby computer programs improve performance when doing a particular task through learning and improving, and without explicit programming (Jordan and Mitchell, 2015). ML has recently emerged as a powerful tool for

modelling the adsorption processes, for example: metal adsorption onto biochars (Zhu et al., 2019; El Hanandeh et al., 2021) dye adsorption on surface-modified municipal waste adsorbent (Ahmad et al., 2020); and heavy metal adsorption (Hafsa et al., 2020). ML algorithms, specifically artificial neural networks (ANN) (Goodfellow et al., 2016) and RF (Breiman, 2001), have been most widely used to model adsorption processes. These ML algorithms are particularly suited to ADS, as the interactive effects of adsorbent properties and adsorption conditions on adsorption capacity appear to be non-linear. Open-source libraries for ML - for example, Scikit-learn (Pedregosa et al., 2011), TensorFlow (Abadi et al., 2016) and recently FastAI (Howard and Gugger, 2020) - have matured and become more accessible for non-computer science researchers (Jordan and Mitchell, 2015; Yang et al., 2020). Recent applications of ML algorithms with various adsorption processes (Jordan and Mitchell, 2015; Zhu et al., 2019; Ahmad et al., 2020) demonstrates the potential of ML models to generate predictive models and untangle the interacting properties and process parameters of zeolite desulphurization.

Predicting adsorption capacity using adsorbent properties and process parameters is fundamentally a regression problem. The RF algorithm is a meta-estimator that averages ensembles of decision trees (aggregation of models and bootstrapping of datasets also known as bagging), in order to generate regression or statistical classification models (Breiman, 2001). Predictive models generated by RF algorithms are widely used, due to their interpretability and low computational resource requirements (Bernard et al., 2010; Biau, 2012). Furthermore, the ability of RF to handle small datasets and missing data has made it very useful in training on data obtained from literature surveys where datasets of around 50-1000 entries are common - see the examples listed in the reference list (Jordan and Mitchell, 2015; Zhu et al., 2019; Ahmad et al., 2020). The interactive effects of zeolite properties, together with process parameters and how these determine adsorption capacity, can be established experimentally,

which is the conventional approach. However, in addition to the challenge of experimental design, such experiments are prohibitive to most researchers in terms of material and time resource requirements. Recent studies, such as (Jordan and Mitchell, 2015; Zhu et al., 2019; Ahmad et al., 2020) have demonstrated that data from existing studies can be leveraged to compile datasets for generating ML predictive models.

In this study, datasets compiled from a literature survey of the adsorption activity of zeolites were used to investigate and characterise the individual and interactive effects of zeolite properties and process parameters. This work aimed to address the following questions: (i) What is the relative importance of adsorbent properties on adsorption activity?; (ii) What is the relative importance of process parameters on adsorption activity?; (iii) What is the predictive power of the best model? Zeolite ADS studies were surveyed and a dataset compiled, which was analysed with regression analysis tools of increasing complexity. The RF regression model was found to be more suitable than multiple linear regression for generating a predictive model for zeolite ADS.

4.2 Materials and methods

4.2.1 Literature survey and data collection

The adsorption experimental data used in this work is based on zeolites data gathered from tables and graphs reported in the literature. The criteria used for data inclusion was the availability of most characterisation data of the adsorbent and all process parameters. The WebPlotDigitzer online software was used to extract data points from graphs (https://apps.automeris.io/wpd/). The dependent or response variable used was adsorption capacity (mg/g). Twelve input/output variables were used and divided into three groups: adsorbent properties, adsorbate properties and adsorption conditions. Adsorbent properties included in the dataset were surface area, microporous volume, mesoporous volume, pore size,

Si/Al ratio, zeolite metal ion and metal ion amount. Corresponding process parameters were also collected, i.e. adsorbate, initial adsorbate concentration, solvent, model fuel to adsorbent ratio and operating temperature; while the adsorbate properties were sulphur compound and adsorbate dipole moment. Initial concentration (C_0) was obtained from the literature texts and, where not available, it was calculated using equilibrium concentrations (Ce) obtained from graphs (equilibrium isotherms) based on equation 4.1.

$$q_e = \frac{(C_0 - C_e)V}{\rho m} \qquad (4.1)$$

Where: q_e (mg/g) is equilibrium adsorption capacity; V is model fuel volume (ml); m (kg) is the mass of adsorbent (g); ρ (g/cm^3) is the density of model fuel; C_0 (ppm) is initial concentration; Ce (ppm) is equilibrium concentration. Where the analysis was carried out at room temperature, the standard temperature of 20 °C was used.

4.2.2 Data pre-processing and exploratory analysis

Data from the literature were pre-processed using a custom Python script, with the variables (continuous and categorical) analysed for their distributions. Categorical variables (adsorbent, adsorbate and solvent) were encoded into dummy/indicator variables using one-hot encoding. For metal ion amount (m^{n+}/Al), zeros were used where values were not available. Missing values were imputed on a variable-by-variable basis. Missing values for features (pore size, micropore volume and mesopore volume) were imputed using group means, with the adsorbent identity used as the grouping variable. This imputation approach was based on the assumption that the properties would be shared based on similar three-dimensional structures, given that they are the same zeolite adsorbents. Statistical significance of differences before and after imputation was assessed using the non-parametric Kolmogorov-Smirnov test implemented in the R function ks.test.

Pairwise linear correlations between the continuous variables in the data were assessed using Pearson's correlation coefficient and corresponding significant tests, as implemented in the cor and cor.mtest functions, respectively, in R (ver. 3.6.1) (R Core Team, 2019). Simple linear regression analysis of the predictor variable (features) and the response variable (adsorptive capacity) was also conducted for comparison with existing theory and the empirical findings in the literature. Furthermore, this step was conducted to gain insight into the relationship between these variables and adsorptive capacity. Assumptions of linear regression in the generated models were assessed and the assumption of linearity was of particular importance. To this end, the normality of residuals and other linear model assumptions were evaluated using the Global Validation of Linear Models Assumptions (gvlma) package (ver. 1.0.0.3) (Peña and Slate, 2006), using the gvlma function.

4.2.3 Relative importance of properties and process parameters on adsorptive desulphurization

To address the question of the relative importance of adsorbent properties and process parameters on adsorption activity, two approaches were used: multiple linear regression (MLR) and RF analysis. The rationale for our approach was to assess the performance of the more widely used MLR, as linearity of predictors is assumed, and then use RF, as the assumption of linearity is not required.

4.2.4 MLR analysis

MLR analysis of explanatory variables comprising encoded and standardised zeolite properties including process parameters (56 variables including encoded variables) set as predictor variables; and the adsorption capacity as the response variable. Briefly, the analysis was carried out using the lm function implemented in the R statistical environment by fitting a linear model of the response variable against all the predictor variables. A stepwise feature and model

selection strategy was then carried out by iteratively adding and removing features in a forward and backward search space, respectively, using the stepAIC function in the Modern Applied Statistics with S (MASS) (Venables and Ripley, 2002) package (ver. 7.3-53.1). The results of the initial multiple regression linear model were used as input. The stepAIC function finds the best model by minimising information loss as measured by the Akaike Information Criteria (AIC) value under the default maximum of 1000 steps. To determine the relative importance of variables, the rel weights R function obtained from Kabacoff, (2015) was used, and the relative importance of the variables in terms of their percentage contribution to R^2 were calculated.

4.2.5 RF regression analysis

An ensemble RF regressor implemented in the Scikit-learn Python module was used to train a predictive ML model of ADS using 80 % of the pre-processed data obtained from the literature survey. The Scikit-learn RF regressor implementation in the sklearn.ensemble.RandomForestRegressor (ver.0.24.1) class is an averaging algorithm of regression decision trees that generates a predictive model from bootstrapped (with replacement) sub-samples of the training set. The performance of the RF model and splitting of the nodes in the decision tree was based on the mean absolute error (MAE) criterion.

A brute-force search strategy was used to tune hyperparameters for the maximum number of features (max_features) and the number of trees (n_estimators). With this approach, the value max_feature was iteratively increased from 1 to 56 features with a step of one feature, while the estimators were also iteratively increased from 5 to 1000 with a step of 5 trees. The ranges of hyper-parameters for the best RF predictive model were identified by selecting the models with the best values of MAE and R^2. Hyper-parameter ranges obtained from the best

performing models were combined with additional hyper-parameters for the number of samples and node depth (max_depth, min_samples_split and min_samples_leaf), and further optimised using randomised cross-validation. To achieve this, the RandomizedSearchCV function in the Scikit-learn module under 1000 fits (10-fold cross-validation for 100 iterations) was used. Training the RF regressor was then repeated with the identified hyper-parameters set and a new RF predictive model was generated using 80 % of the dataset. The performance of the RF model was then determined using the test data and the predicted adsorption capacity values compared with values from the dataset. Furthermore, the relative importance of features in the RF model was calculated.

4.3 Results and discussion

Zeolite ADS is receiving interest due to its demonstrated environmental benefits and cost-effectiveness. However, there remain significant gaps in understanding the zeolite ADS process. To address this challenge, we surveyed 17 studies and compiled a dataset of 31 continuous variables and 3 categorical variables with a total of 356 entries (see Supplementary Tables A1-3). We used analysis tools of increasing complexity, starting from exploring the simple pairwise linear relationships with adsorption capacity to MLR and, finally, a more complex ML RF model. Our goal was to understand the parameters (adsorbent properties, process parameters and adsorbate properties) that have a dominating influence on adsorption capacity, in order to provide insight into adsorption process design.

4.3.1 Dataset exploratory analysis

Statistical distributions of the continuous variable data revealed varying distributions with the majority of variables showing outliers (Figure A1). The response variable, adsorptive capacity, showed a right-skewed distribution ranging between 0.5 and 60.8 mgS/g (mean = 39.7 and SD 51.8). Under zeolite adsorbent properties, the surface area ranged between 141 and 720 m^2/g, which is comparable to the surface area of other adsorbents like activated carbon and low surface MOFs (Chen et al., 2018; Garg and Das, 2020). The median Si/Al ratio was 2.93, which is typical of Y- zeolites, and which confirms that they are the most studied zeolites (see Figure A2). Y- zeolites are probably most studied because of their high ability for cation exchange and their structural stability (Li et al., 2010; Liu et al., 2016). Categorical predictor variables in the dataset were also analysed for their representation in the dataset (Figure A2). The dataset had 15 different adsorbents, with MCM-22 being the most represented, with a relative abundance of 16.9 %. For adsorption conditions, the median adsorption temperature was 30 °C, which suggests that most of the experimental work was carried out at ambient conditions, which is one of the advantages of ADS (Lee and Valla, 2019). Ten different solvents were found, with iso-octane being the most represented at 32.9 % and three different adsorbates were found where TP was the most represented, at 57.9 %. The high representation of the two compounds - TP and octane - indicates that the major test for zeolites has been with model gasoline.

Missing variables in the dataset - excluding the metal ions, where it is not applicable - was determined, and three variables were identified to have missing data. See Figure 4.1 and Supplementary Table A4 for all variables.

Figure 4.1: Missing data rates for zeolite property variables in the dataset.

The highest rate of missing data was found in mesopore volume and pore size, with missing data rates of 73.3 % and 40.5 %, respectively. This suggests that adsorbent characterisation remains a challenge in terms of zeolite ADS investigation. Whether this lack of adsorbent characterisation data is due to equipment or methodological limitations is unclear, and researchers are encouraged to characterise the materials they use in full.

Missing values were imputed and changes in variable distributions were assessed (Figure 4.2). The Kolmogorov-Smirnov test found no statistically significant differences in the raw and imputed micropore data, while significant differences were found for the mesopore volume and pore size data after imputation (Supplementary Table A5). The general approach for dealing with variables with high rates of missing data - for example, the 73.3 % missing rate observed in the mesopore data - is to delete the data. This was the approach taken in similar ML studies, for example in the work done on metal sorption onto biochars (Zhu et al., 2019). However, given the established link between the three variables (mesopore, micropore and pore size) with surface area and adsorption capacity, it was determined that these variables should not be deleted, and imputed for missing data.

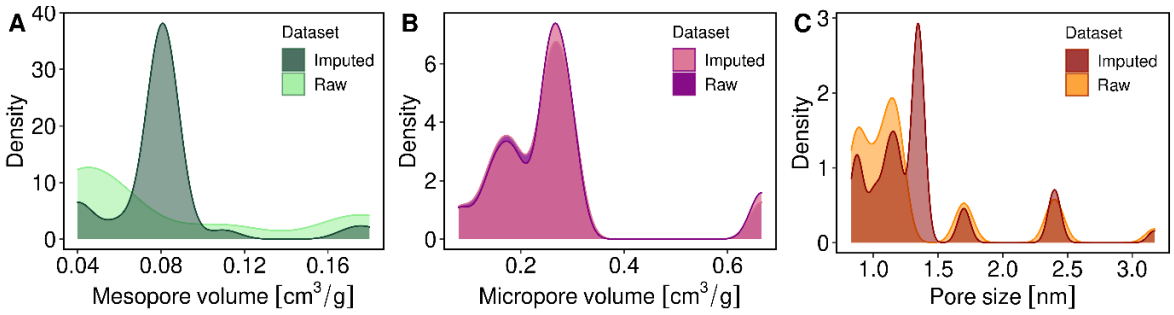

Figure 4.2: Comparison of the distribution of variables with missing data before (raw) and after imputation (imputed): (A) mesopore volume; (B) micropore; (C) pore size.

Pairwise Pearson's correlation coefficients and the corresponding p-values for all continuous variables were also analysed post-imputation (Figure 4.3 and A3 for metal related properties). Initial concentration (C_0) showed the highest correlation with adsorptive capacity, where a moderate significant correlation ($R = 0.59$, $p < 0.01$) was determined. This shows the high influence of C_0 on adsorption activity. Statistically significant correlations were also found among zeolite properties. For example, micropore volume and surface area showed a moderate significant correlation ($R = 0.34$, $p < 0.01$). This correlation is understandable since an increase in microporous volume is known to lead to an increase in the surface area (Na and Somorjai, 2015).

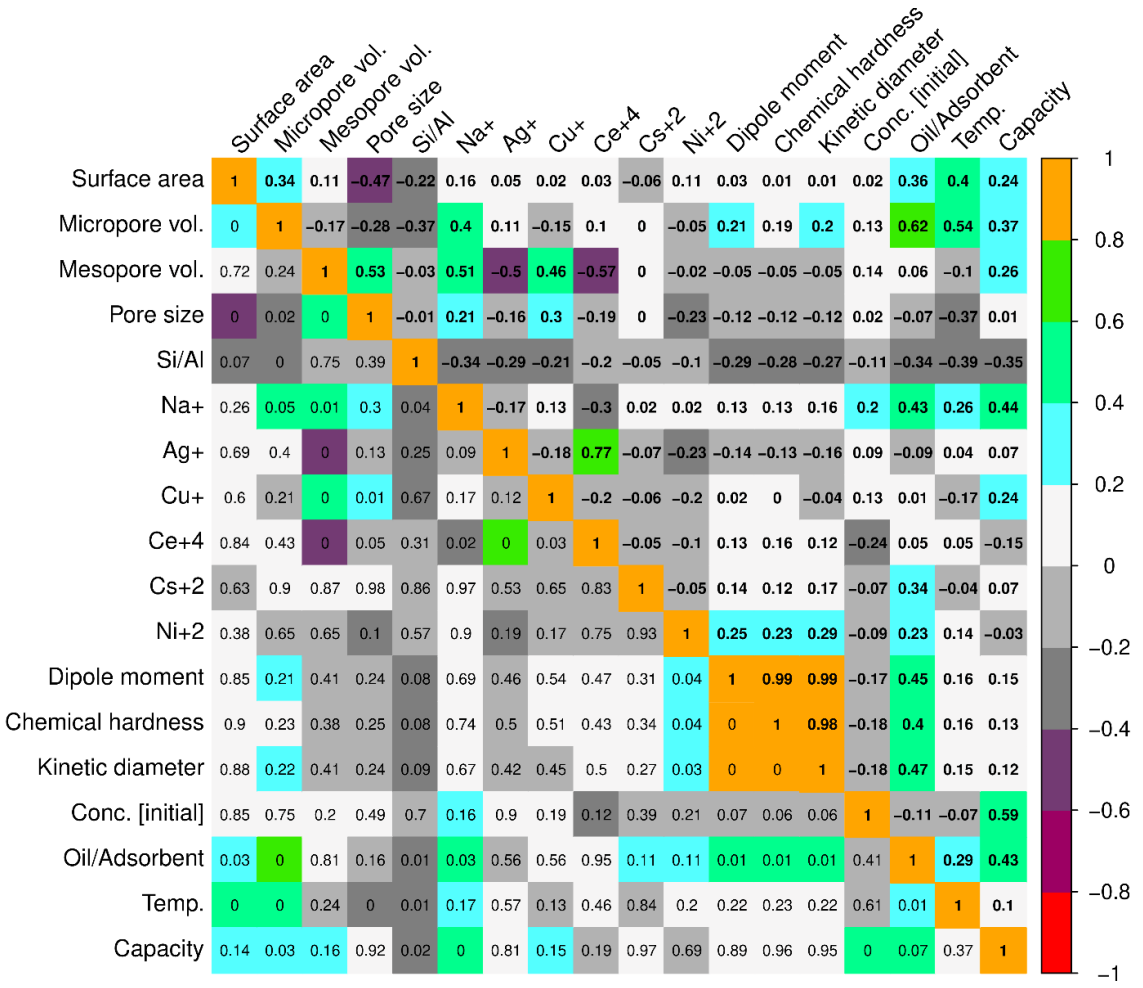

Figure 4.3: Correlation heatmap of variables in the dataset with colours corresponding to Pearson's correlation coefficient (R). The coefficients are provided in the top triangle (right of the diagonal), while the corresponding p-values are provided in the bottom triangle (left of the diagonal).

There was also a moderately negative significant correlation (R = -0.37, $p < 0.01$) between micropore volume and the Si/Al ratio. This phenomenon has been reported in other studies and was attributed to reduced crystallinity and reduction of unit cell size due to delamination processes (Keawkumay et al., 2019; Golubev et al., 2021). Statistically significant correlations were also observed between Si/Al ratio and other structural framework variables, i.e.: surface area, pore size and mesoporous volume. This may be attributed to the phenomenon of reduced crystallinity described earlier. Negative moderate insignificant correlations were also observed between the Si/Al ratio and four metal ions: Na^{+}, Ag^{+}, $Cu^{+}$and Ce^{4+}.

These moderate correlations, results are consistent with the substitution of Si^{4+}ions by Al^{3+}ions resulting in a net negative charge in the tectosilicate framework (Moshoeshoe et al., 2017). The negative sites are usually balanced by metal cations - hence the correlation. Finally, the correlation between chemical hardness, dipole moment and kinetic diameter was high (R values around 0.99); therefore one of them should be excluded so as to avoid collinearity during regression analysis.

Linear regression models for adsorptive capacity against all continuous variables were also fitted and the best performing features were identified among the three variable groups, See Figure 4.4 and Supplementary Table A6 for all variables.

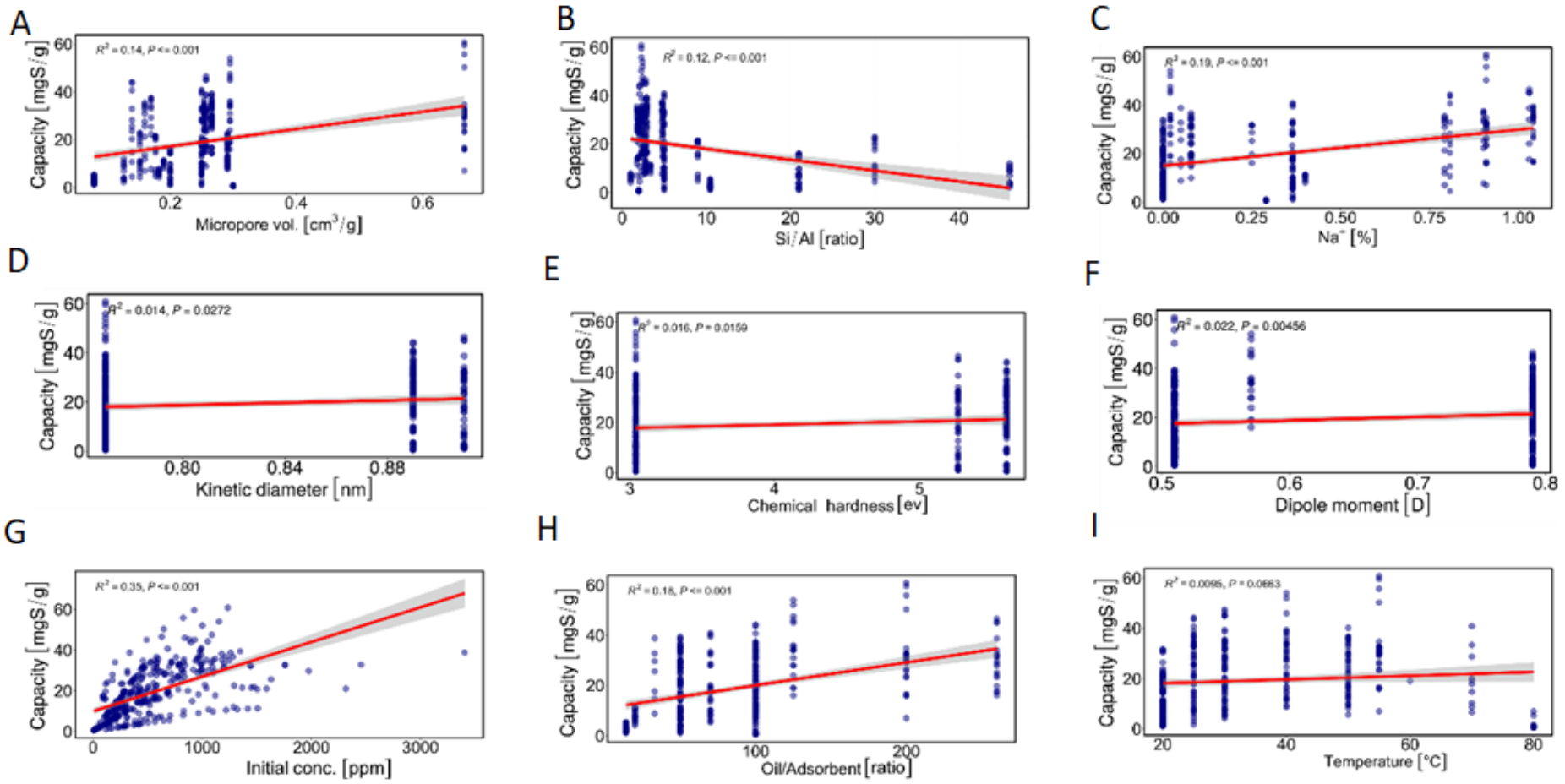

Figure 4.4: Linear regression models of variables against adsorptive capacity: A-C - zeolite adsorbent properties; D-F - adsorbate properties; G-I - ADS conditions.

The regression models for all the continuous variables against adsorptive capacity showing the distribution of residuals around the fitted regression line are provided in the supplementary material (Figure A4). The highest explanatory power of the variation in adsorptive capacity was observed under adsorption conditions for C_0 where an R^2 value of 0.35 was calculated (Figure 4.4G). Under zeolite properties, micropore volume and Si/Al ratio showed low significant R^2 values of 0.17 and 0.12 with adsorption capacity, respectively (Figures 4.4A-B). For mesopore volume, we found that the R^2 was significant, but relatively low ($R^2 = 0.07$; p-value < 0.01), explaining a very small proportion of the variation in adsorptive capacity. Zeolite metal properties showed moderate explanatory power of adsorption capacity with electro-negativity and metal amount showing the highest values within the group of variables with significant R^2 values of 0.2 and 0.19 respectively (Supplementary Table A6). It is highly likely that the imputation of zeros for unavailable data for the metal properties resulted in spurious correlations among the variables. Furthermore, significant results were also observed for ionic radius, however, the caveat is that these relationships with adsorption capacity may be spurious and a result of the imputation strategy.

Plots of residuals against fitted values generated by the linear models (Figure A5) and together with results of the gvlma analysis did not support a linear relationship with adsorptive capacity (Supplementary Table A7). This was supported by the results of the Shapiro-Wilk normality test, as all variables were significant (p-value < 0.05) for non-normality (Supplementary Table A8). Numerous hypotheses may be provided for this violation of normality in residual data. The majority of the predictor variables contained outliers (Figure A2), while a strategy of removal of outliers is conventional and has been suggested (see for example (Keawkumay et al., 2019)). In this study, outlier removal was not carried out, as it would have resulted in a significant loss of data and sacrifice of predictive power.

Furthermore, such an approach would have required the application of some criteria, the current work was conceptualised to address such questions. Literature on the Shapiro-Wilk test suggests it is not sensitive to outliers; however, its weakness with long-tailed datasets has been documented (Royston, 1992). On the other hand, it is important to note that explanations for some of the results, for example, the high explanatory power of C_0 are intuitively supported by knowledge of the experimental system and empirical data (Zhu et al., 2019; Ullah et al., 2020; Wang et al., 2020; El Hanandeh et al., 2021).

These pairwise linear models of adsorption capacity versus other predictive variables illustrate the limited power of using single variable analysis to understand ADS, with a maximum of 35% of the variation explained by C_0. The violation of assumptions of linearity is problematic; however, some of the results offer nuanced insight that agrees with our current understanding of the adsorption capacity, and the models could be improved by transformation or the use of a variance stabilising approach, as reviewed by Lin et al., (2008) and Morgenthaler and Staudte, (2012).

4.3.2 MLR model performance

Using all the predictor variables against adsorption capacity, MLR analysis was carried out, with the caveat of violations of linearity that had already been identified using the simple pairwise linear model analysis. The rationale for proceeding with MLR analysis was to gain insight into the extent that an MLR model could provide an explanation of the variation in adsorption capacity. Using the stepwise feature and model selection with StepAIC, 25 predictors were found to generate the best predictive model. Multiple linear regression analysis was then carried out using the selected features, which provided a coefficient of determination (R^2) of 0.83 (p-value < 0.01) (Table 4.1).

Diagnostic plots (Figure A6) were also used to assess assumptions of multiple linear regression analysis, and bias introduced by outliers was also observed. Violation of the assumption of normality was observed using the Shapiro-Wilk normality test (W = 0.91841, p-value < 0.001).

Table 4.1: Multiple linear regression model metrics for the best performing combination of 25 predictor variables for the ADS process.

R^2	adjusted R^2	Sigma	Statistic	p-value
0.83	0.82	0.424	65.8	< 0.001

The list of predictor variables used in the best performing model and estimates of regression coefficients are also available (Supplementary Table A9). The relative importance of variables and their contribution to the R^2 was also determined (Figure 4.5).

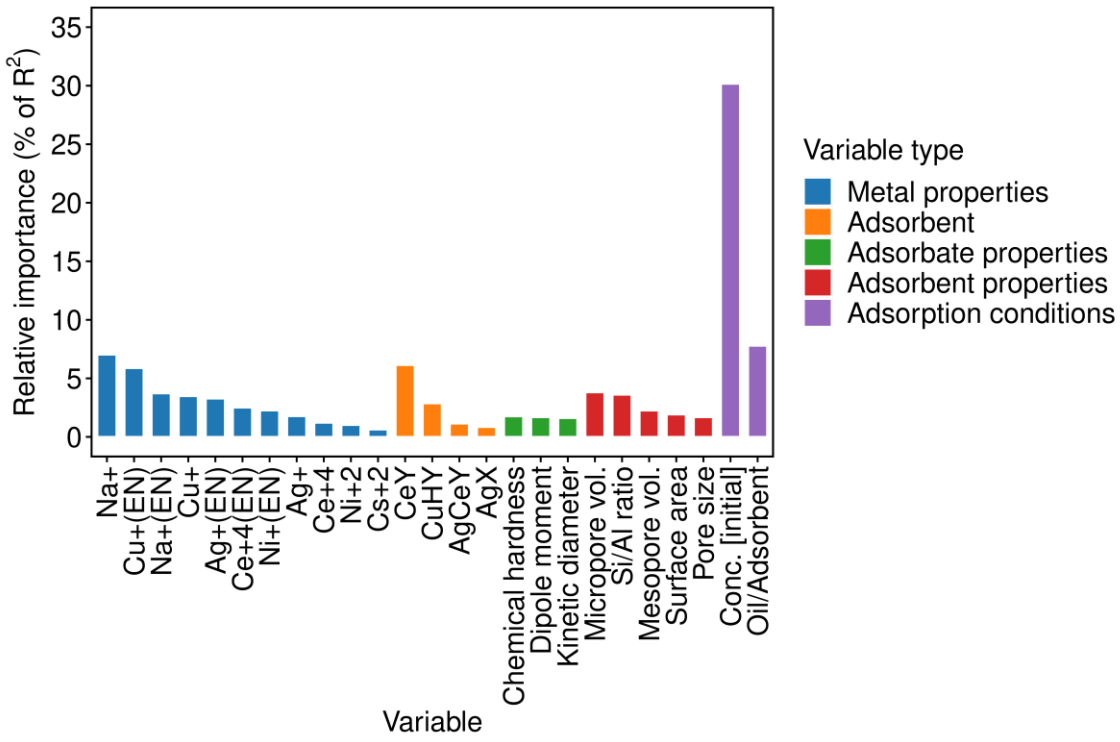

Figure 4.5: Relative importance of predictors in the best performing multiple linear model and their percentage contribution to the R^2 of 0.83.

The results of the best performing MLR model for relative importance showed that the process condition predictor C_0 explained the most variation in adsorption capacity, with a relative importance of 30.2 %. Another process condition predictor, the oil/adsorbent ratio, was also observed and showed the relative importance of 9.7 %. The identity of the adsorbent showed the third-highest relative importance, with adsorbent CeY explaining 6.5 % of the adsorption capacity variation.

4.3.3 RF model performance

The best performing number of trees and feature hyper-parameters using the predictive RF model were identified by an iterative search strategy by identifying the range of hyper-parameters that maximised and minimized the R^2 and root mean square error (RMSE), value respectively (Figure 4.6).

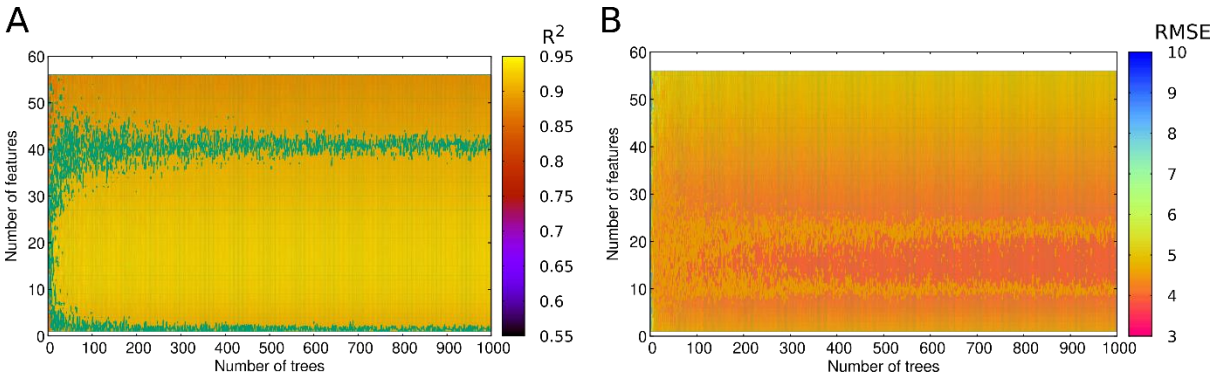

Figure 4.6**:** Hyper-parameter tuning for the number of trees and number of features in the RF model.

RF hyper-parameter tuning revealed that the best model number of trees and number of feature hyper-parameters were about 8 and 18, respectively. Additional hyper-parameters identified by the 10-fold cross-validations that were used to generate the final RF model are provided in Supplementary Table A10. The generated predictive model was found to have an R^2 of 0.93 (p-value < 0.01). (See Figure 4.7 and Supplementary Table A11 for additional model evaluation metrics.) This high R^2 value demonstrates the better predictive ability of the RF model.

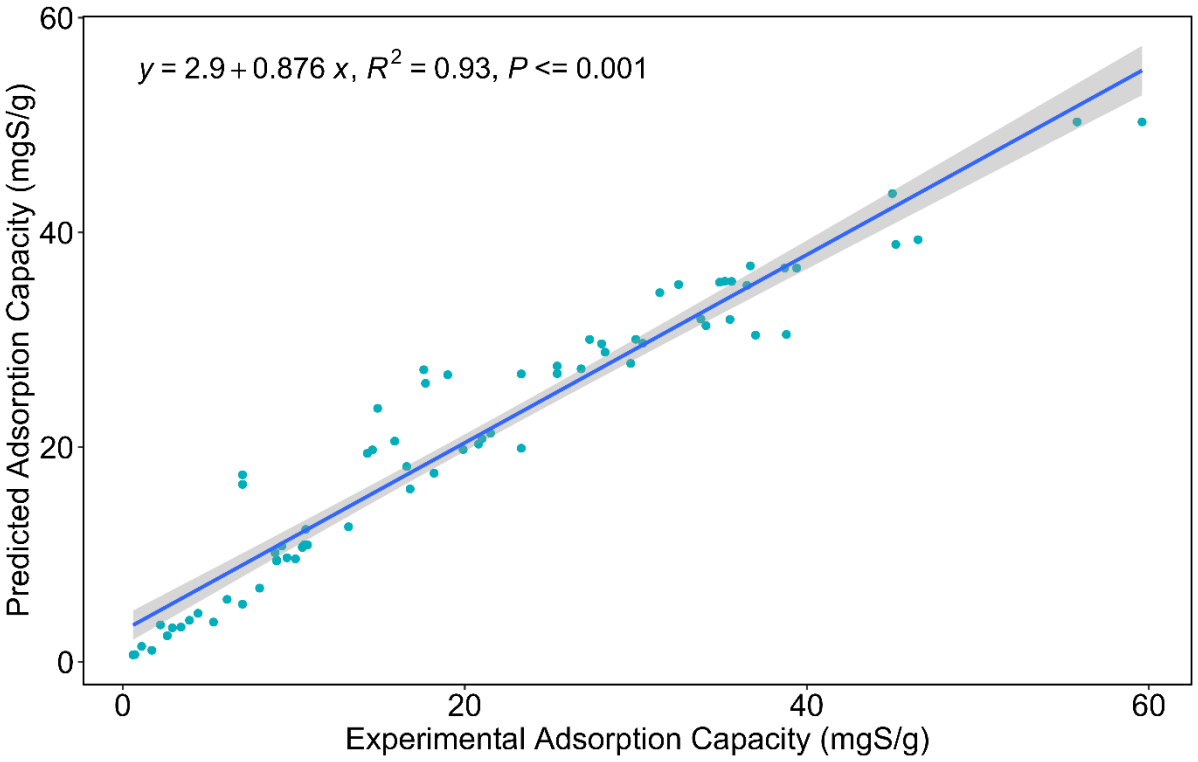

Figure 4.7: Regression analysis of predicted adsorption capacity generated by the RF model compared to experimental adsorption capacity data obtained from the literature survey.

The relative importance of RF features showed that, when summed, adsorption conditions, adsorbent properties and adsorbate properties had variable importance of 71.3%, 24.3% and 4.4%, respectively. (See Figure 4.8 and Supplementary Table A12 for the full list of predictors.)

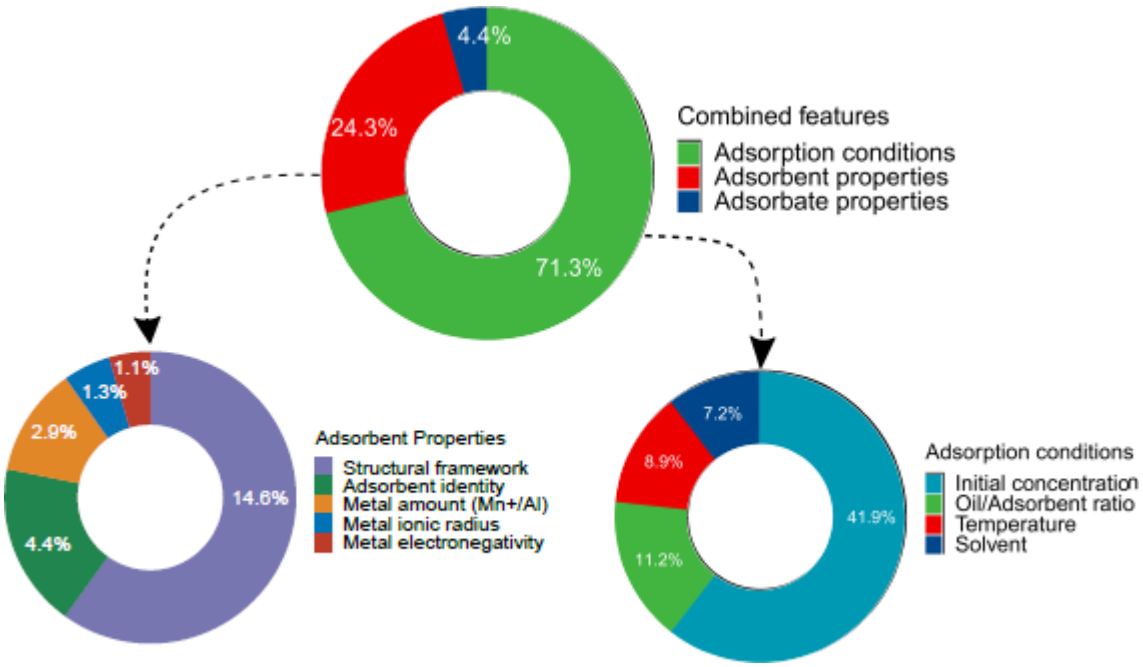

Figure 4.8**:** The overall relative importance of RF model for variables of ADS.

With adsorption conditions, C_0 showed the highest variable relative importance of 41.9 %, and the oil/adsorbent ratio, temperature and solvent showing 11.2 %, 8.9 % and 7.2 %, respectively (Figure 4.8). This high relative importance of C_0 is consistent with the observations made by Zhu et al., 2019. However, the C_0 process parameter cannot be controlled to increase adsorption capacity; instead, the C_0 parameter is determined by the fuel to be treated. The high influence of C_0 on adsorption capacity may also be explained by the high correlation (R = 0.59). However, for the variable Na^+, which also had a moderately high correlation with adsorptive capacity (R = 0.44), the relative importance was relatively lower than that of C_0. The high influence of C_0 suggests that comparing the activity of different adsorbents using adsorption capacity when the process is carried out at varying concentrations does not give a true picture of the activity of each adsorbent. Therefore, the partition coefficient (PC) (see equation 4.2) is the ideal variable to use to compare the activity of adsorbents assessed at different concentrations, because adsorption capacity is not an objective metric for use in a meaningful assessment of the actual performance of sorbents if initial concentrations of adsorbate are different (Al-Wabel et al., 2019).

$$PC = q_e/C_e \quad (4.2)$$

Where: q_e and C_e are the adsorption capacity (mg/g) and sulphur content for the equilibrium of the batch adsorption, respectively. However, there was even less information reported on the values of PC for ADS.

The oil/adsorbent ratio showed the second-highest relative influence on adsorption activity under adsorption conditions. This was expected since the number of sites available is positively correlated to the amount of adsorbent. The relatively high combined influence of the solvent identity on adsorption activity suggests that varying solvents for model fuels is not a "good" practice. It is also important to note that iso-octane showed the highest relative importance among the solvents.

The combined adsorbent properties showed a relative importance of 24.3 %, with the order of influence being: structural framework, adsorbent identity and metal ion amount, see Figure 4.9. This result suggests that, in order to improve ADS, more attention should be paid to adsorbent modification. In terms of the adsorbent properties, the metal ion amount and metal properties showed a total relative importance of 9.7 %, which demonstrates the important role played by metals in ADS. These results are consistent with the accepted understanding that ADS proceeds via pi-bonding, acid-base interactions and σ-bonds (Hernández-Maldonado et al., 2005; Lee and Valla, 2019). Metals facilitate adsorption modes, and the RF models showed the most promising metal ions as follows, in descending order: Na^{+}, Cu^{+}, Ce^{+4}, Ni^{+2}, Ag^{+} and Cs^{+2}.

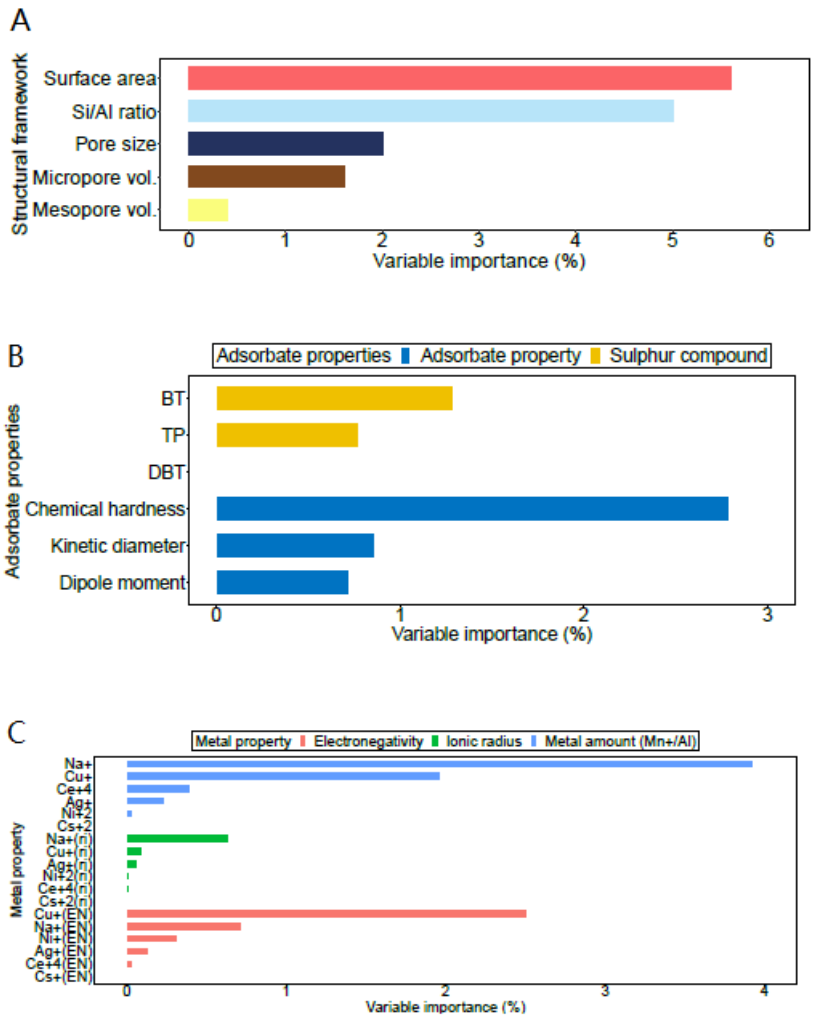

Figure 4. 9**:** RF model of the relative importance of variables for ADS A) structural framework B) adsorbate properties and C) Metal property

Among the structural framework features, surface area (5.8 %) showed the highest impact on adsorption activity. This is consistent with the expectation that an increase in the surface area results in an increase in the number of active sites; and, in this case, the surface area is paramount to even loading the metal ion, which has also been found to show a relatively high relative importance. In addition, under the structural framework, the Si/Al ratio (5.2 %) is known to influence the exchange capacity of zeolites and influence the hydrophobicity of zeolites, as stated earlier. Furthermore, zeolites with a low Si/Al ratio possess a significant amount of acid sites and these improve adsorption (Ganiyu and Lateef, 2021).

However, acidity has to be balanced with zeolite stability, which decreases with a low Si/Al ratio. Microporous volume (1.6 %) has a good correlation with surface area, as per Figure 4.3, which could have contributed to its high importance. Beyond the good correlation, adsorption activity is known to increase with micropore volume given that the adsorbate can access the pore structure of the adsorbent (Triantafyllidis and Deliyanni, 2014). Pore size (2 %) had the next highest influence, and it is also known that the kinetic diameter of TP, BT and DBT are 5.3 Å, 6 Å and 8 Å, respectively (Contreras et al., 2008). Their ability to access the pore structure is dependent on zeolite pore size. Finally, mesoporosity (0.3 %) is known to circumvent the steric hindrance and diffusion limitation in microporous materials (Chen et al., 2009; Sentorun-Shalaby et al., 2011). Tian et al., (2012) further suggested that mesoporosity also weakens the micropore-filling effect of the microporous adsorbent, and thus suppresses the non-selective adsorption of solvents. With the caveat that mesoporous volume had the highest missing data for characterisation of the adsorbent (see Figure 4.1), the displayed low influence in this work may be attributed to the data that was used did not include the highly steric derivatives of benzothiophene.

4.3.4 A machine learning model of adsorptive desulphurization

This study compared the performance of the traditional, interpretable and restrictive linear regression approach to the more advanced RF approach that uses no restrictive assumptions. The RF model outperformed the MLR model in terms of predictive accuracy. Furthermore, as discussed earlier, the MLR model violated the assumptions of a linear model. However, both approaches were in agreement about variables C_0 and the oil/adsorbent ratio being the two most influential variables in terms of explaining adsorption capacity. This affirms the challenge that researchers should be cognisant of adsorption conditions when comparing the activity of adsorbents carried out at different C_0.

The importance of the zeolite structure was also observed in both models. For example, the correlation (Figure 4.3) and linear model analysis (Figure 4.4) showed a positive relationship between adsorption capacity and the other variables, with the exception of the Si/Al ratio and the metal ion amounts of Ni^{2+} and Ce^{4+}. This negative relationship between Si/Al ratio and adsorption capacity suggests that a lower Si/Al ratio is desirable, while the literature suggests the lower limit being the stability of zeolites. With the RF model, the variables that showed more influence in terms of ADS were surface area, micropore volume, metal amounts (m^{n+}/Al ratio), Si/Al ratio and mesopore volume. There are a number of correlations/observations that we could not explain. These could be due to the current limited understanding of the adsorption process using zeolites or due to spurious correlations. The high significance of Na^{+} when the current understanding is that its substitution by transitional metal like Ag improves zeolite adsorbent activity. It is also difficult to understand why metals correlations are different, some negative and others positive, while the current understanding is that metal loading should increase with a decrease in Si/Al ratio. Finally, the high influence of metal amount and electronegativity was only observed for Cu^{+} and Na^{+}.

One of the main limitations of this study was missing data for three variables: mesopore volume, micropore volume and pore size. There are numerous algorithms and approaches for addressing the challenge of missing data and imputation (Harel and Zhou, 2007; Rässler et al., 2013), and the researchers chose a simple group mean and basic mean imputation approach for micropore volume, mesopore volume and pore size, based on the adsorbent identity. The challenges of mean imputation increasing variance, Type I errors due to reduced standard errors, and distorting relationships are well established (Stef van, 2018). As discussed earlier, significant changes in the individual distributions of the imputed variables were found, i.e. mesopore volume and pore size.

However, with micropore volume, imputation did not result in a significant change in the distribution, which was attributed to the relatively low rate of missing data compared to the other variables (Figure 4.1). Micropore volume was also found to be the 6th and 8th most influential variables for the RF and MLR models, respectively, while mesopore and pore size showed lower relative importance. Therefore, the results for the imputed variables and the resulting model require nuanced interpretation. Variability in the identity and number of metals used in the adsorbents resulted in cases where there was no data available for some entries. This data was imputed using zeros and resulted in a distribution that is not representative of the data. How this imputation strategy affected the models was not assessed and requires further study.

The correlation analysis of the continuous variables revealed multi-collinearity between some of the independent variables, with a high correlation between metals and their properties (Figure 4.3). The general approach for dealing with such variables when doing regression analysis is to remove one of the variables with a high correlation - see for example (Zhu et al., 2019). The variance inflation factor (VIF) is also commonly used to assess multicollinearity, with variables that score above a set threshold being removed (Zuur et al., 2010). In this study, variables were not explicitly dropped for multi-collinearity. The StepAIC approach used to select the best linear model minimizes the AIC score, while dropping variables where there is high multi-collinearity (Venables and Ripley, 2002) - therefore this step did not have to be carried out. The MLR model saw 22 variables being dropped and 25 variables in the selected model, including adsorption capacity, compared to the full list of 57. In contrast, the RF algorithm is robust, so multicollinearity and highly correlated variables were not removed.

Generating ML predictive models for adsorption conditions for a variety of adsorbents and processes has been the focus of several recent studies (Foroughi et al., 2020; Hafsa et al., 2020; Zuur et al., 2010). The general approach in these studies is to compare the accuracy and predictive performance of ML algorithms - usually ANN and RF. In this study, the researchers compared the more traditional approach of regression linear modelling to RF, to study ADS. First, the pairwise linear models of the individual predictor variables were analysed compared to the response variable adsorptive capacity (Figure 4.4). Next, the more complex MLR and RF models were used to understand the interactive effects of the variables. These approaches were chosen for their interpretability and insight into variable importance (Marchese Robinson et al., 2017). A deep learning ANN predictive model could have provided better accuracy and predictive power than the RF approach; however, interpretability of ANN models is a challenge (He et al., 2020) and RF was chosen instead. Therefore, interpretability was prioritised over accuracy, as there are trade-offs in satisfying each criterion (reviewed by (Bratko, 1997; Stiglic et al., 2020)). The over-arching aim of this work was to use literature survey data to address gaps and inconsistencies in the literature about which factors have the most influence on adsorption capacity in terms of ADS. Although some of the results provided here are challenging to interpret in light of our current understanding of ADS, insight into the process has been provided.

4.4 Conclusion

ADS of model fuels using zeolites was analysed using ML. Compared to MLR analysis, we found that the ML RF model provides the highest predictive power, with an R^2 value of 0.93. These results demonstrate the utility of RF over traditional linear regression approaches that are restricted by their assumption criteria. Our analysis provides a comprehensive insight into the process of ADS, ranging from the relationship between variables to the relative importance of zeolite properties and process parameters. When analysed individually, the process parameter C_0 had the highest influence on ADS activity. We also found that, when combined, the relative importance of zeolite adsorption conditions had the highest influence on ADS activity, with the most influential zeolite adsorbent properties being the structural framework and metal ion properties. Zeolites will become increasingly important as concerns over environmental protection increase. ML algorithms such as RF are useful and inexpensive approaches for gaining additional insight into zeolite ADS; however, more data and experiments are required to understand how zeolite properties and process parameters interact to influence ADS activity.

Acknowledgements

The authors are grateful for the support received from the University of South Africa (UNISA), the University of Stellenbosch, the National Research Foundation (NRF) and the Department of Science and Technology (DST) of South Africa.

Appendix A. Supplementary data

Supplementary data related to this article can be found at: **Appendix A.**

References

Abadi, M., Barham, P., Chen, J., Chen, Z., Davis, A., Dean, J., Devin, M., Ghemawat, S., Irving, G., Isard, M., Kudlur, M., Levenberg, J., Monga, R., Moore, S., Murray, D.G., Steiner, B., Tucker, P., Vasudevan, V., Warden, P., Wicke, M., Yu, Y., Zheng, X., 2016. TensorFlow: A System for Large-Scale Machine Learning, in: Proceedings of the 12th USENIX Conference on Operating Systems Design and Implementation, OSDI'16. USENIX Association, USA, pp. 265–283.

Ahmad, M.B., Soomro, U., Muqeet, M., Ahmed, Z., 2020. Adsorption of Indigo Carmine dye onto the surface-modified adsorbent prepared from municipal waste and simulation using deep neural network. J. Hazard. Mater. 124433. https://doi.org/10.1016/j.jhazmat.2020.124433

Ahmed, I., Jhung, S.H., 2016. Adsorptive desulphurization and denitrogenation using metal-organic frameworks. J. Hazard. Mater. 301, 259–276. https://doi.org/10.1016/j.jhazmat.2015.08.045

Al-Wabel, M., Elfaki, J., Usman, A., Hussain, Q., Ok, Y.S., 2019. Performance of dry water- and porous carbon-based sorbents for carbon dioxide capture. Environ. Res. 174, 69–79. https://doi.org/10.1016/j.envres.2019.04.020

Bernard, S., Heutte, L., Adam, S., 2010. A Study of Strength and Correlation in Random Forests, in: Huang, D.-S., McGinnity, M., Heutte, L., Zhang, X.-P. (Eds.), Advanced Intelligent Computing Theories and Applications. Springer Berlin Heidelberg, Berlin, Heidelberg, pp. 186–191.

Biau, G., 2012. Analysis of a Random Forests Model. J. Mach. Learn. Res. 13, 1063–1095.

Bratko, I., 1997. Machine Learning: Between Accuracy and Interpretability, in: Della Riccia, G., Lenz, H.-J., Kruse, R. (Eds.), Learning, Networks and Statistics. Springer Vienna, Vienna, pp. 163–177.

Breiman, L., 2001. Random Forests. Mach. Learn. 45, 5–32. https://doi.org/10.1023/A:1010933404324

Chen, H., Wang, Y., Yang, F.H., Yang, R.T., 2009. Desulphurization of high-sulphur jet fuel by mesoporous π-complexation adsorbents. Chem. Eng. Sci. 64, 5240–5246. https://doi.org/10.1016/j.ces.2009.08.031

Chen, Y., Mu, X., Lester, E., Wu, T., 2018. High efficiency synthesis of HKUST-1 under mild conditions with high BET surface area and CO2 uptake capacity. Prog. Nat. Sci. Mater. Int. 28, 584–589. https://doi.org/10.1016/j.pnsc.2018.08.002

Contreras, R., Cuevasgarcia, R., Ramirez, J., Ruizazuara, L., Gutierrezalejandre, A., Puentelee, I., Castillovillalon, P., Salcedoluna, C., 2008. Transformation of thiophene, benzothiophene and dibenzothiophene over Pt/HMFI, Pt/HMOR and Pt/HFAU: Effect of reactant molecular dimensions and zeolite pore diameter over catalyst activity. Catal. Today 130, 320–326. https://doi.org/10.1016/j.cattod.2007.10.007

Dehghan, R., Anbia, M., 2017. Zeolites for adsorptive desulphurization from fuels: A review. Fuel Process. Technol. 167, 99–116. https://doi.org/10.1016/j.fuproc.2017.06.015

El Hanandeh, A., Mahdi, Z., Imtiaz, M.S., 2021. Modelling of the adsorption of Pb, Cu and Ni ions from single and multi-component aqueous solutions by date seed derived biochar: Comparison of six machine learning approaches. Environ. Res. 192, 110338. https://doi.org/10.1016/j.envres.2020.110338

Foroughi, M., Ahmadi Azqhandi, M.H., Kakhki, S., 2020. Bio-inspired, high, and fast adsorption of tetracycline from aqueous media using Fe3O4-g-CN@PEI-β-CD nanocomposite: Modeling by response surface methodology (RSM), boosted regression tree (BRT), and general regression neural network (GRNN). J. Hazard. Mater. 388, 121769. https://doi.org/10.1016/j.jhazmat.2019.121769

Ganiyu, S.A., Lateef, S.A., 2021. Review of adsorptive desulphurization process: Overview of the non-carbonaceous materials, mechanism and synthesis strategies. Fuel 294, 120273. https://doi.org/10.1016/j.fuel.2021.120273

Garg, S., Das, P., 2020. Microporous carbon from cashew nutshell pyrolytic biochar and its potential application as CO2 adsorbent. Biomass Convers. Biorefinery 10, 1043–1061. https://doi.org/10.1007/s13399-019-00506-1

Golubev, I.S., Dik, P.P., Kazakov, M.O., Pereyma, V.Yu., Klimov, O.V., Smirnova, M.Yu., Prosvirin, I.P., Gerasimov, E.Yu., Kondrashev, D.O., Golovachev, V.A., Vedernikov, O.S., Kleimenov, A.V., Noskov, A.S., 2021. The effect of Si/Al ratio of zeolite Y in NiW catalyst for second stage hydrocracking. Catal. Today S0920586121000444. https://doi.org/10.1016/j.cattod.2021.01.014

Goodfellow, I., Bengio, Y., Courville, A., Bengio, Y., 2016. Deep learning. MIT press Cambridge.

Hafsa, N., Rushd, S., Al-Yaari, M., Rahman, M., 2020. A Generalized Method for Modeling the Adsorption of Heavy Metals with Machine Learning Algorithms. Water 12. https://doi.org/10.3390/w12123490

Harel, O., Zhou, X.-H., 2007. Multiple imputation: review of theory, implementation and software. Stat. Med. 26, 3057–3077. https://doi.org/10.1002/sim.2787

He, C., Ma, M., Wang, P., 2020. Extract interpretability-accuracy balanced rules from artificial neural networks: A review. Neurocomputing 387, 346–358. https://doi.org/10.1016/j.neucom.2020.01.036

Hernández-Maldonado, A.J., Yang, F.H., Qi, G., Yang, R.T., 2005. Desulphurization of transportation fuels by π-complexation sorbents: Cu(I)-, Ni(II)-, and Zn(II)-zeolites. Fuel Process. PEM Fuel Cells Adv. Cataysts Adsorbents Electrocatalysts 56, 111–126. https://doi.org/10.1016/j.apcatb.2004.06.023

Howard, J., Gugger, S., 2020. Fastai: A Layered API for Deep Learning. Information 11. https://doi.org/10.3390/info11020108

Jacobs, P.A., Flanigen, E.M., Jansen, J.C., Bekkum, H. van, 2001. Introduction to zeolite science and practice. Elsevier science.

Jordan, M.I., Mitchell, T.M., 2015. Machine learning: Trends, perspectives, and prospects. Science 349, 255. https://doi.org/10.1126/science.aaa8415

Kabacoff, R., 2015. R in Action: Data Analysis and Graphics with R. Manning Publications Co., USA.

Keawkumay, C., Rongchapo, W., Sosa, N., Suthirakun, S., Koleva, I.Z., Aleksandrov, H.A., Vayssilov, G.N., Wittayakun, J., 2019. Paraquat adsorption on NaY zeolite at various Si/Al ratios: A combined experimental and computational study. Mater. Chem. Phys. 238, 121824. https://doi.org/10.1016/j.matchemphys.2019.121824

Lee, K.X., Valla, J.A., 2019. Adsorptive desulphurization of liquid hydrocarbons using zeolite-based sorbents: a comprehensive review. React. Chem. Eng. 4, 1357–1386. https://doi.org/10.1039/C9RE00036D

Li, Q., Zhang, Y., Cao, Z., Gao, W., Cui, L., 2010. Influence of synthesis parameters on the crystallinity and Si/Al ratio of NaY zeolite synthesized from kaolin. Pet. Sci. 7, 403–409. https://doi.org/10.1007/s12182-010-0085-x

Lin, S.M., Du, P., Huber, W., Kibbe, W.A., 2008. Model-based variance-stabilizing transformation for Illumina microarray data. Nucleic Acids Res. 36, e11–e11. https://doi.org/10.1093/nar/gkm1075

Liu, Z., Shi, C., Wu, D., He, S., Ren, B., 2016. A Simple Method of Preparation of High Silica Zeolite Y and Its Performance in the Catalytic Cracking of Cumene. J. Nanotechnol. 2016, 1–6. https://doi.org/10.1155/2016/1486107

Ma, L., Yang, R.T., 2007. Heats of Adsorption from Liquid Solutions and from Pure Vapor Phase: Adsorption of Thiophenic Compounds on NaY and 13X Zeolites. Ind. Eng. Chem. Res. 46, 4874–4882. https://doi.org/10.1021/ie070336i

Mahmoudi, R., 2016. A Systematic Study on the Effect of Desilication of Clinoptilolite Zeolite on its Deep-Desulphurization Characteristics 9.

Marchese Robinson, R.L., Palczewska, A., Palczewski, J., Kidley, N., 2017. Comparison of the Predictive Performance and Interpretability of Random Forest and Linear Models on Benchmark Data Sets. J. Chem. Inf. Model. 57, 1773–1792. https://doi.org/10.1021/acs.jcim.6b00753

Mguni, L.L., Yao, Y., Liu, X., Yuan, Z., Hildebrandt, D., 2019. Ultra-deep desulphurization of both model and commercial diesel fuels by adsorption method. J. Environ. Chem. Eng. 7, 102957. https://doi.org/10.1016/j.jece.2019.102957

Morgenthaler, S., Staudte, R.G., 2012. Advantages of Variance Stabilization. Scand. J. Stat. 39, 714–728.

Moshoeshoe, M., Nadiye-Tabbiruka, M.S., Obuseng, V., 2017. Zeolites, Zeolite crystal structure, Zeolite applications, Zeolite properties. Am. J. Mater. Sci. 26.

Na, K., Somorjai, G.A., 2015. Hierarchically Nanoporous Zeolites and Their Heterogeneous Catalysis: Current Status and Future Perspectives. Catal. Lett. 145, 193–213. https://doi.org/10.1007/s10562-014-1411-5

Pedregosa, F., Varoquaux, G., Gramfort, A., Michel, V., Thirion, B., Grisel, O., Blondel, M., Prettenhofer, P., Weiss, R., Dubourg, V., Vanderplas, J., Passos, A., Cournapeau, D., Brucher, M., Perrot, M., Duchesnay, E., 2011. Scikit-learn: Machine Learning in Python. J. Mach. Learn. Res. 12, 2825–2830.

Peña, E.A., Slate, E.H., 2006. Global Validation of Linear Model Assumptions. J. Am. Stat. Assoc. 101, 341–354. https://doi.org/10.1198/016214505000000637

R Core Team, 2019. R: A Language and Environment for Statistical Computing. R Foundation for Statistical Computing, Vienna, Austria.

Rässler, S., Rubin, D.B., Zell, E.R., 2013. Imputation. WIREs Comput. Stat. 5, 20–29. https://doi.org/10.1002/wics.1240

Royston, P., 1992. Approximating the Shapiro-Wilk W-test for non-normality. Stat. Comput. 2, 117–119. https://doi.org/10.1007/BF01891203

Sentorun-Shalaby, C., Saha, S.K., Ma, X., Song, C., 2011. Mesoporous-molecular-sieve-supported nickel sorbents for adsorptive desulphurization of commercial ultra-low-sulphur diesel fuel. Appl. Catal. B Environ. 101, 718–726. https://doi.org/10.1016/j.apcatb.2010.11.014

Sharma, N., 2018. Ways to Detect and Remove the Outliers. Data Sci.

Shi, Y., Yang, X., Tian, F., Jia, C., Chen, Y., 2012. Effects of toluene on thiophene adsorption over NaY and Ce(IV)Y zeolites. J. Nat. Gas Chem. 21, 421–425. https://doi.org/10.1016/S1003-9953(11)60385-X

Song, Hua, Gao, H., Song, Hualin, Yang, G., Li, X., 2016. Effects of Si/Al Ratio on Adsorptive Removal of Thiophene and Benzothiophene over Ion-Exchanged AgCeY Zeolites. Ind. Eng. Chem. Res 55, 3813−3822.

Stef van, B., 2018. Flexible Imputation of Missing Data, 2nd ed. Chapman & Hall/CRC, Boca Raton.

Stiglic, G., Kocbek, P., Fijacko, N., Zitnik, M., Verbert, K., Cilar, L., 2020. Interpretability of machine learning-based prediction models in healthcare. WIREs Data Min. Knowl. Discov. 10, e1379. https://doi.org/10.1002/widm.1379

Szulejko, J.E., Kim, K.-H., Parise, J., 2019. Seeking the most powerful and practical real-world sorbents for gaseous benzene as a representative volatile organic compound based on performance metrics. Sep. Purif. Technol. 212, 980–985. https://doi.org/10.1016/j.seppur.2018.11.001

Tan, P., Jiang, Y., Sun, L.-B., Liu, X.-Q., AlBahily, K., Ravon, U., Vinu, A., 2018. Design and fabrication of nanoporous adsorbents for the removal of aromatic sulphur compounds. J. Mater. Chem. A 6, 23978–24012. https://doi.org/10.1039/C8TA09184F

Tian, F., Yang, X., Shi, Y., Jia, C., Chen, Y., 2012. Adsorptive desulphurization over hierarchical beta zeolite by alkaline treatment. J. Nat. Gas Chem. 21, 647–652. https://doi.org/10.1016/S1003-9953(11)60414-3

Triantafyllidis, K.S., Deliyanni, E.A., 2014. Desulphurization of diesel fuels: Adsorption of 4,6-DMDBT on different origin and surface chemistry nanoporous activated carbons. Chem. Eng. J. 236, 406–414. https://doi.org/10.1016/j.cej.2013.09.099

Ullah, S., Hussain, S., Ahmad, W., Khan, H., Khan, K.I., Khan, S.U., Khan, S., 2020. Desulphurization of Model Oil through Adsorption over Activated Charcoal and Bentonite Clay Composites. Chem. Eng. Technol. 43, 564–573. https://doi.org/10.1002/ceat.201900203

Velu, S., Ma, X., Song, C., 2003. Selective adsorption for removing sulphur from jet fuel over zeolite-based adsorbents. Ind. Eng. Chem. Res. 42, 5293–5304.

Velu, S., Song, C., Engelhard, M.H., Chin, Y.-H., 2005. Adsorptive Removal of Organic Sulphur Compounds from Jet Fuel over K-Exchanged NiY Zeolites Prepared by Impregnation and Ion Exchange. Ind. Eng. Chem. Res. 44, 5740–5749. https://doi.org/10.1021/ie0488492

Venables, W.N., Ripley, B.D., 2002. Modern Applied Statistics with S, Fourth. ed. Springer, New York.

Wang, J., Zhang, Q., Yang, H., Qiao, C., 2020. Adsorptive Desulphurization of Organic Sulphur from Model Fuels by Active Carbon Supported Mn (II): Equilibrium, Kinetics, and Thermodynamics. Int. J. Chem. Eng. 2020, 1–12. https://doi.org/10.1155/2020/2813946

Wang, L. k, Pereira, N.C., Hung, Y.-T., 2005. Advanced air and noise pollution control. Human Press Inc, Totowa, New Jersey.

Xiao, J., Li, Z., Liu, B., Xia, Q., Yu, M., 2008. Adsorption of benzothiophene and dibenzothiophene on ion-impregnated activated carbons and ion-exchanged Y zeolites. Energy Fuels 22, 3858–3863.

Yang, W., Fidelis, T.T., Sun, W.-H., 2020. Machine Learning in Catalysis, From Proposal to Practicing. ACS Omega 5, 83–88. https://doi.org/10.1021/acsomega.9b03673

Zhou, D.-H., Wang, Y.-Q., He, N., Yang, G., 2006. The π-complexation mechanisms of Cu(I), Ag(I)/zeolites for desulphurization. Acta Phys. -Chim. Sin. 22, 542–547.

Zhu, X., Wan, Z., Tsang, D.C.W., He, M., Hou, D., Su, Z., Shang, J., 2021. Machine learning for the selection of carbon-based materials for tetracycline and sulfamethoxazole adsorption. Chem. Eng. J. 406, 126782. https://doi.org/10.1016/j.cej.2020.126782

Zhu, X., Wang, X., Ok, Y.S., 2019. The application of machine learning methods for prediction of metal sorption onto biochars. J. Hazard. Mater. 378, 120727. https://doi.org/10.1016/j.jhazmat.2019.06.004

Zuur, A.F., Ieno, E.N., Elphick, C.S., 2010. A protocol for data exploration to avoid common statistical problems. Methods Ecol. Evol. 1, 3–14. https://doi.org/10.1111/j.2041-210X.2009.00001.x

5. ADSORPTION DESULPHURIZATION USING COMMERCIAL ADSORBENTS

This work was has been published in the Journal of Environmental Chemical Engineering, Volume 7, Issue 2, 2019, 102957, ISSN 2213-3437. 102957.

Summary

Selective adsorption for removing sulphur from diesel fuel has emerged as a potential economically viable and effective alternative method to achieve the stringent environmental regulations for sulphur levels in diesel. In this chapter, the sulphur removing activity of three different types of activated charcoal (AC, T103 and T104) and two molecular sieves (MS)-13X and 5 A- were investigated, using both model diesel and commercial diesel. It was observed that AC, T103 and T104 displayed similar good sulphur removing activity and stability with both the model diesel (initial sulphur content: 1000 ppm) and commercial diesel (initial sulphur content: 43 ppm), with the sulphur removal efficiency varying from 60% up to 90% under the reaction conditions used in this work. These results also suggested that the adsorbents were better suited to polishing low sulphur diesel, to achieve ultra-low sulphur content. The experimental data for the adsorption of DBT fitted the pseudo-second-order kinetic equation more closely, which suggests chemical adsorption activity between DBT and the adsorbents AC, T103, T104 and MS 13X. Further experimental work, using commercial diesel with 43 ppm sulphur content, revealed that the adsorption affinity for different sulphur compounds in conventional diesel decreases in the following order: 4- MDBT≫ 4,6-DMDBT˜4 E,6-MDBT˜2,4,6-TMDBT˜1,4,6-TMDBT. It is believed this is due to steric hindrance. The decrease in activity with molecular weight epitomizes the limitations of the adsorbents in removing refractory organic sulphur. In conclusion, activated charcoals are much more suitable for the task of deep desulphurization of diesel fuels than are molecular sieves.

Keywords: sulphur; model diesel; commercial diesel; adsorption; activated carbon; molecular sieves.

5.1 Introduction

Deep desulphurization of diesel has gained significant importance because crude oil has a high sulphur content. Global concern has arisen due to the combustion of the sulphur compounds present in diesel. These compounds include thiophene, mercaptan and sulfides, which combust to form SO_2, which, in turn, reacts with oxygen to produce SO_3 (Shiraishi et al., 2002). Both SO_2 and SO_3 are the main chemicals that are precursors to acid rain, which is detrimental to the environment. Another reason for the attempts by fuel producers to reduce the sulphur content is that it affects fuel cell applications (Ma et al., 2002b; Tran et al., 2018) and catalytic converters (Chandra Srivastava, 2012).

Although the new stringent environmental regulations have succeeded in reducing the sulphur level in diesel produced locally, diesel fuel from Africa has a considerably higher sulphur content than diesel made in the developed countries. This topic has, therefore, become a priority for researchers and engineers in Africa. At present, oil desulphurization technology can be divided into two broad categories: conventional hydrodesulphurization (HDS) and non-HDS (NHDS) (Duarte et al., 2011). Although HDS is a mature technology, it has several shortcomings, for example, the expense attributable to the high pressure and high temperature required for the reaction, and the need for large amounts of hydrogen (Xuemei et al., 2008). It is, therefore, necessary to develop alternative processes to produce low-sulphur fuels. There are a number of methods that offer a potential solution. These include the use of ionic liquids, oxidation, adsorption, solvent extraction, and photochemical, biochemical, catalytic and electrochemical processes.

Using adsorbents to selectively remove the sulphur compounds in liquid hydrocarbon fuels is one of the promising approaches for producing ultra-clean fuel (Kim et al., 2006; Tang et al., 2016). A number of researchers have reported on the activity of a variate of adsorbents; these include: activated carbon (Kim et al., 2006; Yu et al., 2013); metal/metal oxides (Jeevanandam et al., 2005; Selvavathi et al., 2009; Shakirullah et al., 2009); bimetallics (Al. Swat et al., 2017; Danmaliki and Saleh, 2017; Saleh et al., 2018); zeolites (Salem, 1994; Velu et al., 2003). The use of activated carbon as a desulphurization adsorbent has been reported frequently; these are widely used because of their porous structure and large surface area. Adsorption of dibenzothiophene (DBT) has been reported to be dependent on the carboxylic group/acidic strength of the adsorbent and the pore structure (Yu et al., 2005; Yang et al., 2007; Seredych and Bandosz, 2010).

It has been further suggested by some researchers that the presence of methyl groups on DBT enhances selective adsorption of these sulphur compounds on activated carbon. This has been attributed to an increase in electron density of the aromatic system or an increase in the delocalized π electrons (Selvavathi et al., 2009; Yu et al., 2013). Contrarily, other researchers (Kim et al., 2006) have observed smaller sulphur compounds being adsorbed faster, which they attribute to steric hindrances encountered by bigger sulphur compounds.

For purposes of understanding the adsorption kinetics of sulphur compounds, model diesel has generally been used. Adsorption of conventional diesel has been investigated by a few researchers (Ma et al., 2002a; Bu et al., 2011). Most of the work that has been done on commercial fuel has focused on overall sulphur removal (Sano, 2004; Han et al., 2014; Olajire et al., 2017; Shah et al., 2018). In the work done by Hernández-Maldonado and Yang, 2004, four individual sulphur compounds (BT, DBT, 4MDBT and 4,6DMDBT) were looked at, using a fixed bed, and the researchers reported that the breakthrough of the four compounds occurred instantly. To the best of our knowledge, no work has been reported on the adsorption affinity of sulphur in commercial diesel, including trimethyl dibenzothiophene (TMDBT).

The adsorption mechanism for sulphur compounds over activated carbon is still not fully understood (Selvavathi et al., 2009; Sarda et al., 2012). The adsorption of sulphur becomes more complex with conventional diesel, as there are many compounds that can potentially compete with sulphur compounds; these include: monoaromatics, polyaromatics, nitrogen-heterocyclic aromatics and additives. In a multiple-adsorbing system, the adsorbates compete for the available adsorption sites on the adsorbent. In this case, the equilibrium loading (q_{eq}) of adsorbate depends on the equilibrium concentration of all adsorbates, as given by equation 5.1 below. This demonstrates the complexity of multi-solute adsorption and underlines the difficulty of determining complete mixture equilibria by experimental measurements (Worch, 2012).

$$q_{eq,i} = f(c_{eq,1}, c_{eq,2}, c_{eq,3}, \ldots\ldots, c_{eq,N}) \qquad (5.1)$$

Where: $q_{eq,i}$ is equilibrium loading of component i; C_{eqi} is equilibrium concentration for a system with N components.

Because of this complex system, there is a challenge in that the adsorbent could competitively adsorb the non-sulphur containing hydrocarbons. However, surface functionalization has been reported to improve selectivity (Shah et al., 2017).

In this work, the adsorption performance of five kinds of adsorbents was investigated for desulphurization using both model diesel and commercial diesel. The adsorbents used in this work include: three kinds of activated carbons, i.e. AC, T103 and T104; and two kinds of molecular sieves, i.e. 13X and 5A. Of these, T103 and T104 are the commercial adsorbents used for gas-phase sulphur removal, and these have not been reported for use in liquid phase sulphur removal. The effect of adsorbent quantity, initial concentration and adsorption time was also investigated. Additionally, the adsorption kinetics of the model and conventional diesel are discussed in this work. Finally, a comparative study was done on the adsorption affinity of different sulphur compounds when using conventional diesel.

5.2 Materials and method

5.2.1 Material

Hexadecane (99 %), toluene (99.5 %) and DBT (98 %) were obtained from Sigma Aldrich. The commercial diesel was bought from a garage in Johannesburg, South Africa. The absorbents used for this work - activated charcoal (AC) and molecular sieves 13X and 5A - were also obtained from Sigma Aldrich. The activated carbon T103 and T104 (T103 and T104) were obtained from Tongxing Chemical Co., Ltd, Henan Province, China. All the absorbents were dried overnight in an oven and then crushed and sieved. The particles in the range 2000-1180 µm were used in the adsorption experiments.

5.2.2 Adsorption experiments

Adsorption experiments were carried out with commercial diesel and model diesel. The model diesel was synthesized using 85 v/v% hexadecane, 15 v/v% toluene and varying amounts of DBT, so as to create different initial sulphur concentrations. The adsorption experiments were carried out using a stirred basket reactor at atmospheric pressure and the adsorbent quantity was varied as a weight percentage of the total diesel mass.

5.2.3 Analysis

Samples taken during adsorption experiments were analyzed using a 7890B Agilent Gas Chromatograph (GC) with two detectors - FID and Pulsed Flame Photometric Detector (PFPD). A J&W DB-1 GC capillary column (30 m length, 0.32 mm internal diameter, and 0.25 µm film thickness) was used. The temperature of the detector was set at 300 °C. The oven temperature was initially held at 50 °C for 0.5 min, then increased at a rate of 10 °C/min to 300 °C, and then held at 300 °C for 5 min. Nitrogen gas was used as a gas carrier at a flow rate of 1.2 mL/min.

After the separation of each component in the diesel by the GC capillary column, the sulphur substances were detected and quantified by the PFPD detector. Figure 5.1 shows the sulphur components analysis when using GC-PFPD for both the model diesel and commercial diesel

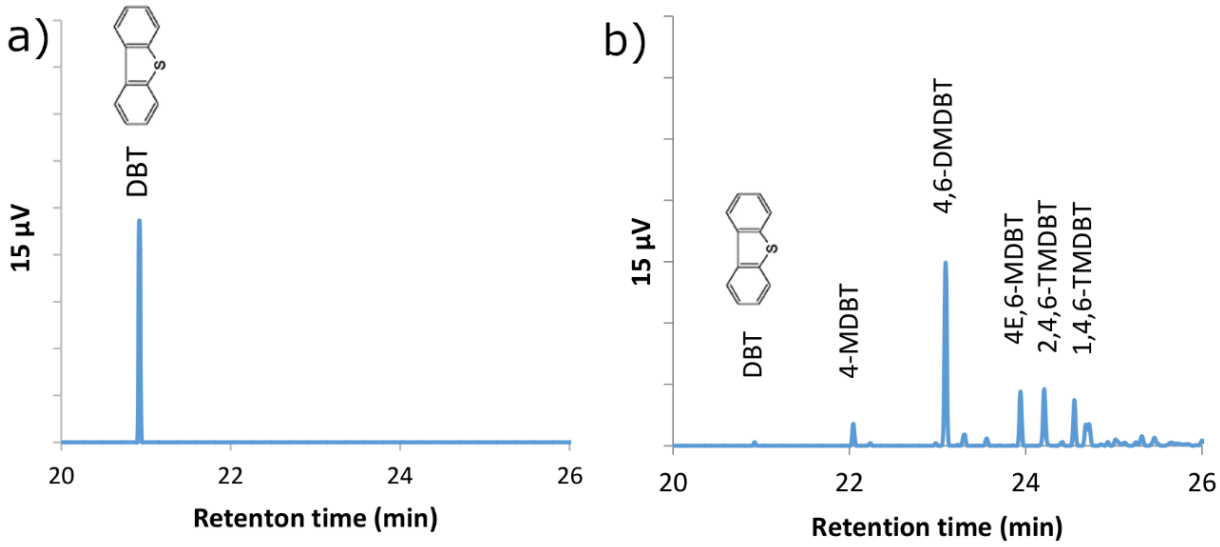

Figure 5.1: Diesel chromatogram from GC-PFPD for: a) model diesel; b) commercial diesel

Quantification of the major sulphur compounds was carried out using a normalization method (Safa et al., 2017), with the concentration of each sulphur compound being determined by the following equation (5.2):

$$C_{s,i} = C_{s,ref} \frac{A_i^{0.5}}{A_{ref}^{0.5}} \qquad (5.2)$$

Where: $C_{S,\ ref}$ is the sulphur concentration in the reference sample; A_i is the peak area corresponding to the sulphur compound to be measured - i; and A_{ref} is the area of the reference peak in the GC-PFPD chromatograms. The relative error for analysis of the sulphur compounds is less than 6 %.

5.2.4 Characterisation

Fourier-Transform Infrared Spectroscopy (FTIR) recordings were done using a Bruker Tensor 27 ATR in the range 4000–400 cm^{-1} to determine functional groups in the adsorbents. The adsorbents were mixed with KBr to produce pellets for analysis. Boehm's titration was carried out on adsorbents to determine the acid strength of different surface groups (Momcilovic et al., 2012). The Brunauer–Emmett–Teller (BET) analysis was performed to determine the surface area and pores distribution by N_2 adsorption, using NOVA 1200e.

The structure of the catalyst system was analyzed using a Philips PW 3040/60 X-ray diffraction machine with a CuKα (λ=1.54) radiation. Samples were scanned over a 2θ range of 5–90°, a 0.02° step size and a scan speed of 0.04 s/step.

5.3 Results and discussion

5.3.1 Characterisation

The comparison of the FTIR results for the fresh adsorbents and the used adsorbents is shown in Figure 5.2. Activated charcoal and activated carbon T103 and T104 had similar bands before and after the reaction. The major bands observed before adsorption were at 1000, 1312, 1714, 2991 and 3500 cm^{-1}. Bands between 1000 and 1450 cm^{-1} indicate oxygen surface functional groups, namely alcoholic, phenolic and carboxylic (C–O stretching and O–H bending). The band observed at 1714 cm^{-1} was assigned either to lactone groups or to non-aromatic carboxyl groups. Adsorption bands below 950 cm^{-1} can be assigned to the out of plane deformation vibration of C-H groups that are located at the edges of aromatic planes (Moreno-Castilla et al., 2000; Mahalakshmy et al., 2009). After adsorption, the bands that were observed were 1533, 1724, 2853, 2922 and 2960 cm^{-1}. These well-established bands were attributed to -CH_2- and CH_3 from hexadecane (Patiño-Herrera et al., 2015). With molecular sieves, the vibration of their framework gives rise to typical bands in the mid and far-infrared range. These are due to external and internal vibrations of the $TO_4/_2$ tetrahedra (T = Si or Al). An intense band at around 990 cm^{-1} along with a weak shoulder ~1100 cm^{-1} corresponds to T-O-T asymmetric stretching vibration. In addition: a band appearing at around 745 cm^{-1} could be attributed to symmetrical stretching vibrations related to external linkages of TO_4 units in the molecular sieve structure; a band at around 605 cm^{-1} corresponds to the presence of a double ring in the molecular sieve framework (Sharma et al., 2016).

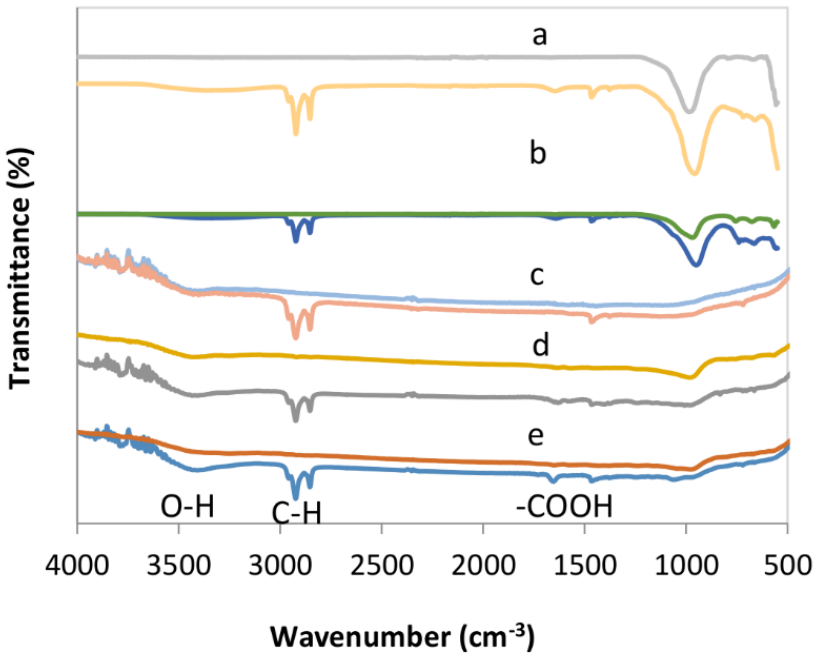

Figure 5. 2: FTIR for adsorbents: a) MS 5 A; b) MS 13X; c) AC; d) AC T104; e) AC T103

MS 13X was observed to have major peaks at 5.99º, 9.95º, 15.47º, 23.42º and 26.76º; these were attributed to "distorted" sodalite units (with point symmetry Td) in tetrahedral coordination, with each sodalite unit connected to its neighbour by six bridge oxygen ions. While the major peaks for MS 5 A were 7.10º, 10.13º, 12.44º, 21.70 º and 24.00º, these were attributed to sodalite units (with point symmetry Oh) in a simple cubic arrangement. The three AC samples were observed to have broad diffraction peaks at 24º and 43º, which is consistent with graphitic carbon (see Figure 5.3).

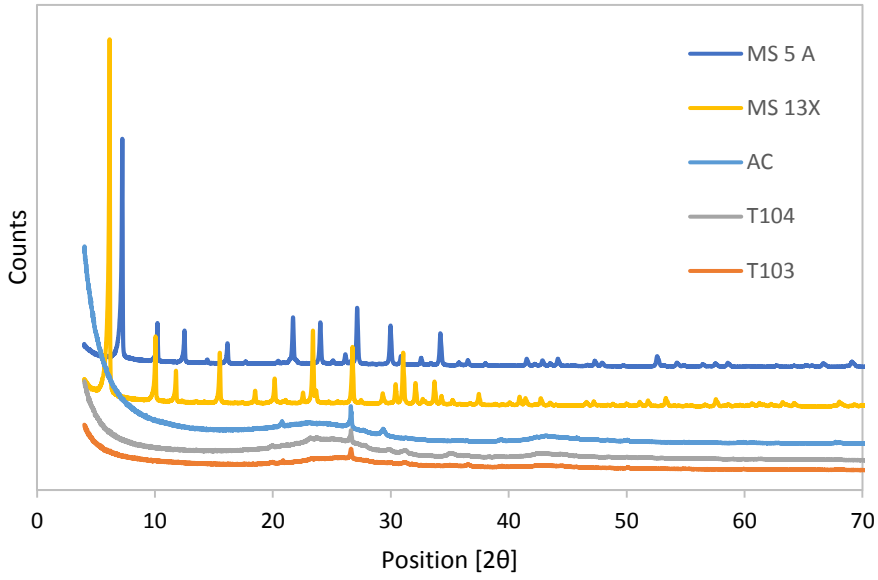

Figure 5. 3: XRD spectrum for adsorbents

Boehm's titration results are given in Table 5.1 below. The results show the presence of phenolic, lactonic and carboxylic groups, as indicated in the FTIR results. Little difference in the acid strength of adsorbents was observed. Therefore, any difference in activity cannot be attributed to acidity.

Table 5.1: Boehm's titration and BET results

	Phenolic µmol/g	Lactonic µmol/g	Carboxylic µmol/g	Total µmol/g	BET m^2/g
AC	908	105	445	1458	602
T104	913	93	458	1463	526
T103	900	95	425	1420	506
MS 13X	-	-	-	-	405
MS 5A	-	-	-	-	416

From the BET results, it was observed that AC had the biggest surface area. In summary, the surface area for the adsorbents was observed to decrease in the following order: AC> T104~ T103>MS 5A~MS 13X. The isotherm curves for T103, T104, MS 13X and MS 5A were observed to have a well-defined plateau and can, therefore, be classified as Type 1, in

accordance with the IUPAC classification (highly microporous). On the other hand, AC was observed to exhibit hysteresis, which suggests its mesoporosity (Figure 5.4).

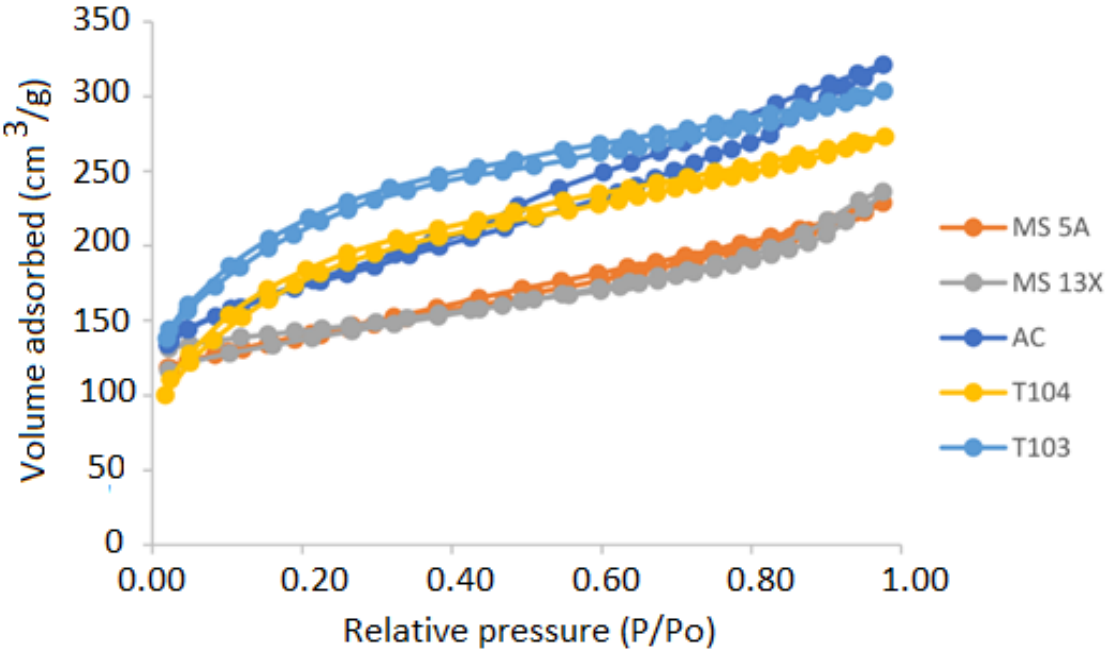

Figure 5.4: Adsorption isotherms for activated charcoal, activated carbon T104 and T103, and molecular sieve 5A, 13X.

5.3.2 Model diesel adsorption

Effect of adsorption time

The adsorption activity of DBT using the five selected adsorbents was analysed at 10 wt% of adsorbents, with respect to model diesel. In Figure 5.5 it can be seen that AC, MS 13X, T103 and T104 showed similar activity. MS 5A showed the lowest activity, even though it had a similar surface area to that of MS 13X. The poor activity relative to MS 13X could be due to its different crystal structure, even though they both have the same building block of the sodalite (Broussard and Shoemaker, 1960). This is consistent with our XRD results. These results are also consistent with the work done by Salem (Salem, 1994), where MS 5A showed poorer activity in desulphurizing naphtha than did MS 13X. Due to its poor activity, molecular sieve 5A was not considered for further testing. For the other four adsorbents, the initial

adsorption rate, i.e. within the first 60 min, was rapid; thereafter, it became very slow until equilibrium was achieved at about 240 min.

The rapid initial adsorption rate was due to a vacant adsorption site and hence a high solute gradient. With time, the remaining vacant sites were further from the adsorbent surface, as DBT had to travel further and deeper into the micro-pores, while encountering much resistance and repulsion from the adsorbed solute - hence the decrease in adsorption rate. The FID results (not presented here) showed no adverse effect on the model diesel's hydrocarbons, which suggests that the adsorption that took place was mainly for DBT. Overall, the poor activity of MS 5A could be due to small pore size, which suggests it is not good for big sulphur molecule adsorption.

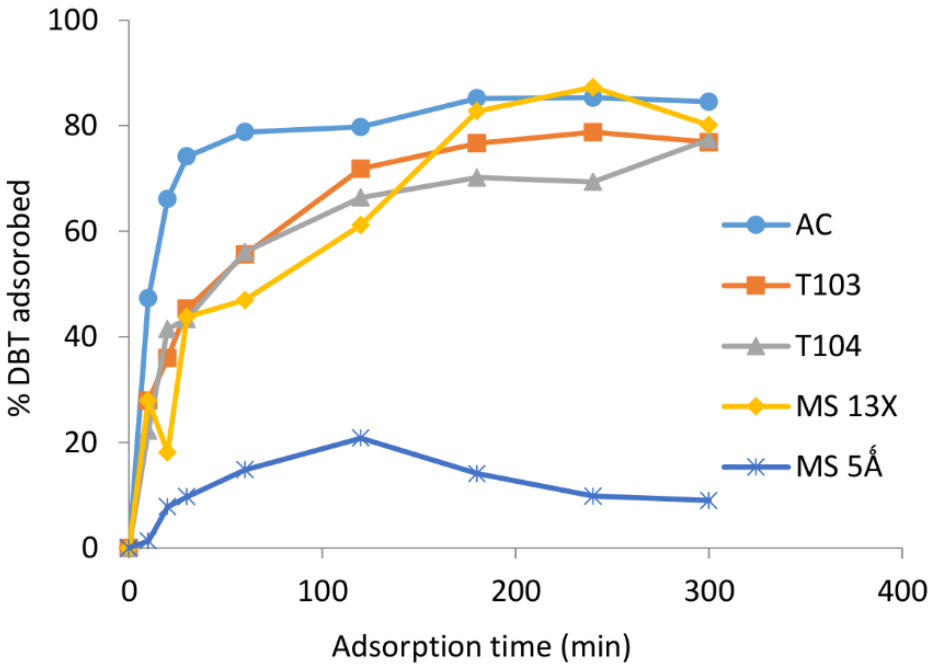

Figure 5.5: Effect of adsorption time for adsorbents (10 wt% adsorbent) with conditions: 25 ℃, atmospheric pressure, stirring speed of 800 rpm and 1000 ppm initial model diesel sulphur concentration.

Effect of adsorbent quantity

The percentage of DBT adsorbed was observed to increase with an increase in adsorbent quantity, as expected for activated charcoal, activated carbon T103 and T104, as shown in Figure 5.6. As the adsorbent quantity increases from 5 wt% to 15 wt%, the number of sites available for DBT increases - hence a faster adsorption rate and quantity. The adsorption activity of molecular sieve 13X did not show a consistent trend. The amount of DBT adsorbed by MS 13X first increased from 73 % to 86 %, as expected, but then decreased to 77 % at 15

wt%. During the experiments, the stirring speed was set at 800 rpm for all the runs and it was maintained at that setting point for most of the runs. However, when a 15 wt% molecular sieve 13X was used in the experiments, the stirring speed was out of control at times, which may be due to difficulty in mixing at a high adsorbate weight percentage.

Poor mixing is believed to have led to lower sulphur removal, due to increased mass transfer resistance. While percentage DBT adsorbed was observed to increase with adsorbent quantity, the amount of sulphur (q_e) loading on the adsorbent decreased, as shown in Table 5.2. The decrease in adsorbent loading is due to the same total sulphur quantity in the feed, but more adsorbent.

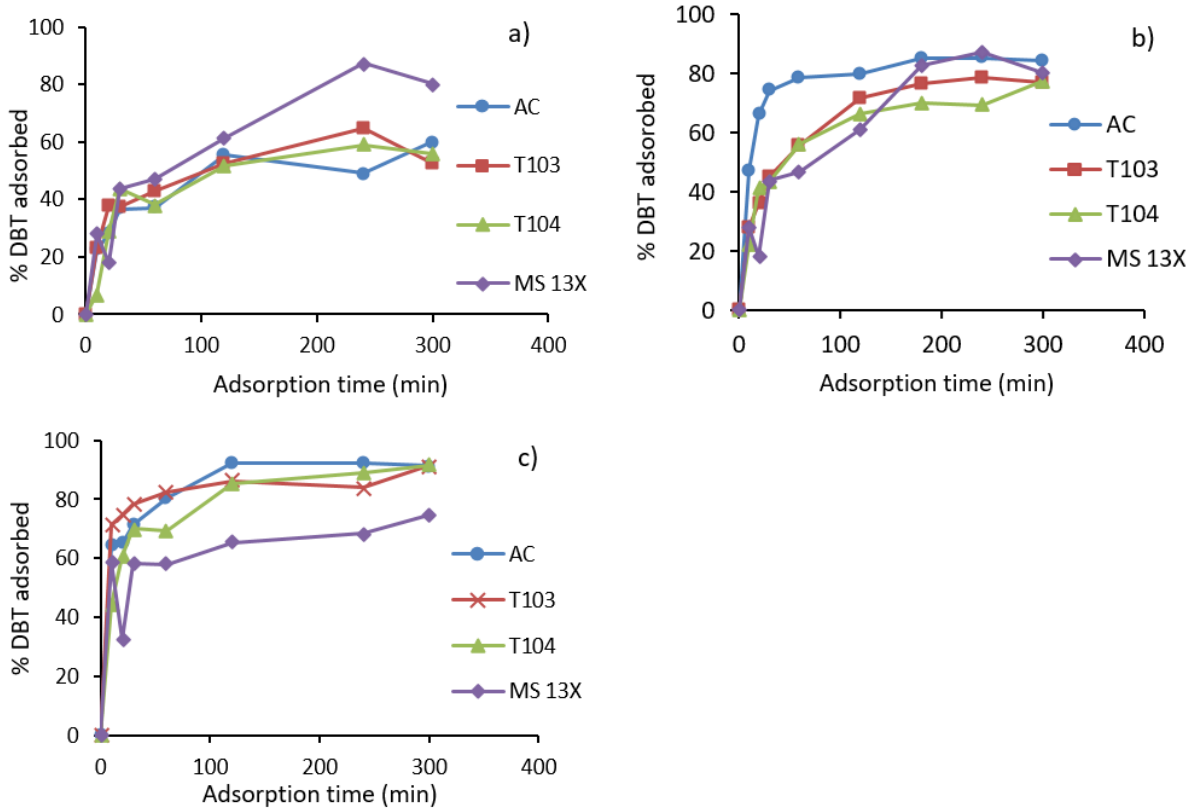

Figure 5.6: Effect of adsorbent quantity with condition: 25 ℃, atmospheric pressure, stirring speed of 800 rpm and 1000 ppm initial model diesel sulphur concentration. (a) 5 wt%. (b) 10 wt%. (c) 15 wt%.

Effect of initial DBT concentration

The amount of DBT loaded on the adsorbents (q_e) was observed to increase with an increase in the initial DBT concentration from 250 ppm to 1000 ppm for all absorbents, as shown in Table 5.2. This is likely due to the increased probability of DBT bumping into the adsorbent. Overall, ultra-low sulphur concentrations were not achieved for all tests presented in table 5.2, below.

Table 5.2: Effect of adsorbent quantity (initial concentration 1000ppm) and initial DBT concentration (5 wt.% adsorbent) on equilibrium adsorption capacity.

	Adsorption capacity (mg/g)					
	Adsorbent quantity (wt%)			**Initial DBT concentration (ppm)**		
	5	**10**	**15**	**250**	**500**	**1000**
AC	10.80 (459)	8.22 (178)	6.10 (85)	2.15 (143)	7.30 (137)	10.8 (459)
T104	11.34 (433)	7.74 (226)	6.01 (98)	2.21(82)	7.10 (129)	11.3 (433)
T103	10.94 (443)	7.69 (231)	6.11 (84)	3.35(139)	7.40 (145)	10.9 (443)
MS13X	15.54 (278)	8.66 (134)	5.18 (223)	2.66 (157)	4.40 (277)	15.5 (278)

(NB: Values in brackets represent the final sulphur concentration.)

The percentage of DBT adsorbed from solution (C_e) increased when the initial concentration was increased from 250 to 500 ppm and then dropped when the DBT concentration was doubled to 1000 ppm. The drop in the percentage of DBT adsorbed (as shown in Figure 5.7) suggests a saturation of the adsorption site - hence a significant amount is not adsorbed at 1000 ppm. The saturated adsorption capacity of the three adsorbents are 43 mg/g, 44 mg/g and 46 mg/g for activated charcoal, T103, and T104, respectively. These values are comparable with those reported by other researchers (Kim et al., 2006; Yang et al., 2007; Saleha and Danmaliki, 2016).

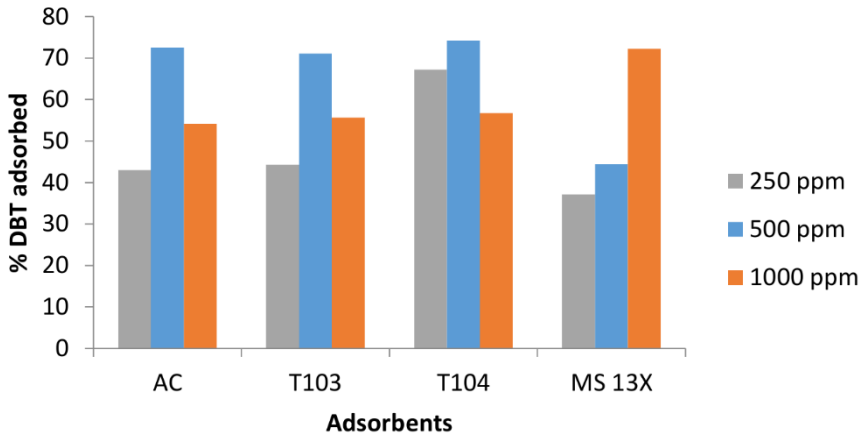

Figure 5.7: Effect of the initial DBT concentration on DBT removing with time on stream with conditions: 25 ^{o}C, atmospheric pressure, stirring speed of 800 rpm, adsorption loading of 5 %.

The saturation adsorption capacity of the studied activated carbons is closely comparable with that reported by Saleha and Danmaliki, 2016, which was produced by steam activation at 900 ^{o}C, followed by a sulphuric acid wash. But the acid-washed samples were 3-4 times more active compared to those produced by thermal treatment. Although the sulphur removal capacity is similar for the four kinds of adsorbents, Figure 5.7 indicates that T104 has the potential to remove sulphur at low concentrations, while 13 X is better at high sulphur concentrations.

Kinetics of adsorption of DBT

In order to understand the adsorption process commonly used in kinetic models, a pseudo-first-order model and the pseudo-second-order model were used. Predicting the adsorption kinetics is necessary for the design of adsorption columns (Srivastav and Srivastava, 2009; Kumar et al., 2011). Pseudo-first-order and pseudo-second-order models were tested by fitting the experimental data to equation 5.3 and equation 5.4, respectively, as given below.

$$\log(q_e - q_t) = log q_e - \frac{K_{ad} t}{2.303} \qquad (5.3)$$

Where: q_e is the amount of adsorbate loaded on the adsorbent under equilibrium; q_t is the amount of adsorbate loaded on adsorbent at time t; $k_{ad}/2.303$ is the pseudo-first-order rate constant.

$$\frac{t}{q_t} = [K_s {q_e}^2] + \frac{t}{q_e} \qquad (5.4)$$

Where: $[K_s {q_e}^2] = h$ is the initial adsorption rate (mg/g min) as $t \to 0$

In Table 5.3, it can be seen that, with pseudo-first-order, the q_e-experimental and q_e-calculated were very different and the regression coefficients were very low. Contrarily, the q_e-experimental matches the q_e-calculated with the pseudo-second-order. This suggests that the experimental data fit the pseudo-second-order more closely. This is consistent with the work done on desulphurization by many researchers (Kumar et al., 2011; Saleha and Danmaliki, 2016). These results suggest chemical adsorption between DBT and adsorbents in this work.

Table 5.3: Adsorbent loading comparison between the experimental data and the pseudo-first-order rate and pseudo-second-order rate equations.

Adsorbent	q_{exp}	q_{cal}	k_{ad}	R^2	
Pseudo-first-order					
Activated charcoal	0.433	6.41	0.0166	0.7945	
T103	0.552	6.03	0.0076	0.8089	
T104	0.403	4.00	0.0140	0.6574	
Molecular sieves 13x	0.408	4.62	0.0203	0.6519	
Pseudo-second-order	q_{exp}(mg/g)	q_{actual} (mg/g)	k_s (g/mg min)	h (mg/g min)	R^2
Activated charcoal	6.45	6.45	0.03059	1.2717	0.9990
T103	6.29	6.03	0.05033	1.19882	0.9981
T104	4.04	4.00	0.16231	2.6476	0.9959
Molecular sieves 13x	4.94	4.62	0.100354	2.4497	0.9920

5.3.4 Commercial diesel adsorption

Commercial diesel with a total sulphur content of about 43 ppm was used for the study. Dilute systems are normally used for studying adsorption systems, to enable ideal behaviour to be displayed in both the liquid phase and the adsorbed phase. A chromatogram for diesel is shown in Figure 5.1, with some of the major compounds identified. 4-MDBT and 4,6-MDBT were observed to contribute approximately 4 % and 35 %, respectively, of the sulphur in the diesel. Activated charcoal and activated carbon T103 and T104 have been mainly used in experimental work using commercial diesel.

Effect of adsorption time

A similar trend was observed where model diesel was used, i.e.: adsorption activity was fast within the first 120 min; thereafter, sulphur compounds were slowly adsorbed, until equilibrium was achieved at about 300-420 min. However, even though shorter adsorption times could be used, all equilibrium data measurements were done after 24 h. The nature of the

adsorbent and its available adsorption sites affects the time needed to reach equilibrium. In Figure 5.8, it can be seen that the data between time on stream, of 420 min and 1500 min, are quite close to each other for the three adsorbents. This indicates that adsorption was very stable during the life of the experimental work.

It was also observed that there was little difference in the activity of the three adsorbents, which suggests they have a similar nature. These results are consistent with FTIR, Boehm's titration, XRD and BET results, which showed similar characteristics for these adsorbents. The sulphur removing activity of T104 is a little higher than that of AC, and the same trend is shown in Figure 5.7, with 250ppm DBT initial concentration. This indicates that T104 is a good adsorbent for low-sulphur concentration removal.

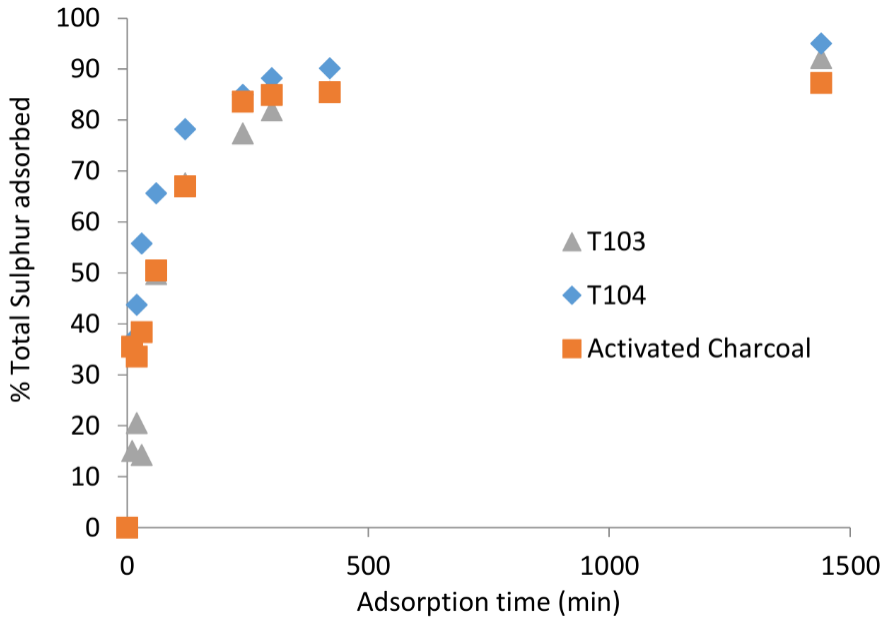

Figure 5.8: Effect of adsorption time, adsorbent loading 15wt% with conditions: 25℃, atmospheric pressure, stirring speed of 800 rpm.

Effect of adsorbent quantity

The activity of the three adsorbents was seen to increase with an increase in the adsorbent amount, as expected. (See Figure 5.9.) The increase in activity was lowest between 10 and 15 wt%. MS 13X, which had shown similar activity to AC with model diesel, was observed to have poor activity with commercial diesel, where the percentage removal is 13% for a single point run at 10 wt%. (See Figure 5.9.). Salem, 1994 pointed out that competition between the aromatics and the sulphur compounds for the sites may be the main reason for the lower efficiency of MS 13X. MS 13X is not suitable for sulphur removal from the commercial diesel used in this experiment. It was also observed that as the percentage removal of sulphur increased with adsorbent quantity, the amount of sulphur loaded on the adsorbent (q_e) decreased. This could be due to the same total sulphur quantity in the feed, but more adsorbent quantity - as explained earlier in section 3.2.2 in relation to DBT.

The highest adsorbent loading (qe) statistics for the three adsorbents were 0.84, 0.64, 0.6 mg/g for activated charcoal, activated carbon T103 and T104, respectively; this was with 2.5 wt% adsorbent loading, however, these are not saturation capacity (q_m) figures, since qe was still increasing.

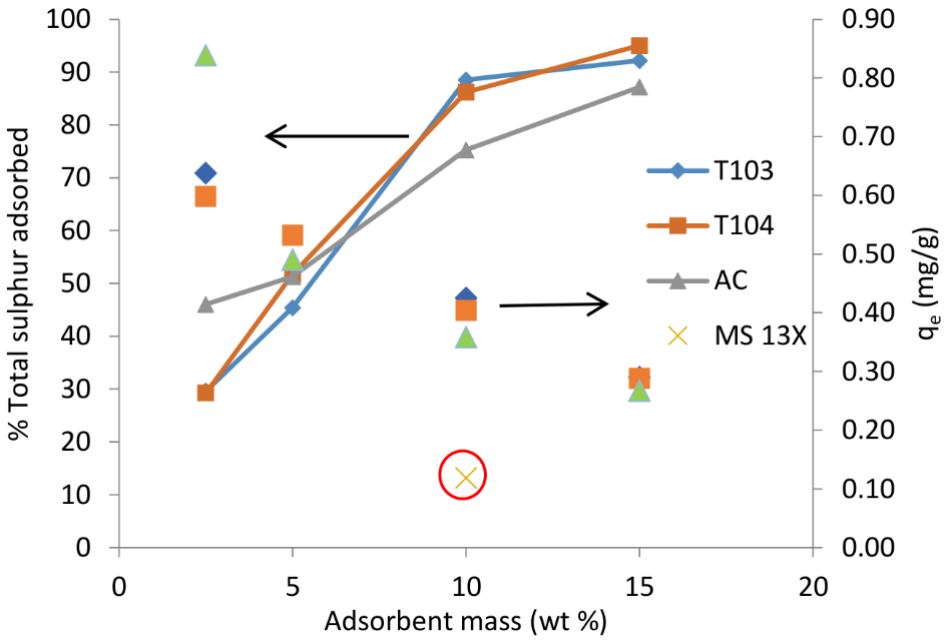

Figure 5.9: Effect of adsorbent quantity on 43 ppm conventional diesel.

Adsorption kinetics of individual compounds

Understanding the adsorption affinity for each sulphur compound is paramount, in order to improve the overall removal efficiency of adsorbents. If adsorption affinity by different adsorbents is different for different compounds, this would enable adsorbent blending and thus enable maximum adsorption of different sulphur compounds. Adsorption trends for individual major compounds are given in Figure 5.10. Similar adsorption trends were observed with the three adsorbents. The 4-MDBT concentration decrease was faster than with all other major compounds, while there was little difference between the other four. This phenomenon was further investigated using the concept of adsorption affinity.

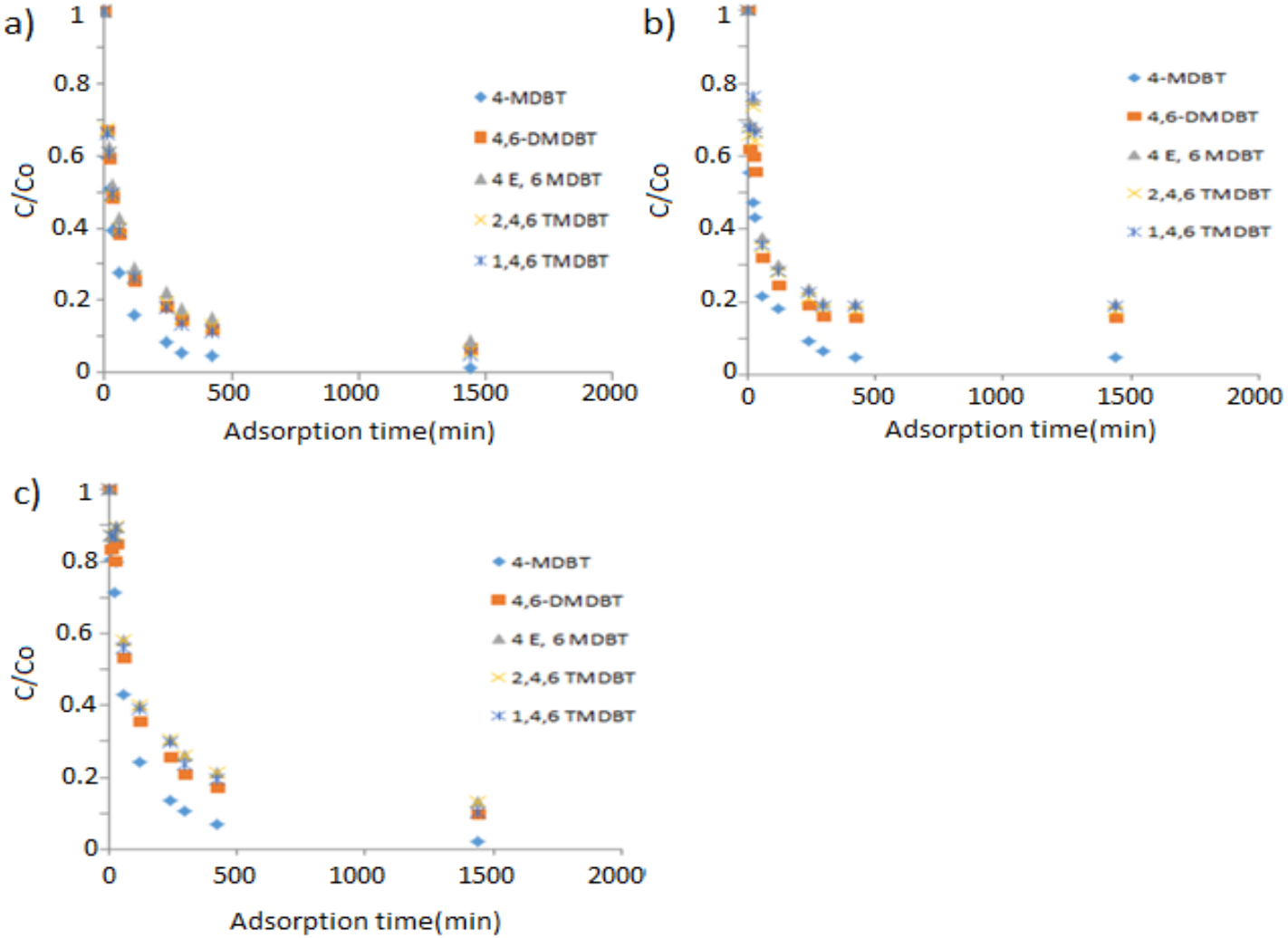

Figure 5.10: Adsorption of a five-component adsorbate mixture. (a) Activated charcoal. (b) Activated carbon T104. (c) Activated carbon T103.

An analysis of the adsorption affinity for five major compounds (4-MDBT, 4,6-DMDBT, 4E, 6 MDBT, 2,4,6 TMDBT and 1,4,6 TMDBT) in conventional diesel toward AC, T103 and T104 was done. In Figure 5.11 it is seen that adsorption affinity occurred in the following decreasing order: 4-MDBT>> 4,6 DMDBT~4 E, 6 MDBT~2,4,6 TMDBT~1,4,6 TMDBT.

These results are contrary to what has been observed by a number of researchers when using model diesel and activated carbon (Yu et al., 2013). It has been reported that adsorbent activity increases in the following order: BT<DBT<MDBT<4,6 DMDBT. This has been attributed to the increase in electron density of the aromatic system or the increase in delocalized π electrons. This discrepancy with model diesel results could be due to the sulphur compounds loading to already-highly-loaded surfaces and the smaller molecules have a better adsorption chance because of a lower steric hindrance.

Additionally, as stated in the introduction, the adsorption rate is also a function of adsorbate concentrations. The presence of steric hindrances is consistent with the mechanism expected for chemical adsorption, i.e. the second–order-pseudo adsorption model.

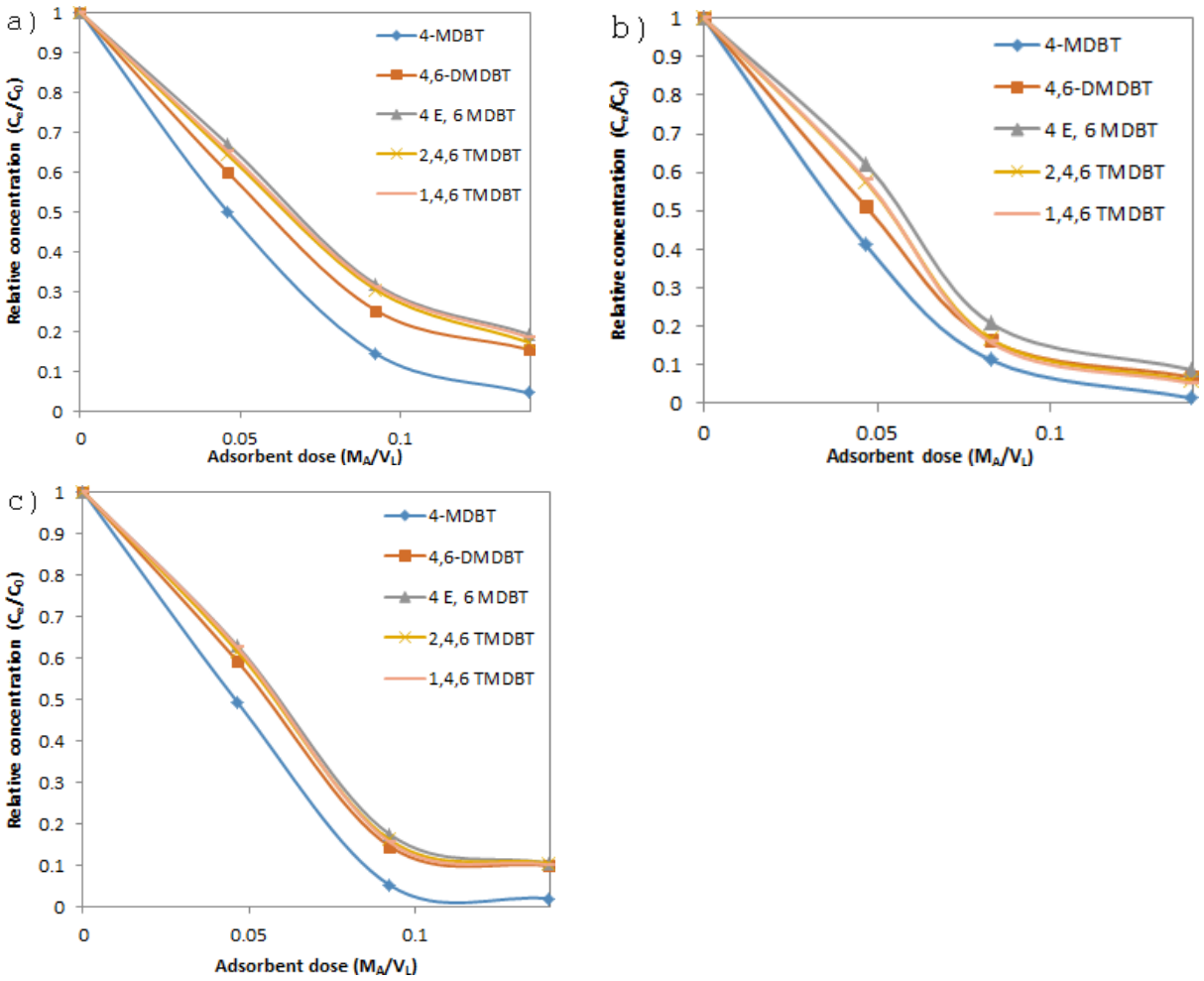

Figure 5.11: Adsorption affinity of a five-component adsorbate mixture. (a) Activated charcoal. (b) Activated carbon T104. (c) Activated carbon T103.

5.4 Conclusion

Deep desulphurization has gained significant importance because of environmental issues and the effect that sulphur has on fuel cells and catalytic converters. Desulphurization of model diesel and conventional diesel was investigated using molecular sieves (MS), activated charcoal (AC), and activated carbon T103 and T104. The characterization of adsorbents was done by FTIR, BET and Boehm's titration analysis, which showed similar characteristics for these adsorbents of AC, T104 and T103. MS 5A showed poor activity, and it is believed this is due to the crystal structure of the molecular sieve. MS 13X showed fair activity with model diesel but had poor stability. The adsorption of DBT to these adsorbents was observed to be pseudo-second-order, which suggests chemical adsorption. Finally, when using model diesel, saturation adsorption capacity for AC, T103 and T104 were observed to be 4.3, 4.4 and 4.6 mg/g, respectively.

From the experimental work carried out using 43 ppm conventional diesel, it was observed that activated charcoal, T104 and T103 delivered a good sulphur removing performance: high removing capacity and good stability. Adsorption affinity of different sulphur compounds decreased in the following order for the three adsorbents (activated charcoal, T104 and T104): 4-DBT>> 4,6 DMDBT~ 4 E, 6 MDBT~ 2,4,6 TMDBT~1,4,6 TMDBT. This is contrary to the commonly reported order when using model diesel, i.e. activity increases with an increase in molecular weight. This might be due to steric hindrance from already-loaded poly-aromatic compounds. In addition, MS 13X showed good activity with model diesel sulphur removing, but poor sulphur removing behaviour with conventional diesel. In conclusion, the ability of successful desulphurization using adsorption lies in good selectivity of sulphur compounds - hence adsorbent-sulphur bonds will be important.

Acknowledgments

The authors are grateful for the support received from the University of South Africa (UNISA), the National Research Foundation (NRF), the South African Research Chairs Initiative (SARChI), the Technology and Human Resources for Industry Programme (THRIP), the South African National Energy Research Institute (SANERI), the Technology Innovation Agency (TIA) and the Department of Science and Technology (DST).

References

Al. Swat, A.A., Saleh, T.A., Ganiyu, S.A., Siddiqui, M.N., Alhooshani, K.R., 2017. Preparation of activated carbon, zinc oxide and nickel oxide composites for potential application in the desulphurization of model diesel fuels. J. Anal. Appl. Pyrolysis 128, 246–256. https://doi.org/10.1016/j.jaap.2017.10.004

Broussard, L., Shoemaker, Dp., 1960. The structures of synthetic molecular sieves. J. Am. Chem. Soc. 82, 1041–1051.

Bu, J., Loh, G., Gwie, C.G., Dewiyanti, S., Tasrif, M., Borgna, A., 2011. Desulphurization of diesel fuels by selective adsorption on activated carbons: Competitive adsorption of polycyclic aromatic sulphur heterocycles and polycyclic aromatic hydrocarbons. Chem. Eng. J. 166, 207–217.

Chandra Srivastava, V., 2012. An evaluation of desulphurization technologies for sulphur removal from liquid fuels. RSC Adv 2, 759–783. https://doi.org/10.1039/C1RA00309G

Danmaliki, G.I., Saleh, T.A., 2017. Effects of bimetallic Ce/Fe nanoparticles on the desulphurization of thiophenes using activated carbon. Chem. Eng. J. 307, 914–927. https://doi.org/10.1016/j.cej.2016.08.143

Duarte, F.A., Mello, P. de A., Bizzi, C.A., Nunes, M.A.G., Moreira, E.M., Alencar, M.S., Motta, H.N., Dressler, V.L., Flores, É.M.M., 2011. Sulphur removal from hydrotreated petroleum fractions using ultrasound-assisted oxidative desulphurization process. Fuel 90, 2158–2164. https://doi.org/10.1016/j.fuel.2011.01.030

Han, X., Lin, H., Zheng, Y., 2014. Understanding capacity loss of activated carbons in the adsorption and regeneration process for denitrogenation and desulphurization of diesel fuels. Sep. Purif. Technol. 133, 194–203. https://doi.org/10.1016/j.seppur.2014.06.020

Hernández-Maldonado, A.J., Yang, R.T., 2004. New sorbents for desulphurization of diesel fuels via π-complexation. AIChE J. 50, 791–801. https://doi.org/10.1002/aic.10074

Jeevanandam, P., Klabunde, K.J., Tetzler, S.H., 2005. Adsorption of thiophenes out of hydrocarbons using metal impregnated nanocrystalline aluminum oxide. Microporous Mesoporous Mater. 79, 101–110. https://doi.org/10.1016/j.micromeso.2004.10.029

Kim, J.H., Ma, X., Zhou, A., Song, C., 2006. Ultra-deep desulphurization and denitrogenation of diesel fuel by selective adsorption over three different adsorbents: A study on adsorptive selectivity and mechanism. Catal. Today 111, 74–83. http://dx.doi.org/10.1016/j.cattod.2005.10.017

Kumar, S., Srivastava, V.C., Badoni, R.P., 2011. Studies on adsorptive desulphurization by zirconia based adsorbents. Fuel 90, 3209–3216. https://doi.org/10.1016/j.fuel.2011.06.029

Ma, X., Sprague, M., Sun, L., Song, C., 2002a. Deep desulphurization of diesel fuels by novel integrated approach (DOE Technical Progress Report No. M/S 921-107). Pennsylvania State University.

Ma, X., Sun, L., Song, C., 2002b. A new approach to deep desulphurization of gasoline, diesel fuel and jet fuel by selective adsorption for ultra-clean fuels and for fuel cell applications. Catal. Today 77, 107–116. https://doi.org/10.1016/S0920-5861(02)00237-7

Mahalakshmy, R., Indraneel, P., Viswanathan, B., 2009. Surface functionalities of nitric acid treated carbon- A density funtinal theory based vibrational analysis. Indian J. Chem. 48A, 352–356.

Mguni, L., Yao, Y., Nkomzwayo, T., Xinying, L., Hildebrandt, D., Glasser, D., 2018. Desulphurization of diesel fuels using intermediate Lewis acids loaded on activated charcoal and alumina. Chem. Eng. Commun. https://doi.org/10.1080/00986445.2018.1511983

Momcilovic, M.Z., Onjia, A.E., Purenovic, M.M., Zarubica, A.R., Randelovic, M.S., 2012. Removal of a cationic dye from water by activated pinecones. J. Serbian Chem. Soc. 77, 761–774.

Moreno-Castilla, C., Lopez-Ramon, M.V., Carrasco-Marına, F., 2000. Changes in surface chemistry of activated carbons by wet oxidation. Carbon 38, 1995–2001.

Olajire, A.A., Abidemi, J.J., Lateef, A., Benson, N.U., 2017. Adsorptive desulphurization of model oil by Ag nanoparticles-modified activated carbon prepared from brewer's spent grains. J. Environ. Chem. Eng. 5, 147–159. https://doi.org/10.1016/j.jece.2016.11.033

Patiño-Herrera, R., González-Alatorre, G., Estrada-Baltazar, A., Escoto-Chavéz, S.E., Pérez, E., 2015. Hydrophobic coatings for prevention of dental enamel erosion. Surf. Coat. Technol. 275, 148–154.

Safa, M.A., Al-Shamary, T., Al-Majren, R., Bouresli, R., Ma, X., 2017. Reactivities of Various Alkyl Dibenzothiophenes in Oxidative Desulphurization of Middle Distillate with Cumene Hydroperoxide. Energy Fuels 31, 7464–7470. https://doi.org/10.1021/acs.energyfuels.7b01272

Saleh, T.A., Al-Hammadi, S.A., Tanimu, A., Alhooshani, K., 2018. Ultra-deep adsorptive desulphurization of fuels on cobalt and molybdenum nanoparticles loaded on activated carbon derived from waste rubber. J. Colloid Interface Sci. 513, 779–787. https://doi.org/10.1016/j.jcis.2017.11.076

Saleha, T.A., Danmaliki, G.I., 2016. Adsorptive desulphurization of dibenzothiophenefrom fuels by rubber tyres-derived carbons:Kinetics and isotherms evaluation. Process Saf. Environ. Prot. 102, 9–16.

Salem, A.B.S.H., 1994. Naphtha desulphurization by adsorption. Ind Eng Chem Res 33, 336–340.

Sano, Y., 2004. Adsorptive removal of sulphur and nitrogen species from a straight run gas oil over activated carbons for its deep hydrodesulphurization. Appl. Catal. B Environ. 49, 219–225. https://doi.org/10.1016/j.apcatb.2003.12.007

Sarda, K.K., Bhandari, A., Pant, K.K., Jain, S., 2012. Deep desulphurization of diesel fuel by selective adsorption over Ni/Al2O3 and Ni/ZSM-5 extrudates. Fuel 93, 86–91. https://doi.org/10.1016/j.fuel.2011.10.020

Selvavathi, V., Chidambaram, V., Meenakshisundaram, A., Sairam, B., Sivasankar, B., 2009. Adsorptive desulphurization of diesel on activated carbon and nickel supported systems. Sel.

Pap. Catal. Future Fuels 18th Natl. Symp. INDO-US Semin. Catal. Indian Inst. Pet. Dehradun India April 16-18 2007 141, 99–102. https://doi.org/10.1016/j.cattod.2008.05.009

Seredych, M., Bandosz, T.J., 2010. Adsorption of Dibenzothiophenes on Nanoporous Carbons: Identification of Specific Adsorption Sites Governing Capacity and Selectivity †. Energy Fuels 24, 3352–3360. https://doi.org/10.1021/ef9015087

Shah, S.S., Ahmad, I., Ahmad, W., Ishaq, M., Gul, K., Khan, R., Khan, H., 2018. Study on adsorptive capability of acid activated charcoal for desulphurization of model and commercial fuel oil samples. J. Environ. Chem. Eng. 6, 4037–4043. https://doi.org/10.1016/j.jece.2018.06.008

Shah, S.S., Ahmad, I., Ahmad, W., Ishaq, M., Khan, H., 2017. Deep Desulphurization Study of Liquid Fuels Using Acid Treated Activated Charcoal as Adsorbent. Energy Fuels 31, 7867–7873. https://doi.org/10.1021/acs.energyfuels.7b00914

Shakirullah, M., Ahmad, I., Ishaq, M., Ahmad, W., 2009. Study on the role of metal oxides in desulphurization of some petroleum fractions. J. Chin. Chem. Soc. 56, 107–114.

Sharma, P., Song, J.-S., Hee Han, M., Cho, C.-H., 2016. GIS-NaP1 zeolite microspheres as potential water adsorption material: Influence of initial silica concentration on adsorptive and physical/topological properties (Scientific Reports No. 6:22734).

Shiraishi, Y., Naito, T., Hirai, T., Komasawa, I., 2002. A Desulphurization Process for Light Oils Based on the Formation and Subsequent Adsorption of N-Tosylsulfimides. Ind. Eng. Chem. Res. 41, 4376–4382. https://doi.org/10.1021/ie010620o

Srivastav, A., Srivastava, V.C., 2009. Adsorptive desulphurization by activated alumina. J. Hazard. Mater. 170, 1133–1140. https://doi.org/10.1016/j.jhazmat.2009.05.088

Tang, X., Lu, H., Li, J., Chen, L., 2016. Adsorption desulphurization performance and mechanism over nanocrystalline NiO/Al 2 O 3-1 adsorbent. Russ. J. Appl. Chem. 89, 2043–2049.

Tran, D.T., Palomino, J.M., Oliver, S.R.J., 2018. Desulphurization of JP-8 jet fuel: challenges and adsorptive materials. RSC Adv. 8, 7301–7314. https://doi.org/10.1039/C7RA12784G

Velu, S., Ma, X., Song, C., 2003. Selective Adsorption for Removing Sulphur from Jet Fuel over Zeolite-Based Adsorbents. Ind. Eng. Chem. Res. 42, 5293–5304. https://doi.org/10.1021/ie020995p

Worch, E., 2012. Adsorption technology in water treatment: fundamentals, processes, and modeling. Walter de Gruyter.

Xuemei, C., Yufeng, H., Jiguang, L., Liang, Q., Yansheng, L., Zhang, X., Xiaoming, P., Wenjia, Y., 2008. Desulphurization of diesel fuel by extraction with [BF4]−-based ionic liquids. Chin. J. Chem. Eng. 16, 881–884.

Yang, Y., Lu, H., Ying, P., Jiang, Z., Li, C., 2007. Selective dibenzothiophene adsorption on modified activated carbons. Carbon 45, 3042–3044.

Yu, C., Fan, X., Yu, L., Bandosz, T.J., Zhao, Z., Qiu, J., 2013. Adsorptive Removal of Thiophenic Compounds from Oils by Activated Carbon Modified with Concentrated Nitric Acid 27, 1499−1505.

Yu, G., Lu, S., Chen, H., Zhu, Z., 2005. Diesel fuel desulphurization with hydrogen peroxide promoted by formic acid and catalyzed by activated carbon. Carbon 43, 2285–2294. https://doi.org/10.1016/j.carbon.2005.04.008

6. MODIFIED ACTIVATED CARBON ADSORBENTS

This work was has been published in the Chemical Engineering Communications, 206:5, 572-580, DOI: 10.1080/00986445.2018.1511983. Part of this work was presented at the following conference:

National University of Lesotho International Science and Technology Innovation Conference and Expo (NULISTICE): 23 – 26 January 2018, Maseru, Lesotho
Catalysis Society of South Africa (CATSA), Pilanesberg, North-West (19-22th Nov 2017)

Summery

According to Pearson's hard/soft (Lewis) acids/bases concept, sulphur compounds in diesel will prefer to interact with intermediate or soft Lewis acid sites since they are soft to intermediate bases. In this work, intermediate Lewis metal oxides (MO) acids were loaded on activated carbon (AC) and alumina (Al_2O_3) to desulphurize diesel using adsorption. For carbon-loaded MO, NiO showed the highest desulphurization activity of 89 % and 50 % when using both model diesel and conventional diesel, respectively. The activity of Al_2O_3 and Al_2O_3 supported MO was approximately four times less than that of AC for model diesel desulphurization. It is suggested that the low activity of Al_2O_3 is due to lower surface area, pore distribution, and the strong acidity nature of Al_2O_3 since the adsorbates are soft to intermediate Lewis bases. Lower activity, 2–4 times, was observed when treating conventional diesel compared to model diesel. This lower activity is due to competitive adsorption with compounds such as naphthalene and indole. Despite this difference, the activity trends were generally maintained suggesting that the use of model diesel is not a bad technique for screening adsorbents. Selectivity on AC was observed to decrease in this order: 4-MDBT > 1,4,6-TMDBT > 4,6-DMDBTZ ~ 4E,6-MDBT ~ 2,4,6-TMDBT. This suggests that steric hindrances dominate selectivity for these high-molecular-weight molecules. Finally, it was observed that the challenge with the regeneration of adsorbent (AC) that treated conventional diesel using solvent extraction is the competitive desorption of hydrocarbons and sulphur compounds.

Keywords: Desulphurization; Diesel; Metal oxides; Activated carbon; Alumina

6.1 Introduction

The removal of sulphur to produce "sweet" diesel has gained attention because of environmental effects associated with the combustion of sulphur compounds and the desire to use diesel to generate off-grid electricity using fuel cells (Ruberti, 2003). The sulphur compounds found in diesel are derivatives of dibenzothiophene. Although intensive work has been done using conventional hydrodesulphurization (HDS) to decrease the sulphur content in diesel, sulphur has not been completely removed because of many unreactive chemical species like; benzothiophene (BT), 4-methyl-dibenzothiophene (4-MDBT), 4,6-dimethyl-dibenzothiophene (4,6-DMDBT), 2,4,6-Trimethyldibenzothiophene (2,4,6-TMDBT) and 1-methylnaphthalene (Muzic et al., 2008; Hernández-Maldonado and Yang, 2004; Jeevanandam et al., 2005). Efforts to reduce sulphur content below the concentration of 50 ppm results in a considerable escalation in cost, because of the need to work with hydrogen at an elevated temperature and high pressure (Jeevanandam et al., 2005; Xuemin et al., 2008).

There are a number of methods that offer potential solutions. These include the use of ionic liquids, oxidation, adsorption, solvent extraction, and photochemical, biochemical, catalytic, and electrochemical processes. Adsorption processes seem to be the most promising approach to remove sulphur from fuels (Triantafyllidis and Deliyanni, 2014). An effective adsorbent has to provide an active surface, i.e., a surface with correct surface chemistry, high surface area, and proper pore size distribution. It has been suggested that sulphur compounds found in fuels are intermediate to soft bases and hence prefer to interact with intermediate or soft Lewis acid sites (Maes et al., 2011). Some researchers have shown a good correlation between acid groups in activated carbon (AC) and desulphurization (Saleh and Danmaliki, 2016a). The acids groups in AC can be modified by acid treatment of AC (Saleh and Danmaliki, 2016a); Bu et al., 2011**;** Fallah and Azizian, 2012**;** Zhou et al., 2009; Zhao et al., 2008) and thermal activation (Yu et

al., 2009). Another way of modifying the acidity of adsorbents is the introduction of Lewis acids like metal oxides and metal halides.

All sorts of metal oxides (MO) from hard to soft Lewis acids have been reported for desulphurization of fuels (M. Shakirullah et al., 2009) Srivastav and Srivastava, 2009; Saleh et al., 2017). (M. Shakirullah et al., 2009) reported on the activity of Al_2O_3, ArO_3, MgO_2, MnO_2, PbO_2, SiO_2, and ZnO_2. They reported that the highest activity of 54.5 % was observed for a soft metal oxide PbO_2 at around 6wt% (MO/diesel) after 6 h. Al_2O_3 and ZrO_2, hard acids, have been investigated and they showed removal efficiency of DBT of 59 % and 50 % after 24 and 22 h respectively (Srivastav and Srivastava, 2009; Kumar et al., 2011). The results are difficult to compare because of the different working condition such as adsorption time, adsorbent loading and initial sulphur concentration of model diesel.

AC loaded with metal/metal oxides has been investigated by a number of researchers (Arturo J. Hernández-Maldonado et al., 2005); Seredych and Bandosz, 2007). The practice of loading metal oxides/metal on support is for increasing the available active surface for adsorption. Saleh et al., 2017 investigated the effect of loading MnO_2 on AC, and they reported that AC-manganese oxide composite showed significant adsorptive desulphurization efficiency. Unfortunately, no comparison was done with AC alone. A number of researchers have conducted desulphurization experimental work using model diesel fuel which contained the sulphur compounds thiophene, BT, DBT, 4-MDBT and 4,6 DMDBT. They have reported a higher removal efficiency for DBTs compounds. This has been attributed to high delocalized electrons in these compounds hence π-complexation bonding (Saleh and Danmaliki, 2016a). Wang and Yang, 2007 reported that $PbCl_2$/AC improved selectivity for sulphur compounds compared to AC for desulphurization of JP-5 jet fuel and also indicated that AC was better support for π-complexation compared to Al_2O_3.

Other supports have also been investigated, and these include zeolites, SBA-15, MCM 41 and clays (Wang et al., 2008; Ahmad et al., 2017). The loading of metal oxide/ metal has been achieved by a number of methods these include: impregnation (Hernandez et al., 2010; Danmaliki et al., 2017), hydrothermal synthesis (Yan et al., 2012), xerogel process (Tang et al., 2016a) and co-precipitation (Gaddafi I. Danmaliki and Saleh, 2017). The advantage of impregnation is the simplicity of the method and hence the industrial application of the technique.

Most of the work that has been discussed above and available in the literature is based on model diesel. Hence, these represent the adsorption of low molecular sulphur compounds. To the best of our knowledge, no work has been reported on the activity of high molecular sulphur compounds, TMDBT, on a system based exclusively on intermediate Lewis metal oxides (MO) acids loaded on AC and Al_2O_3.

In this work, the adsorptive desulphurization of both model diesel and commercial diesel were investigated by using exclusively intermediate Lewis metal oxides (MO) acids loaded on both AC and Al_2O_3. The effect of these Lewis metal oxides, as well as the supports on the adsorption performance (activity and selectivity) of the model and conventional diesel, were compared.

6.2 Materials and method

6.2.1 Material

Hexadecane (98 %), Toluene (99 %), Octane (98 %), heptane (98 %), dibenzothiophene (98 %), nickel (II) nitrate hexahydrate (98.5 %) and zinc nitrate hexahydrate (>98 %) were obtained from Sigma-Aldrich, whereas copper (II) nitrate trihydrate (>98 %) and cobalt (II) nitrate hexahydrate (99 %) were purchased from Merck. All reagents were used as received.

6.2.2 Adsorbents synthesis

AC and Al_2O_3, with a particle size of 1-2 mm, were loaded via incipient impregnation with aqueous solutions of different metal nitrate salts. 15 g of AC and Al_2O_3 were loaded with the appropriate amount of metal nitrate to achieve 5 wt% dissolved in 3.9 cm^3 and 10 cm^3 of water respectively based on their pore volumes of 0.262 cm^3/g and 0.72 cm^3/g. The mixtures were dried by evaporation at 80 ^oC for 2 h, then dried at 110 ^oC overnight and then finally calcined at 400 ^oC temperature for 4 h in nitrogen and air for AC and Al_2O_3 respectively.

6.2.3 Batch adsorption experiments and regeneration

Experiments were carried out using diesel from a garage, Johannesburg, South Africa and model diesel. The model diesel was synthesized using 85 v/v% of hexadecane, 15 v/v% toluene and a fixed amount of DBT to create a concentration of 100 ppm sulphur, other properties of diesel are given in Table 6.1. 3.7 g of adsorbent was added to 90 ml of model diesel to achieve 5 wt% adsorbent loading. The adsorption experiments were carried out on a 100 ml three-neck flask placed on a water bath on top of the heating magnetic stirrer. A digital Thermoregulatory regulated the heat supply to maintain a set temperature by the heating magnetic stirrer. Adsorption was carried out at atmospheric pressure and a temperature of 25 ^oC. Samples for the quantification of sulphur were taken at predetermined time intervals. To evaluate the regeneration ability of the adsorbent (AC), the adsorbate was first washed with 50 ml of heptane. Subsequently, 100 mL of octane was heated to 90 ^oC and the adsorbent washed with heptane was added.

The desorption experiment was carried out for 3 h, with samples taken at time intervals to analyze desorbing hydrocarbons and sulphur compounds. The regenerated adsorbent was then dried at 120 ^{o}C overnight, and it was used in the subsequent adsorption experiment.

Table 6. 1: Properties of model diesel and Conventional diesel

	Model diesel	Conventional diesel
type	85%hexadecane/15%toluene/DBT	SHELL GARAGE
Total Sulphur content (ppm)	100	103
Density (g/ml)	0.81	0.84
viscosity (mPa s @ 20)	3.04	2.64

6.2.4 Characterisation

The adsorbent's specific surface area, pore-volume, and average pore width were determined by nitrogen adsorption/desorption isotherms at 77 K using NOVA 1200e. Prior to the measurements, the sorbents were degassed by Ar at 300 ◦C for 2h. While the adsorbent surface

pH was determined by adding a 0.1 g sample of dry adsorbent into 5 ml of distilled water and the suspension was stirred overnight to reach equilibrium. Then the pH of the filtrate was measured.

6.2.5 Analysis

Samples taken during adsorption experiments were analyzed to determine sulphur concentration as well as the hydrocarbons in diesel. A7890B Agilent-GC with two detectors PFPD and FID was used to quantify the sulphur components and hydrocarbons respectively.

The relative adsorption factor of adsorbents towards different sulphur compounds in diesel was calculated using equations 6.1 and 6.2 below.

$$K_d = \frac{q_e}{c_e} \qquad (6.1)$$

Where K_d is the distribution coefficient, q_e is the adsorption capacity (mg/g), and C_e (mg/L) is the equilibrium concentration.

$$k = \frac{K_{d\,(c)}}{K_{d\,4MDBT}} \qquad (6.2)$$

where k expresses the relative adsorption factor, $K_{d\,(c)}$ is the distribution coefficient, and the subscript (c) is the competing molecule.

In this chapter, a group of experiments was conducted using the methods mentioned above. The desulphurization activity of AC with/without MO and Al_2O_3 with/without MO were investigated. The sulphur removal activity, selectivity and the effect of regeneration were analyzed.

6.3 Results and discussion

From Table 6.2 it was observed that for AC loaded with CuO and NiO there was a slight increase in surface area. This was attributed to most of the metal oxide loading on the exterior of the support while the drop in the surface area for AC/ZnO, could be due to the oxide depositing within the pores hence a decrease in surface area. In the case where Al_2O_3 was used as the support, there was a slight increase in surface area for all metal oxides suggesting mainly external surface deposition. The pore sizes were observed to be large enough (3 nm) to allow easy accessibility of sulphur compounds which range between 7 and 10 .5 Å in critical diameter. The addition of metal oxides on AC was observed to decrease adsorbent acidity while it was found to increase acidity for Al_2O_3 systems except for NiO/Al_2O_3.

Table 6. 2: BET analysis and surface pH for adsorbent

ADSORBENT	Surface area (m^2/g)	Average pore size (nm)	Surface acidity pH
AC	564.45	3.25	7.34
AC/CoO	426.99	3.25	8.36
AC/NiO	635.42	3.26	8.05
AC/CuO	611.46	3.58	7.98
AC/ZnO	535.65	5.36	8.55
Al_2O_3	200.85	3.58	6.80
Al_2O_3/CoO	222.24	3.25	6.22
Al_2O_3/NiO	229. 29	3.25	8.36
Al_2O_3/CuO	254.80	3.25	6.14
Al_2O_3/ZnO	219.08	3.30	5.70

Figure 6.1 presents adsorption-desorption isotherm for AC systems and Al_2O_3. It was observed that for AC systems the highest volume adsorbed was for AC/NiO and the least for AC/CoO; this is consistent with surface area results for AC systems since the pore sizes were similar. For all AC adsorbents systems, no apparent plateau was observed suggesting adsorption occurs over the entire pressure interval indicating the presence of a wide range of pore diameters even though overall the adsorbent was mesoporous (Kumar and Jena, 2016). Al_2O_3 systems showed a type II IUPAC classification of adsorption isotherms suggesting multilayer adsorption and a macroporous adsorbent.

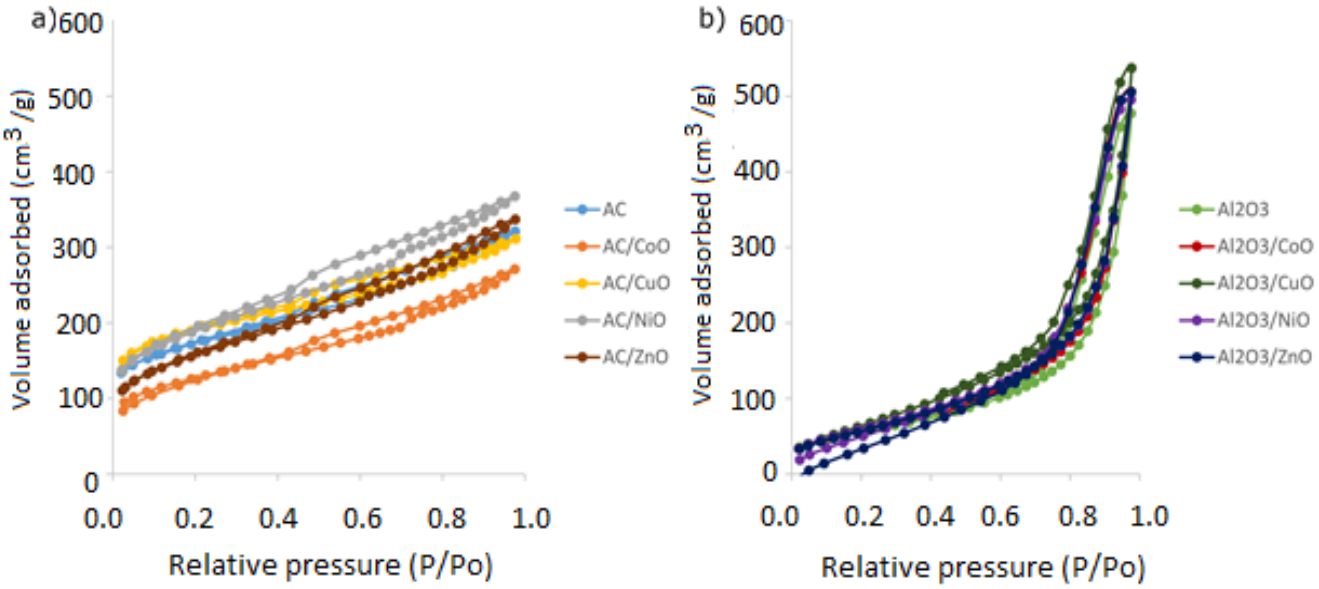

Figure 6.1: Nitrogen adsorption-desorption isotherms for a) MO/AC and b) MO/Al_2O_3

Conventional diesel with a total sulphur content of around 103 ppm was used for the study. A chromatogram for the diesel is shown in Figure 6.2 below, with some of the primary compounds identified. It was observed that the most abundant sulphur compounds are 4,6 DMDBT and TMDBT with the latter being never used in model diesel work.

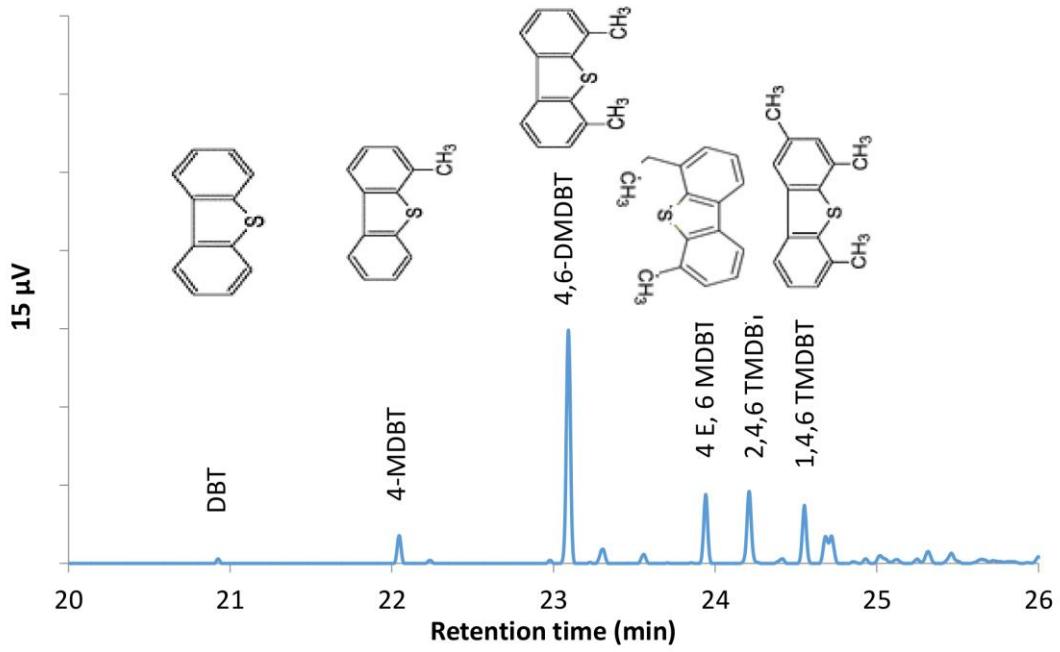

Figure 6. 2: Conventional diesel chromatogram from GC-PFPD

The activity of metal oxides supported on Al_2O_3 and AC were investigated using model diesel; the results are presented in Figure 6.3. It was observed that AC and AC/MO had higher activity compared to Al_2O_3 and Al_2O_3/MO systems. It was also observed that adsorption was fast within the first 60 min for AC based systems. Then it slowed down to achieve pseudo equilibrium around 120 min. The rapid initial adsorption rate was due to the vacant adsorption site and hence a high solute gradient. With time, the remaining vacant sites were further from the adsorbent surface, DBT had to travel further and deeper into micro-pores encountering much resistance and repulsion from adsorbed solute hence a decrease in adsorption rate (Srivastav and Srivastava, 2009). On the other hand, adsorption of DBT from model diesel using Al_2O_3-based adsorbents was observed to be highest at 20/30 min, and after that, it dropped. The drop might be due to a poor adsorbent-DBT bond, which breaks easily. A comparison between AC and Al_2O_3 supported adsorbents suggests that AC is better support for adsorption which is consistent with work reported by Wang and Yang, 2007. The poor activity of Al_2O_3 might be

explained by Pearson's hard/soft (Lewis) acids/bases concept since Al_2O_3 is a known strong acid, hence poor activity since DBT is a soft-intermediate base. Furthermore, the addition of these metal oxides on both supports showed no benefit suggesting the metal oxides added were replacing more active acids sites under these condition on AC as observed in Table 6.2 by a drop in surface acidity. Contrary to this, the interactions between the metal oxides and Al_2O_3 produced even more acidic adsorbates hence poor activity.

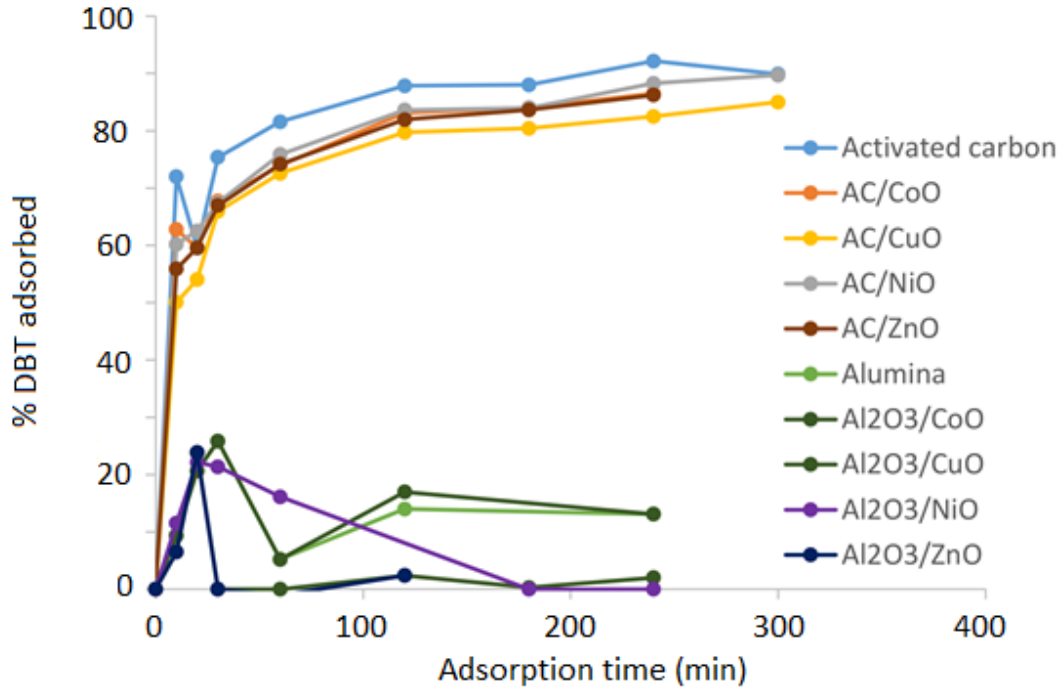

Figure 6.3: Adsorption comparison of 5 wt% MO/AC versus MO/Al_2O_3 at 5 wt% adsorbent: model diesel at 25 ^oC and atmospheric pressure.

The results comparing the activity of AC-based adsorbents on model diesel and conventional diesel are presented in Figure 6.4 below. It was observed that when treating model diesel the difference among the five adsorbents was not so pronounced.

However, when treating conventional diesel it became more pronounced, and the activity is in this order: AC> AC-NiO >>AC-CuO >AC-CoO >AC-ZnO. The difference in activity when treating conventional diesel and model diesel might be due to competitive adsorption on the

adsorbents with some compounds found in diesel which have a similar chemical structure to sulphur compounds, such as, naphthalene and indole. It is important to note that adsorption trends of adsorptive desulphurization for both model diesel and conventional diesel are maintained, i.e. highest activities were observed for AC and AC/NiO for both systems. The addition of MO showed no benefit.

These results are contrary to what has been found by some researchers who have reported improved activity of AC upon addition of metal oxides (Saleh et al., 2017). This difference could be due to different sulphur compounds being treated. In work done by Saleh, 2018 and (Danmaliki and Saleh, 2017) it has been shown that activity improvement is significant for low molecular weight sulphur compounds (lower than DBT) but for higher molecular sulphur compounds little increase was observed. In this work DBT and higher molecular weight sulphur compounds were used.

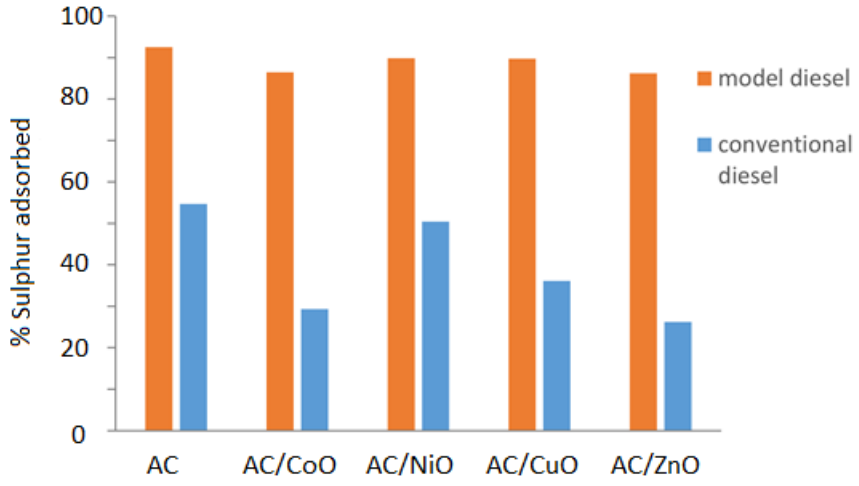

Figure 6.4: Adsorption comparison of 5wt% MO/AC for model diesel versus conventional diesel at 5 wt% adsorbent: model diesel (or conventional diesel) at 25 ^{o}C and atmospheric pressure.

Because of poor activity of Al_2O_3 supported metal oxides in desulphurizing model diesel as observed in Figure 6.3, 10 wt% metal oxide was used to investigate the adsorption of conventional diesel. The support, Al_2O_3, showed the highest removal efficiency of 34 % while

a negligible difference was observed for NiO, CuO and ZnO supported on Al_2O_3. The poor activity of Al_2O_3 supported metal oxides as shown in Figure 6.5 might be attributed to a lower surface area and poor affinity for sulphur compounds as observed by desorption after 20 min. The poor activity for Al_2O_3 could also be due to a highly macroporous structure as shown by the type II IUPAC classification. A number of researchers have reported a good correlation between microporosity of adsorbent and adsorption activity (Deliyanni et al., 2009; Seredych et al., 2009; Seredych and Bandosz, 2010). These researchers suggest that adsorption of most sulphur compounds takes place in the microporous sites hence these sites play a critical role in the adsorption capacity of an adsorbent. Finally, the poor activity of Al_2O_3 could be due to the strong acidic nature of Al_2O_3 as explained earlier.

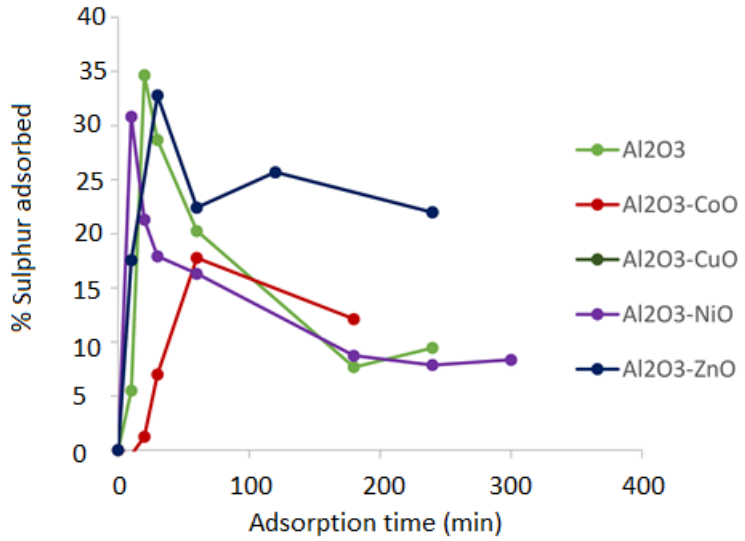

Figure 6.5: Adsorption of sulphur from conventional diesel using 10 wt% MO/Al_2O_3 at 5 wt% adsorbent: conventional diesel at 25 ^oC and atmospheric pressure.

The relative selectivity of the most active adsorbent, AC, for different sulphur compounds in conventional diesel was calculated based on the equation (6.1) and (6.2). It was observed from Table 6.3 that selectivity was decreasing in this order: 4-MDBT> 1,4,6 TMDBT> 4,6 DMDBT> 4E,6 MDBT> 2,4,6 TMDBT. This suggests that the most adsorbed is the smallest in size and hence the adsorption might be controlled by steric hindrances.

This work is in agreement with work done by some researchers that reported that activity improved with an increase in molecular size from thiophene to DBT and thereafter, a decrease in activity was reported (Tang et al., 2011; Saleh, 2018). However, it should be stated that the work reported was based on molecules smaller than the ones reported in this work. The results of this work is also in agreement with work done by Safa et al., (2017) for an oxidative desulphurization for molecules similar to the ones investigated in this work that steric hindrances significantly affect activity.

Table 6. 3: Activated carbon selectivity

Compound	Selectivity
4-MDBT	1.00
4,6 DMDBT	0.33
4 E, 6 MDBT	0.33
2,4,6 TMDBT	0.33
1,4,6 TMDBT	0.56

6.3.1 Kinetics of DBT adsorption from Model diesel using AC

To understand the adsorption process of the most active adsorbent, AC, experimental data was fitted to the pseudo-first-order model and the pseudo-second-order model. Pseudo-first order and pseudo-second-order models were tested by fitting the experimental data to equations 6.3 and 6.4 given below respectively.

$$\log(q_e - q_t) = logq_e - \frac{K_{ad}t}{2.303} \qquad (6.3)$$

Where q_e is the amount of adsorbate loaded on the adsorbent under equilibrium, q_t is the amount of adsorbate loaded on adsorbent at time t, and $k_{ad}/2.303$ is the pseudo-first-order rate constant.

$$\frac{t}{q_t} = \frac{1}{[K_s q_e{}^2]} + \frac{t}{q_e} \qquad (6.4)$$

Where $[K_s {q_e}^2] = h$ is the initial adsorption rate (mg/g min) as $t \to 0$

The regression coefficients were observed to be 0.795 and 0.999 for the pseudo-first-order and pseudo-second-order models respectively, shown in Figure 6.6. The results suggest that the experimental data fit more closely pseudo-second-order reactions. This is consistent with the work of many researchers on desulphurization (Saleha and Danmaliki, 2016). These results suggest mainly chemical adsorption between adsorbent and DBT this could also explain the dependence of selectivity on steric hindrances.

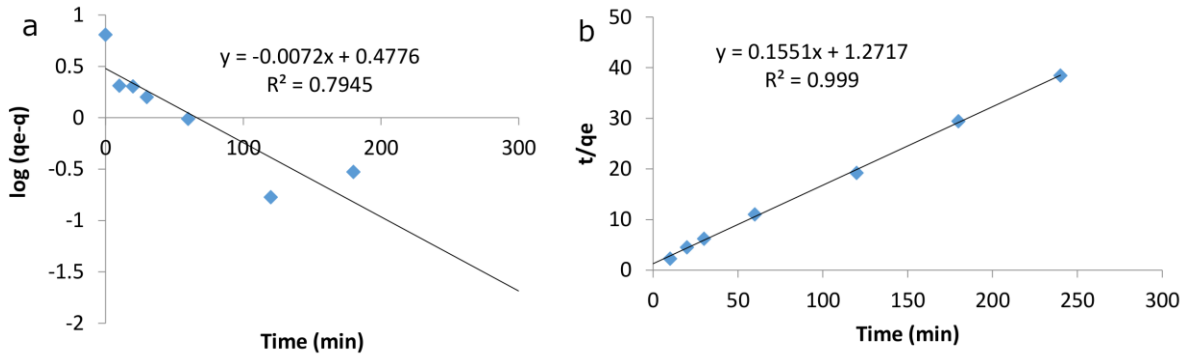

Figure 6.6: Kinetic models for DBT adsorption from model diesel using AC: a) Pseudo-first order and b) Pseudo-second order model

6.3.2 Regeneration

The regeneration of the AC treating conventional diesel and model diesel were carried out using solvent extraction of adsorbed compounds. The solvent used was octane which has been reported to show good activity (Li et al., 2016). It was observed that there was a decrease in activity with each regeneration and it reached 60% and 43% of its initial activity on the fourth run for model diesel and conventional diesel respectively as shown in Figure 6.7.

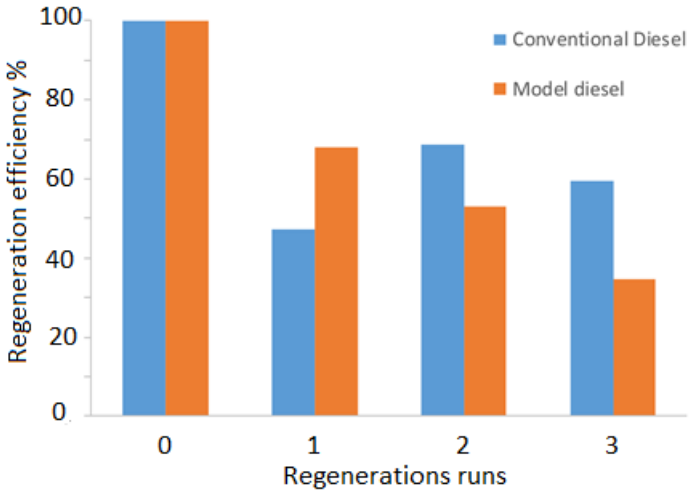

Figure 6.7: Regeneration stability of AC treating model and conventional diesel (50 ^{o}C, 180 min with n-octane)

The poor regeneration of AC treating conventional diesel has been suggested to be due to competitive desorption between polycyclic aromatic hydrocarbons (PAHs) and S-compounds (Li et al., 2016). This is consistent with the analysis results of the extraction/regeneration solvent. Some hydrocarbons were observed to desorb competitively with lower sulphur compounds. The chromatogram showing the hydrocarbons in diesel and those observed during desorption is presented in Figure 6.8. The two large peaks on the chromatogram represent the extraction solvents. The other reason for poor activity with regeneration which could also explain a drop in activity when treating model diesel is poor desorption of sulphur compounds under the experimental conditions, and this is consistent with Li et al., (2016) work.

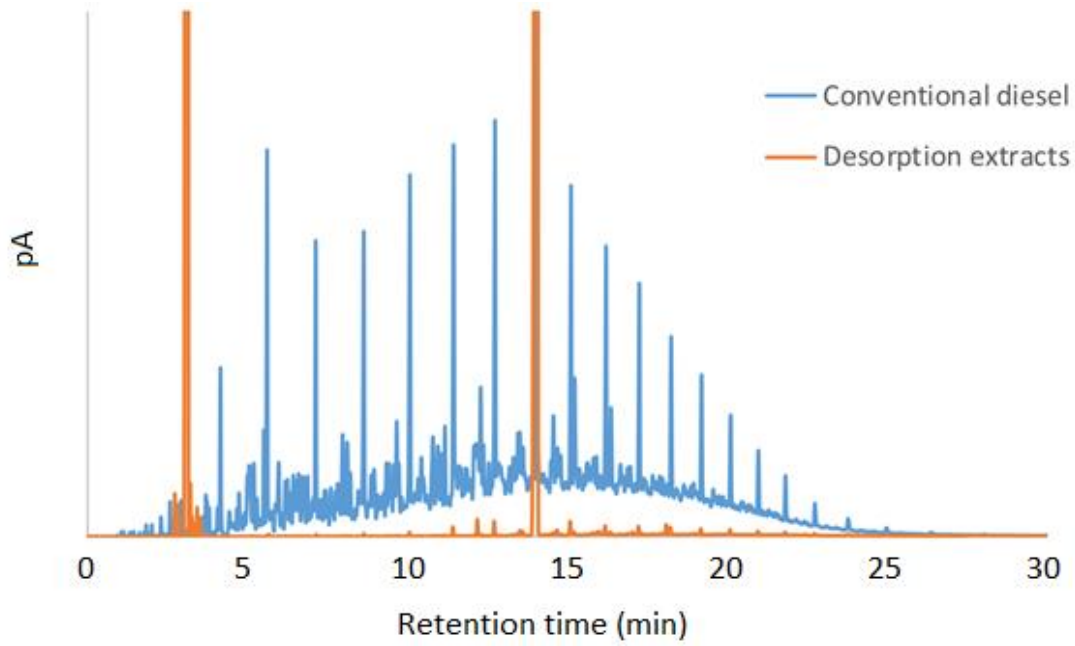

Figure 6.8: Desorption compounds chromatogram observed on FID (hydrocarbons)

6.3.3 Mechanism of adsorption

The adsorbent was observed to show good selectivity towards DBT in the presence of toluene and hexadecane when treating model diesel. However, when conventional diesel was treated, poor activity was observed because of poor selectivity. Since the kinetics suggested adsorption was mainly chemical, pseudo-second-order, we propose that adsorption was primarily via π-bonding. The chemical bonding via sulphur atom was eliminated because the presence of non-sulphur PAHs would not have affected activity when treating conventional diesel.

6.4 Conclusion

In this work intermediate, Lewis metal oxides (MO) acids were loaded on activated carbon (AC) and alumina (Al_2O_3) to desulphurize diesel using adsorption. The following metal oxides were used; CoO, NiO, CuO, and ZnO. The experimental data indicate that adding Lewis metal oxides acids on both activated carbon and alumina had no significant benefits under the experimental condition investigated. For carbon loaded metal oxides, NiO showed the highest activity when using both model diesel and conventional diesel. Alumina has demonstrated to be bad support for the metal oxides as the activity of alumina and alumina supported metal oxides was approximately 4 times less than of activated carbon for model diesel desulphurization. A comparison between the activity of model diesel and conventional diesel has shown that activity based on model diesel although higher it does reflect activity in a real system of conventional diesel and hence use of model diesel to screen adsorbents is not a "bad" practice. Finally, it was observed that the challenge with the regeneration of adsorbent that treated real diesel is due to the competitive desorption of hydrocarbons and sulphur compounds.

References

Ahmad, W., Ahmad, I., Ishaq, M., and Ihsan, K. (2017). Adsorptive desulphurization of kerosene and diesel oil by Zn impregnated montmorollonite clay. Arab. J. Chem. *10*, S3263–S3269.

Bu, J., Loh, G., Gwie, C.G., Dewiyanti, S., Tasrif, M., and Borgna, A. (2011). Desulphurization of diesel fuels by selective adsorption on activated carbons: Competitive adsorption of polycyclic aromatic sulphur heterocycles and polycyclic aromatic hydrocarbons. Chem. Eng. J. *166*, 207–217.

Danmaliki, G.I., and Saleh, T.A. (2017). Effects of bimetallic Ce/Fe nanoparticles on the desulphurization of thiophenes using activated carbon. Chem. Eng. J. *307*, 914–927.

Danmaliki, G.I., Saleh, T.A., and Shamsuddeen, A.A. (2017). Response surface methodology optimization of adsorptive desulphurization on nickel/activated carbon. Chem. Eng. J. *313*, 993–1003.

Deliyanni, E., Seredych, M., and Bandosz, T.J. (2009). Interactions of 4,6-Dimethyldibenzothiophene with the Surface of Activated Carbons. Langmuir *25*, 3352–3360.

Fallah, R.N., and Azizian, S. (2012). Removal of thiophenic compounds from liquid fuel by different modified activated carbon cloths. Fuel Process. Technol. *93*, 45–52.

Hernandez, S.P., Fino, D., and Russo, N. (2010). High performance sorbents for diesel oil desulphurization. Chem. Eng. Sci. *65*, 603–609.

Hernández-Maldonado, and Yang, R.T. (2004). New sorbents for desulphurization of diesel fuels via π-complexation. AICHE J *50*, 791–801.

Hernández-Maldonado, A.J., Qi, G., and Yang, R.T. (2005). Desulphurization of commercial fuels by π-complexation: Monolayer CuCl/γ-Al2O3. Appl. Catal. B Environ. *61*, 212–218.

Jeevanandam, P., Klabunde, K.J., and Tetzler, S.H. (2005). Adsorption of thiophenes out of hydrocarbons using metal impregnated nanocrystalline aluminum oxide. Microporous Mesoporous Mater. *79*, 101–110.

Kumar, A., and Jena, H.M. (2016). Preparation and characterization of high surface area activated carbon from Fox nut (Euryale ferox) shell by chemical activation with H 3 PO 4. Results Phys. *6*, 651–658.

Kumar, S., Srivastava, V.C., and Badoni, R.P. (2011). Studies on adsorptive desulphurization by zirconia based adsorbents. Fuel *90*, 3209–3216.

Li, W., Chen, J., Cong, G., Tang, L., Cui, Q., and Wang, H. (2016). Solvent desulphurization regeneration process and analysis of activated carbon for low-sulphur real diesel. RSC Adv. *6*, 20258–20268.

Maes, M., Trekels, M., Boulhout, M., Schouteden, S., Vermoortele, F., Alaerts, L., Heurtaux, D., Seo, Y.-K., Hwang, Y.K., Chang, J.-S., et al. (2011). Selective Removal of N-Heterocyclic Aromatic

Contaminants from Fuels by Lewis Acidic Metal-Organic Frameworks. Angew. Chem. *123*, 4296–4300.

Muzic, M., Sertic-Bionda, K., and Gomzi, Z. (2008). Kinetic and Statistical Studies of Adsorptive Desulphurization of Diesel Fuel on Commercial Activated Carbons. Chem. Eng. Technol. *31*, 355–364.

Ruberti, T. (2003). Off-grid hybrids: Fuel cell solar-PV hybrids. Refocus *4*, 54–57.

Safa, M.A., Al-Shamary, T., Al-Majren, R., Bouresli, R., and Ma, X. (2017). Reactivities of Various Alkyl Dibenzothiophenes in Oxidative Desulphurization of Middle Distillate with Cumene Hydroperoxide. Energy Fuels *31*, 7464–7470.

Saleh, T.A. (2018). Simultaneous adsorptive desulphurization of diesel fuel over bimetallic nanoparticles loaded on activated carbon. J. Clean. Prod. *172*, 2123–2132.

Saleh, T.A., and Danmaliki, G.I. (2016). Influence of acidic and basic treatments of activated carbon derived from waste rubber tires on adsorptive desulphurization of thiophenes. J. TheTaiwan Inst. Chem. *60*, 460–468.

Saleh, T.A., Sulaiman, K.O., AL-Hammadi, S.A., Dafalla, H., and Danmaliki, G.I. (2017). Adsorptive desulphurization of thiophene, benzothiophene and dibenzothiophene over activated carbon manganese oxide nanocomposite: with column system evaluation. J. Clean. Prod. *154*, 401–412.

Saleha, T.A., and Danmaliki, G.I. (2016). Adsorptive desulphurization of dibenzothiophenefrom fuels by rubber tyres-derived carbons:Kinetics and isotherms evaluation. Process Saf. Environ. Prot. *102*, 9–16.

Seredych, M., and Bandosz, T.J. (2007). Template-Derived Mesoporous Carbons with Highly Dispersed Transition Metals as Media for the Reactive Adsorption of Dibenzothiophene. Langmuir *23*, 6033–6041.

Seredych, M., and Bandosz, T.J. (2010). Adsorption of Dibenzothiophenes on Nanoporous Carbons: Identification of Specific Adsorption Sites Governing Capacity and Selectivity. Energy Fuels *24*, 3352–3360.

Seredych, M., Lison, L., Jans, U., and Bandosz, T.J. (2009). Textural and chemical factors affecting adsorption capacity of activated carbon in highly efficient desulphurization of diesel fuel. Carbon *47*, 2491–2500.

Shakirullah, M., Ahmad, I., Ishaq, M., and Ahmad, W. (2009). Study on the role of metal oxides in desulphurization of some petroleum fractions. J. Chin. Chem. Soc. *56*, 107–114.

Srivastav, A., and Srivastava, V.C. (2009). Adsorptive desulphurization by activated alumina. J. Hazard. Mater. *170*, 1133–1140.

Tang, K., Hong, X., Zhao, Y.H., and Wang, Y.G. (2011). Adsorption Desulphurization on a Nanocrystalline NaY Zeolite Synthesized Using Carbon Nanotube Templated Growth. Pet. Sci. Technol. *29*, 779–787.

Tang, X., Lu, H., Li, J., and Chen, L. (2016). Adsorption desulphurization performance and mechanism over nanocrystalline NiO/Al2O3-1 adsorbent. Russ. J. Appl. Chem. *89*, 2043–2049.

Triantafyllidis, K.S., and Deliyanni, E.A. (2014). Desulphurization of diesel fuels: Adsorption of 4,6-DMDBT on different origin and surface chemistry nanoporous activated carbons. Chem. Eng. J. *236*, 406–414.

Wang, Y., and Yang, R.T. (2007). Desulphurization of Liquid Fuels by Adsorption on Carbon-Based Sorbents and Ultrasound-Assisted Sorbent Regeneration. Langmuir *23*, 3825–3831.

Wang, Y., Yang, R.T., and Heinzel, J.M. (2008). Desulphurization of jet fuel by π-complexation adsorption with metal halides supported on MCM-41 and SBA-15 mesoporous materials. Chem. Eng. Sci. *63*, 356–365.

Xiao, J., Li, Z., Liu, B., Xia, Q., and Yu, M. (2008). Adsorption of Benzothiophene and Dibenzothiophene on Ion-Impregnated Activated Carbons and Ion-Exchanged Y Zeolites. Energy Fuels *22*, 3858–3863.

Xuemin, C., Yufeng, H., Jiguang, L., Qianqing, L., and Wenjia, Y. (2008). Desulphurization of Diesel Fuel by Extraction with [BF4] based Ionic Liquids. Chin. J. Chem. Eng. *16*, 881–884.

Yan, Z., Wang, J., Zou, R., Liu, L., Zhang, Z., and Wang, X. (2012). Hydrothermal Synthesis of CeO_2 Nanoparticles on Activated Carbon with Enhanced Desulphurization Activity. Energy Fuels *26*, 5879–5886.

Yu, M., Li, Z., Ji, Q., Wang, S., Su, D., and Lin, Y.S. (2009). Effect of thermal oxidation of activated carbon surface on its adsorption towards dibenzothiophene. Chem. Eng. J. *148*, 242–247.

Zhao, D., Zhang, J., Duan, E., and Wang, J. (2008). Adsorption equilibrium and kinetics of dibenzothiophene from n-octane on bamboo charcoal. Appl. Surf. Sci. *254*, 3242–3247.

Zhou, A., Ma, X., and Song, C. (2009). Effects of oxidative modification of carbon surface on the adsorption of sulphur compounds in diesel fuel. Appl. Catal. B Environ. *87*, 190–199.

7. EFFECT OF SUPPORT ON SELECTED LEWIS ACID METAL OXIDE

This work has been prepared in the form of a paper for future publication. Part of this work was presented at the following conference:

Catalysis Society of South Africa (CATSA), Waterberg, Limpopo (11-14th Nov 2018)

Summary

In this work, NiO was loaded on different supports - activated carbon (AC), alumina (Al_2O_3), silica (SiO_2) and titania (TiO_2) - with the aim of investigating the effect on desulphurization. The adsorbent system was characterised using FTIR, XRD, SEM, TPD-pyridine, TGA and BET. The addition of NiO was observed to cause a slight increase in activity at 30 ^oC and low loading (~5% NiO/support). Thereafter, a decrease in activity was observed with an increase in NiO loading, which is attributed to agglomeration with high NiO loading. NiO loading was also observed to decrease activity and selectivity towards high molecular weight sulphur compounds for AC and Al_2O_3, while it had a positive effect on SiO_2 and no effect on TiO_2. This positive effect was a result of synergy between NiO and SiO_2 since pure NiO was observed to favour the adsorption of low molecular weight sulphur molecules, i.e. DBT and 4MDBT. Another positive synergy was that the addition of NiO on SiO_2 reduced hydrocarbon adsorbed by the system, and hence improved its overall selectivity. Finally, when conventional diesel was used, it was observed that the addition of NiO (5 %) on these supports led to an increase in activity at a higher temperature (60 ^oC). The higher activity at a high temperature of 60 ^oC was attributed to poor adsorption of polyaromatic hydrocarbon at this temperature and increased involvement of chemical bonds

Keywords: adsorption desulphurization; nickel oxide; polyaromatic hydrocarbon; activated carbon

7.1 Introduction

Sulphur is the third most abundant element in diesel fuel after carbon and hydrogen (Gawande and Kaware, 2016). Dibenzothiophene (DBT) and its derivatives are the main organosulphur compounds in fuels. When it undergoes combustion, sulphur in diesel produces SO_X gases that are precursors of acid rain and smog. It is of paramount importance to reduce the sulphur content in diesel for environmental reasons and also to prevent the deactivation of the catalytic converter catalyst. The presence of sulphur in diesel has also prevented the use of diesel as a source of H_2 because sulphur deactivates the fuel cell catalyst (Ming et al., 2002).

Hydrodesulphurization has been used conventionally for desulphurization and it is very effective in removing thiols (Lee, 2020). However, due to its inability to remove highly alkylated DBT in fuels efficiently, several methods are being investigated, and adsorption has been seen as a potential solution (Tang et al., 2016). As one of the promising approaches, adsorptive desulphurization can deeply remove sulphur compounds under atmospheric pressure and ambient temperature (Tang et al., 2016). However, poor selectivity has been reported to reduce sulphur adsorbed, due to competitive adsorption of compounds like polycyclic aromatic hydrocarbons found in diesel (Bu et al., 2011; Xiao et al., 2012). The other challenge with adsorption is low adsorption capacity. Adsorption capacity is a function of morphology and the number of active sites available, which is, in turn, a function of the synthesis method used. Highly dispersed active sites of the correct size should lead to better activity (De Gisi et al., 2016; Aslam et al., 2021).

A number of both soft and intermediate acids have been reported to be active for adsorptive desulphurization, including NiO, ZnO, MgO, CuO, Zn and PbCl (Xiao et al., 2008; Vilarrasa-García et al., 2010; Shakirullah et al., 2009; Rodrigues et al., 2014). A common practice is to load these Lewis acids on a support material. The principal aim of providing the support being: i) to allow dispersion of the metal oxide (MO) on the support and hence increase the surface area, as well as to improve the mechanical properties of the active material, which is achieved with inert support; ii) to improve the activity of the MO through synergy between the MO and the support. This requires an understanding of the adsorption mechanism and the support used. MO has been supported on different supports, such as alumina (Al_2O_3), activated carbon (AC), titania (TiO_2), and silica (SiO_2). The advantage of using AC as support is that its pore structure and the internal surface can be widely varied using different treatment methods.

Furthermore, the expensive metals used in the active phase can be recovered easily from the spent adsorbent by burning off the carbon support (Jüntgen, 1986). The support common phases of TiO_2 are anatase and rutile phase. The anatase phase is known to have a strong interaction with metal, whilst the interaction with rutile are usually weaker (Jongsomjit et al., 2005). The challenge with TiO_2 is the limited surface area, and hence the low adsorption ability. Al_2O_3 and SiO_2 are known to be acidic supports, with Al_2O_3 being more acidic. The use of these different supports (with different characteristics) natures to achieve the same objective of desulphurization suggests a trial and error approach. This work analyses the rationale of supporting MO on the support for adsorption desulphurization.

Several studies have shown the superior performance of Ni as a desulphurization adsorbent. In reported studies, Ni has been used as Ni^0 or as Ni^{2+} and the major sulphur compounds used were BT, DBT, 4MDBT and 4,6 DMDBT (Hernandez et al., 2010; Sentorun-Shalaby et al., 2011; Sarda et al., 2012; Mansouri et al., 2014). It has been reported that the removal of DBT decreases with an increase in the methyl groups on the DBT structure. This has been attributed to the adsorption being via the Ni-S bond (Velu et al., 2005; Kim et al., 2006). When using Ni^{+2}, π-complex bands have been observed to dominate sulphur compounds adsorption. The advantage of using Ni^{+2} is that its production does not require adsorbent reduction under H_2 and a high temperature, as with the Ni^0 adsorbent synthesis. The Ni^{+2} adsorbent also usually requires low-temperature adsorption, unlike Ni^0 adsorbents. There is limited information regarding selectivity and the mechanism of the Ni-based adsorbent (Sentorun-Shalaby et al., 2011) and even fewer reports on commercial diesel treatment (Sarda et al., 2012).

In this work, intermediate Lewis acid MO NiO was supported on TiO_2, SiO_2, Al_2O_3 and AC. This study shows the effect of different supports on the ability of NiO to remove sulphur from diesel fuels. The effects of support were analysed using thermogravimetric analysis (TGA) and temperature-programmed desorption (TPD)-pyridine, and by analysis of the selectivity of these adsorbents for different sulphur compounds when using model diesel and conventional diesel.

7.2 Materials and method

7.2.1 Material

99 % hexadecane, 99.5 % toluene, 98 % dibenzothiophene (DBT), 4 MDBT (4-methyl dibenzothiophene) and 4,6 DMDBT (4,6-dimethyl dibenzothiophene) were obtained from Sigma Aldrich. The absorbents used for this work were obtained also from Sigma Aldrich, i.e. activated charcoal, titanium, alumina and silica

7.2.2 Adsorbent Synthesis

Support synthesis

TiO_2 (Degussa P25 containing 17 % rutile) was mixed with deionised water in a mass ratio of 1:1 and dried in air at 120 °C for 16 h. The dried support was then calcined in air at 650 °C for 2 h to achieve 78 % rutile (Mguni et al., 2013). SiO_2, AC and Al_2O_3 were used as received.

Adsorbent preparation

NiO/support sorbents with different Ni loads (40, 30, 15, 10 and 5wt %) were prepared via incipient wetness impregnation, using different supports. The supports used were TiO_2 (with a surface area of 15 m^2/g), Al_2O_3 (210 m^2/g), SiO_2 (372 m^2/g) and AC (848 m^2/g). Following impregnation, the sorbents were dried overnight at 100 ^oC and calcined at 450 ^oC for 4h, and then ground and sieved to obtain a particle size of 300 – 200 µm for desulphurization.

Preparation of NiO Nanocrystals.

NiO nanocrystals were prepared by dissolving Ni $(NO_3)_2.6H_2O$ (5.815g) in 20 mL of methanol and then stirring at room temperature for 60 min. 5.0 M NaOH was added dropwise to a 20 mL solution of 1.0 M $Ni(NO_3)_2.6H_2O$, 1.0 M, which was stirred vigorously by a magnetic stirring apparatus for 120 min at room temperature. The mixture was then dried at 100-110 ^oC for 1 h, and a light green powder was produced. The product was then transferred to a porcelain crucible and calcined at 450 ^oC for 1 h.

7.2.3 Adsorption experiments

Adsorption experiments were carried out with diesel and model diesel. The model diesel was synthesized using 85 v/v% hexadecane, 15 v/v% toluene and a fixed amount of DBT, 4MDBT and 4,6 DMDBT, in order to achieve 100 ppm, 100 ppm, and 300 ppm, respectively. The adsorption experiments were carried out at atmospheric pressure and the adsorbent quantity was varied as a weight percentage of total diesel mass.

A sample for quantification of sulphur was taken at time intervals and analysed using a Gas Chromatography–Pulsed Flame Photometric Detector (GC-PFPD).

The selectivity of the adsorbents was calculated based on equation 7.1 below.

$$selectivity = \frac{\frac{q_{e\,i}}{c_{e\,i}}}{\frac{q_{e\,DBT}}{c_{e\,DBT}}} \qquad (7.1)$$

Where: q_{ei}- is equilibrium adsorbent loading of component i; C_{ei}- is the equilibrium concentration of component i, $q_{e\ DBT}$ and $C_{e\ DBT}$ are equilibrium adsorbent loading and equilibrium concentrations of reference compound DBT, respectively.

7.2.4 Characterisation

FTIR spectra were recorded using a Bruker Tensor 27 ATR in the range 4000–400 cm^{-1}, so as to determine the functional groups in the adsorbents. The adsorbents were mixed with KBr to produce pellets for analysis. The structure of the catalyst system was analysed using a Rigaku SmartLab X-ray diffraction (XRD) apparatus with CuKα (λ=1.54) radiation. Samples were scanned over a 2θ range of 5–90° with a 0.01° step size and a scan speed of 0.12 s/ step. The mean crystallite size of NiO in the catalyst sample was estimated from the full width at half maxima of the diffraction peak using the Scherrer equation and a shape factor of 0.94. The BET analysis was performed to determine the surface area and pore distribution by N_2 adsorption using NOVA 1200e. Temperature programmed desorption (TPD) experiments were conducted using a Micromeritics AutoChemII Chemisorption Analyzer. 200 mg of adsorbent sample was pre-treated at 250 °C under He flow for 4 h. After cooling to room temperature in a He atmosphere, the gas was switched to pyridine vapour with He. After physically adsorbed pyridine was purged by He flow at room temperature, the sample was heated to 350 °C at 10 ^{o}C/min, and the liberated pyridine was monitored continuously utilising a CIRRUS quadrupole mass spectrometer. TGA was carried using a Universal Analysis 2000. A sample of 10 mg was heated from 50 °C to 900 ^{o}C at a heating rate of 10 ^{o}C/min under an N_2 atmosphere.

7.3 Results and Discussion

7.3.1 Characterization results

Figure 7.1 shows the XRD patterns for the adsorbents after calcination. The major peaks for NiO that appear at 2θ: 37.101°, 43.301°, 62.871°, 76.501° and 79.221° can be readily indexed as (111), (200), (220), (311) and (222) crystal planes of the bulk NiO, respectively (El-Kemary et al., 2013). These peaks were observed after supporting different supports, which confirms that the calcination temperature was sufficient for decomposing $Ni(NO_3)_2$ on all supports. The supports XRD patterns were observed to be in good agreement with the standard XRD patterns. Major diffraction peaks for anatase and rutile phases were observed for TiO_2 at 25° and 28°, respectively. A broad peak centred at 2θ = 23.2° was observed for SiO_2, which indicates that the SiO_2 was amorphous (Zhong et al., 2010). The $10\%NiO/Al_2O_3$ was observed to be a combination of γ-Al2O3 and NiO peaks. Finally, the carbon samples have two broad diffraction peaks at around 2θ = 24° and 43° in the XRD patterns, which are consistent with that of graphitic carbon (Xu et al., 2015).

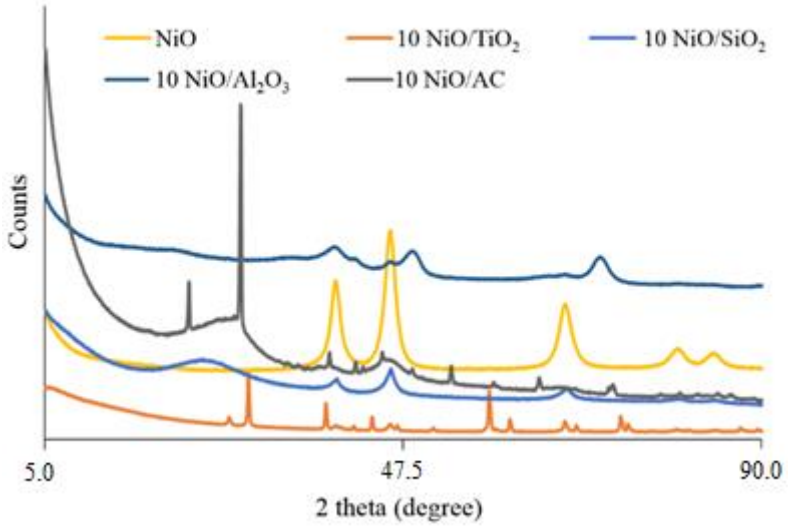

Figure 7.1: XRD spectrum for adsorbents after calcination

The SEM and EDX results presented in Figure 7.2 show that Ni was evenly distributed on four supports. The activated carbon was observed to contain several contaminants (including Si, Fe, Cu, Al, S and Ca), while no contaminants were observed with the other supports.

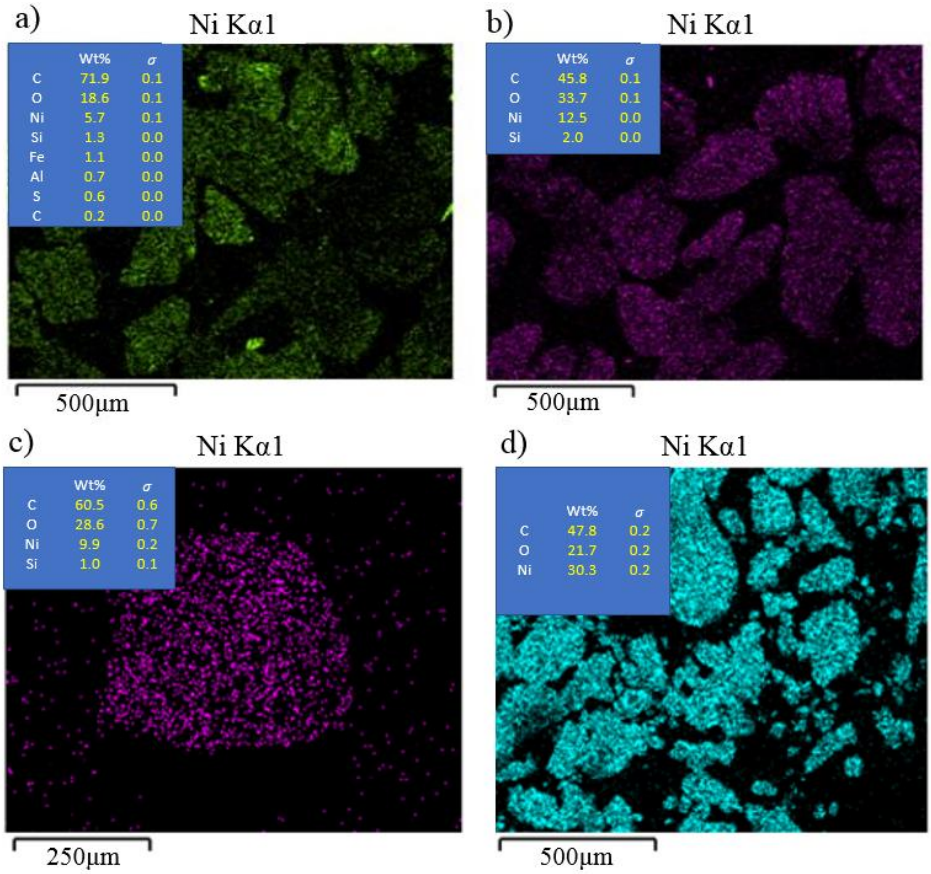

Figure 7.2. Map images, with an EDX inset a) NiO/AC b) NiO/SiO_2 c) NiO/Al_2O_3 d) NiO/TiO_2 e) NiO

The surface area and average pore size for the adsorbents are presented in Table 7.1. There was little difference in the surface area before and after loading NiO on the support. The surface area was observed to follow this decreasing order: AC>SiO_2>Al_2O_3 >NiO>TiO_2. The pore size had the following increasing order: AC<SiO_2<NiO<Al_2O_3<TiO_2.

Table 7. 1: BET Surface area and average pore of adsorbents

Adsorbent	Surface area m^2/g	Average pore size nm
AC	845	2.09
5%NiO/AC	786	2.66
SiO_2	372	3.49
5%NiO/SiO_2	363	3.03
Al_2O_3	210	16.35
5%NiO/Al_2O_3	192	16.43
TiO_2	15	38.81
5%NiO/TiO_2	16	34.72
NiO	153	6.3

The desorption experiments that used TGA showed the influence of metal oxide on the adsorption of molecules. (See Figure 7.3.) The model diesel used was composed of toluene, hexadecane, DBT, 4MDBT and 4,6 DMDBT. The addition of NiO was observed to have a different effect on the support's major desorption temperature. This major peak point is believed to be made up of sulphur compounds, based on work done by Yu et al. (2007). The major last desorption peak temperature was observed to be in this increasing order: Al_2O_3<AC<5Ni/Al_2O_3<SiO_2≈5Ni/SiO_2 < < TiO_2≈5Ni/TiO_2< NiO. These results suggest that the addition of NiO on alumina increases the bonding strength between the adsorbate and adsorbent, as the desorption peak increased from 249 to 512 ^{o}C. The TGA results also suggest that AC had many active sites of different strength from 180 ^{o}C to 520 ^{o}C. The many active sites might be due to many metal contaminates on the adsorbate. The addition of NiO on TiO_2 and SiO_2 seems to not influence the adsorption strength of the sulphur compounds.

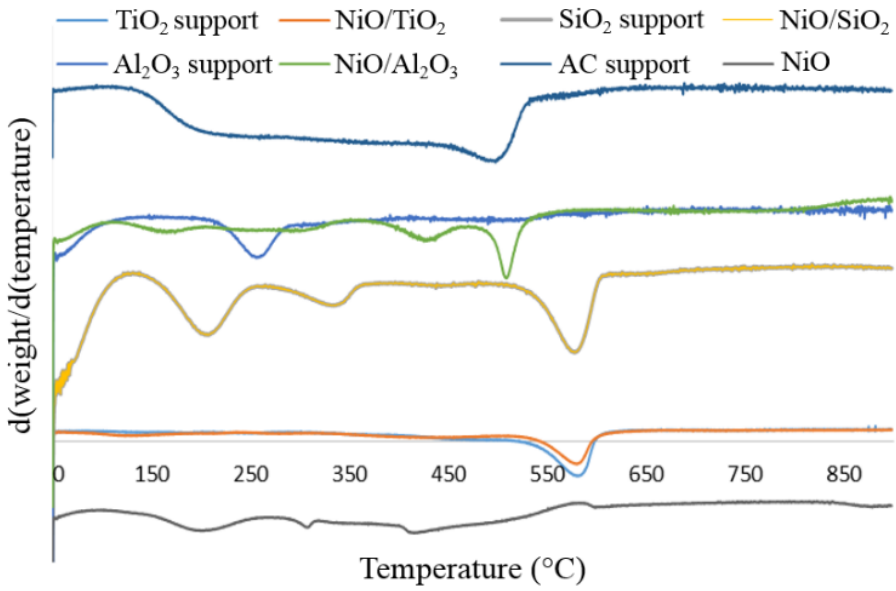

Figure 7.3. Desorption analysis using TGA for MO and MO/support

The quantity of adsorbed compounds was mainly a function of the support. The exception was SiO_2, where the addition of NiO reduced the amount of solvent adsorbed by the adsorbent. The amount of solvent adsorbed by the different supports were in this decreasing order: SiO_2 (23 %) >AC (19 %) >Al_2O_3 (13 %) >NiO (11 %) >TiO_2 (4 %). TGA results are useful for determining regeneration temperature, and the results (Figure 7.3) suggest that the temperatures when using nitrogen are 520 ^oC, 529 ^oC, 562 ^oC, 595 ^oC and 595 ^oC for AC, Al_2O_3, NiO, SiO_2, and TiO_2, respectively. However, it should be noted that Ni/AC mass did not level off or stabilise, which suggests that the presence of NiO on AC provides the O_2 to oxidise carbon. Hence, heat treatment would not be an appropriate method for regeneration.

The effect of loading NiO on acid sites was investigated using TPD-pyridine. No significant difference in terms of acid sites was observed for adsorbents based on SiO_2, Al_2O_3, and TiO_2 supports before and after loading NiO (Figure 7.4). However, with supports based on AC, a synergistic combination was observed, which led to an increase in acid sites for the NiO/AC adsorbent.

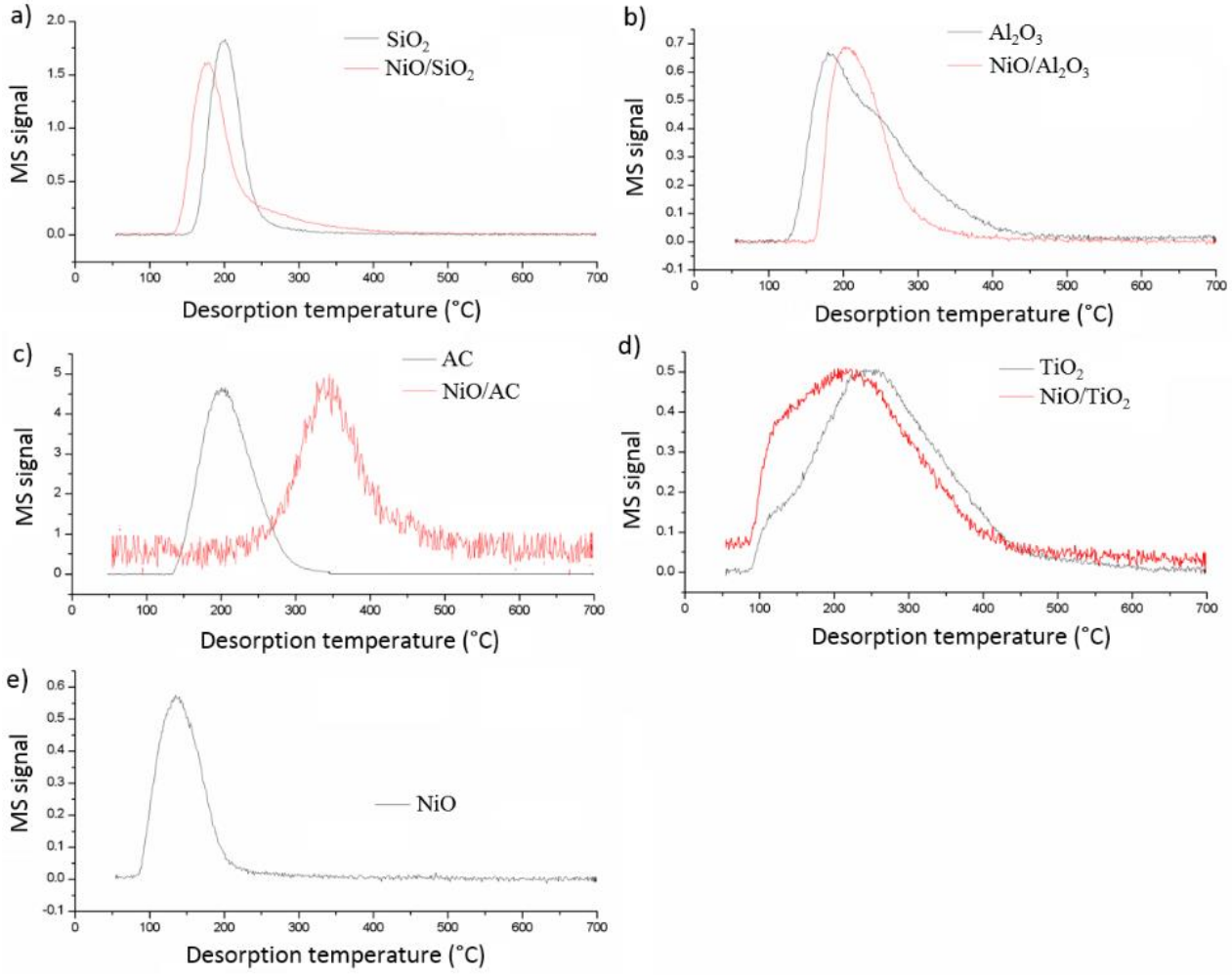

Figure 7.4. Temperature Programmed Desorption: Pyridine for a) SiO_2 and NiO/SiO_2 b) Al_2O_3 and NiO/Al_2O_3 c) AC and NiO/AC d) TiO_2 and NiO/TiO_2 e) NiO adsorbents

7.3.2 Effect of contact time on desulphurization using supports

The activity of the four supports is presented in Figure 7.5. The activity was observed to decrease in this order: $AC>SiO_2>TiO_2>Al_2O_3$. The adsorption order follows a similar order to the amount of pyridine adsorbed. Highly acidic alumina showed the least activity, which is consistent with the HASB theorem because the adsorbates that are to be adsorbed are soft to intermediate bases (Chen et al., 2020). The high activity of AC could be due to many active sites of different strengths, as observed by TGA analysis (Figure 7.3), and a high surface area (Table 7.1). Further analysis was done of activity per surface area, and the adsorption order was TiO_2 > AC > SiO_2 > Al_2O_3. The acidity cations of the metal oxides also follow the same order of softness (Marks, 1990). These results show that TiO_2 has high activity per surface area, i.e. fifteen times that of AC. The high activity may be attributed to a broad range of acid sites, i.e. from 100 ^oC to 700 ^oC. (See Figure 7.4.)

Table 7. 2: Adsorption capacity of supports

Support	Conversion %	Adsorption capacity mg/g	Conversion/area %/(m^2/g)	Q/area mg/m^2
AC	59	6.139	0.0698	0.0073
SiO_2	20.4	2.04	0.0548	0.0064
TiO_2	13	1.629	0.8666	0.1081
Al_2O_3	4	0.939	0.019	0.0045

Figure 7.5 presents the adsorption results of DBT, 4-MDBT and 4,6 DMDBT. It can be seen that the adsorption of sulphur was fast within the first 60 min, but it then slowed down. The adsorption order of each sulphur compound was observed to be dependent on the support. The adsorption order for the sulphur compound on AC and Al_2O_3 was observed to be the same, i.e. DBT<4-MDBT<4,6 DMDBT. The increase in sulphur removal with an increase in the alkyl group for these supports suggests π-bonding, and hence stronger adsorption for larger molecules (4 MDBT) than for smaller ones (DBT) (Kim et al., 2006). The higher activity towards 4,6 DMDBT compared to 4 MDBT could be because 4,6 DMDBT had a higher initial sulphur concentration (300 ppm) than the other two sulphur compounds (DBT 100 ppm and 4 MDBT 100 ppm). TiO_2 and SiO_2 were observed to have this adsorption order: DBT>4-MDBT. The higher activity towards DBT could be due to no steric hindrance by this adsorbate. These results are consistent with TGA results (Figure 7.3), i.e. SiO_2 and TiO_2 showed a higher desorption temperature for sulphur compounds (612 ^oC) than AC and Al_2O_3 (512 and 542 ^oC, respectively). This suggests a stronger adsorbent-sulphur bond (shorter bond length) for SiO_2 and TiO_2.

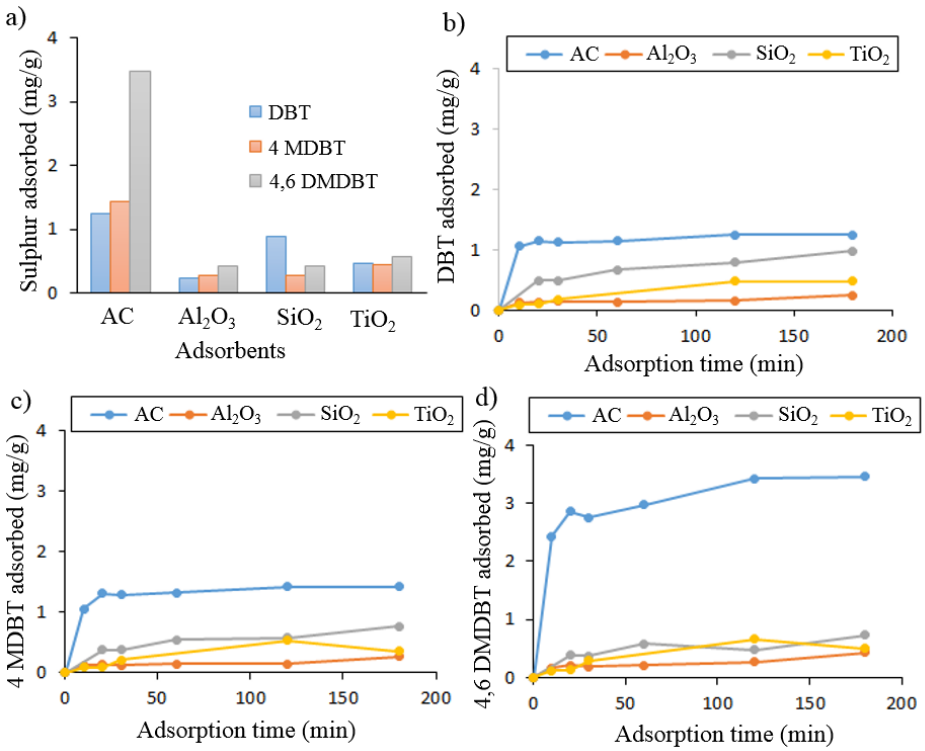

Figure 7.5: Adsorption individual sulphur compounds in model diesel by supports at 30 ^{o}C and atmospheric pressure a) overall activity b) adsorption of DBT c) 4 MDBT d) 4,6 DMDBT

7.3.3 Effect of NiO loading

The effect of the content of NiO supported on different supports on the desulphurization activity is detailed in Figure 7.6. There was a slight increase in activity for adsorbent at a NiO concentration equal to or less than 5 wt%. Thereafter, activity decreased and approached the activity of pure NiO. The decrease in activity might be because of the pore blocking and agglomeration of NiO (Hernandez et al., 2010; Sentorun-Shalaby et al., 2011; Sarda et al., 2012). The adsorption activity was observed to follow this order: NiO/AC> NiO/SiO_2> NiO/TiO_2> NiO/Al_2O_3. This order is similar to that of pure supports, which suggests that the support has a significant effect on activity. A similar adsorption order for different sulphur compounds was observed.

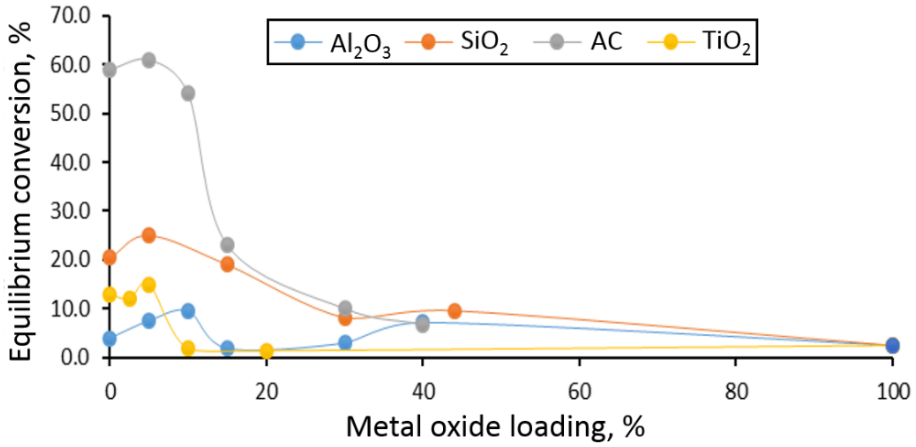

Figure 7.6: Effect of loading NiO on sulphur adsorption on supports at 30 ^{o}C and atmospheric pressure, 1300 rpm stir speed and 3h run time

NiO loading had a different selectivity effect on different support, as indicated in Table 7.3. The selectivity factor is a function of equilibrium concentration, which is important since it also caters for different initial concentrations of the adsorbate. Equation 7.1 was used to calculate the selectivity of removing a sulphur compound relative to the amount of DBT i.e the relative selectivity of DBT is one. With silica, it was observed that the presence of NiO improved the adsorption activity towards larger sulphur compounds slightly, i.e 4-MDBT and 4,6 DMDBT. This suggests a good synergy between SiO_2 and NiO. When titania was used as the support, no change in selectivity was observed. Finally, when alumina and activated carbon were used, there was a slight decrease in selectivity for 4-MDBT and 4,6 DMDBT with an increase in NiO loading. The decrease in selectivity for AC and Al_2O_3 towards 4-MDBT and 4,6 DMDBT with NiO loading is a result of an increase in the chemical bond (Ni-S). This is consistent with the behaviour of NiO as observed with pure NiO, where it favours the adsorption of a low molecular molecule (DBT).

Table 7.3: Effect of metal oxide loading on relative selectivity

Adsorbent	4-MDBT	4, 6 DMDBT
SiO_2	0.7	0.1
5% NiO/SiO_2	0.8	0.3
15% NiO/SiO_2	0.8	0.2
30% NiO/SiO_2	0.9	0.4
44% NiO/SiO_2	0.9	0.4
TiO_2	0.7	0.3
2.5% NiO/TiO_2	0.7	0.3
5% $NiO2/TiO_2$	0.7	0.3
AC	1.5	0.8
10% NiO/AC	1.5	0.9
15% NiO/AC	1.2	0.5
30% NiO/AC	0.9	0.4
40% NiO/AC	0.9	0.4
Al_2O_3	1.2	0.6
5% NiO/Al_2O_3	1	0.5
10% NiO/Al_2O_3	1.1	0.5
30% NiO/Al_2O_3	0.9	0.3
40% NiO/Al_2O_3	1	0.2
NiO	0.5	0.3

7.3.4 Kinetics of adsorption

Kinetic data analysis was done using pseudo-first and second-order kinetic models and the equations used are in section 5.3.2. Adsorption of all the supports was observed to follow the pseudo-second-order kinetics, as per Table 7.2. The calculated equilibrium sulphur adsorption was observed to be 5.540, 1.627, 1.474 and 0.594 mg/g for AC, SiO_2, TiO_2 and Al_2O_3, respectively. Generally, the addition of NiO was seen to lead to an increase in adsorption activity, and the adsorption rate increased based on the adsorption rate constant (k_2) and the initial adsorption rate (h). The pseudo-second-order model suggests mainly chemical bonding, which is consistent with the suggested mechanisms for the supports, i.e π-bond and adsorbent-sulphur bond.

Table 7. 4: Pseudo-first-order rate and Pseudo-second-order rate constants for supports

Pseudo first order	q_{cal}[a] (mg/g)	k_{ad}	R^2	
AC	2.496	0.034	0.912	
Al_2O_3	0.634	0.005	0.527	
TiO_2	1.367	0.022	0.891	
SiO_2	1.443	0.008	0.484	
Second order	q_{cal} (mg/g)	k_2	h (mg/g min)	R^2
AC	5.540	0.028	1.142	0.999
5NiO/AC	5.643	0.074	2.342	1.000
Al_2O_3	0.594	0.087	0.087	0.994
$5Ni/Al_2O_3$	0.815	0.379	0.252	1.000
SiO_2	1.627	0.018	0.115	0.998
$5Ni/SiO_2$	2.714	0.023	0.167	0.988
TiO_2	1.474	0.005	0.011	0.996
$5Ni/TiO_2$	1.626	0.347	0.919	0.998

Where: q_{cal} is adsorption capacity estimated using the kinetic models.

7.3.5 Effect temperature

The effect of temperature was investigated and a summary of the results is presented in Figure 7.7. It shows that both the adsorption temperature and the type of support had a different effect on the activity of ADS. For TiO_2 and Al_2O_3, there was a decrease in activity with a decrease in temperature. With SiO_2, there was an increase in activity with an increase in temperature from 30 to 60 ^oC. This is consistent with the work reported by Koriakin et al. (2010), who observed an increase in activity up to 45 ^oC. In our work, a further increase in temperature to 90 ^oC was observed to lead to a decrease in adsorbent loading, which might be due to desorption at higher temperatures. Finally, the activity of NiO/AC was observed to increase with temperature.

The increase in temperature for the NiO/AC system could potentially promote the participation of metal contaminants in terms of sulphur adsorption and improved mass transfer.

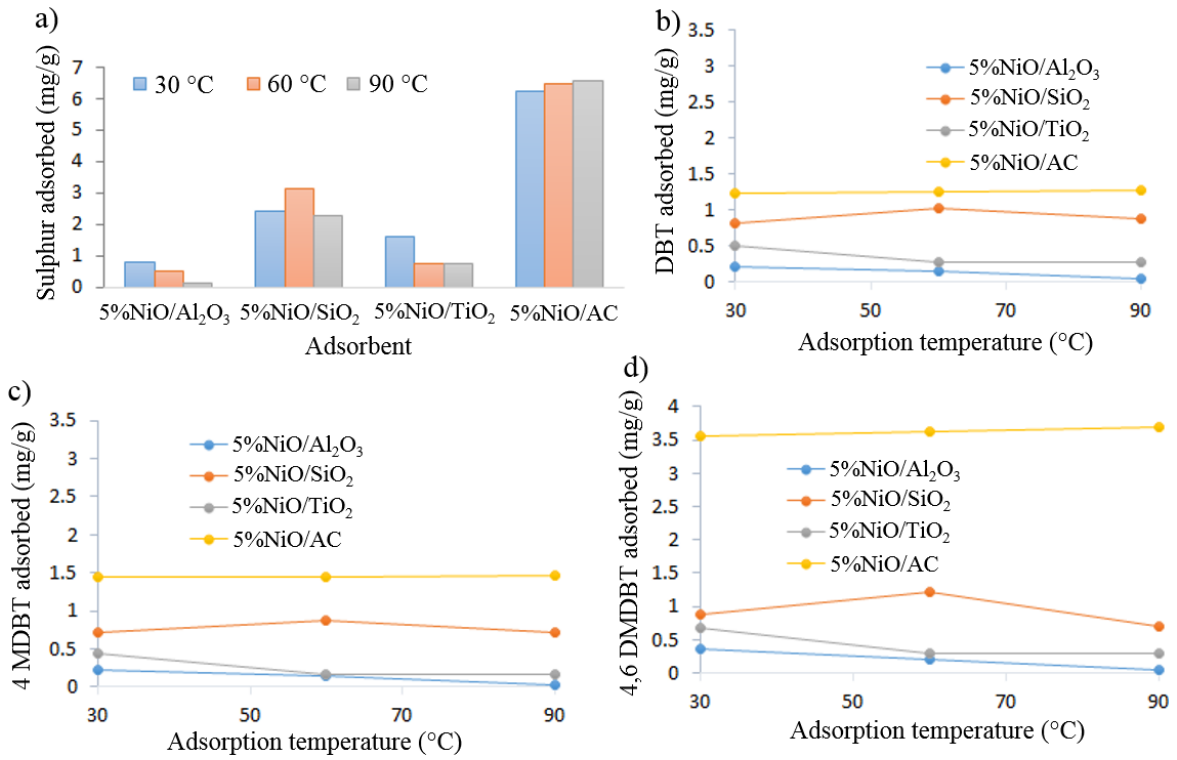

Figure 7.7: Effect of adsorption temperature on adsorption at these conditions atmospheric pressure, 1300 rpm stir speed and 3 h run time, a) overall activity b) adsorption of DBT c) 4 MDBT d) 4,6 DMDBT

7.3.6 Conventional diesel

Based on the finding that increasing temperature to 60 ^{o}C led to an increase in activity (see Figure 7.7) and the findings of our earlier work (i.e. that polycyclic aromatic hydrocarbons desorption occurred at 50 ^{o}C when regenerating AC (Mguni et al., 2018)). The activity of the two promising supports, i.e. SiO_2 and AC were tested, using conventional diesel fuel with 100 ppm sulphur at 60 ^{o}C. (See Figure 7.8.) The effect of loading NiO was also investigated. It was observed that: the adsorption order of the sulphur compounds was similar for the two systems (i.e. SiO_2 and AC); the addition of NiO did not change sulphur compound selectivity significantly, but it improved the adsorption activity significantly. This improvement was more pronounced than when model diesel was used at 30 ^{o}C (Figure 7.5). The significant increase in activity suggests that an increase in temperature increases the participation of NiO in adsorption. This is consistent with exceptions of increase in chemical bonding with an increase in temperature and also increased rate of intraparticle diffusion of molecules into the pores of the adsorbent (Tan et al., 2007).

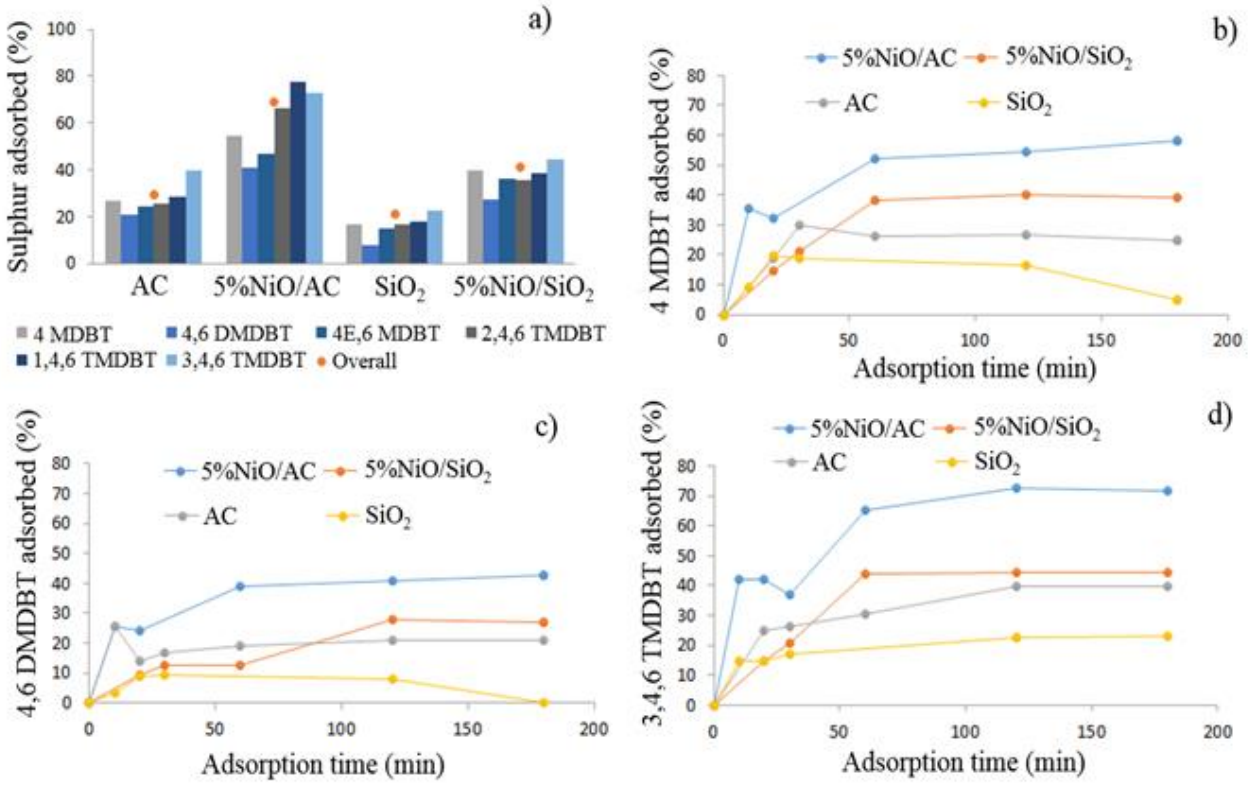

Figure 7.8: Adsorption activity at 60 ^{o}C, atmospheric pressure using conventional diesel and AC, 5%NiO/AC, SiO_2 and 5%NiO/SiO_2. a) overall activity b) adsorption of 4 MDBT c) 4,6 DMDBT d) 3,4,6 TMDBT

The activity of 5%NiO/SiO_2 and 5%NiO/AC were compared for model and conventional diesel - see Figure 7.9. The activity of AC was observed to decrease when treating conventional diesel, which is attributed to competitive adsorption by polyaromatic compounds. There was no significant difference in activity for the 5%NiO/SiO_2 adsorbent when treating model or conventional diesel, which suggests a good selection for the silica-based adsorbent. However, higher activity was observed for the adsorption of both model and conventional diesel over 5%NiO/AC than that obtained over 5%NiO/SiO_2.

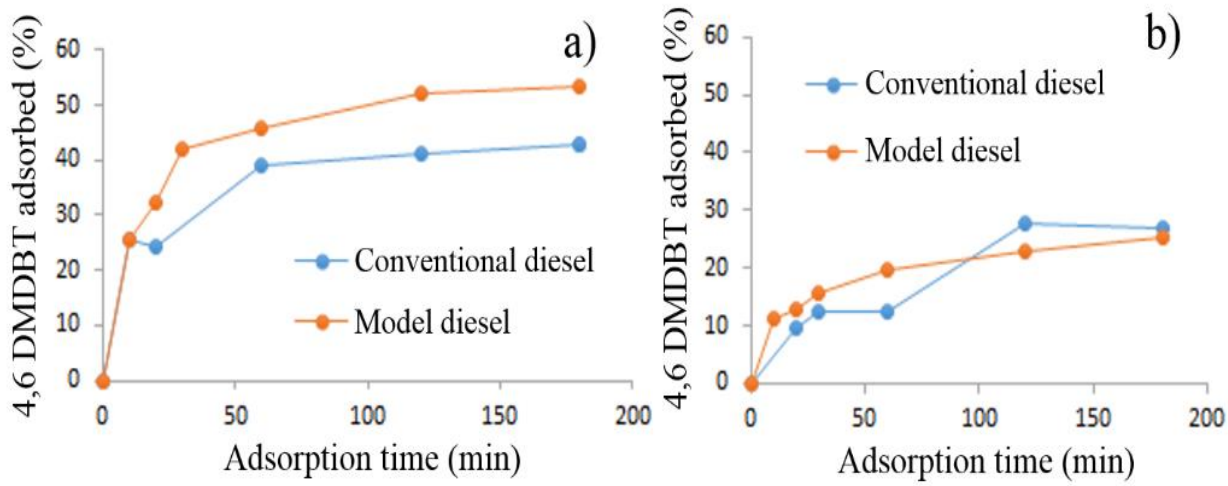

Figure 7.9: A comparison on adsorption activity of model diesel versus conventional diesel a) 5%NiO/AC and b) 5%NiO/SiO_2

7.4 Conclusion

Adding NiO had a different effect on different supports (AC, SiO_2, Al_2O_3 and TiO_2). NiO addition on Al_2O_3 increased the adsorption strength for sulphur compounds significantly, while no significant change in bond strength was observed with the other supports. AC support showed the highest activity, which was attributed to the many active sites of different strengths observed in AC. These active sites have been ascribed to different metals and a high surface area. Per surface area, TiO_2 has been observed to have twice the activity of AC. Since adsorption is a surface phenomenon, these results suggest that adsorbent screening should be based on per surface area and that effort should be put into producing high surface materials, based on these promising highly active materials.

The addition of NiO was observed to cause a slight increase in activity at 30 ^oC and low loading (~5% NiO/support). It was also observed to affect selectivity. The good synergy between SiO_2 and NiO was observed to produce an adsorbent that favoured the adsorption of high molecular weight compounds, i.e 4MDBT and 4,6 DMDBT. However, it did not have any effect on TiO_2 and had a detrimental effect on AC and Al_2O_3. The synergy with SiO_2 was observed to reduce hydrocarbon adsorbed by SiO_2 and thereby improve overall selectivity.

Finally, when conventional diesel was treated at 60 ^oC, NiO activity improved compared to the activity seen at 30 ^oC. This was attributed to the involvement of NiO in chemical bonding at high temperatures and reduced competitive adsorption since polyaromatic compounds desorb at these temperatures.

References

Aslam, M.M-A., Kuo, H-W., Den, W., Usman, M., Sultan, M., Ashraf, H., 2021. Functionalized Carbon Nanotubes (CNTs) for Water and Wastewater Treatment: Preparation to Application. Sustainability 13, 5717. https://doi.org/10.3390/su13105717

Bu, J., Loh, G., Gwie, C.G., Dewiyanti, S., Tasrif, M., Borgna, A., 2011. Desulphurization of diesel fuels by selective adsorption on activated carbons: Competitive adsorption of polycyclic aromatic sulphur heterocycles and polycyclic aromatic hydrocarbons. Chem. Eng. J. 166, 207–217. https://doi.org/10.1016/j.cej.2010.10.063

Chen, K., Li, W., Biney, B.W., Li, Z., Shen, J., Wang, Z., 2020. Evaluation of adsorptive desulphurization performance and economic applicability comparison of activated carbons prepared from various carbon sources. RSC Adv. 10, 40329–40340. https://doi.org/10.1039/D0RA07862J

De Gisi, S., Lofrano, G., Grassi, M., Notarnicola, M., 2016. Characteristics and adsorption capacities of low-cost sorbents for wastewater treatment: A review. Sustain. Mater. Technol. 9, 10–40. https://doi.org/10.1016/j.susmat.2016.06.002

El-Kemary, M., Nagy, N., El-Mehasseb, I., 2013. Nickel oxide nanoparticles: Synthesis and spectral studies of interactions with glucose. Mater. Sci. Semicond. Process. 16, 1747–1752. https://doi.org/10.1016/j.mssp.2013.05.018

Gawande, P., Kaware, J., 2016. Removal of sulphur from liquid fuels using low cost activated carbon - A review. Int. J. Sci. Eng. Appl. Sci. 2, 64–69.

Hernandez, S.P., Fino, D., Russo, N., 2010. High performance sorbents for diesel oil desulphurization. Chem. Eng. Sci. 65, 603–609. https://doi.org/10.1016/j.ces.2009.06.050

Jongsomjit, B., Wongsalee, T., Praserthdam, P., 2005. Study of cobalt dispersion on titania consisting various rutile: anatase ratios. Mater. Chem. Phys. 92, 572–577. https://doi.org/10.1016/j.matchemphys.2005.02.016

Jüntgen, H., 1986. Activated carbon as catalyst support: A review of new research results. Fuel 65, 1436–1446. https://doi.org/10.1016/0016-2361(86)90120-1

Kim, J.H., Ma, X., Zhou, A., Song, C., 2006. Ultra-deep desulphurization and denitrogenation of diesel fuel by selective adsorption over three different adsorbents: A study on adsorptive selectivity and mechanism. Catal. Today 111, 74–83. https://doi.org/10.1016/j.cattod.2005.10.017

Koriakin, A., Ponvel, K.M., Lee, C-H., 2010. Denitrogenation of raw diesel fuel by lithium-modified mesoporous silica. Chem. Eng. J. 162, 649–655. https://doi.org/10.1016/j.cej.2010.06.014

Lee, K., 2020. Liquid Phase Adsorptive Desulphurization using Modified Zeolites for Transportation and Fuel Cell Applications 197.

Mansouri, A., Khodadadi, A.A., Mortazavi, Y., 2014. Ultra-deep adsorptive desulphurization of a model diesel fuel on regenerable Ni–Cu/γ-Al2O3 at low temperatures in absence of hydrogen. J. Hazard. Mater. 271, 120–130. https://doi.org/10.1016/j.jhazmat.2014.02.006

Marks, T.J. (Ed.), 1990. Bonding Energetics in Organometallic Compounds, ACS Symposium Series. American Chemical Society, Washington, DC. https://doi.org/10.1021/bk-1990-0428

Mguni, L., Yao, Y., Nkomzwayo, T., Xinying, L., Hildebrandt, D., Glasser, D., 2018. Desulphurization of diesel fuels using intermediate Lewis acids loaded on activated charcoal and alumina. Chem. Eng. Commun. https://doi.org/10.1080/00986445.2018.1511983

Mguni, L.L., Mukenga, M., Jalama, K., Meijboom, R., 2013. Effect of calcination temperature and MgO crystallite size on MgO/TiO2 catalyst system for soybean oil transesterification. Catal. Commun. 34, 52–57. https://doi.org/10.1016/j.catcom.2013.01.009

Ming, Q., Healey, T., Allen, L., Irving, P., 2002. Steam reforming of hydrocarbon fuels. Catal. Today 77, 51–64. https://doi.org/10.1016/S0920-5861(02)00232-8

Rodrigues, A.K.O., Ramos, J.E.T., Cavalcante Jr, C.L., Rodríguez-Castellón, E., Azevedo, D.C., 2014. Pd-loaded mesoporous silica as a robust adsorbent in adsorption/desorption desulphurization cycles. Fuel 126, 96–103. https://doi.org/10.1016/j.fuel.2014.02.019

Sarda, K.K., Bhandari, A., Pant, K.K., Jain, S., 2012. Deep desulphurization of diesel fuel by selective adsorption over Ni/Al2O3 and Ni/ZSM-5 extrudates. Fuel 93, 86–91. https://doi.org/10.1016/j.fuel.2011.10.020

Sentorun-Shalaby, C., Saha, S.K., Ma, X., Song, C., 2011. Mesoporous-molecular-sieve-supported nickel sorbents for adsorptive desulphurization of commercial ultra-low-sulphur diesel fuel. Appl. Catal. B Environ. 101, 718–726. https://doi.org/10.1016/j.apcatb.2010.11.014

Shakirullah, M., Ahmad, I., Ishaq, M., Ahmad, W., 2009. Study on the role of metal oxides in desulphurization of some petroleum fractions. J. Chin. Chem. Soc. 56, 107–114. https://doi.org/10.1002/jccs.200900015

Tan, I.A.W., Hameed, B.H., Ahmad, A.L., 2007. Equilibrium and kinetic studies on basic dye adsorption by oil palm fibre activated carbon. Chem. Eng. J. 127, 111–119. https://doi.org/10.1016/j.cej.2006.09.010

Tang, X., Lu, H., Li, J., Chen, L., 2016. Adsorption desulphurization performance and mechanism over nanocrystalline NiO/Al2O3-1 adsorbent. Russ. J. Appl. Chem. 89, 2043–2049. https://doi.org/10.1134/S1070427216120168

Velu, S., Ma, X., Song, C., Namazian, M., Sethuraman, S., Venkataraman, G., 2005. Desulphurization of JP-8 jet fuel by selective adsorption over a Ni-based adsorbent for micro solid oxide fuel cells. Energy Fuels 19, 1116–1125. DOI: 10.1039/D0RA07862J

Vilarrasa-García, E., Infantes-Molina, A., Moreno-Tost, R., Rodríguez-Castellón, E., Jiménez-López, A., Cavalcante, C.L., Azevedo, D.C.S., 2010. Thiophene adsorption on microporous activated

carbons impregnated with PdCl2. Energy Fuels 24, 3436–3442. https://doi.org/10.1021/ef901611k

Xiao, J., Li, Z., Liu, B., Xia, Q., Yu, M., 2008. Adsorption of benzothiophene and dibenzothiophene on ion-impregnated activated carbons and ion-exchanged Y zeolites. Energy Fuels 22, 3858–3863. https://doi.org/10.1021/ef800437e

Xiao, J., Song, C., Ma, X., Li, Z., 2012. Effects of aromatics, diesel additives, nitrogen compounds, and moisture on adsorptive desulphurization of diesel fuel over activated carbon. Ind. Eng. Chem. Res. 51, 3436–3443. https://doi.org/10.1021/ie202440t

Xu, J., Gao, Q., Zhang, Y., Tan, Y., Tian, W., Zhu, L., Jiang, L., 2015. Preparing two-dimensional microporous carbon from pistachio nutshell with high areal capacitance as supercapacitor materials. Sci. Rep. 4. https://doi.org/10.1038/srep05545

Yu, M., Li, Z., Xia, Q., Xi, H., Wang, S., 2007. Desorption activation energy of dibenzothiophene on the activated carbons modified by different metal salt solutions. Chem. Eng. J. 132, 233–239. https://doi.org/10.1016/j.cej.2007.01.003

Zhong, L., Shi, T., Guo, L., 2010. Preparation and morphology of porous SiO2 ceramics derived from fir flour templates. J. Serbian Chem. Soc. 75, 385–394. https://doi.org/10.2298/JSC090410010Z

8. MODULATED SYNTHESIZED Ni BASED MOF WITH IMPROVED ADSORPTIVE DESULPHURIZATION ACTIVITY

This work has been published to the *Journal of Cleaner Production, 2021, 323, 129196, doi.org/10.1016/j.jclepro.2021.129196.* Part of this work was presented at the following conference:

Catalysis Society of South Africa (CATSA), Club Mykonos, Langebaan, Cape Town (10-13th Nov 2019)

Abstract

Metal-organic frameworks (MOFs) are promising adsorbents for adsorptive desulphurization (ADS) because MOF structures can be tuned to match the application. However, data on the ADS of liquid fuels using Ni-BDC are still scarce. In this study, modulated synthesis was used to prepare a group of Ni-doped MOF absorbents using formic acid as the modulator. The activities of these adsorbents for the ADS of model fuels were investigated, with initial sulphur concentrations of 150, 151, and 153 ppm for thiophene (TH), dibenzothiophene (DBT), and 4,6-dimethyldibenzothiophene (4,6 DMDBT), respectively. Although Ni-doping decreased the crystallinity and crystallite size of the MOFs, the addition of formic acid significantly increased both the crystallite size and crystallinity of all the (xNi/Zn)-BDC materials. In addition, it was observed that modulated synthesis reduced the interpenetration of the MOF-5 crystallites. The adsorption experimental results showed that the modulated synthesis of Ni-BDC using formic acid improved the overall adsorptive activity of Ni-BDC almost twofold. This increase in activity was attributed to increased crystallinity and a higher number of atoms with low coordination for modulated Ni-BDC compared with MOF-5 (100). Formic acid as a modulator was observed to have three effects: i) accelerating MOF synthesis, ii) modulating crystallite size, and iii) controlling crystallinity. The most active adsorbent, Ni-BDC treated with formic acid, was observed to have higher activity toward TH than DBT and 4,6 DMDBT. The overall adsorption capacity and partition coefficient for this adsorbent was 4.14 mg/g and 0.053 mg/g/ppm, respectively.

Keywords: MOF; nickel; desulphurization; formic acid; acid sites, modulation

8.1 Introduction

The production of clean and environmentally friendly liquid fuels is an important aspect of protecting the earth from the harmful effects of toxic and corrosive emissions, such as SO_x. The need to reduce the sulphur content in fuels has led to intensified research on the economic removal of sulphur. Conventional hydrodesulphurization technology operates in the gas phase at extremely high pressures and temperatures, making it energy-intensive and expensive (Hernández‐Maldonado and Yang, 2004; Tailleur, 2019). Liquid-phase desulphurization by adsorption is a promising technology that is being investigated, as it operates under milder conditions, resulting in lower energy consumption.

High-surface-area porous materials, such as metal-organic frameworks (MOFs), activated carbon (AC), and zeolite (Dehghan and Anbia, 2017), have been tested for the adsorptive desulphurization (ADS) of liquid fuels. MOFs are an emerging class of porous materials that are constructed from a variety of inorganic nodes (i.e., metal clusters or ions) and organic linkers with a number of metal-organic combinations; therefore, the structural possibilities are almost endless (Howarth et al., 2016). MOF-5 is a three-dimensional ultra-high porosity MOF with the formula $Zn_4O(BDC)_3$. It possesses adsorption properties for thiophenic compounds from liquid fuels (Jia et al., 2017). However, there is little published research on ADS using MOF-5.

The current challenges with MOFs, especially those based on intermediate-soft Lewis metals (such as Zn-based MOF-5), are that they are moisture sensitive, and their structural decomposition leads to poor reproducibility and decreased activity (Wiβmann et al., 2012; Ren et al., 2014). Moisture sensitivity necessitates special care during handling, making these MOFs unsuitable for industrial use. Several strategies can be used to reduce moisture sensitivity and improve activity (Ma et al., 2011; Ren et al., 2017; Yuan et al., 2018; Ding et al., 2019). Among these is the metal doping of MOF-5 with various metal ions, which has been used to improve stability (Li et al., 2012; Ming et al., 2015). According to the literature, using nickel (Li et al., 2012; Yang et al., 2014a) and cobalt (Jia et al., 2017) with a mixed solvent of ethanol and N, N-dimethylformamide (DMF) improved the stability of synthesized MOF-5. The previous work by the authors of the present study, which involved the use of several intermediate Lewis acids, showed that Ni is one of the most promising metals for diesel fuel desulphurization (Mguni et al., 2019b). Therefore, it would be interesting to investigate the effect of the Ni concentration on Ni-doped MOF-5 for ADS.

The experimental parameters that are usually investigated when using MOFs for ADS include the effects of central metal nodes (Li et al., 2012; Khan and Jhung, 2013; Wang et al., 2015), organic linkers (Zhang et al., 2012), pore functionality (Sun et al., 2012), operating temperature, and regeneration procedures (Ahmed and Jhung, 2015). Modulated synthesis, especially that for high-valence metals, has been investigated by several researchers for hydrogen storage applications (Wiβmann et al., 2012; Ren et al., 2014; Zahn et al., 2015). It has been reported that modulated synthesis improves the crystallinity of the material, varies the crystal size of the MOFs, improves ease of handling, and decreases reaction time and degree of aggregation (Wiβmann et al., 2012). Recent publications have reported the modulated synthesis of MOF-5 using ethanol (Lv et al., 2018) and acetic acid (Wang et al., 2018) as modulator solvents. These strategies produced monodispersed MOF-5 crystals with controllable sizes and shapes. Crystallite size and crystallinity have been reported to affect several reactions (Montero et al., 2009; Zhang et al., 2010). To the best of our knowledge, the effect of the crystallite size and crystallinity (produced via modulated synthesis using formic acid) on ADS has not been previously reported.

In the present study, a group of (xNi/Zn)-BDC adsorbents with varying Ni contents were subjected to modulated synthesis, and the performance of these materials in the ADS of model diesel was investigated. After preparation, the materials were characterized using Fourier-transform infrared spectroscopy (FTIR), Brunauer–Emmett–Teller (BET) theory, scanning electron microscopy (SEM), X-ray diffraction analysis (XRD), X-ray photoelectron spectroscopy (XPS), and temperature-programmed desorption (TPD). The effect of the Ni content and the modulated synthesis method on the morphology of the material (surface area, crystallite size, and crystallinity) and its desulphurization activity were investigated. Thereafter, the results obtained in the current study were compared with those reported in the literature. Finally, the optimal Ni-doped MOF (Ni-BDC) material was selected for ADS. This study provides valuable information regarding the design of alternative materials for removing thiophenic compounds from liquid fuels under mild operating conditions.

8.2 Experimental procedure

8.2.1 Materials

The following materials were purchased from Merck: 1,4-benzenedicarboxylic acid (H_2BDC) (98 %), zinc (II) nitrate hexahydrate ($Zn(NO_3)_2 \cdot 6H_2O$), nickel (II) nitrate hexahydrate ($Ni(NO_3)_2 \cdot 6H_2O$) (97 %), hexadecane (98 %), thiophene (98 %), dibenzothiophene (DBT) (98 %), 4,6 dimethylbenzothiophene (98 %), and commercial activated carbon. N,N-dimethylformamide (DMF, 99.8 %) and formic acid (85 %) were purchased from Associated Chemical Enterprises (Pty) Ltd. (ACE Chemicals).

8.2.2 (xNi/Zn)-BDC synthesis

To prepare the MOF-5, H_2BDC (0.33 g), $Zn(NO_3)_2 \cdot 6H_2O$ (1.78 g), and DMF (45 mL) were mixed using a sonicator, then added to a Teflon-lined steel autoclave and hydrothermally treated at 130 °C for 8 h. The same procedure was repeated to investigate the effects of nickel doping and the quantity of the modulator used. To prepare the Ni-doped MOF, a mass of *x* g nickel nitrate and (1.78-*x*) g zinc nitrate was used, with *x* set to reach 25 %, 50 %, 75 %, and 100 % Ni on (xNi/Zn)-BDC. To determine the effect of the modulator, a varying molar equivalent amount (eq) of formic acid (with respect to the metal nitrate) was added to the reaction mixture. For example, MOF-5 100 eq means that if 0.006 mol of $Zn(NO_3)_2 \cdot 6H_2O$ was used in the adsorbent synthesis, 0.6 mol of formic acid was added. A summary of the adsorbents synthesized is presented in Table B1 (Supplementary data). The synthetic products (white or green crystalline powders) were isolated by centrifugation. The solid was washed three times with 20 mL of DMF and then dried under vacuum at 80 °C for 8 h. To remove any traces of DMF, the dried powder was washed three times with CH_2Cl_2 and soaked for three days in the solution. Finally, the product was activated at 120 °C for at least 12 h under vacuum. The product was stored in sample vials for later use. A schematic diagram of the adsorbent synthesis process is shown in Figure B1 (Supplementary Data). The theoretical yield was calculated based on the empirical formula of MOF-5 and Ni-BDC using H_2BDC as the limiting reagent. The yields of MOF-5 and Ni-BDC were 54 % and 77 %, respectively. The MOF-5 yield was comparable to that reported by Tranchemontagne et al. (2008) and Li et al. (2012).

8.2.3 Characterization of MOF

The FTIR spectra in the range of 4000–400 cm^{-1} were measured using a Bruker Tensor 27 ATR in order to determine the functional groups in the adsorbent samples. XPS analysis was performed using a Thermo ESCALAB 250Xi-XPS photoelectron spectrometer with an Al Kα X-ray source to determine the structure and composition of the samples. BET analysis was performed to determine the surface area (SA) and pore size distribution by N_2 adsorption at 77 K using a Micromeritics ASAP 2000 instrument. TPD experiments were conducted using a Micromeritics AutoChemII chemisorption analyzer. The adsorbent sample (200 mg) was pre-treated at 250 °C under He flow for 4 h. After cooling to room temperature (25-30 °C) in a He atmosphere, the gas was switched to a pyridine vapour–He mixture. After the physically adsorbed pyridine was purged via He flow at room temperature, the sample was heated to 350 °C at 10 °C/min, and the liberated pyridine was monitored continuously using a CIRRUS quadrupole mass spectrometer. The structure of the adsorbent was analyzed using a Rigaku Ultima IV X-ray diffractometer with CuKα radiation (λ=1.54). The samples were scanned over a 2θ range of 3–90° with a 0.01° step size and a scan speed of 0.02 s/step. The mean crystallite size of the adsorbent samples was estimated from the full width of the diffraction peak at half maxima using the Scherrer equation, using a shape factor of 0.9. The SEM was conducted using a Joel Philips SEM 505 instrument at a working distance of 10 mm, a spot size of 20, and a voltage of 20 kV. In this work, the crystallinity of the synthesized MOF was determined using the TOPAS single line fitting method (Bruker Axs, Inc., 2005).

8.2.4 Adsorption experiment

The model liquid fuel for the adsorption experiments was synthesized using hexadecane and three sulphur compounds, namely thiophene (TH), dibenzothiophene (DBT), and 4,6-dimethyldibenzothiophene (4,6 DMDBT), at concentrations of 150, 153, and 151 ppm, respectively. The adsorption experiments were performed using a batch stirred basket reactor. Ten millilitres of model fuel and 200 mg of adsorbent were placed in the reactor and thereafter, the reactor switched on with the magnetic stirrer speed set to 1300 rpm. The adsorption time was measured using a second chronograph, and the adsorption process was performed for 120 min for each run. A schematic representation of the ADS experiments is shown in Figure 8.1. A three-neck round-bottom flask with a magnetic stirrer was used as the reactor, and a water bath was used to control the temperature of the reactor (see Figure 8.1).

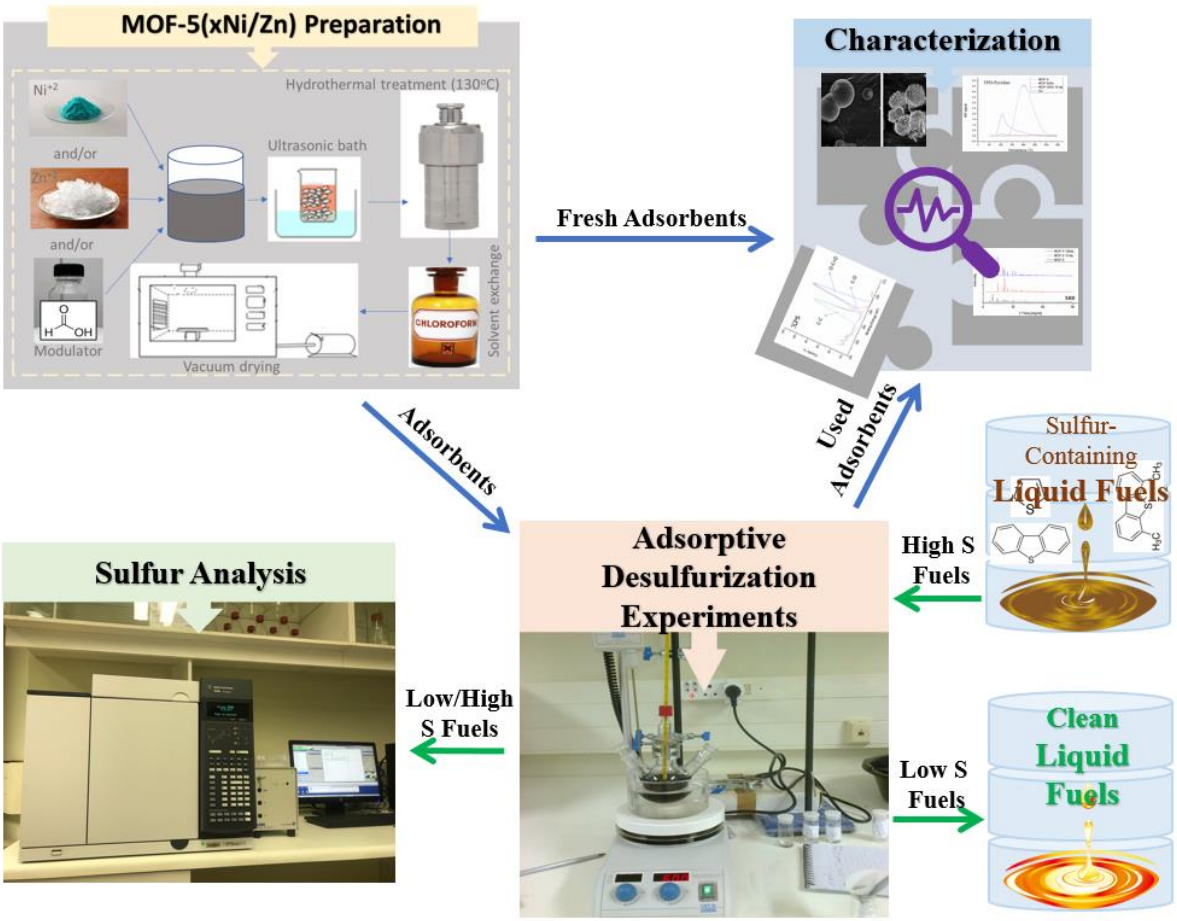

Figure 8.1: Schematic of the setup for the ADS experiments.

8.2.5 Sulphur analysis

The model diesel was analyzed before and after the adsorption process using a 7890 B Agilent Gas Chromatograph (GC) with two detectors: a flame ionization detector (FID) and a pulsed flame photometric detector (PFPD). The sulphur was quantified as described in our previous study (Mguni et al., 2019a). The relative error for the analysis of sulphur compounds was less than 6 %. Figure 8.2 shows the analysis of the sulphur components when using GC-PFPD on the model diesel. The similar heights of the peaks for the three compounds are in line with the linear and equimolar responses of the PFPDs.

To compare the adsorption performance of different adsorbents or data obtained under different conditions, the adsorption activity, capacity, and partition coefficient (PC) were utilized. The following equations were used to calculate the adsorption activity, adsorption capacity, and PC in this study.

Adsorption activity:

$$\%\, Adsorption = \frac{C_0 - C_t}{C_O} * 100 \qquad (8.1)$$

Adsorption capacity

$$q_t = (C_0 - C_t) W_{Fuel} / W_{ads} \qquad (8.2)$$

PC

$$PC = q_{equ} / C_{equ} \qquad (8.3)$$

Here, C_o and C_t are the sulphur contents in ppm initially and at time t, respectively; q_t is the adsorption capacity (mg/g) at time t; W_{Fuel} and W_{ads} are the mass of the model fuel and adsorbent used, respectively; and q_{equ} and C_{equ} are the adsorption capacity (mg/g) and sulphur content for the equilibrium of the batch adsorption, respectively. The maximum adsorption capacity of an adsorbent representing 100 % breakthrough (BT) was used to calculate the PC.

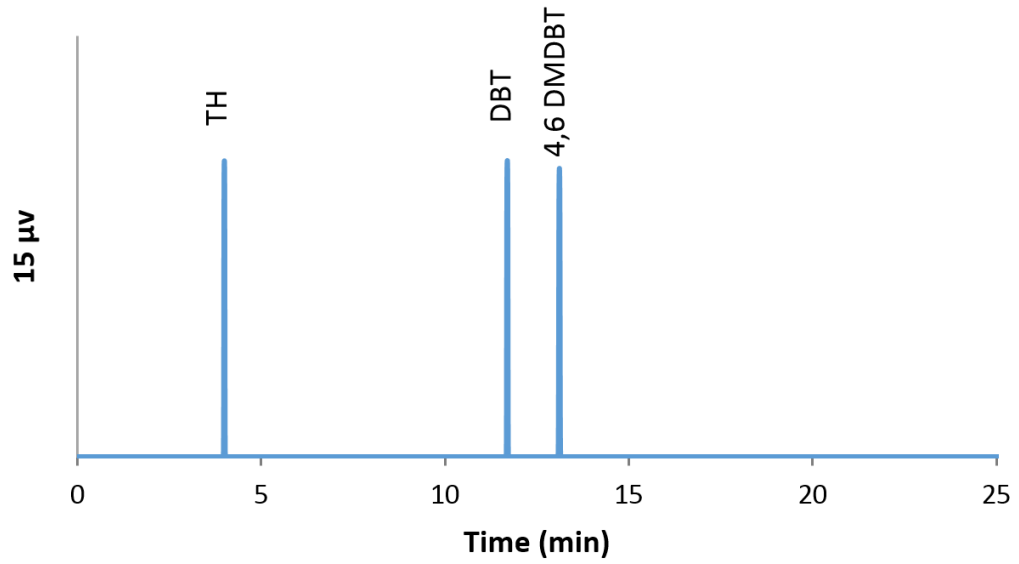

Figure 8.2: GC-PFPD chromatogram of the model diesel comprising: hexadecane; 150 ppm TH; 153 ppm DBT; 151 ppm 4,6DMDBT.

8.3. Results and discussion

8.3.1 Characterizations of fresh (xNi/Zn)-BDC

The MOF-5 was successfully synthesized, and the characteristic peaks at 6.8°, 9.7°, 13.7°, and 15.4°, which correspond to the diffractions of (2 0 0), (2 2 0), (4 0 0), and (4 2 0), respectively, were observed (Wu et al., 2018) (see Figure 8.3 and B2 in the Supplementary Data.). The peak at 13.7° has been reported to be an indication of an interpenetrated structure (Hafizovic et al., 2007). When the formic acid modulator was added, the characteristic peaks disappeared. The disappearance of the peak at 13.7° is consistent with that seen in the SEM images (Figures 8.4a and b), where interpenetration disappeared with the addition of formic acid. When Ni was introduced in the synthesis of MOF-5, most characteristic peaks of MOF-5 were maintained up to 25 % Ni, which suggests that the doped Ni(II) ions were incorporated into the framework and partially substituted Zn(II) ions in the $[Zn4O]^{6+}$ clusters (Li et al., 2012; Yang et al., 2014b). The ability to form MOF-5 up to 25 % Ni is consistent with the study conducted by Botas et al., 2010 and Brozek and Dincă, 2012, who showed that the maximum Ni/Co uptake for MOF-5 was 25 %. Thereafter, a new material, Ni-BDC, was observed. Its peaks are somewhat similar to those of MOF-5, indicating a similar structure. However, this material was attributed to Ni-BDC because similar peaks have been reported by other researchers (Gao et al., 2018; Ahsan et al., 2020). In this work, we report trigonal or truncated cubic Ni-BDC synthesized using a formic acid modulator for the first time. It was observed that with the addition of a formic acid peak, the 9.7° peak split into two peaks. The splitting of the peak at 9.7° in the MOF-5 system has been reported to be due to the distortion of the cubic structure into trigonal symmetry (Tirmizi et al., 2018; Burgaz et al., 2019). Low crystallinity was observed for MOFs that were not subjected to modulated synthesis, as the Ni content increased, which is consistent with the results in Table 8.1.

Table 8.1 shows that both the crystallite size and the crystallinity of all the MOF-5 and (xNi/Zn)-BDC compounds increased with increasing modulator concentration. The increase in crystallite size is due to the competition between deprotonated linker molecules and formate, which reduces the number of nuclei and results in the formation of fewer but larger crystals. This competition also helps to produce highly crystalline products (Yuan et al., 2018). Another observation was that the crystallite size generally decreased with increasing Ni content. This could be due to the replacement of Zn with Ni, which is relatively more electronegative. The introduction of Ni also led to a significant decrease in crystallinity.

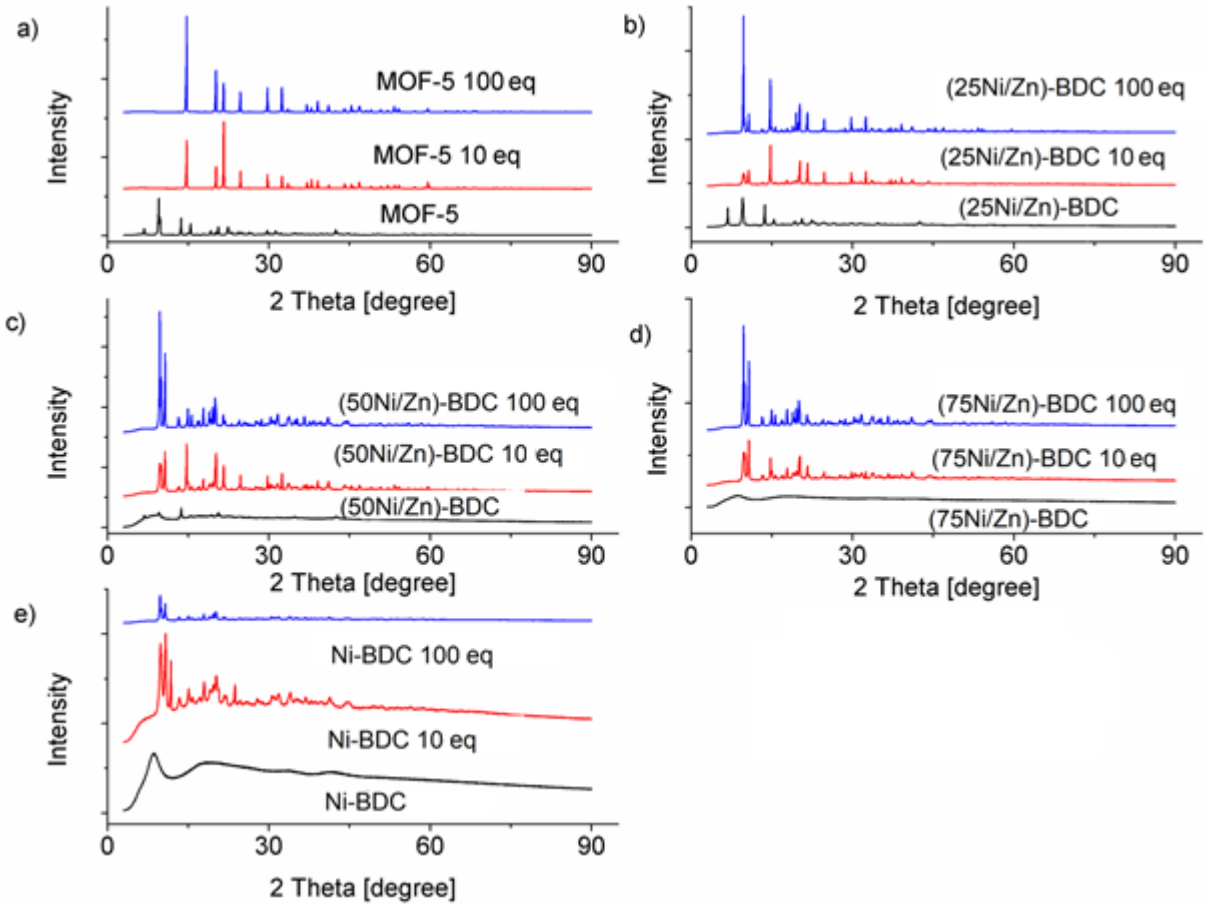

Figure 8.3: XRD spectrum for: a) MOF-5; b) (25Ni/Zn)-BDC; c) (50Ni/Zn)-BDC; d) (75Ni/Zn)-BDC; e) Ni-BDC with varying amounts of the modulator (eq), as indicated in the legends.

The structure of MOF-5 was cubic, as shown in the SEM image in Figure 8.4. However, many wide cracks can be seen on the surface of the cubes, which indicates that the cubes are not single crystals but interpenetrated crystals (Biemmi et al., 2009). The SEM images revealed that the particle size decreased with the addition of the modulator. This decrease is contrary to the observed increase in crystallite size and is believed to be due to a decrease in the intergrowth of crystals, as seen in the SEM images. It was also observed that the addition of the modulator formic acid produced irregularly shaped structures for (75Ni/Zn)-BDC and Ni-BDC (Figure 8.4). These results, that is, the observation of the effect of formic acid on crystalline structures, suggest that formic acid accelerates the formation of the crystalline product. Wiβmann et al. (2012) worked with Zr-fumarate and suggested that accelerated product formation occurred as a result of formic acid being a direct product of the decomposition of DMF with water. Yang et al. (2014) also reported a change in MOF shape when working with Co-doped MOF-5 using acetic acid as a modulator, and they made a similar observation when working with Ni-doped MOF-5 using ethanol.

Table 8.1: Effect of modulator concentration and nickel content on crystallite size and crystallinity

MOF	Modulator equivalent (eq)	Crystallite size (nm)	Crystallinity
MOF-5	0	52.64	64.57
	10	79.12	99.89
	100	74.89	96.48
(25Ni/Zn)-BDC	0	39.41	20.36
	10	56.13	23.93
	100	88.95	33.10
(50Ni/Zn)-BDC	0	-	-
	10	56.85	15.44
	100	79.68	13.09
(75Ni/Zn)-BDC	0	-	-
	10	48.04	15.52
	100	79.34	14.29
Ni-BDC	0	-	-
	10	38.17	15.31
	100	53.25	8.17

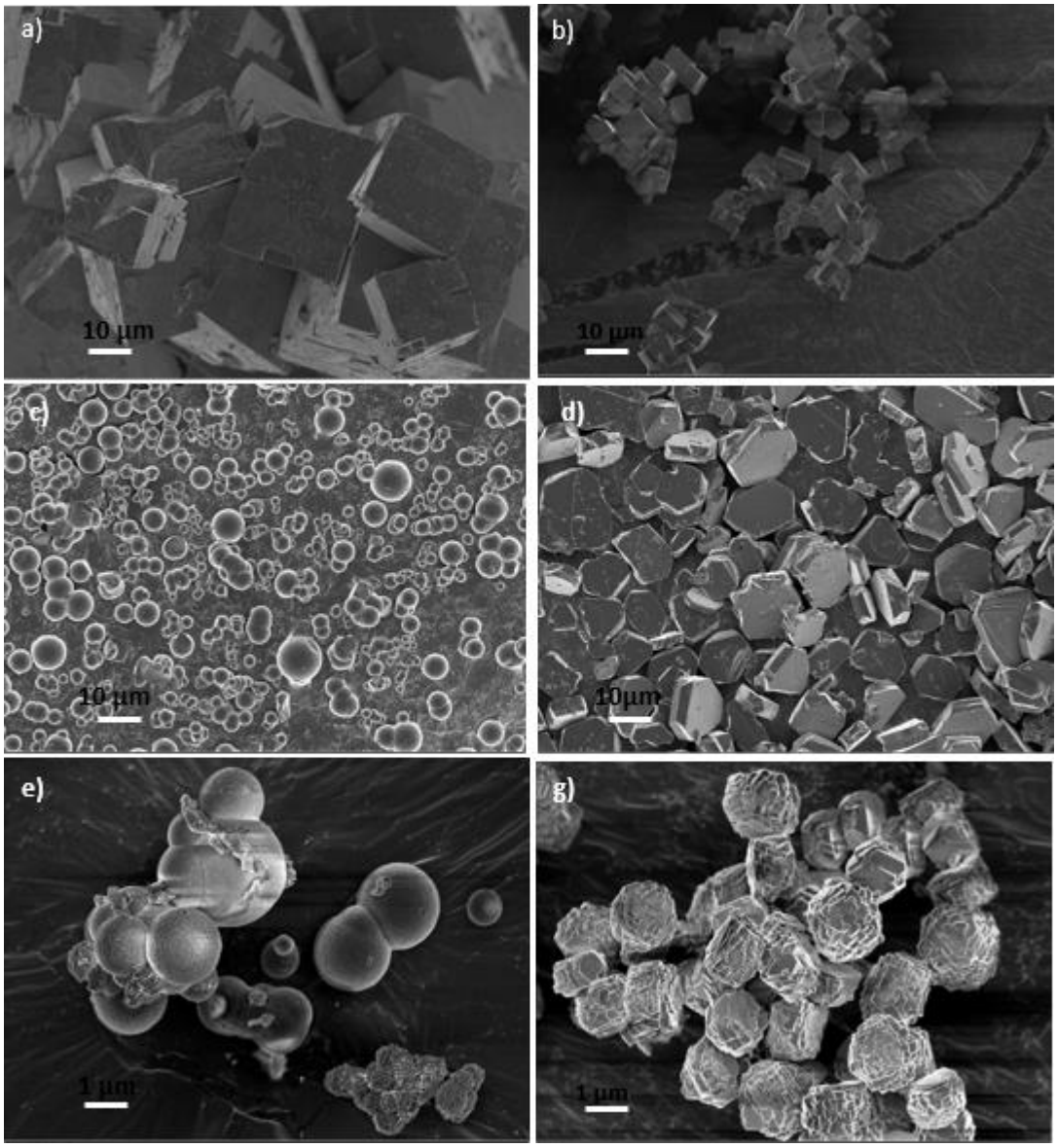

Figure 8.4: SEM images of: a) MOF-5 0 eq; b) MOF-5 100 eq; c) (75Ni/Zn) -BDC 0eq; d) (75Ni/Zn)-BDC 10 eq; e) Ni-BDC (Ni) 0 eq; f) Ni-BDC (Ni) 100 eq.

The FTIR spectrum of the synthesized adsorbents is shown in Figure 8.5 (also see Figure B3 in the Supplementary Data). A broad band was observed at approximately 3200 cm^{-1}, which corresponds to the -OH stretching vibrations of physically adsorbed water. The bands at approximately 1577 and 1384 cm^{-1} correspond to the symmetric and asymmetric stretching vibrations of the C-O bond of the carboxylate in 1,4-benzenedicarboxylate (Wu et al., 2018). The absence of the DMF C=O stretch at ~1650 cm^{-1} indicates the complete removal of DMF by CH_2Cl_2. Furthermore, there is no absorption of protonated BDC (1715–1680 cm^{-1}), which confirms the complete deprotonation of H_2BDC (Burgaz et al., 2019). In conclusion, the FTIR spectra of the MOFs were similar, which suggests similar structures in the synthesized MOFs.

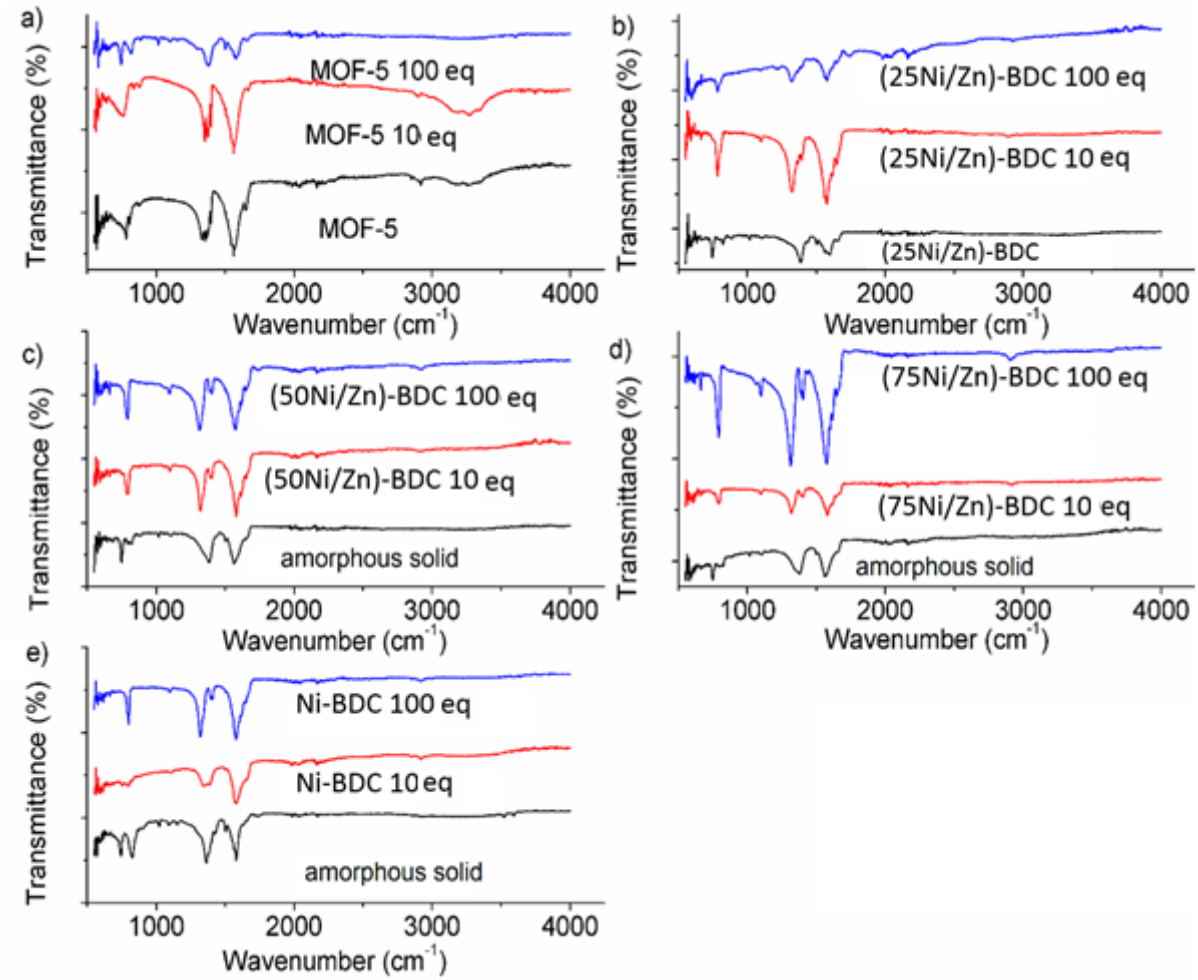

Figure 8.5: FTIR of: a) MOF-5; b) (25Ni/Zn)-BDC; c) (50Ni/Zn)-BDC; d) (75Ni/Zn)-BDC; e) Ni-BDC. The varying amounts of modulator eq, are indicated in the legends.

The elemental surface species and content of MOF-5 and Ni-BDC were measured using XPS. The MOF-5 XPS spectrum is consistent with that reported by other authors (Zhen et al., 2015; Wu et al., 2018). The main peaks were observed at 284.2, 531.9, and 1022.7. eV, which correspond to C 1s, O 1s, and Zn 2p, respectively. Similarly, for Ni-BDC, C 1s and O 1s were observed at 284.3 and 532, while the Ni 2p peak was seen at 856.3 (see Figure 8.6 a). The adsorbents had similar C 1s and O 1s spectra. The deconvolution of C 1s led to three peaks at 284.3, 285.6, and 288.8, corresponding to C-C, C=O, and C-O groups, respectively. The O 1s peak was deconvoluted to C-O (531.5) and C=O (532.5) (see Figure 8.6b and c).

The C 1s and O 1s spectra were similar for both adsorbents (see Figure B4 in the Supplementary Data). This is consistent with the XRD and FTIR data for the two compounds.

The metal peaks differ between the two compounds; the binding energy of Zn2p corresponds to Zn/ZnO, while the Ni 2p peak is at 856.3 eV, which corresponds to Ni (OH). The absence of significant amounts of chlorine and nitrogen suggests that the activation temperature was appropriate for removing the DMF and chloroform molecules from the two adsorbents, although small amounts of nitrogen (DMF) were observed with MOF-5.

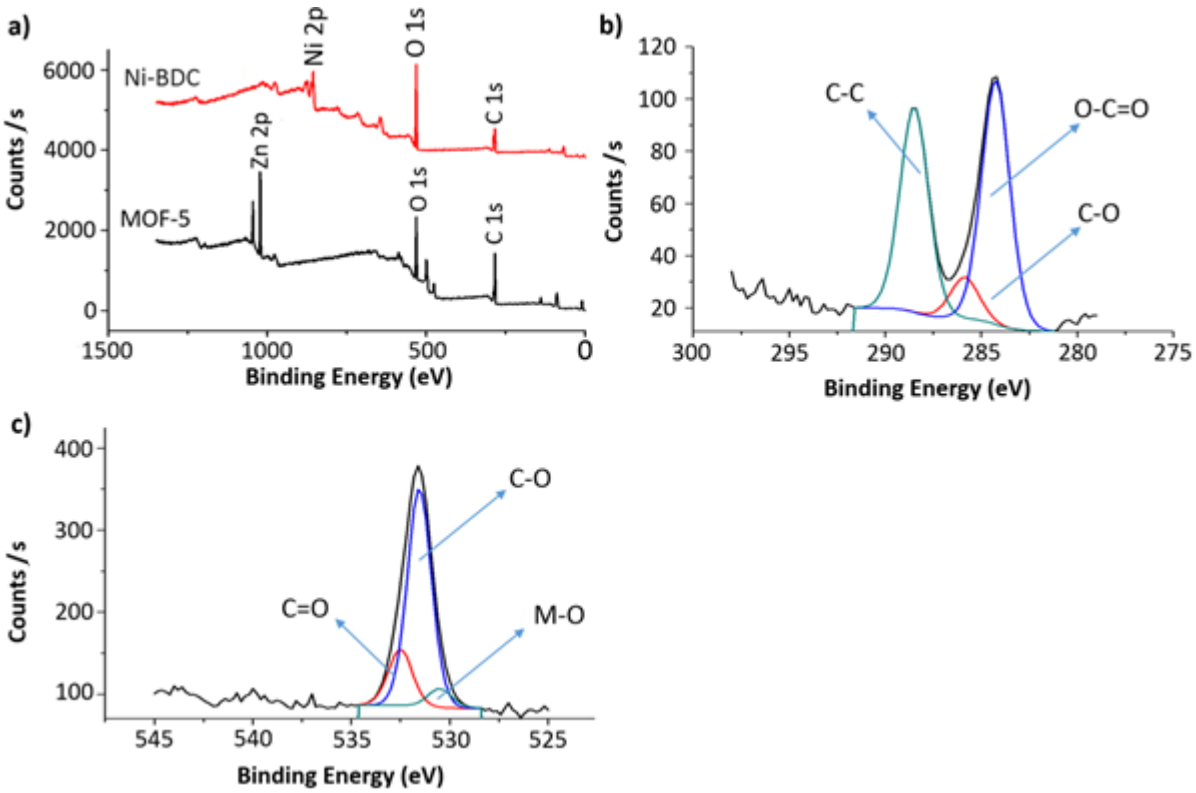

Figure 8.6: Full XPS spectrum of the (a) Ni-BDC and MOF-5, and close up survey at: (b) C for Ni-BDC and (c) O for the Ni-BDC core level.

8.3.2 Adsorptive desulphurization

Effect of adsorption time

The adsorption activity of MOF-5 with time on stream is shown in Figure 8.7. The highest MOF-5 activity was observed to generally take place within the first 15 min, except for that of the MOF-5 100 eq. This high activity within the first 15 min suggests that MOF-5 has a high affinity for organic sulphur compounds. MOF-5 modulated with 10 eq showed slightly higher activity for DBT and 4,6 DMDBT. This increase in activity could be attributed to a decrease in particle size (as observed in the SEM images) and an increase in the external surface area. The poor activity at 100 eq could be due to excessive solvent, which resulted in the dilution of the ligand and metal ion concentrations, which in turn led to poor conversion.

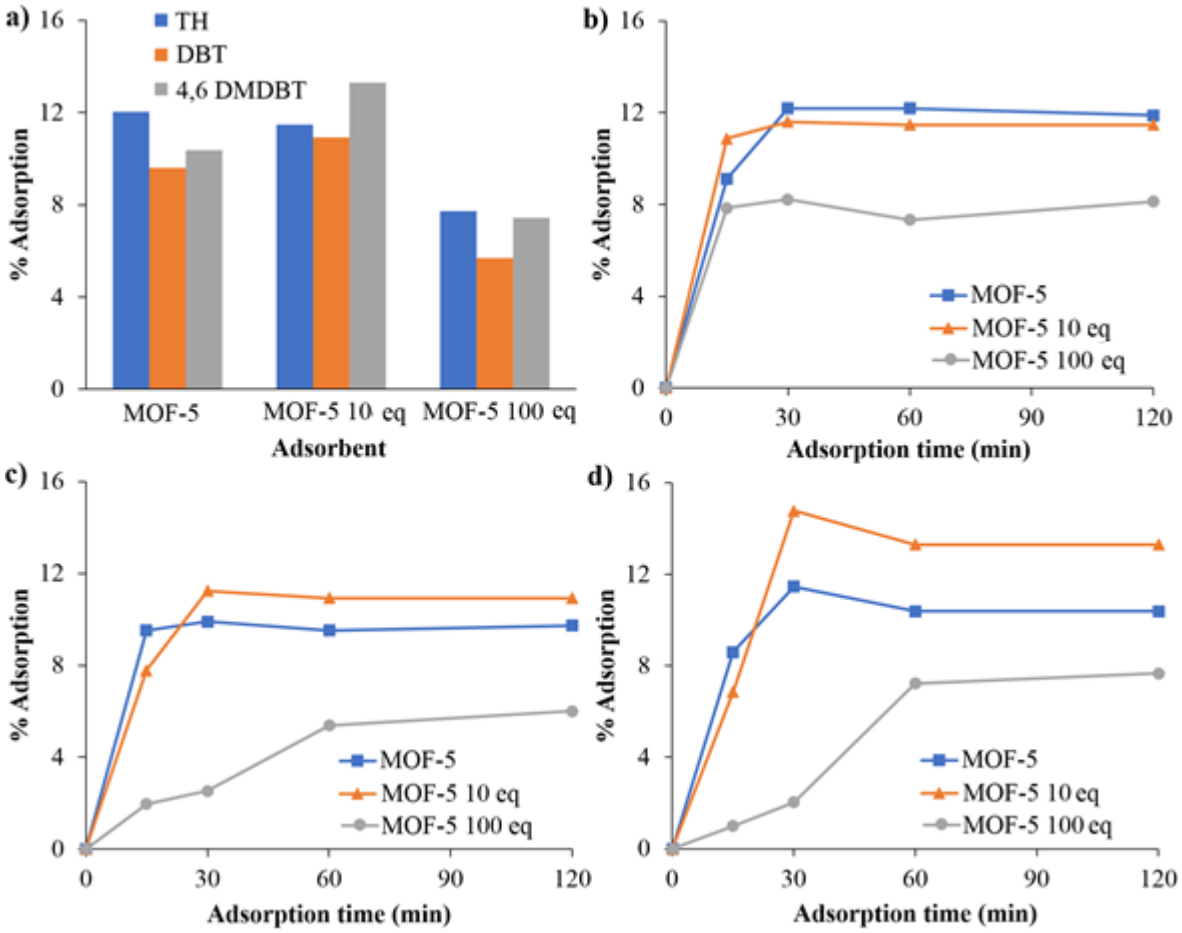

Figure 8.7: MOF-5 activity with varying amounts of modulator eq, as indicated in the legends: a) adsorption at 120 min; b) TH adsorption with time on stream; c) DBT adsorption with time on stream; d) 4,6DMDBT adsorption with time on stream at 25 ^{o}C, 2.5 wt% adsorbent and 1300 rpm stirring speed.

To compare the activity of MOF-5 and (xNi/Zn)-BDC compounds synthesized with other adsorbents, a commercial activated carbon (AC) (Sigma Aldrich) was also used for desulphurization, using the adsorption procedures described for the MOF-5 and (xNi/Zn)-BDC compounds (see Section 2.4). The adsorption of AC was higher than that of MOF-5, as shown in Figure 8.8. It was also observed that adsorption of AC took almost 120 min to reach equilibrium, compared to MOF-5, which had high activity within the first 15 min. This difference could be due to the different affinities for sulphur compounds and the pore structure of the two adsorbents.

The adsorption of AC was as follows, in decreasing order: 4,6DMDBT>>DBT>TH. The order suggests dependence only on the electron density of the organic sulphur compounds. This is consistent with the pore size, which is large enough to accommodate all sulphur compounds (see Table 8.2). This suggests that π–π interactions occur between sulphur compounds and AC (Bu et al., 2011).

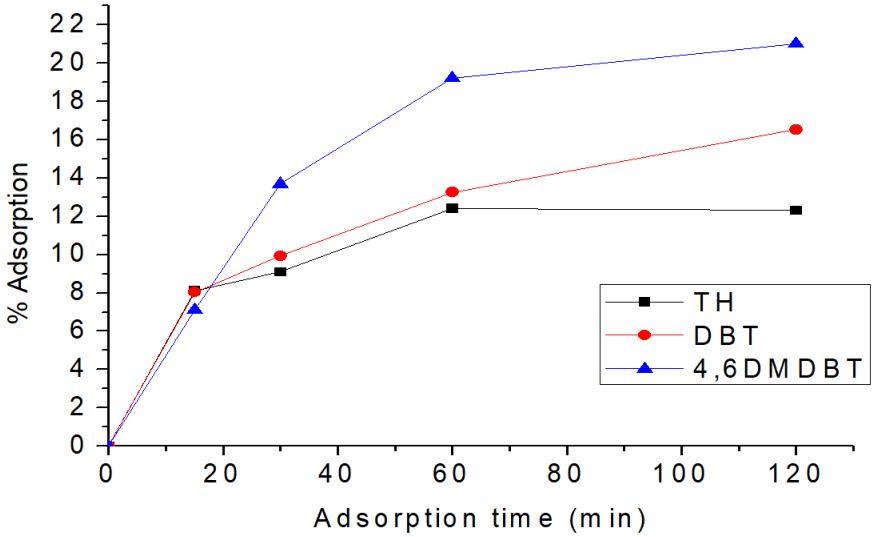

Figure 8.8: Effect of adsorption time on adsorption efficiency of AC for compounds TH DBT, and 4,6DMDBT with: at a temperature of 25 °C; 2.5 wt% adsorbent; 1300 rpm stirring speed.

Figures 8.7 and 8.8 show that the maximum adsorption efficiency is in the range of 10–20 %. This low adsorption activity may be due to the low dosage of adsorbents used in the experiments, the low adsorptive ability of the adsorbents, and the experimental setup. Low activity is expected when using a batch reactor for ADS under these conditions (Khaled, 2015; Sikarwar et al., 2018; Ullah et al., 2020; Saha et al., 2021). The experiments were intentionally conducted at a low adsorbent dosage (corresponding to a low adsorption activity (%) as a basis for easily discerning the influences of the Ni content and the amount of the formic acid treatment on the adsorption activity. These influences are discussed in the following sections.

Effect of nickel content and modulated synthesis on sulphur removal

Figure 8.9 shows that activity decreased with increased Ni content for non-modulated (xZn/Ni)-BDC. This decrease in activity may be attributed to a decrease in crystallinity, as observed in Figure 8.3. In contrast, the activity was observed to increase with increasing Ni content for modulated (xZn/Ni)-BDC. This increase in activity might be attributed to an increase in crystallinity and a higher affinity of sulphur compounds for Ni compared to Zn, as other authors have observed this in other systems, e.g., in zeolites (Hernández-Maldonado et al., 2005; Xiao et al., 2008). It was also observed that the highest activity for any (xNi/Zn)-BDC was observed for the compound treated with 10 eq formic acid. The selectivity for sulphur compounds was observed to follow the adsorption order: TH>>4,6DMDBT>DBT. In general, MOF-5 and Ni-BDC showed high activity for TH. This high adsorption activity/loading of TH was expected since MOF-5/Ni-BDC has an aperture opening of 7–8 Å (Zhao et al., 2009). Hence, TH is the only molecule that can easily access the internal structure of the MOF-5/ Ni-BDC. The slightly higher activity of 4,6DMDBT compared to DBT for most adsorbents may be attributed to a higher electron density, which suggests π-complexation bonding between the MOF and the adsorbates (Zuhra et al., 2019). A direct sulphur-MOF bond would have favored DBT bonding, since 4,6DMDBT offers higher steric hindrance because of the methyl groups.

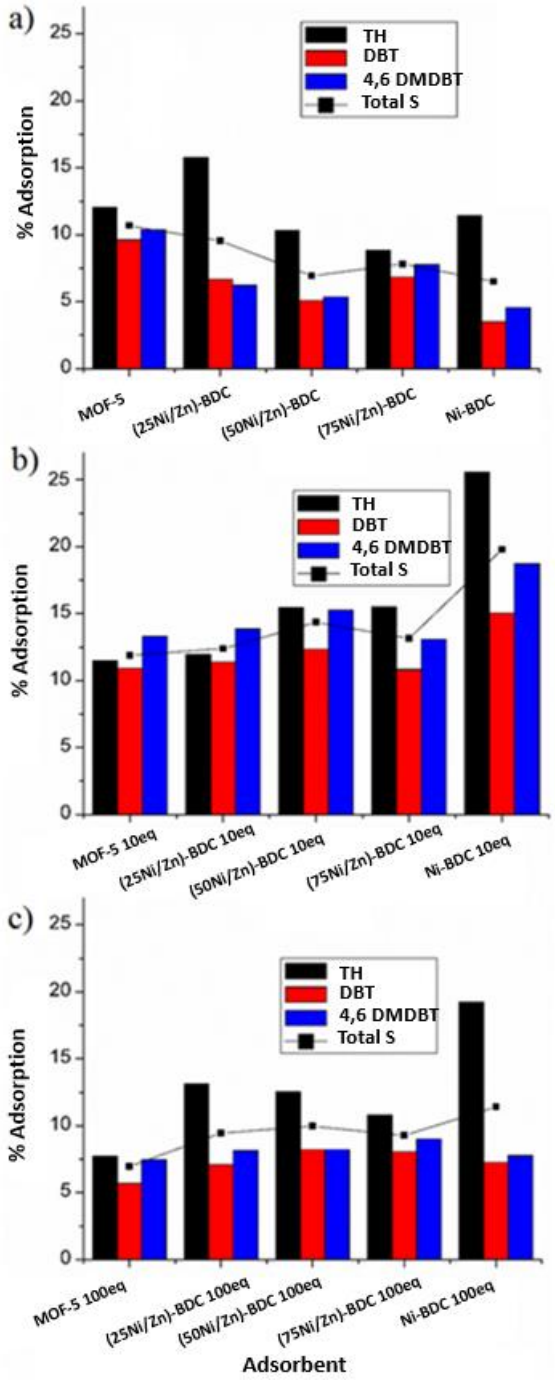

Figure 8.9: Effect of Ni content on adsorption efficiency for: a) no formic acid; b) 10 equivalent formic acid; c) 100 equivalent formic acid. Adsorption conditions: at 25 °C with 2.5 wt% adsorbent at 1300 rpm stirring speed.

8.2.3 Optimizing modulated synthesis

As addressed in the previous section, the modulated Ni-BDC showed the most promising activity. This adsorbent was used to optimize the amount of formic acid required for modulated synthesis. The surface area and crystallinity of the synthesized adsorbents are shown in Table 8.2 (see also Table B2 in the Supplementary Data). MOF-5 showed the greatest surface area, and the addition of formic acid during the synthesis of MOF-5 produced material with a smaller surface area. The smaller surface area is consistent with the XRD results: R_1 (9.7° to 6.8° ratio) was observed to be very high, with the peak at 6.8° becoming negligible (Chen et al., 2010; Greer et al., 2016). In contrast, the addition of formic acid to Ni-BDC led to an increase in surface area. However, the surface area of Ni-BDC was 3–4 times smaller than that of MOF-5 and smaller than that reported in the literature (Yang et al., 2014a). The average pore size was observed to be approximately 7.6 Å for most adsorbents. An analysis of the surface area versus crystallinity showed a good correlation with that of Ni-BDC, on which the surface area increased with increasing crystallinity (see Figure B.5 in Supplementary Data).

Table 8.2: Surface area, pore width and crystallinity for the various adsorbents

Adsorbent	Surface Area (m^2/g) BET	Langmuir	Median Pore Width (Å)	Crystallinity (%)
AC	845.56	-	20.89	
MOF-5	785.83	1 142.8	7.696	
MOF-5 10 eq	1.001	0.61	8.123	
MOF-5 100 eq	2.39	2.95	8.145	
Ni-BDC	4.02	4.89	7.751	-
Ni-BDC 10 eq	178.93	235.93	7.697	7.7
Ni-BDC 25 eq	241.99	306.8	7.659	22.4
Ni-BDC 50 eq	208.20	340.84	7.675	19.5
Ni-BDC 75 eq	211.64	327.70	7.668	15.7
Ni-BDC 100 eq	170.54	231.38	7.684	8.7

The Ni-BDC activity increased with the quantity of formic acid added, reaching a maximum at 15 eq (see Figure 8.10). Thereafter, the activity levelled off and started dropping after 50 eq, as shown in Figure 8.10. The increase in activity may be attributed to increased crystallinity (see Figure 8.11). The decrease in crystallinity after 50 eq could be due to the excessive dilution of the MOF synthesis reagents by formic acid.

It was also observed generally (see Figure 8.10) that Ni-BDC had better activity for TH compared to DBT and 4,6DMDBT. This is because of the pore structure, as discussed earlier, section 3.2.2. The experimental results indicate that the Ni-based MOF absorbents show good potential for the desulphurization of fluid catalytic cracking gasoline, with thiophenic sulphur representing over 80 % of the total sulphur content (Fihri et al., 2016).

To further understand the effect of crystallinity and crystallite size on adsorption, a correlation analysis of the activity versus crystallinity and activity versus crystallite size was performed for each sulphur compound (see Figure 8.11). Figure 8.11(a) shows that the TH activity was directly proportional to the crystallinity. The dependence of TH adsorption on crystallinity could be a result of increased crystallinity, leading to an increase in the number of Ni crystallite sites. This could be important because TH can penetrate the Ni-BDC structure and access these active sites. However, crystallinity has no significant effect on the adsorption activity of either DBT or 4,6DMDBT because adsorption occurs only on the external surface. There was no correlation between crystallite size and TH activity, but an inverse relationship (R-negative) was observed between DBT and 4,6DMDBT activity and crystallite size (see Figure 8.11(b)). This result suggests that because TH can penetrate the MOF structure, the crystallite size has no bearing on its adsorption. However, DBT and 4,6DMDBT depend on crystallite size, as their adsorption occurs on the external surface; hence, a larger crystallite size translates into a smaller external surface area and lowers the adsorption of these compounds.

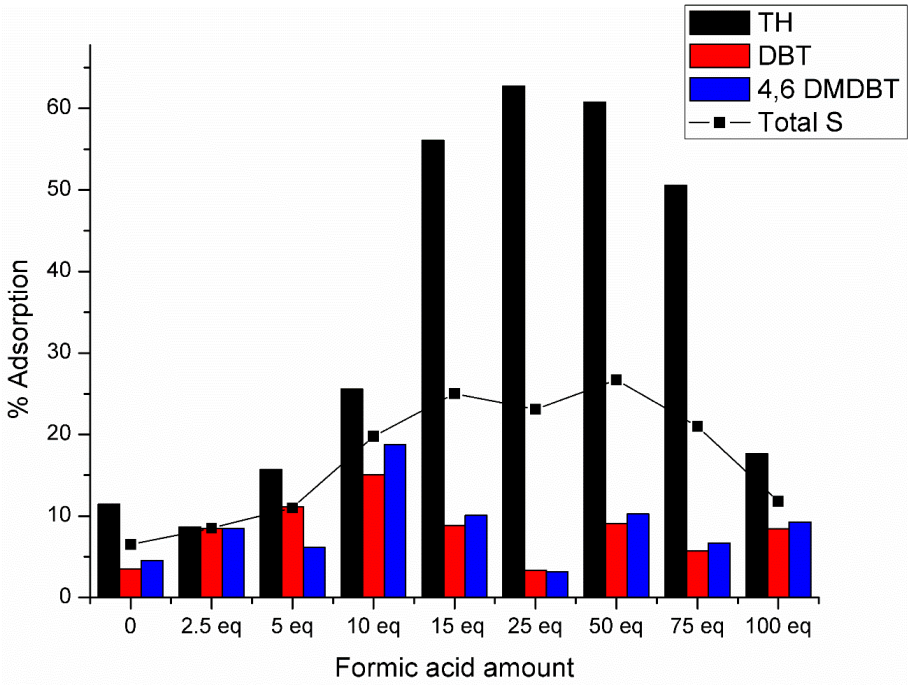

Figure 8.10: Effect of the amount of formic acid modulator added on the adsorption performance of Ni-BDC. Adsorption conditions: 25 °C, 2.5 wt% adsorbent, and 1300 rpm stirring speed.

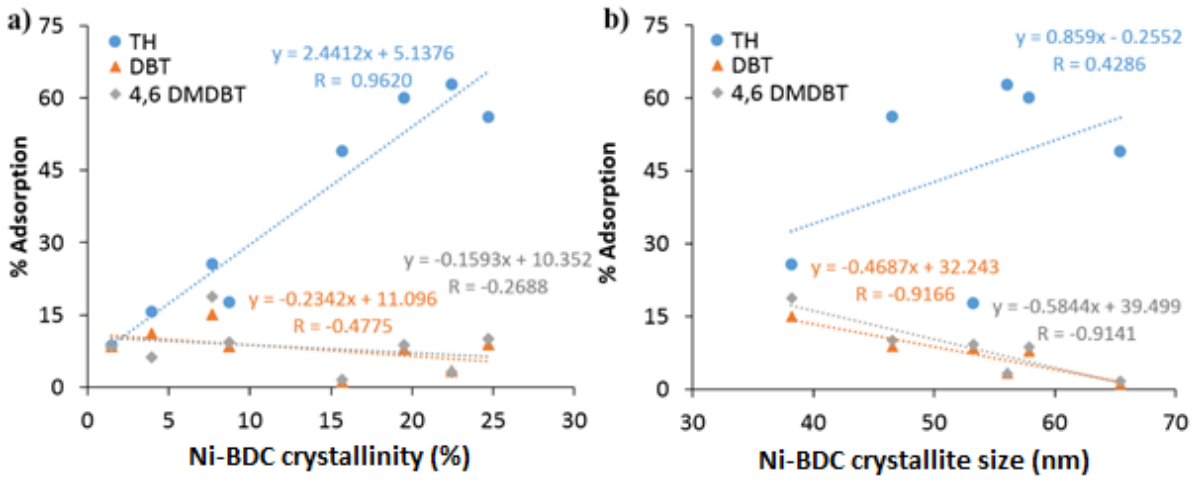

Figure 8.11: Modulated Ni-BDC activity correlation against: a) crystallinity (%); b) crystallite size (nm). Adsorption conditions: 25 °C, 2.5 wt% adsorbent, and 1300 rpm stirring speed.

The adsorption capacities and PCs of the four adsorbents (AC, MOF-5, Ni-BDC, and Ni-BDC 15 eq) are summarized in Table 8.3. The replacement of Zn by the Ni metal ion in the MOF reduced the activity of the adsorbent by nearly half. This decrease in activity is attributed to the poor crystallinity of Ni-BDC (see Figure 8.4). Finally, the activity of Ni-BDC 15 eq after modulated synthesis was 3.5 times higher than that of Ni-BDC. This was ascribed to two factors: the improved crystallinity (Table B2), even though interpenetration of crystallites was still observed on SEM, and an increase in the number of atoms with low coordination planes compared to cubic-MOF-5 (see Figure 8.3). The increase in microcrystallinity led to more unsaturated metal sites and a stronger adsorption effect (Zhu et al., 2018). It should also be noted that the improvement in the activity of Ni-BDC 15 eq compared to MOF-5 was primarily due to the nearly five-fold increase in the adsorption of TH. This high increase in activity towards TH suggests that Ni-BDC 15eq is best suited for the adsorption of smaller sulphur compounds.

The adsorption capacity of MOF 5 was comparable to that reported by Shi et al., 2011 and Jia et al., 2017, even though different initial sulphur concentrations were used. The modified Ni-BDC 15 eq showed higher activity towards TH compared to MOF 5, as reported by Jia et al. (2017), and it had a similar adsorption time, with both experiments carried out in batch mode. However, the adsorbent in this work had lower activity compared to the work performed by Cychosz et al., (2008) and Li et al., (2015). The effect of the initial concentration of the adsorbate can be considered by using a PC (Vikrant and Kim, 2019). Adsorption capacity is not an objective metric for meaningfully assessing the actual performance of sorbents if the initial adsorbate concentrations are different (Al-Wabel et al., 2019).

Therefore, the authors have reported their PCs to enable meaningful comparisons with this work. The PC values reported for other researchers (see Table 8.3) were estimated by taking the first derivative of adsorption capacity versus the equilibrium adsorbate concentration in the region where Henry's law is applicable or per the equations given in the literature (Speight, 2018; Szulejko et al., 2019).

The highest PC value reported in the present study was 4.54×10^{-2} mg/ppm for TH, which is comparable to the estimated PC reported by Khan et al. (2011) for benzothiophene adsorption using MIL-53(Al) and MIL-53(Cr), where PC values of 3.294×10^{-2} and 7.647×10^{-2} mg/ppm were obtained, respectively, for adsorption at 25 °C. However, the PC values for DBT and DMDBT were lower than those of the MOF-5 adsorbent reported by Cychosz et al. (2008), with PC values estimated to be 2.857×10^{-2} mg/g/ppm and 5.556×10^{-2} mg/g/ppm, respectively (see Table 8.3). We believe this may be due to the competitive absorption of TH, DBT, and DMDBT. Further research must be conducted to compare the adsorptive capacity and PC values when using only a single sulphur component to those obtained when using a mixture of sulphur components.

Table 8.3**:** Sulphur adsorption capacity and PC for tested adsorbates and others reported in the literature.

Adsorbent	Initial Concentration (Final Concentration), ppm					Adsorption capacity, (mg-S/g-adsorbent)					Partition Coefficient (mg/g/ppm× 10^2)					Ref
	TH	BT	DBT	4,6DMDBT	Total	TH	BT	DBT	4,6DMDBT	Total	TH	BT	DBT	4,6DMDBT	Total	
AC	150(132)	---	153(126)	151(120)	454(378)	0.78	---	1.04	1.61	3.43	0.591	---	0.823	1.341	2.755	Current work[a]
MOF-5	150(132)	---	153(138)	151(135)	454(405)	0.62	---	0.53	0.56	1.71	0.469	---	0.384	0.414	1.267	
Ni-BDC	150(132)	---	153(146)	151(143)	454(421)	0.63	---	0.22	0.28	1.13	0.477	---	0.151	0.195	0.823	
Ni-BDC 15eq	150(68)	---	153(139)	151(136)	454(343)	3.09	---	0.5	0.55	4.14	4.544	---	0.359	0.404	5.307	
MOF-5	500	---	---	---	500	1.25	---	---	---	1.25	---		---	---	---	(Jia et al., 2017)
	---	500	---	---	500	---	1.03	---	---	1.03	---		---	---	---	
	---	---	500	---	500	---	---	0.52	---	0.52	---		---	---	---	
MOF-5	---	---	35	---	35	---	---	0.461	---	0.4608	---		---	---	---	(Shi et al., 2011)
	---	---	1006	---	1006	---	---	11.1	---	11.104	---		---	---	---	
MOF-5	550	---	---	---	550	7.36	---	---	---	7.36	---		---	---	---	(Li et al., 2015)
	---	550	---	---	550	---	2.56	---	---	2.56	---		---	---	---	
MOF-5	---	---	(~210)	---	(~210)	---	---	~6	---	~6	---	---	~2.857	---	~2.857~	(Cychosz et al., 2008)
	---	---	---	(~117)	(~117)	---	---	---	~6.5	~6.5	---	---	---	~5.556	~5.556	
MIL-53(Al)	---	~500(~425)	---	---	~500(~425)	---	~14	---	---	~14	---	~3.294	---	---	~3.294	(Khan et al., 2011)
MIL-53(Cr)	---	~500(~340)	---	---	~500(~340)	---	~26	---	---	~26	---	~7.647	---	---	~7.647	

TH refers to Thiophene; BT refers to Benzothiophene; DBT refers to Dibenzothiophene; 4,6 DMDBT refers to 4,6-Dimethyldibenzothiophene

[a] the value of partition coefficient was calculated by using the data obtained when adsorption reached saturated capacity, which represented 100% breakthrough

The nature of the acid sites of the four adsorbents listed in Table 8.3 was analyzed using TPD-pyridine (see Figure 8.12). AC had the highest number of acid sites and the highest number of strong acid sites. The overall order of the acid sites was as follows: AC>> Ni-BDC 15 eq>MOF-5> Ni-BDC. The results are consistent with the adsorption order for total sulphur for the MOFs, that is, Ni-BDC 15 eq>MOF-5> Ni-BDC. The low overall activity of AC was due to its low activity toward TH. Although AC had the highest number of acidic sites, the pore structure (pore size: 20.89 Å) was not comparable to the kinetic diameter of TH (7.6 Å), leading to TH not fully experiencing the electronic field of AC. An analysis of Ni-BDC and Ni-BDC 15 eq suggests that there may be some correspondence between crystallinity and the number of acid sites. The experimental results show the benefit of the modulated synthesis of Ni-BDC for removing sulphur components from liquid fuels.

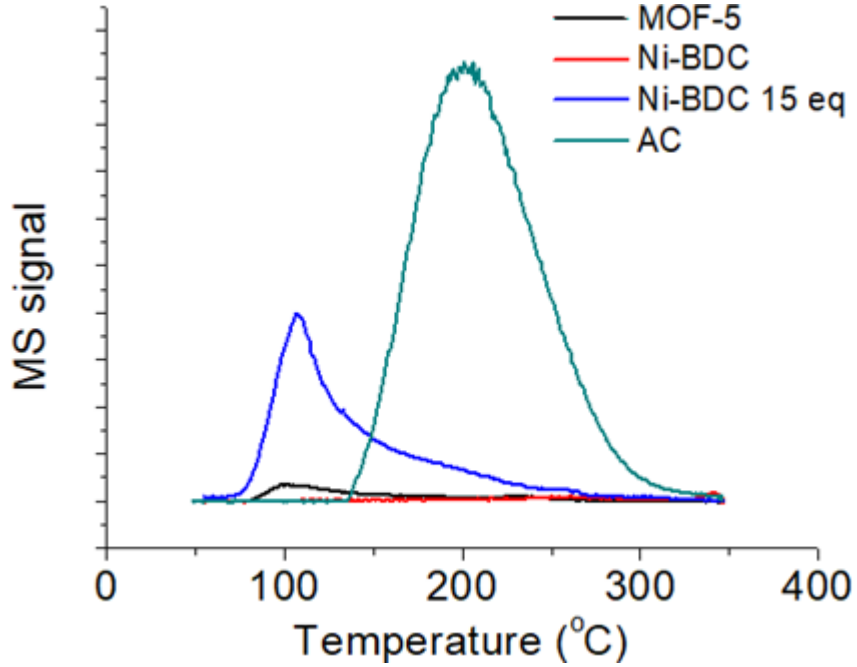

Figure 8.12: Temperature programmed desorption of pyridine for AC, MOF-5, Ni-BDC and Ni-BDC 15 eq.

8.3.4 Stability of MOF-5 and (xNi/Zn)-BDC samples

The stability of adsorbents for desulphurization is another important factor in practice. Therefore, the XRD patterns of the dried MOF-5 and (xNi/Zn)-BDC samples after the adsorption experiments were collected to compare them with those of the as-prepared samples. As shown in Figure 8.13, the split peak of MOF-5 near 2θ=9.5° was caused by the adsorption of water in the experiments. The XRD diffraction spectrum of the other MOF samples did not indicate any clear signs of structural destruction when compared to the as-prepared samples. This suggests that the MOF-5 and (xNi/Zn)-BDC samples are stable enough to be employed as adsorbents for the desulphurization of liquid fuels.

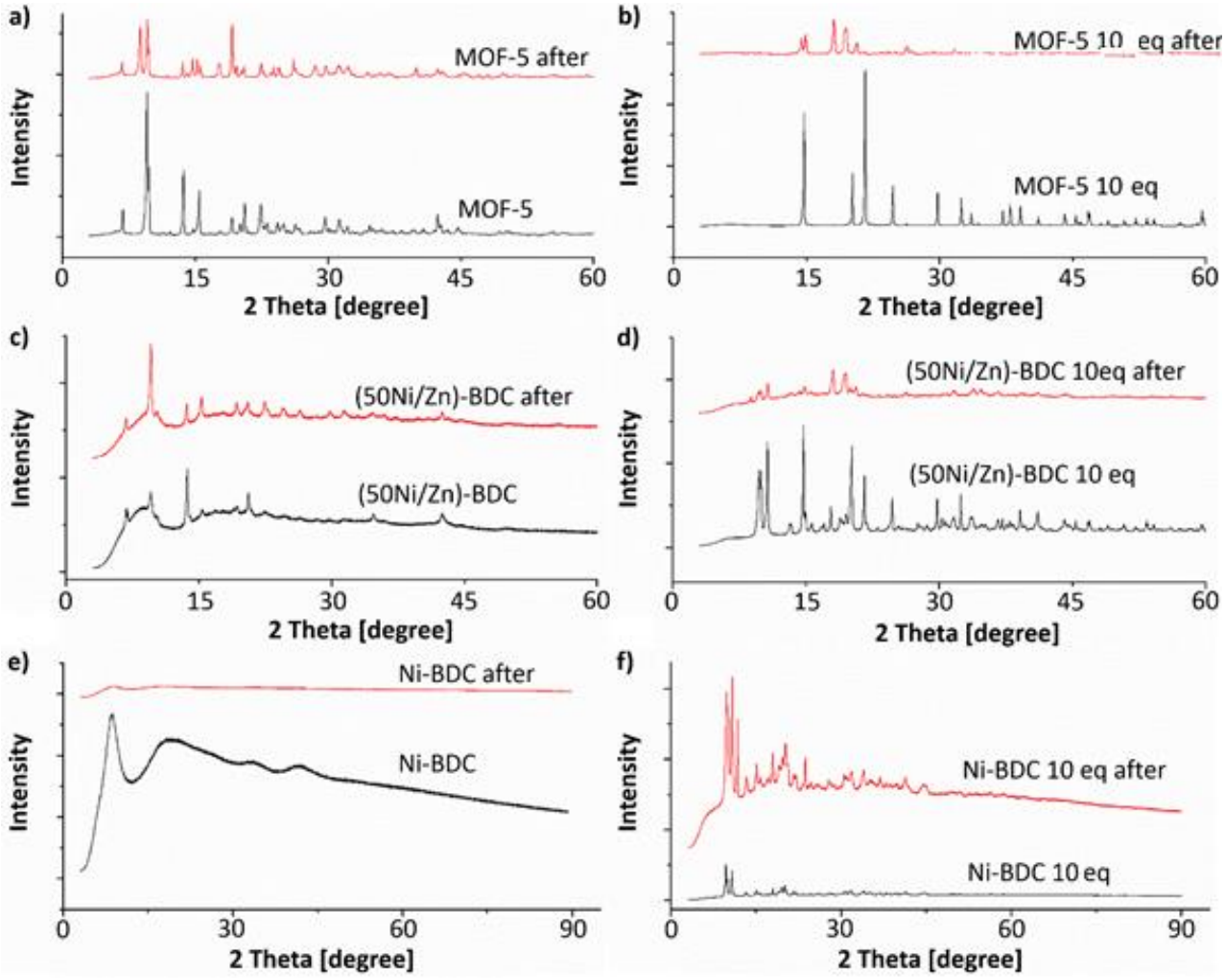

Figure 8.13: XRD spectrum before and after adsorption: a) MOF-5; b) MOF-5 10eq; c) (50Ni/Zn)-BDC; d) (50Ni/Zn)-BDC10eq; e) Ni-BDC; f) Ni-BDC 10eq.

8.4 Conclusion

A group of Ni-doped MOFs with varying Ni content (xNi/Zn) was successfully synthesized using different amounts of the modulator (formic acid), and these MOFs were evaluated in terms of their adsorptive performance for desulphurization of model diesel. The introduction of Ni changed the shape of the synthesized MOF from cubic to irregularly shaped structures and led to a decrease in the crystallinity and crystallite size of the adsorbents. Nevertheless, the addition of formic acid significantly increased both the crystallite size and crystallinity of the (xNi/Zn)-BDC materials.

It was shown that Ni-doping and modulation with formic acid improved the activity in the adsorption of sulphur components from model diesel, with the order of activity of Ni-BDC 10 eq > (xNi/Zn)-BDC 10 eq > MOF-5 > (xNi/Zn)-BDC ~ (xNi/Zn)-BDC 100 eq. This trend is attributed to the increase in the crystallinity resulting from the use of formic acid as a modulator for the preparation of MOFs and the higher affinity of sulphur compounds for Ni compared to that of Zn. The different behaviour observed between Ni-BDC 10 eq (high adsorption capacity) and Ni-BDC 100 eq (low adsorption capacity) enabled us to optimize the amount of modulator added in the preparation of the absorbents.

Another group of Ni-BDC samples was subjected to modulated synthesis by adding different amounts of formic acid. Increasing the amount of formic acid initially led to an increase in both crystallite size and crystallinity, which reached a maximum at 15 eq (Ni-BDC 15 eq). Increasing the amount of modulator led to the further dilution of the reagents, which had an adverse effect on the properties of Ni-BDC. The highest total adsorption capacity was obtained for Ni-BDC 15 eq, which had an overall capacity of 4.14 (mg-S/g-adsorbent) and a PC of 5.31×10^{-2} mg/g/ppm. The relative activity for adsorbing TH, DBT, and 4,6DMDBT depends on the material crystallinity and crystallite size. The activity data also correlated with the number of acid sites, which indicates that there is a relationship between the crystallinity and the number of acid sites in Ni-BDC. These results show that the modulated synthesis of Ni-BDC is a promising adsorbent for sulphur removal from liquid fuels, especially for the TH compound. Further investigation is recommended to determine how Zn and Ni are incorporated into (xNi/Zn)-BDC and how to improve the adsorptive capacity of modulated Ni-BDC for larger molecules such as DBT and DMDBT.

Acknowledgements

The authors are grateful for the support received from the University of South Africa (UNISA), the National Research Foundation (NRF), and the Department of Science and Technology (DST). The authors are also grateful for the characterization assistance provided by Prof. M. M. Nindi and Dr. H. Nyoni. We are also grateful for the opportunity to make use of the laboratories at the Council for Scientific and Industrial Research (CSIR), South Africa.

Appendix B. Supplementary data

Supplementary data related to this article can be found at: **Appendix B.**

References

Ahmed, I., Jhung, S.H., 2015. Effective adsorptive removal of indole from model fuel using a metal-organic framework functionalized with amino groups. J. Hazard. Mater. 283, 544–550. https://doi.org/10.1016/j.jhazmat.2014.10.002

Ahsan, Md.A., Jabbari, V., Imam, M.A., Castro, E., Kim, H., Curry, M.L., Valles-Rosales, D.J., Noveron, J.C., 2020. Nanoscale nickel metal organic framework decorated over graphene oxide and carbon nanotubes for water remediation. Sci. Total Environ. 698, 134214. https://doi.org/10.1016/j.scitotenv.2019.134214

Al-Wabel, M., Elfaki, J., Usman, A., Hussain, Q., Ok, Y.S., 2019. Performance of dry water- and porous carbon-based sorbents for carbon dioxide capture. Environ. Res. 174, 69–79. https://doi.org/10.1016/j.envres.2019.04.020

Biemmi, E., Christian, S., Stock, N., Bein, T., 2009. High-throughput screening of synthesis parameters in the formation of the metal-organic frameworks MOF-5 and HKUST-1. Microporous Mesoporous Mater. 117, 111–117.

Botas, J.A., Calleja, G., Sánchez-Sánchez, M., Orcajo, M.G., 2010. Cobalt Doping of the MOF-5 Framework and Its Effect on Gas-Adsorption Properties. Langmuir 26, 5300–5303. https://doi.org/10.1021/la100423a

Brozek, C.K., Dincă, M., 2012. Lattice-imposed geometry in metal–organic frameworks: lacunary Zn4O clusters in MOF-5 serve as tripodal chelating ligands for Ni2+. Chem. Sci. 3, 2110. https://doi.org/10.1039/c2sc20306e

Bruker Axs, INC., 2005. Bruker Advanced X-ray solutions, 3. Bruker Axs, INC., Karlsruhe, West Germany.

Bu, J., Loh, G., Gwie, C.G., Dewiyanti, S., Tasrif, M., Borgna, A., 2011. Desulphurization of diesel fuels by selective adsorption on activated carbons: Competitive adsorption of polycyclic aromatic sulphur heterocycles and polycyclic aromatic hydrocarbons. Chem. Eng. J. 166, 207–217. https://doi.org/10.1016/j.cej.2010.10.063

Burgaz, E., Erciyes, A., Andac, M., Andac, O., 2019. Synthesis and characterization of nano-sized metal organic framework-5 (MOF-5) by using consecutive combination of ultrasound and microwave irradiation methods. Inorganica Chim. Acta 485, 118–124.

Chen, B., Wang, X., Zhang, Q., Xi, X., Cai, J., Qi, H., Shi, S., Wang, J., Yuan, D., Fang, M., 2010. Synthesis and characterization of the interpenetrated MOF-5. J. Mater. Chem. 20, 3758–3767.

Cychosz, K.A., Wong-Foy, A.G., Matzger, A.J., 2008. Liquid Phase Adsorption by Microporous Coordination Polymers: Removal of Organosulphur Compounds. J. Am. Chem. Soc. 130, 6938–6939. https://doi.org/10.1021/ja802121u

Ding, M., Cai, X., Jiang, H.-L., 2019. Improving MOF stability: approaches and applications. Chem. Sci. 10, 10209–10230. https://doi.org/10.1039/C9SC03916C

Fihri, A., Mahfouz, R., Shahrani, A., Taie, I., Alabedi, G., 2016. Pervaporative desulphurization of gasoline: A review. Chem. Eng. Process. - Process Intensif. 107, 94–105. https://doi.org/10.1016/j.cep.2016.06.006

Gao, S., Sui, Y., Wei, F., Qi, J., Meng, Q., He, Y., 2018. Facile synthesis of cuboid Ni-MOF for high-performance supercapacitors. J. Mater. Sci. 53, 6807–6818. https://doi.org/10.1007/s10853-018-2005-1

Greer, H.F., Liu, Y., Greenaway, A., Wright, P.A., Zhou, W., 2016. Synthesis and Formation Mechanism of Textured MOF-5. Cryst. Growth Des. 16, 2104–2111. https://doi.org/10.1021/acs.cgd.5b01785

Hafizovic, J., Bjørgen, M., Olsbye, U., Dietzel, P.D., Bordiga, S., Prestipino, C., Lamberti, C., Lillerud, K.P., 2007. The inconsistency in adsorption properties and powder XRD data of MOF-5 is rationalized by framework interpenetration and the presence of organic and inorganic species in the nanocavities. J. Am. Chem. Soc. 129, 3612–3620.

Hernández-Maldonado, A.J., Yang, F.H., Qi, G., Yang, R.T., 2005. Desulphurization of transportation fuels by π-complexation sorbents: Cu (I)-, Ni (II)-, and Zn (II)-zeolites. Appl. Catal. B Environ. 56, 111–126.

Hernández‐Maldonado, A.J., Yang, R.T., 2004. Desulphurization of Transportation Fuels by Adsorption. Catal. Rev. 46, 111–150. https://doi.org/10.1081/CR-200032697

Howarth, A.J., Peters, A.W., Vermeulen, N.A., Wang, T.C., Hupp, J.T., Farha, O.K., 2016. Best practices for the synthesis, activation, and characterization of metal–organic frameworks. Chem. Mater. 29, 26–39.

Jia, X.-Y., Song, Z.-Y., Zhu, L.-J., Xia, D.-H., 2017. Synthesis of transition metal-doped MOF-5 and their application for adsorptive desulphurization, in: 2nd Annual International Conference on Energy, Environmental & Sustainable Ecosystem Development (EESED 2016). Presented at the 2nd Annual International Conference on Energy, Environmental & Sustainable Ecosystem Development (EESED 2016), Atlantis Press, Kunming, China. https://doi.org/10.2991/eesed-16.2017.76

Khaled, M., 2015. Adsorption performance of multiwall carbon nanotubes and graphene oxide for removal of thiophene and dibenzothiophene from model diesel fuel. Res. Chem. Intermed. 41, 9817–9833. https://doi.org/10.1007/s11164-015-1986-5

Khan, N.A., Jhung, S.H., 2013. Effect of central metal ions of analogous metal-organic frameworks on the adsorptive removal of benzothiophene from a model fuel. J. Hazard. Mater. 260, 1050–1056. https://doi.org/10.1016/j.jhazmat.2013.06.076

Khan, N.A., Jun, J.W., Jeong, J.H., Jhung, S.H., 2011. Remarkable adsorptive performance of a metal–organic framework, vanadium-benzenedicarboxylate (MIL-47), for benzothiophene. Chem Commun 47, 1306–1308. https://doi.org/10.1039/C0CC04759G

Li, Huanhuan, Shi, W., Zhao, K., Li, Han, Bing, Y., Cheng, P., 2012a. Enhanced hydrostability in Ni-doped MOF-5. Inorg. Chem. 51, 9200–9207.

Li, Huanhuan, Shi, W., Zhao, K., Li, Han, Bing, Y., Cheng, P., 2012b. Enhanced Hydrostability in Ni-Doped MOF-5. Inorg. Chem. 51, 9200–9207. https://doi.org/10.1021/ic3002898

Li, Y.-X., Jiang, W.-J., Tan, P., Liu, X.-Q., Zhang, D.-Y., Sun, L.-B., 2015. What matters to the adsorptive desulphurization performance of metal-organic frameworks? J. Phys. Chem. C 119, 21969–21977.

Lv, Y., Wang, S., Zhang, R., Zhang, D., Yu, H., Lu, G., 2018. PH-modulated formation of uniform MOF-5 sheets. Inorg. Chem. Commun. 97, 30–33. https://doi.org/10.1016/j.inoche.2018.09.003

Ma, D., Li, Y., Li, Z., 2011. Tuning the moisture stability of metal–organic frameworks by incorporating hydrophobic functional groups at different positions of ligands. Chem. Commun. 47, 7377–7379.

Mguni, L.L., Yao, Y., Liu, X., Yuan, Z., Hildebrandt, D., 2019a. Ultra-deep desulphurization of both model and commercial diesel fuels by adsorption method. J. Environ. Chem. Eng. 7, 102957. https://doi.org/10.1016/j.jece.2019.102957

Mguni, L.L., Yao, Y., Nkomzwayo, T., Liu, X., Hildebrandt, D., Glasser, D., 2019b. Desulphurization of diesel fuels using intermediate Lewis acids loaded on activated charcoal and alumina. Chem. Eng. Commun. 206, 572–580.

Ming, Y., Purewal, J., Yang, J., Xu, C., Soltis, R., Warner, J., Veenstra, M., Gaab, M., Müller, U., Siegel, D.J., 2015. Kinetic stability of MOF-5 in humid environments: impact of powder densification, humidity level, and exposure time. Langmuir 31, 4988–4995.

Montero, J.M., Gai, P., Wilson, K., Lee, A.F., 2009. Structure-sensitive biodiesel synthesis over MgO nanocrystals. Green Chem. 11, 265–268.

Ren, J., Langmi, H.W., North, B.C., Mathe, M., Bessarabov, D., 2014. Modulated synthesis of zirconium-metal organic framework (Zr-MOF) for hydrogen storage applications. Int. J. Hydrog. Energy 39, 890–895.

Ren, J., Ledwaba, M., Musyoka, N.M., Langmi, H.W., Mathe, M., Liao, S., Pang, W., 2017. Structural defects in metal–organic frameworks (MOFs): Formation, detection and control towards practices of interests. Coord. Chem. Rev. 349, 169–197. https://doi.org/10.1016/j.ccr.2017.08.017

Saha, B., Vedachalam, S., Dalai, A.K., 2021. Review on recent advances in adsorptive desulphurization. Fuel Process. Technol. 214, 106685. https://doi.org/10.1016/j.fuproc.2020.106685

Shi, F., Hammoud, M., Thompson, L.T., 2011. Selective adsorption of dibenzothiophene by functionalized metal organic framework sorbents. Appl. Catal. B Environ. 103, 261–265. https://doi.org/10.1016/j.apcatb.2010.07.016

Sikarwar, P., Kumar, U.K.A., Gosu, V., Subbaramaiah, V., 2018. Synergetic Effect of Cobalt-Incorporated Acid-Activated GAC for Adsorptive Desulphurization of DBT under Mild Conditions. J. Chem. Eng. Data 63, 2975–2985. https://doi.org/10.1021/acs.jced.8b00249

Speight, J.G., 2018. Chapter 5 - Sorption, Dilution, and Dissolution, in: Speight, J.G. (Ed.), Reaction Mechanisms in Environmental Engineering. Butterworth-Heinemann, pp. 165–201. https://doi.org/10.1016/B978-0-12-804422-3.00005-5

Sun, L.-B., Li, J.-R., Park, J., Zhou, H.-C., 2012. Cooperative template-directed assembly of mesoporous metal–organic frameworks. J. Am. Chem. Soc. 134, 126–129.

Szulejko, J.E., Kim, K.-H., Parise, J., 2019. Seeking the most powerful and practical real-world sorbents for gaseous benzene as a representative volatile organic compound based on performance metrics. Sep. Purif. Technol. 212, 980–985. https://doi.org/10.1016/j.seppur.2018.11.001

Tailleur, R.G., 2019. Hydrogenation and hydrodesulphurization in gas phase of light hydrocarbons from hydrocracking, desulphurization and delayed coking. I catalyst deactivation. Chem. Eng. Sci. 210, 115195. https://doi.org/10.1016/j.ces.2019.115195

Tirmizi, S.A., Badshah, A., Ammad, H.M., Jawad, M., Abbas, S.M., Rana, U.A., Khan, S.U.-D., 2018. Synthesis of highly stable MOF-5@ MWCNTs nanocomposite with improved hydrophobic properties. Arab. J. Chem. 11, 26–33.

Tranchemontagne, D.J., Hunt, J.R., Yaghi, O.M., 2008. Room temperature synthesis of metal-organic frameworks: MOF-5, MOF-74, MOF-177, MOF-199, and IRMOF-0. Tetrahedron 64, 8553–8557. https://doi.org/10.1016/j.tet.2008.06.036

Ullah, S., Hussain, S., Ahmad, W., Khan, H., Khan, K.I., Khan, S.U., Khan, S., 2020. Desulphurization of Model Oil through Adsorption over Activated Charcoal and Bentonite Clay Composites. Chem. Eng. Technol. 43, 564–573. https://doi.org/10.1002/ceat.201900203

Vikrant, K., Kim, K.-H., 2019. Nanomaterials for the adsorptive treatment of Hg (II) ions from water. Chem. Eng. J. 358, 264–282.

Wang, S., Lv, Y., Yao, Y., Yu, H., Lu, G., 2018. Modulated synthesis of monodisperse MOF-5 crystals with tunable sizes and shapes. Inorg. Chem. Commun. 93, 56–60.

Wang, T., Li, X., Dai, W., Fang, Y., Huang, H., 2015. Enhanced adsorption of dibenzothiophene with zinc/copper-based metal–organic frameworks. J. Mater. Chem. A 3, 21044–21050. https://doi.org/10.1039/C5TA05204A

Wiβmann, G., Schaate, A., Lilienthal, S., Bremer, I., Schneider, A.M., Behrens, P., 2012. Modulated synthesis of Zr-fumarate MOF. Microporous Mesoporous Mater. 152, 64–70.

Wu, Y., Pang, H., Yao, W., Wang, Xiangxue, Yu, S., Yu, Z., Wang, Xiangke, 2018. Synthesis of rod-like metal-organic framework (MOF-5) nanomaterial for efficient removal of U (VI): batch experiments and spectroscopy study. Sci. Bull. 63, 831–839.

Xiao, J., Li, Z., Liu, B., Xia, Q., Yu, M., 2008. Adsorption of benzothiophene and dibenzothiophene on ion-impregnated activated carbons and ion-exchanged Y zeolites. Energy Fuels 22, 3858–3863.

Yang, J.-M., Liu, Q., Sun, W.-Y., 2014a. Shape and size control and gas adsorption of Ni (II)-doped MOF-5 nano/microcrystals. Microporous Mesoporous Mater. 190, 26–31.

Yang, J.-M., Liu, Q., Sun, W.-Y., 2014b. Co (II)-doped MOF-5 nano/microcrystals: Solvatochromic behaviour, sensing solvent molecules and gas sorption property. J. Solid State Chem. 218, 50–55.

Yuan, S., Feng, L., Wang, K., Pang, J., Bosch, M., Lollar, C., Sun, Y., Qin, J., Yang, X., Zhang, P., 2018. Stable metal–organic frameworks: design, synthesis, and applications. Adv. Mater. 30, 1704303.

Zahn, G., Schulze, H.A., Lippke, J., König, S., Sazama, U., Fröba, M., Behrens, P., 2015. A water-born Zr-based porous coordination polymer: Modulated synthesis of Zr-fumarate MOF. Microporous Mesoporous Mater. 203, 186–194.

Zhang, H.-X., Huang, H.-L., Li, C.-X., Meng, H., Lu, Y.-Z., Zhong, C.-L., Liu, D.-H., Yang, Q.-Y., 2012. Adsorption Behavior of Metal–Organic Frameworks for Thiophenic Sulphur from Diesel Oil. Ind. Eng. Chem. Res. 51, 12449–12455. https://doi.org/10.1021/ie3020395

Zhang, J., Liu, Y., Tian, S., Chai, Y., Liu, C., 2010. Reactive adsorption of thiophene on Ni/ZnO adsorbent: Effect of ZnO textural structure on the desulphurization activity. J. Nat. Gas Chem. 19, 327–332.

Zhao, Z., Li, Z., Lin, Y., 2009. Adsorption and diffusion of carbon dioxide on metal− organic framework (MOF-5). Ind. Eng. Chem. Res. 48, 10015–10020.

Zhen, W., Li, B., Lu, G., Ma, J., 2015. Enhancing catalytic activity and stability for CO_2 methanation on Ni@MOF-5 via control of active species dispersion. Chem. Commun. 51, 1728–1731. https://doi.org/10.1039/C4CC08733J

Zhu, L., Jia, X., Bian, H., Huo, T., Duan, Z., Xiang, Y., Xia, D., 2018. Structure and adsorptive desulphurization performance of the composite material MOF-5@ AC. New J. Chem. 42, 3840–3850.

Zuhra, Z., Mu, C., Tang, F., Zhou, Y., Zhang, L., Zhao, Z., Qin, L., 2019. Enhanced adsorptive desulphurization by iso-structural amino bearing IRMOF-3 and IRMOF-3@ Al 2 O 3 versus MOF-5 and MOF-5@ Al 2 O 3 revealing the predominant role of hydrogen bonding. Dalton Trans. 48, 14792–14800.

9. MODULATED SYNTHESIS OF NICKEL-BASED METAL-ORGANIC FRAMEWORK COMPOSITE FOR THE ADSORPTIVE DESULPHURIZATION OF LIQUID FUELS

This work was has been published in the Industrial & Engineering Chemistry, 206:60, 2021, 10997-11008, https://doi/abs/10.1021/acs.iecr.1c01082.

Summary

Removing sulphur from liquid fuels has become an important issue in a global society. Modulated synthesis has been known to improve the: crystallinity of materials; ease of handling; control of crystallite size; and degree of aggregation. A group of adsorbents (activated carbon (AC), a novel synthesized Ni-based metal-organic framework (Ni-BDC) and composites of AC@Ni-BDC treated with different concentrations of nitric acid and modulator (formic acid)) were characterized using XRD, HR-TEM, FT-IR, BET and TPD-pyridine. The adsorbents were also evaluated for adsorptive desulphurization. The quantities of both AC and the modulator were observed to influence: the nucleation of Ni-BDC; crystallite size; and crystallinity. The adsorption activity of the composite towards thiophene (TH) was the average of the two materials (i.e AC and Ni-BDC) while the activity doubled towards dibenzothiophene (DBT) and 4, 6-dimethyldibenzothiophene (4, 6 DMDBT) with respect to the excepted average. The improved activity was attributed to enhanced pore structure, crystallinity and synergistic effects that produced stronger acidic sites.

Keywords: MOF; nickel; desulphurization; formic acid; activated carbon; acid sites, modulation

9.1 Introduction

Human activity in the modern world is having a negative impact on the environment. During the operation of internal combustion engines, the sulphur in diesel and gasoline produces SO_x gases, which are precursors to acid rain and smog. The natural pH level of rain is 5, but acid rain has been measured to have pH levels below 3, which corresponds with that of vinegar (Wright and Institute of Marine Engineers, 2000). Therefore, legislation has been put in place in the fuel sector to limit the amount of sulphur in diesel and gasoline (Aribike et al., 2020). The sulphur compounds found in gasoline and diesel include sulphides, mercaptans, thiophenes (TH) and cyclic compounds (benzothiophene (BT), dibenzothiophene (DBT), 4-methyl dibenzothiophene (4-MDBT) and 4,6-dimethyl dibenzothiophene (4,6-DMDBT)), which must be treated as per stringent environmental regulations (Sarda et al., 2012).

Among the options available to do the treatment, adsorptive desulphurization is considered a potential solution to reducing the sulphur content in liquid fuels, due to the ease of operation at ambient conditions. Since adsorptive desulphurization is a surface phenomenon, the characteristics of a suitable adsorbent depend on several parameters, e.g. surface area, porosity, adsorbate-adsorbent bond and mechanical strength. Activated carbon (AC) has been used as an adsorbent, and it has been reported to offer: a porous structure with high surface area and high pore volume,(Yu et al., 2009; Al. Swat et al., 2017; Moreira et al., 2017) good mechanical strength (Sumathi et al., 2009) and moderate activity (Mguni et al., 2019). AC has been reported to have high selectivity for high molecular weight (MW) sulphur substances, such as DBT, 4-MDBT and 4,6-DMDBT (Al. Swat et al., 2017; Saleh et al., 2018). However, relatively low activity and poor selectivity towards low MW thiophenic compounds, has been identified as a challenge (Bu et al., 2011).

Efforts have been made to change functional groups on AC using loaded metals and acid/base/heat treatments (Fallah and Azizian, 2012; Olajire et al., 2017; Arcibar-Orozco et al., 2019a). AC adsorbents have shown limited potential for engineering structural changes, i.e. to improve the selectivity of light thiophenic compounds, such as TH and BT.

In contrast, metal-organic frameworks (MOFs) are a new class of porous adsorbents that offer more straightforward structural engineering and infinite structural possibilities (Greer et al., 2016; Abdelhameed et al., 2017; Kampouraki et al., 2019; Ullah et al., 2019). Ni has been reported to show promise for removing sulphur in systems such as NiSiAl and NiC, (Hernandez et al., 2010) Ni/Al_2O_3, (Sarda et al., 2012) and Ni/ACB (activated carbon beads) with/without carbon nanofibers (Prajapati and Verma, 2017). Cubic nickel-based MOF, Ni-BDC, has been reported for use in a few applications, such as water remediation (Ahsan et al., 2020) and high-performance supercapacitors (Gao et al., 2018). However, there is no information on adsorptive desulphurization of fuels using Ni-BDC (MOF).

Very few studies have been reported that used composites to remove sulphur compounds (Matloob et al., 2019). It has generally been reported that improvement in activity when composites are used is usually a result of the following: i) enhancement of the volume of the composites; (Zhao et al., 2018) ii) formation of an appropriate pore structure for the adsorption of a particular adsorbate;(Ahmed et al., 2013; Shi et al., 2017) and iii) synergistic effects on the edge sites of metal species (Dai et al., 2017; Liang et al., 2018; Crandall et al., 2019; Tan et al., 2018).

As stated, AC has shown good activity for removing high MW sulphur compounds (DBT, 4-MDBT and 4,6-DMDBT) (Al. Swat et al., 2017; Saleh et al., 2018), while MOFs are more suited to removing low MW sulphur compounds (BT and TH). Therefore, it would be interesting to synthesize a composite of AC and Ni-BDC for adsorptive desulphurization.

A Ni-based MOF was chosen due to the high affinity of Ni for sulphur compounds (Hernandez et al., 2010; Sarda et al., 2012).

Li et al., (2019) reported hydrothermal treatment of carbon nanospheres (CNPs) by DMF. CNPs treated by DMF showed relatively higher crystallinity and activity towards dye adsorption compared to CNPs. This was attributed to more active sites of oxygen-containing functional groups. The commonly used method of increasing acidic functional groups of AC is acid treatment. The proposed use of acidic groups is explained by the Lewis acid-base theory, as most thiophenic sulphur compounds are Lewis bases, which adsorb on acidic sites.

Another strategy that has been reported to alter the properties of adsorbents is modulated synthesizes. Modulated synthesis has been reported to: improve the crystallinity of materials; vary the crystal size and shape of MOFs; improve the ease of handling; decrease reaction time and the degree of aggregation (Wiβmann et al., 2012). To the best of our knowledge, the effect of nitric acid, DMF and modulated treatment on the sulphur removing performance of AC and Ni-BDC composites has not been reported to date.

With the aim of designing and developing highly efficient adsorptive desulphurization materials, new modulated composites of AC@Ni-BDC were synthesized and evaluated as composite adsorbents for adsorptive desulphurization. The effect of varying synthesis parameters (such as modulator quantity, nitric acid treatment and DMF treatment) on the adsorptive desulphurization performance of AC, Ni-BDC and the composite of AC and Ni-BDC were investigated. The synthesized composite was expected to show enhanced desulphurization activity with both low and high molecular organic sulphur compounds.

9.2 Experimental procedure

9.2.1 Materials

1,4-benzenedicarboxylic acid (H_2BDC) (98 %); N,N-dimethylformamide (DMF, 99.8 %); formic acid (85 %); chloroform (98 %); $CHCl_3$ and nickel (II) nitrate hexahydrate ($Ni(NO_3)_2{\cdot}6H_2O$) (97 %); hexadecane (98 %); TH (98 %); DBT (98 %); 4,6 DMDBT(98 %).

9.2.2 Ni-BDC synthesis

Ni-BDC was synthesized by dissolving $Ni(NO_3)_2{\cdot}6H_2O$ (1.78 g) and H_2BDC (0.33 g) in DMF (45 ml) and formic acid, for modulated synthesis. The mixture was hydrothermally treated at 130 ^oC for 8 h. The green product was vacuum-dried at 80 ^oC and then soaked in $CHCl_3$ for 3 days. The activation of the synthesized adsorbent was done at 120 ^oC in a vacuum oven overnight. It should be noted that the amount of modulator (formic acid) added was calculated based on the different mole ratios of formic acid to $Ni(NO_3)_2{\cdot}6H_2O$, see equation 9.1. For ease of understanding, examples of how synthesized materials are named are detailed in Table 9.1.

$$Neq = \frac{N_{HCOOH}}{N_{Ni(NO_3)_2.6H_2O}} \qquad (9.1)$$

Where N_{eq} represents the modulator equivalent amount, a ratio of the moles of formic acid to the moles of $Ni(NO_3)_2{\cdot}6H_2O$ (N_{eq} = 0, 5, 15, 25, 50, 75, 100). N_{HCOOH} represents the moles of formic acid and $N_{Ni(NO_3)_2.6H_2O}$ are the moles of $Ni(NO_3)_2{\cdot}6H_2O$ added.

Table 9.1: Specifications for typical materials synthesized in this work.

Name	Specification
Ni-BDC	Modulator (formic acid) was not added during the synthesis of Ni-BDC.
Ni-BDC 25eq	25eq presents the equivalent moles of the formic acid added to a mole of $Ni(NO_3)_2 \cdot 6H_2O$ (the mole of the formic acid added was 25 times higher than the mole of $Ni(NO_3)_2 \cdot 6H_2O$ used during the synthesis of Ni-BDC).
AC-65H	65H indicates that the concentration of the HNO_3 used to treat the AC was 65 %.
40%AC@Ni-BDC	There is 40 % AC in the AC@Ni-BDC composite and no modulator.
40%AC@Ni-BDC 25eq	There is 40 % AC in the AC@Ni-BDC composite and 25 equivalent moles of formic acid.
40%AC-65H@Ni-BDC 25eq	There is 40 % AC in the AC@Ni-BDC composite, the AC was acid-treated by 65 % HNO_3 and 25 equivalent moles of formic acid.

9.2.3 AC treated with nitric acid, DMF and formic acid

Nitric acid treatment

AC was treated with HNO_3 solutions of different concentrations. 5 g of AC was mixed with 80 ml of HNO_3 and refluxed at 90 ^oC for 3 h. The material was then washed with distilled water to remove all the acid and then dried overnight at 110 ^oC. The material produced in this way is referred to as AC-xxH, where: H represents HNO_3; xx represents the concentration of the HNO_3 used to treat the AC (xx=10 %, 30 %, 50 %, 65 %), e.g. AC-65H is an adsorbent produced by treating AC with 65 % HNO_3.

DMF treatment

DMF treatment was done to mimic the conditions that AC experiences when the AC@Ni-BDC composite is synthesized. Therefore, 1.2 g of AC was placed in 45 ml of DMF. The mixture was hydrothermally treated at 130 ^oC for 8 h. The product was then vacuum dried for 8 h at 80 ^oC. Similarly, with DMF treatment of nitric acid-treated AC, AC-xxH was treated as detailed above.

DMF and formic acid treatment

Similar to the DMF treatment, with the DMF and formic acid treatment, 1.2 g of AC was mixed with 45ml DMF and formic acid. The mixture was hydrothermally treated at 130 ^{o}C for 8 h and then vacuum dried overnight at 80 ^{o}C.

9.2.4 AC@Ni-BDC synthesis

A mixture of H_2BDC (0.33 g), $Ni(NO_3)_2 \cdot 6H_2O$ (1.78 g) and DMF (45mL) was mixed ultrasonically for 30 min. AC was then added to the mixture. To achieve different AC loading, the amount of AC added to the mixture was varied. The mixture was sonicated for 1 h. Thereafter, the mixture was hydrothermally treated using the method described above for Ni-BDC. For the modulated synthesis of AC@Ni-BDC, the modulator (formic acid) was added after the addition of AC. This mixture was then further sonicated, and the combination was then subjected to hydrothermal treatment.

9.2.5 Full factorial experimental design

The full factorial experimental design is a useful tool for studying the effect of the various process parameters. In the factorial design approach, the interdependency of process variables can be analysed with respect to targeted responses (Araujo and Brereton, 1996). In this study, a full factorial experimental design was used to identify the individual and interactive effects of the modulator and AC loading on: the AC@Ni-BDC composite; and the modulator and AC treated with different levels of acid concentration. The levels used with each factor are detailed in Table C1.

9.2.6 Characterisation of adsorbent

In order to determine the functional groups in the catalyst samples, Fourier-transform infrared spectroscopy (FTIR) spectra were recorded using a Bruker Tensor 27 ATR in the range of 4000–400 cm^{-1}. BET analysis was performed to determine the surface area and pore size distribution by N_2 adsorption, at a temperature of 77 K, using a Micromeritics ASAP 2000.

Temperature-programmed desorption (TPD) experiments were conducted on a Micromeritics AutoChemII Chemisorption Analyzer. 200 mg of adsorbent sample was pre-treated at 250 ℃ under He for 12 h. After cooling to room temperature in a He atmosphere, the gas was switched to TH vapour with He. After physically adsorbed TH was purged by He flow at room temperature, the sample was heated to 350 °C at 10 ^{o}C/min, and the liberated TH was monitored continuously by means of a CIRRUS quadrupole mass spectrometer.

The structure of the catalyst system was analysed using a Rigaku Ultima IV X-ray diffractometer (XRD), with CuKα (λ=1.54) radiation. Samples were scanned over a 2θ range of 3–90° with a 0.01° step size and a scan speed of 0.02 s/ step. The mean crystallite size of the adsorbent samples was estimated from the full width at half maxima of the diffraction peak using the Scherrer equation and using a shape factor of 0.9. In this work, the crystallinity of synthesized MOF was obtained using the TOPAS single line fitting method (Bruker Axs, Inc., 2005). The morphology of the adsorbents was studied using a Joel 2100 High-Resolution Transmission Electron Microscope (HR TEM) at 200 kV. The samples were prepared for TEM by suspending the adsorbent in ethanol and then dispersing the suspension on a copper slide.

9.2.7 Adsorption experiments

The model diesel used for the adsorption experiments was synthesized using hexadecane and three sulphur compounds, TH, DBT and 4,6 DMDBT, at 150 ppm, 153 ppm and 151 ppm, respectively. The adsorption experiments were carried out using a stirred basket reactor. The stirrer was set at a high stirring rate of 1300 rpm to minimize the mass transfer restriction. 200 mg of adsorbent was added to 10 ml of model diesel, and the adsorption process was carried out at room temperature of 25 ℃ for 180 min/run (excluding the runs for adsorptive desulphurization using AC and Ni-BDC which were held for 120 min/run).

9.2.8 Analysis

The model diesel was analysed before and after the adsorption process using 7890B Agilent Gas Chromatograph (GC) with two detectors: a Flame Ionization Detector (FID) and a Pulsed Flame Photometric Detector (PFPD). The quantification of sulphur was done as described in our previous work (Mguni et al., 2019). The relative error for analysis of the sulphur compounds was less than 6 %.

9.3 Results and discussion

9.3.1 Characterization of materials

The HR TEM characterization results for the Ni-BDC and the composites of AC and Ni-BDC are shown in Figure 9.1. The explanation of how the prepared materials were named is shown in Table 9.1. The synthesized Ni-BDC was observed to be highly photosensitive, and the material was observed to shrink and sometimes change shape when exposed to the electron beam. The unsupported Ni-BDC had a trigonal shape. Ni-BDC was evenly dispersed on AC for 40%AC@Ni-BDC 25eq. The d-spacing of Ni-BDC was d=0.2941 nm and d= 0.3540 nm (see Figure 9.1(c)). When the amount of formic acid was increased to 75, and 100 eq, no difference was observed in the morphology of AC@Ni-BDC. Figure 9.1(d) shows that nickel and copper were the elements observed, and nickel was evenly distributed on AC. The copper observed was from the HR TEM copper slide.

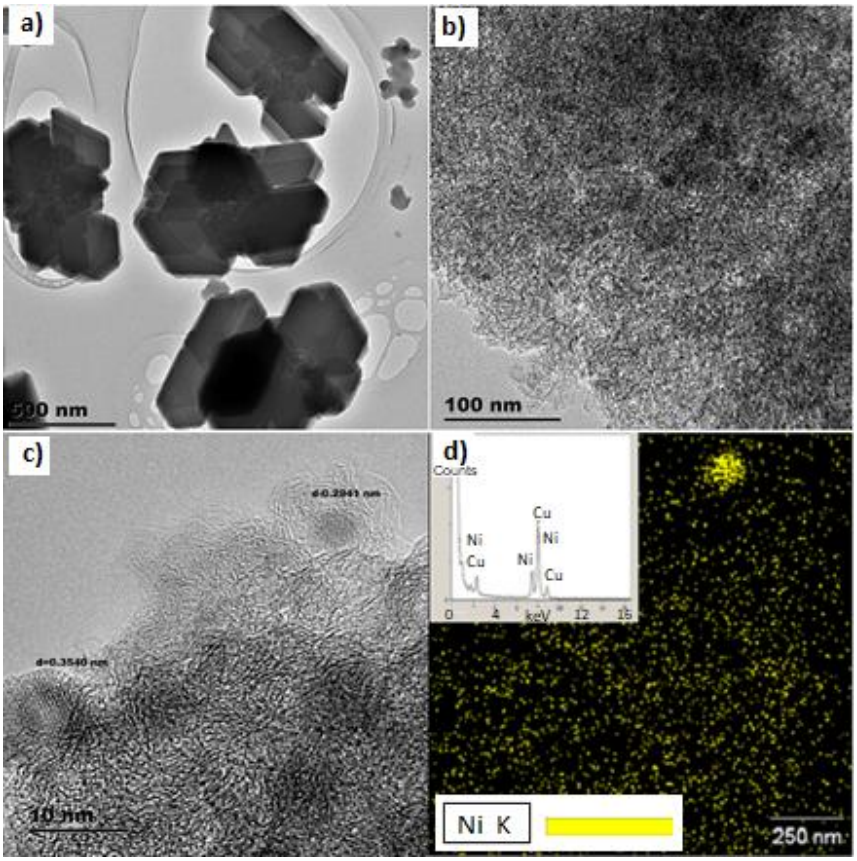

Figure 9.1: HR TEM images: a) Ni-BDC 25 eq; b) 40%AC@Ni-BDC 0 eq; c) 40%AC@Ni-BDC 25 eq; d) EDX and element mapping for 40%AC@Ni-BDC 25 eq.

The XRD patterns for the adsorbents synthesized were plotted - see Figure 9.2 and Figure C1. Figure 9.2 (a) shows that an amorphous phase is obtained without the addition of the formic acid (0 eq); by the addition of a small amount of the modulator (5 eq), the material starts to change from an amorphous phase to a crystalline phase. The peaks attributed to the Ni-BDC were observed when more than 15 equivalent formic acid was used for adsorbent preparation. The XRD pattern of Ni-MOF was similar to the pattern reported by Ahsan et al., (2020) and Gao et al., (2018)

In Figure 9.2 (b-c), at 0 eq and 5 eq formic acid, the pattern observed was for the pure activated carbon; this is because of poor crystallinity of Ni-BDC with small amounts of formic acid. The two peaks observed at 2θ = 25.9° and 45° were attributed to d_{002} and d_{100} reflections. These diffraction peaks are evidence that the samples have a turbostratic structure. This turbostratic model assumes that the sample is made of graphite-like microcrystallites that are bound by the cross-linking network, which consists of several graphite-like layers stacked nearly parallel and equidistant, with each layer having a random orientation (Hashemian et al., 2013). The peak at 9.8˚ was observed to split into two in this work (see Figure C1), for the MOF-5 system the splitting has been reported to be due to distortion of the MOF-5 cubic structure into a trigonal symmetry pattern (Tirmizi et al., 2018; Burgaz et al., 2019).

The phase of the synthesized materials changed from an amorphous to a crystalline phase with the increasing quantity of modulator. The increased intensity of these peaks (attributed to Ni-BDC) seen with an increase in the amount of formic acid used suggests that formic acid enhances the synthesis process and improves the crystallinity of the adsorbent. It has been suggested that the acceleration in the formation of the MOF may be because formic acid is a direct product of the decomposition of the solvent DMF with water; furthermore, it has been reported that the modulators enhance the deprotonation of linker molecules, thereby accelerating the formation of the MOF (Wiβmann et al., 2012; Zahn et al., 2014). The crystallinity was observed to increase

up to 75 eq. A drop in peak intensity at 100 eq was attributed to the dilution effect. This is consistent with results observed in the absence of AC. A comparison of Figure 9.2(b) and Figure 9.2(c) indicates that treating AC using nitric acid did not affect the phases present. Finally, the introduction of the support did not change the XRD pattern of Ni-BDC, which suggests that the addition of AC did not prevent the formation of the Ni-BDC crystalline phase.

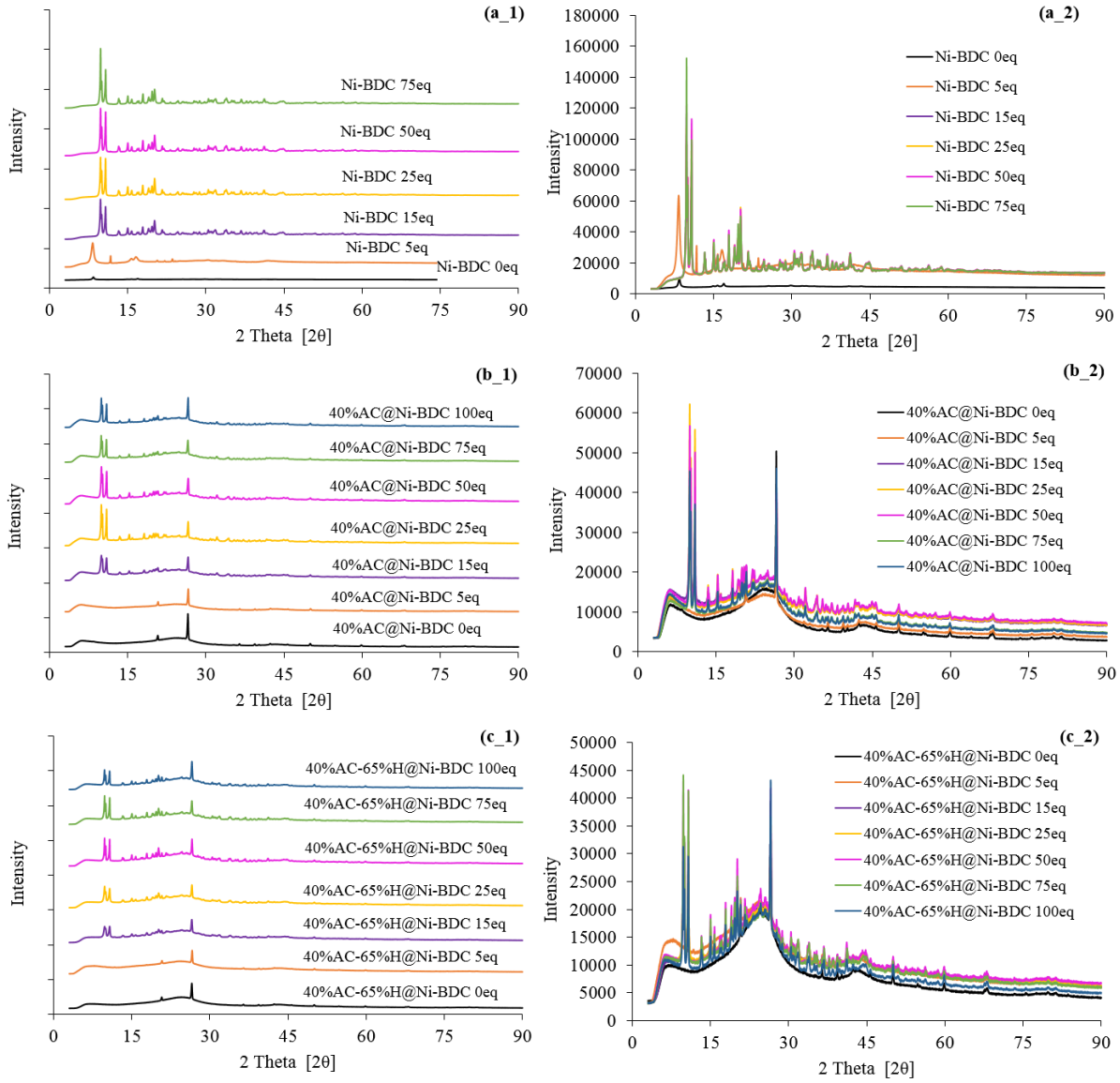

Figure 9.2: XRD spectrum for: a) Ni-BDC b) 40% AC@Ni-BDC composite; c) 40% AC-65H@ Ni-BDC composite.

Table 9.2 provides the corresponding N_2 adsorption-desorption data. The BET surface area of the composites was observed to increase with an increase in AC percentage in the composite (see Table 9.2). The low surface area at high MOF loading is attributed to pore blocking of AC by Ni-BDC, as observed by a drop in pure AC pore size from 31.67 to about 26-27 Å, in the presence of the MOF (Zhu et al., 2018). An increase in the quantity of the modulator was observed to lead to a decrease in the surface area of the composite. This is due to a change in the nature of synthesized Ni-BDC. A change in the acidity of AC was observed to cause no significant change in the surface area of the adsorbent.

Table 9.2: BET surface area and average pore diameter of composites.

Adsorbent	Surface area (m^2/g)	BJH adsorption average pore diameter (Å)
AC	845.0	31.67
AC-65H	829.1	25.65
AC-65H DMF	742.4	26.21
Ni-BDC 25eq	241.9	7.66
20%AC@Ni-BDC 25 eq	501.5	26.84
40%AC@Ni-BDC 25eq	738.5	27.31
60%AC@Ni-BDC 25eq	773.7	26.87
80%AC@Ni-BDC 25eq	781.1	26.48
40%AC@Ni-BDC 5eq	760.6	27.24
40%AC@Ni-BDC 15eq	739.2	29.40
40%AC@Ni-BDC 50eq	738.5	26.95
40%AC@Ni-BDC 75eq	719.3	26.95
40%AC@Ni-BDC 100eq	669.4	26.94
40%AC-10H@ Ni-BDC 50eq	660.0	26.64
40%AC-30H@ Ni-BDC 50eq	656.0	26.06
40%AC-50H@ Ni-BDC 50eq	694.3	27.84
40%AC-65H@ Ni-BDC 50eq	668.5	25.34

The effect of the formic acid modulator on the crystallite size of Ni-BDC with different amounts of AC loading is listed in Table 9.3. The crystallite size of Ni-BDC was observed to increase with an increase in the modulator amount, in the absence of AC. The increase in crystallite size is due to the competition between the deprotonated linker molecules and formate, which reduces the number of nuclei - hence fewer nuclei grow to larger crystals (Yuan et al., 2018). A drop in crystallite size was observed at 100 eq, which may be due to the dilution of reagents caused by

excess formic acid. Burgaz et al., (2019) reported that dilution affected MOF-5 synthesis, even though the metal/ligand (Zn/BDC) molar ratio remained the same. The introduction of AC (20 % and 40 %) reduced the crystallite size of the adsorbent at a low AC quantity. The decrease in crystallite size was attributed to the introduction of many nucleation sites, hence more nucleation sites grow into small crystals (Yuan et al., 2018). A further increase in AC (60, 80 %) leads to an increase in crystallite size, but the cause of this phenomenon is unknown.

Table 9.3: Effect of the formic acid modulator on the crystallite size and crystallinity for x % AC@Ni-BDC

Modulator Equivalent	**Crystallite size (nm) x% AC@Ni-BDC**				
	x=0	**x=20**	**x=40**	**x=60**	**x=80**
15	46.52	24.47	25.56	45.36	50.88
25	56.06	51.93	51.28	55.75	58.64
50	57.82	53.08	49.43	59.08	50.30
75	65.44	50.06	57.52	50.48	54.37
100	53.44	49.65	62.22	63.42	48.67

The FT-IR spectra of Ni-BDC (Figure 9.3) had the expected strong adsorption characteristics for the vibrations of BDC (1599.16 cm^{-1} and 1392.32 cm^{-1}) and a broad-band originating at around 3435 cm^{-1} from adsorbed water. As expected, the FTIR spectrum of the composite is a combination of Ni-BDC and AC; however, a slight shift in the bands - to lower values - was observed at 1600 and 1400 cm^{-1} (see Figure 9.3(b)). This shift may be due to part of the carboxyl group forming an ester bond with hydroxyl on the AC surface, thus verifying the formation of the AC@Ni-BDC composite (Zhu et al., 2018). The shift in bands for 65 % nitric acid-treated carbon was more pronounced, suggesting a stronger Ni-BDC and AC-65H bond.

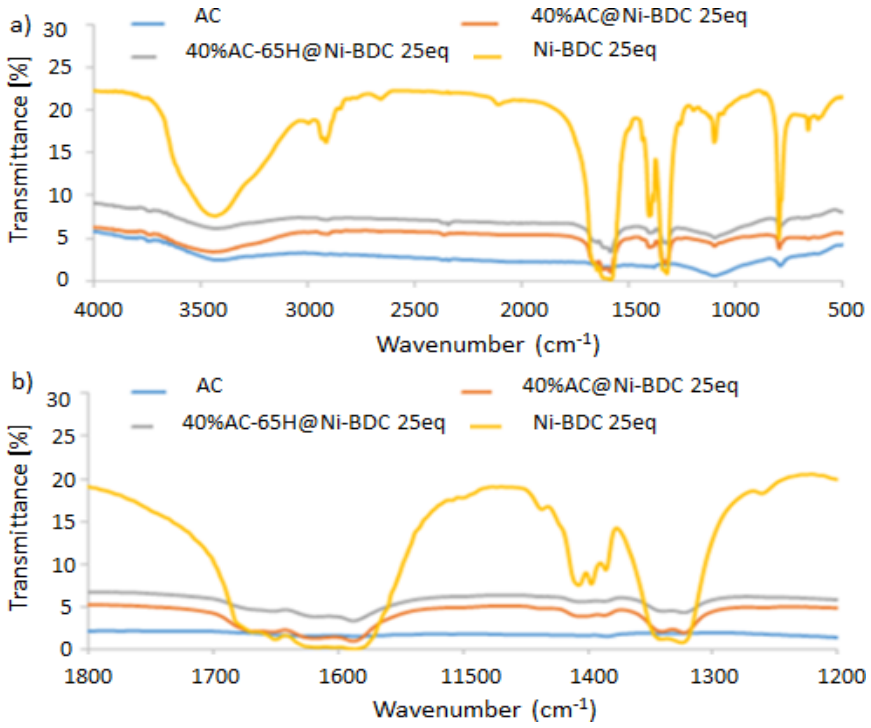

Figure 9.3: FTIR spectra of: a) AC, as-synthesized 40%AC@Ni-BDC, 40%AC-65H@ Ni-BDC 25 eq, and Ni-BDC samples; b) enlarged view

The TPD patterns for pyridine adsorption are depicted in Figure 9.4. The results from Figure 9.4 show the effect of acid treatment, DMF treatment and composite formation on acidic sites of the adsorbents. Ni-BDC 25 eq had the least amount of acid sites. The number of strong acid sites was observed to increase in the order: Ni-BDC 25 eq << AC <AC-65H < AC-65H/DMF < 40%AC@Ni-BDC 25 eq < 40%AC-65@ Ni-BDC 25 eq. The composites produced by Ni-BDC and AC / AC-65 had a synergistic effect, which produced stronger acidic sites.

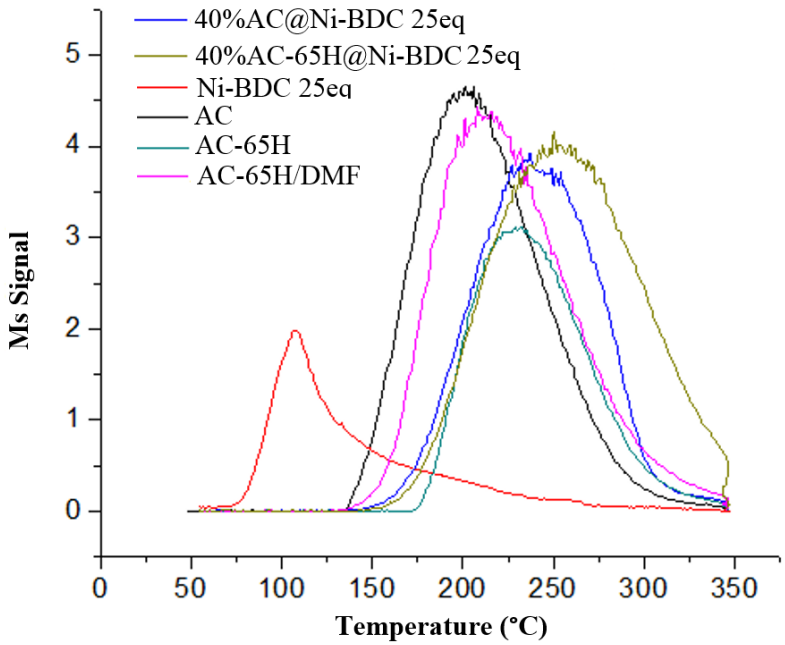

Figure 9.4: Adsorption activity of AC and Ni-BDC a) adsorption capacity at 120 min; b) TH adsorption with time on stream; c) DBT adsorption with time on stream; d) 4,6DMDBT adsorption with time on stream at 25 ^{o}C, 2.5 wt% adsorbent and 1300 rpm stirring speed

9.3.2 Adsorptive desulphurization

Sulphur removal capacity for AC and Ni-BDC

The adsorption activities of AC and Ni-BDC with time on stream are shown in Figure 9.5. The major activity for Ni-BDC was observed to take place within the first 15 min. This high activity within the first 15 min suggests that Ni-BDC has a higher affinity for organic sulphur compounds than AC. The adsorption activity order for Ni-BDC was observed to follow the order TH >> 4, 6 DMDBT > DBT. The adsorption order for this adsorbent is due to pore size that only allows TH access to the internal surface, while the higher activity of 4, 6 DMDBT relative to DBT might be determined by the electron density of the molecules. The overall poor activity of Ni-BDC may be related to poor crystallinity as suggested by Liu et al., (2007) when working with mesoporous Al-MCM-41 materials. The adsorption activity of AC followed the order 4,6DMDBT >> DBT > TH, due to the electron density of the compounds, as suggested by a number of researchers (Fallah et al., 2014).

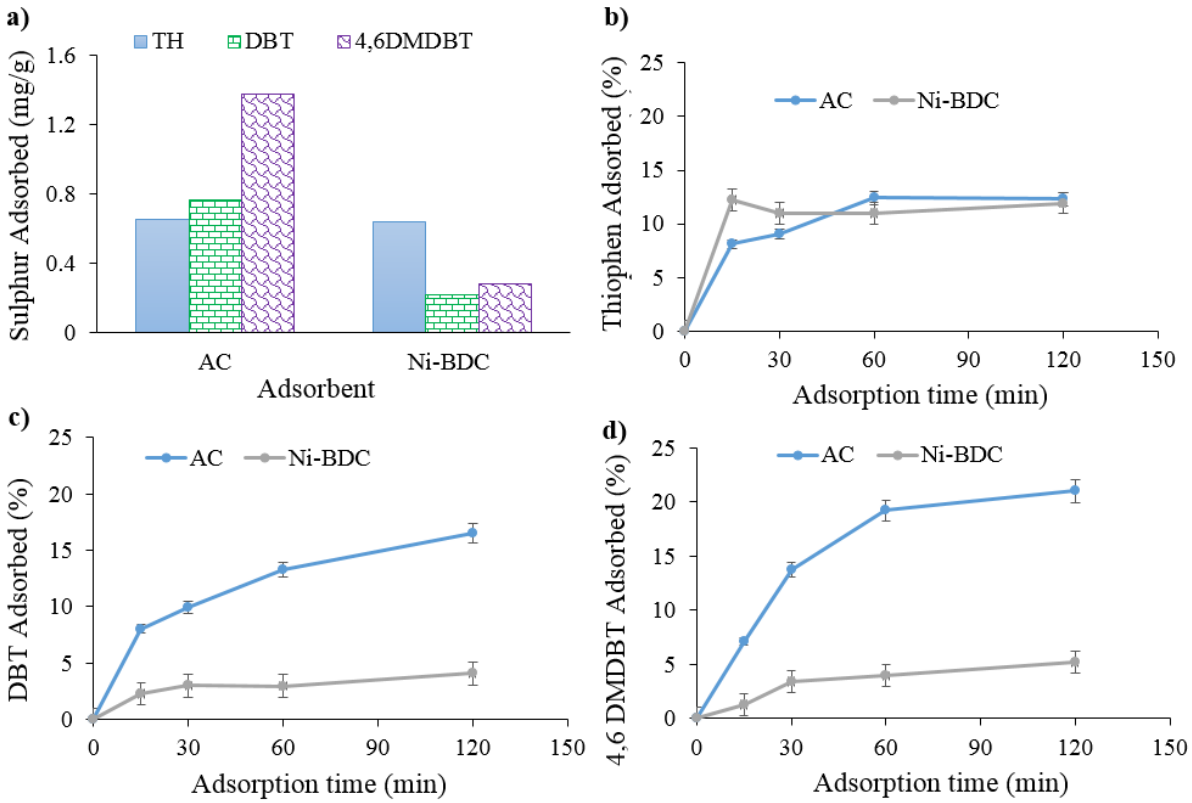

Figure 9.5: Adsorption activity of AC and Ni-BDC a) adsorption capacity at 120 min; b) TH adsorption with time on stream; c) DBT adsorption with time on stream; d) 4,6 DMDBT adsorption with time on stream at 25 ^{o}C, 2.5 wt% adsorbent and 1300 rpm stirring speed

Effect of AC quantity on sulphur removal activity by AC@Ni-BDC

The effect of AC content on the sulphur removing capacity of AC@Ni-BDC was studied, using different quantities of formic acid (see Figure C2). As shown in Figure 9.6, adsorption was carried out at 0 eq and 25 eq, and 25 eq had the highest activity. At 0 eq, the activity of DBT and 4,6 DMDBT was observed to increase with an increase in the percentage of AC. This is consistent with the poor activity of Ni-BDC with these compounds - see Figure 9.5. A slight increase in TH activity was observed up to 40**%**AC@Ni-BDC, which can only be attributed to synergetic interaction between the two materials, Ni-BDC and AC, since they had similar activity. The activity dropped as it approached the lowest value at 100 **%** AC.

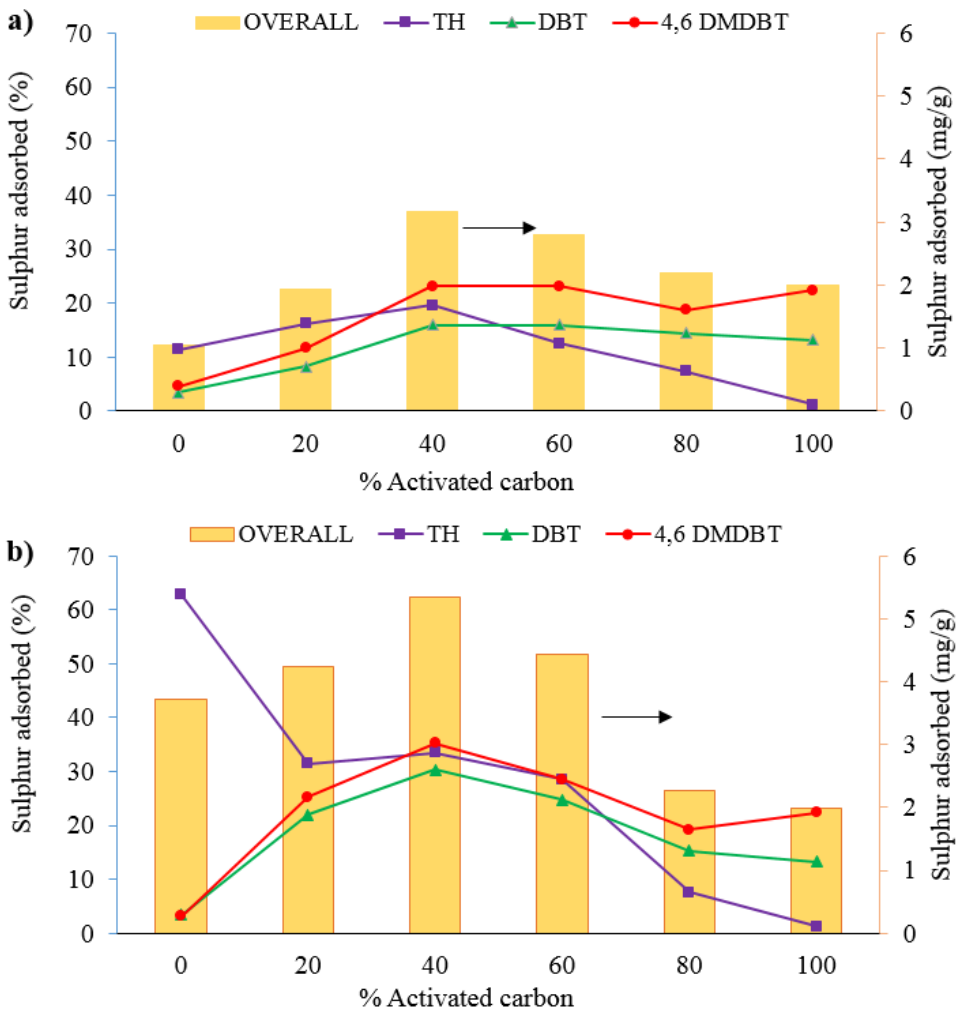

Figure 9.6: Effect of the amount of AC on the adsorption performance of a) *x*%AC@Ni-BDC 0 eq composite b) *x*%AC@Ni-BDC 25 eq composite. Operating condition: dosage – 200 mg/10 ml; stirring speed - 1300 rpm; temperature – 25 ^{o}C.

The activity of Ni-BDC treated with 25 eq was higher than the activity at 0 eq. The improvement in activity may be attributed to improvement in adsorbent crystallinity, which is discussed in detail later. For x%AC@Ni-BDC 25 eq composite, TH adsorption activity was observed to decrease with an increase in AC content. The high activity of Ni-BDC without AC for TH adsorption may be attributed to the adsorbent affinity and the pore size of the Ni-BDC MOF being comparable to the kinetic diameter of TH (Li et al., 2015). The decrease in adsorption activity of TH seen with an increase in AC was expected, as low adsorption activity towards TH was observed when using pure AC. The poor activity of pure AC in terms of TH may be attributed to the pore structure and surface chemistry of this adsorbent.

However, the adsorption activity for DBT and 4,6 DMDBT was observed to increase with AC loading on the composite up to 40 wt%; thereafter, activity dropped. The initial increase in activity with an increase in the amount of AC was attributed to the improvement of the pore structure of the composite compared to Ni-BDC (see Table 9.2). The decrease in activity after 40 wt% of AC is due to the decreased amount of Ni-BDC, which has a better affinity for sulphur compounds relative to the AC surface.

The mean plot of the effects was used to study the differences between the mean of each parameter at different levels. As shown in Figure C3, the lines that connect the mean for each variable level are not horizontal; therefore, the main effects are present with all variables. It is clear from Figure C3 that an increase in the quantity of AC has a significant negative effect on TH adsorption, as discussed earlier. However, with DBT and 4,6 DMDBT, the activity was observed to increase up to 40 wt% AC; thereafter, it decreased, as per the earlier discussion regarding AC@Ni-BDC 25eq. This is consistent with the Pareto analysis results (see Figure C4).

Formic acid treatment of 40%AC@Ni-BDC

The modulator effect was observed to be consistent for all the sulphur compounds, i.e. activity improved with an increase in the formic acid quantity up to 25/50 equivalent amounts (see Figure 9.7). This increase in activity was attributed to the improved crystallinity of the adsorbent (see Figure 9.2). The drop in activity was attributed to the dilution effect, which affects the formation of Ni-BDC, and a decrease in the surface area seen with an increase in equivalent amounts of formic acid for the composites (see Table 9.2). From the mean plot (Figure C3), it is clear that an increase in the quantity of formic acid led to an increase in activity up to 25/50 eq, as discussed earlier. This is in line with the Pareto analysis, where 25 eq and 50 eq had the highest contribution to adsorption activity.

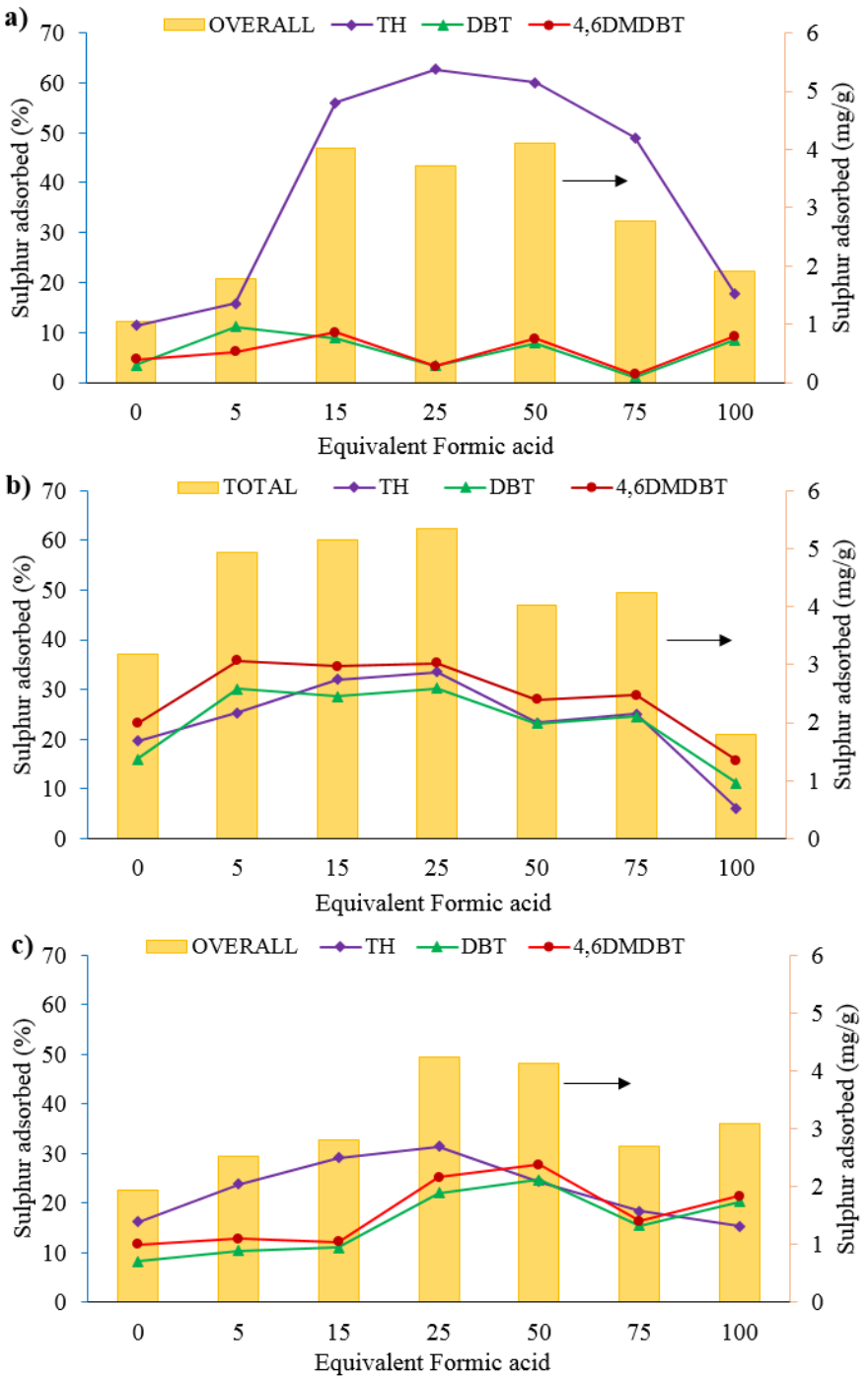

Figure 9.7: Effect of the amount of formic acid modulator on the adsorption performance of a) Ni-BDC xeq composite b) 40%AC@Ni-BDC xeq composite c) 80%AC@Ni-BDC xeq composite. Operating condition: dosage – 200 mg/10 ml; stirring speed - 1300 rpm; temperature – 25 ^{o}C. (xeq represents x equivalent formic acid used: the mole of formic acid added was x times higher than the mole of $Ni(NO_3)_2 \cdot 6H_2O$ used during the synthesis of Ni-BDC.)

9.3.3 Kinetic studies

The transition from the MOF and AC materials to the composite material was analysed using adsorption kinetics. The kinetic data analysis was done using pseudo-first, second-order kinetic and intraparticle diffusion models. The pseudo-first-order kinetic and second-order kinetic models are given in section 5.3.2.

The intraparticle diffusion model is given below by:

$$q_t = K_{id} t^{1/2} + C \qquad (9.2)$$

Where: K_{id} and C are the intraparticle diffusion rate constant and the intercept, respectively; C represents the thickness of the boundary layer, i.e. the greater the C value, the larger the effect of the boundary layer will be. If the plot of qt vs $t^{0.5}$ is linear, it implies that the adsorption process is only controlled by intra-particle diffusion.

Adsorption by Ni-BDC was observed to follow second-order kinetics, while AC adsorption followed first-order kinetics (see Table C2). This suggests that the adsorption activity seen when using Ni-BDC is dominated by chemical adsorption, while it is physical in nature with AC. The initial adsorption rate (h) for Ni-BDC was observed to decrease with molecular weight. This was attributed to the small pore size, which restricted the adsorption of bigger molecules, as stated earlier. The adsorption activity of AC improved with an increase in the MW of the sulphur compounds, which suggests that physical adsorption improves with an increase in the electron density of sulphur compounds.

Composite adsorption kinetics followed the second-order kinetics, which suggests that chemical adsorption dominated the process. This chemical adsorption domination was facilitated by the Ni-BDC surface. The initial adsorption rate for DBT and 4,6 DMDBT was observed to improve for the composite and this was attributed to the high affinity of Ni-BDC and appropriate pore structure for these molecules. A multi-linear plot was observed, it can be separated into two largely linear regions, see Figure C5. This indicates that intra-particle diffusion was not the rate-

controlling step for the overall adsorption process. The first region might be assigned to film diffusion corresponding to the transportation of sulphur compounds to the external surfaces of the adsorbent. The second region includes the gradual adsorption and equilibrium stages (Hu et al., 2017).

Nitric acid, DMF, and both DMF and formic acid treatment to AC

Figure 9.8 is a plot of the desulphurization activity of: AC; AC treated by DMF; AC treated by DMF; formic acid. Treating AC with DMF (0 eq) was observed to lead to a slight decrease in the adsorption of TH. TH was initially adsorbed quickly, and after 60 min TH was desorbed as more DBT and 4,6 DMDBT were adsorbed. This desorption of TH, while DBT and 4,6 DMDBT are adsorbed, suggests that the DMF-treated AC has a poor affinity for TH adsorption. This phenomenon is known as roll-up or rollover for dynamic adsorption and is caused by the displacement of a weaker adsorbate by a stronger one (Kim et al., 2006; Roy and Moharir, 2019). The addition of formic acid had no significant effect on the activity of the adsorbent. It was also observed that changing the quantity of formic acid that was added to the AC did not affect the activity of the adsorbent. This suggests that the weak acid (formic acid) did not change the surface properties of the AC.

In addition, although the adsorption activities for the removal of DBT and 4, 6 DMDBT did not change much after 120 min time on stream (Figure 9.8). The adsorption activity for TH increased, reached a maximum and then decreased with time on stream. These results indicate that the experimental conditions, such as adsorption time, are important factors for desulphurization. More research on the optimisation of the adsorption parameters is needed and in particular, the effect of kinetics, thermodynamics and adsorptive equilibrium isotherm on the process should be considered.

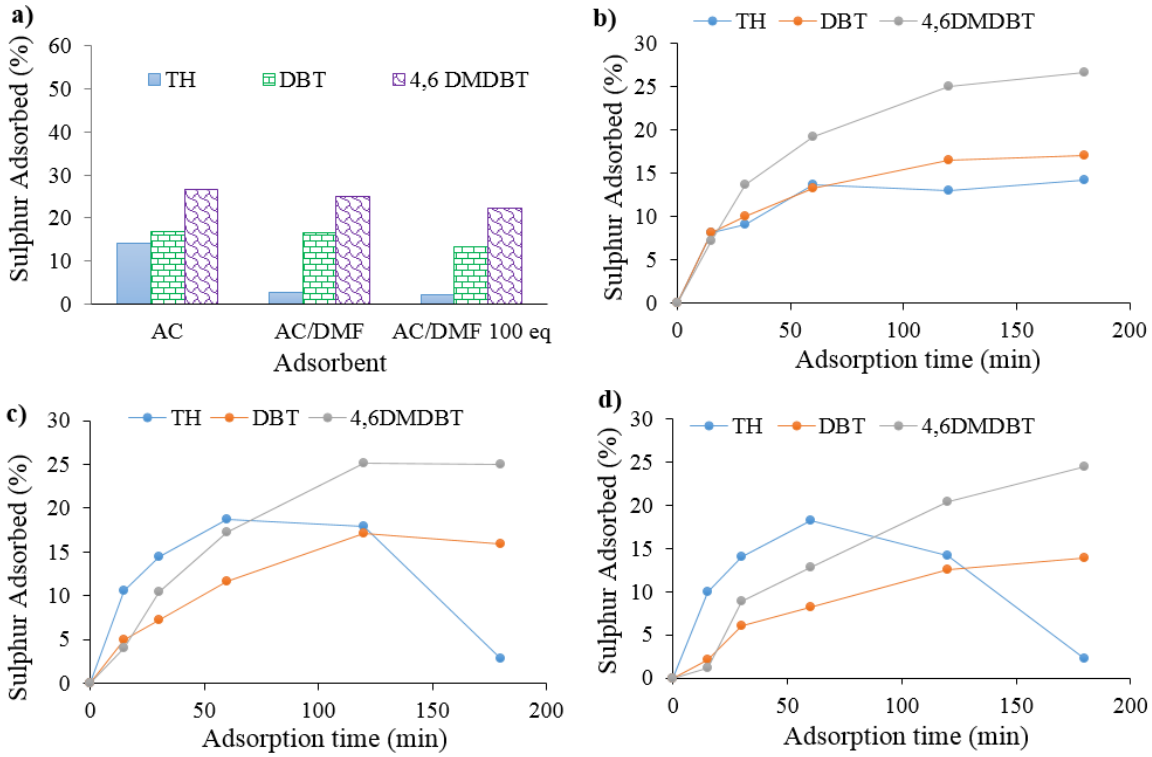

Figure 9.8: Sulphur adsorbed: a) overall; b) AC; c) DMF treated AC; d) DMF and 100 eq formic acid-treated AC. Operating condition: dosage - 200 mg/10 ml; stirring speed - 1300 rpm; temperature – 25 ^{o}C.

In this section, the activity of AC treated with nitric acid and then DMF or formic acid was investigated. The results of the experiment are plotted in Figure 9.9. The activity of AC was observed to increase with an increase in the concentration of nitric acid used to treat the activated carbon.

This increase in activity is consistent with previous work reported, (Yu et al., 2008; Saleh and Danmaliki, 2016) and it has been attributed to an increase in the number of acid sites. Furthermore, the TPD of pyridine results suggest that the increase in activity is due to an increase in the number of stronger acid sites, and not just an increase in the acid sites (see Figure 9.4). Hydrothermal treatment of activated carbon with DMF was observed to lead to an overall increase in activity for acid-treated activated carbon (see Figure 9.9(b)). Treatment by formic acid caused no significant activity change, as stated earlier. The increase in the activity of acid-treated adsorbent when treated by DMF for DBT and 4,6 DMDBT was attributed to the ability

of DMF to further increase the number of strong acid sites, and the potential change in the surface charge, as suggested by Li et al., (2019) when investigating metal ions adsorption (see Figure 9.4). The adsorption order increased with an increase in the π electron density of the sulphur compounds, which suggests that the interaction may include π–π stacking or that π-H interactions may play an important role in adsorption, as reported by a number of researchers who used activated carbon (Kim et al., 2006; Xiao et al., 2012; Wang et al., 2020).

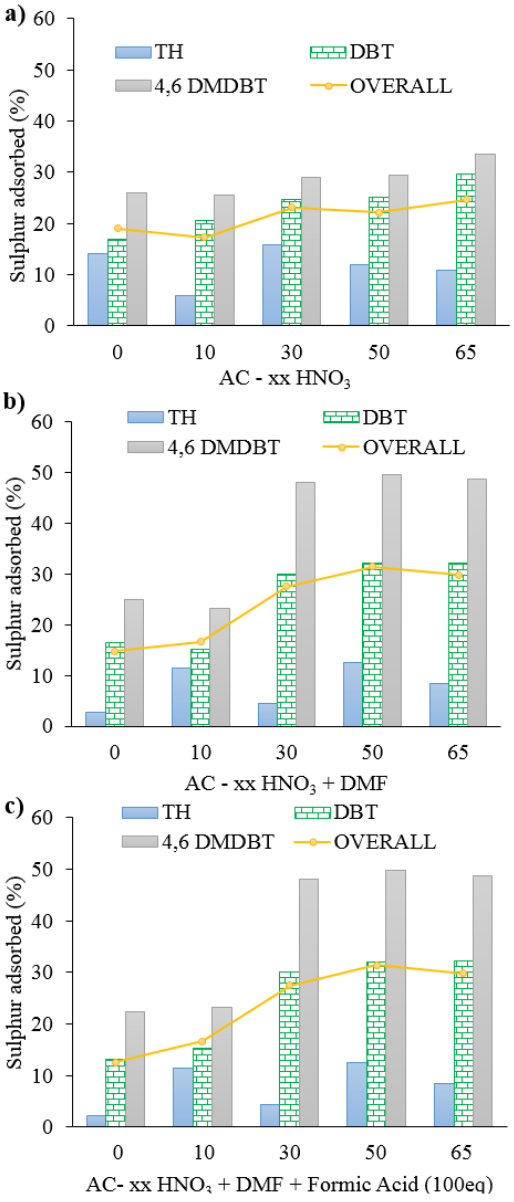

Figure 9.9: Effect of nitric acid treatment on the adsorptive performance of (a) AC; (b) AC treated with DMF; (c) AC treated with both DMF and 100 eq formic acid. Operating condition: dosage – 200 mg/10 ml; stirring speed - 1300 rpm; temperature – 25 ^{o}C.

The optimum 40 wt% AC for AC@Ni-BDC composite, was used to investigate the effect of the two parameters, AC-acidity and modulator quantities-formic acid, using a 2-factor design (see Table C1). AC not treated with nitric acid showed the highest activity (see Figure 9.10.). This high activity of 40%AC@Ni-BDC was attributed to optimum Ni-BDC loading on AC, which suggests that a change in the acidity of the AC leads to a change in the interaction between the AC and Ni-BDC - hence a change in optimum loading. This is consistent with the results obtained for FTIR (Figure 9.3), which showed a more pronounced shift in the bands for 65 % nitric acid-treated carbon, which suggests a stronger Ni-BDC and AC-65H bond. These results also suggest that the best approach for this analysis might be a 3-factor analysis, i.e. for the 3 parameters AC loading, acidity and modulation amount. Another useful finding of this work is that formic acid-treated adsorbents generally had slightly higher activity.

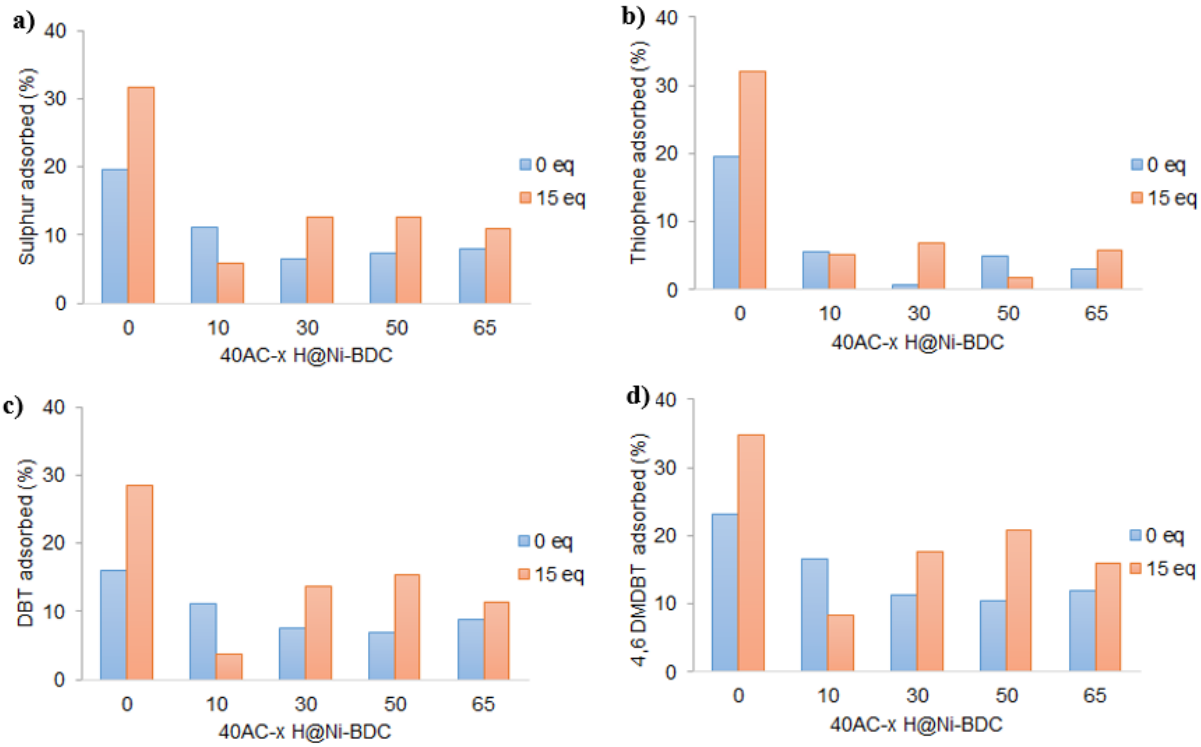

Figure 9.10: Effect of the pre-treatment of AC by different concentration of nitric acid on the adsorptive performance of the composite of 40%AC-yH@Ni-BDC (0 or 15 eq) (concentration of nitric acid y=0 %, 10 %, 30 %, 50 %, 65 %): (a) overall; (b) thiophene; (c) DBT and (d) DMDBT. Operating condition: dosage – 200 mg/10 ml; stirring speed - 1300 rpm; temperature – 25 ^{o}C.

An R-squared regression analysis was carried out for activity versus crystallite size and crystallinity of the synthesized adsorbate (see Table C3 and Table C4). With the two-factorial design of modulator and AC loading on the AC@Ni-BDC composite, it was observed that: for unsupported Ni-BDC, TH adsorption activity depended on crystallinity; for DBT and 4,6 DMDBT, it is dependent on crystallite size. The dependence of TH on crystallinity could be because increased crystallinity leads to an increase in Ni crystallites and low coordination sites, which would be essential since TH can penetrate the Ni-BDC structure. However, DBT and 4,6 DMDBT depend on the crystallite size, since their adsorption is a surface phenomenon - hence a larger crystallite size translates into a smaller external surface area. For x%AC@Ni-BDC, only 40%AC@Ni-BDC showed dependence on crystallinity only (see Table C3 and C2). This suggests that when AC is not at the optimum quantity, another parameter determines the adsorption rate, i.e. not the crystallinity. For all acid-treated activated carbon composites, no correlation was observed with both crystallinity and crystallite size.

As discussed earlier, AC showed higher activity towards larger sulphur compounds, with the adsorption activity following the order: TH <DBT<4,6 DMDBT. It has been reported that adsorption in activated carbons can occur via various mechanisms, including π-π interactions between aromatic rings and acidic-base interactions.(Arcibar-Orozco et al., 2019b) These suggested mechanisms are consistent with the observed increase in adsorption activity with increasing MW of the sulphur compounds – and hence an increase in electron density and basicity.

The adsorption activity of the most active pure nickel-based adsorbent, Ni-BDC 25eq, followed the order: DBT <4,6 DMDBT << TH. The high activity towards TH was attributed to pore structure. The higher activity of Ni-BDC 25eq for 4,6 DMDBT compared to that of DBT was attributed to π-π interactions between aromatic rings and acidic-base interactions with the adsorbent, similar to that observed for AC.

The adsorption order for the composite 40%AC@Ni-BDC 25 eq was: DBT < TH <4,6 DMDBT. This is the same order that would be excepted for the average of two compounds. However, the values of adsorption capacity are higher than the expected averages. This could be as a result of synergistic effects that produced stronger acidic sites. The adsorption capacity of TH was approximately the average of the two materials; this suggests that newly-formed strong acid sites did not affect the adsorption of TH, which is in line with the very weak basic nature of TH in comparison to the other two sulphur compounds (Fallah et al., 2014).

The partition coefficient (PC) is an ideal parameter for comparing the adsorption activity of different adsorbents because it takes into account the effect of the initial adsorbate concentration (Al-Wabel et al., 2019; Vikrant and Kim, 2019). A comparison with MOF-5 based composites was done, based on PC and adsorption capacity - Table C5. The composite in this work based on AC and Ni-BDC 25 eq showed higher activity compared to a composite of MOF-5 and hollow mesoporous silica spheres (HMSS), and a slightly higher PC value compared to MOF-5@AC for an adsorbate with a similar initial total sulphur concentration. The differences might be due to the different central metal and modulated synthesis adopted in this work, which was observed to affect the crystallinity of the composites.

9.4 Conclusions

The aim of this work was to develop novel materials to enhance desulphurization activity for both low and high molecular organic sulphur compounds. The composites of AC@Ni-BDC were successfully synthesized. The TH-removing capacity of AC@Ni-BDC composite was much higher than when using AC as the adsorbent which remedies the disadvantage of AC, i.e. poor adsorptive selectivity of TH. Although the TH-removing activity of AC@Ni-BDC was lower than when using Ni-BDC, the composites exhibited significant improvement in terms of the total sulphur removing capacity, especially for high MW thiophenic compounds.

The improvement in the activity is attributed to the improved pore structure and the introduction of Ni-BDC, which has a higher affinity for sulphur compounds, but a small pore window for these compounds. The nucleation of Ni-BDC, crystallite size and crystallinity were significantly influenced by the amount of AC and the amount of formic acid added during the synthesis of x%AC@Ni-BDC. A comparison of all the materials prepared showed that the 40%AC@Ni-BDC with a 25 equivalent modulator had the best desulphurization activity. This was due to the enhanced pore structure and crystallinity. Hydrothermal treatment of AC in the presence of DMF was observed to improve adsorbate activity in terms of the high molecular sulphur compounds, which is attributed to improved surface chemistry. The synthesized composite has the potential to remove the sulphur compounds with a broad spectrum of MW. Finally, this work shows: the possibility of improving the adsorption capacity of adsorbents in adsorptive desulphurization by varying crystallinity using modulators; and the potential to use hydrothermal treatment for AC to produce more acid sites on AC. Hydrothermal treatment offers an opportunity to treat AC at temperatures above the boiling point of the solvents or acids being used.

Acknowledgements

The authors are grateful for the support received from the University of South Africa (UNISA), University of Johannesburg, the National Research Foundation (NRF) and the Department of Science and Technology (DST).

Appendix C. Supplementary data

Supplementary data related to this article can be found at: **Appendix C.**

References

Abdelhameed, R.M., Emam, H.E., Rocha, J., Silva, A.M.S., 2017. Cu-BTC metal-organic framework natural fabric composites for fuel purification. Fuel Process. Technol. 159, 306–312. https://doi.org/10.1016/j.fuproc.2017.02.001

Ahmed, I., Khan, N.A., Jhung, S.H., 2013. Graphite Oxide/Metal–Organic Framework (MIL-101): Remarkable Performance in the Adsorptive Denitrogenation of Model Fuels. Inorg. Chem. 52, 14155–14161. https://doi.org/10.1021/ic402012d

Ahsan, Md.A., Jabbari, V., Imam, M.A., Castro, E., Kim, H., Curry, M.L., Valles-Rosales, D.J., Noveron, J.C., 2020. Nanoscale nickel metal organic framework decorated over graphene oxide and carbon nanotubes for water remediation. Sci. Total Environ. 698, 134214. https://doi.org/10.1016/j.scitotenv.2019.134214

Al. Swat, A.A., Saleh, T.A., Ganiyu, S.A., Siddiqui, M.N., Alhooshani, K.R., 2017. Preparation of activated carbon, zinc oxide and nickel oxide composites for potential application in the desulphurization of model diesel fuels. J. Anal. Appl. Pyrolysis 128, 246–256. https://doi.org/10.1016/j.jaap.2017.10.004

Al-Wabel, M., Elfaki, J., Usman, A., Hussain, Q., Ok, Y.S., 2019. Performance of dry water- and porous carbon-based sorbents for carbon dioxide capture. Environ. Res. 174, 69–79. https://doi.org/10.1016/j.envres.2019.04.020

Araujo, P.W., Brereton, R.G., 1996. Experimental design III. Quantification. TrAC Trends Anal. Chem. 15, 156–163.

Arcibar-Orozco, J.A., Acosta-Herrera, A.A., Rangel-Mendez, J.R., 2019a. Simultaneous desulphuration and denitrogenation of model diesel fuel by Fe-Mn microwave modified activated carbon: Iron crystalline habit influence on adsorption capacity. J. Clean. Prod. 218, 69–82. https://doi.org/10.1016/j.jclepro.2019.01.202

Arcibar-Orozco, J.A., Acosta-Herrera, A.A., Rangel-Mendez, J.R., 2019b. Simultaneous desulphuration and denitrogenation of model diesel fuel by Fe-Mn microwave modified activated carbon: Iron crystalline habit influence on adsorption capacity. J. Clean. Prod. 218, 69–82. https://doi.org/10.1016/j.jclepro.2019.01.202

Aribike, D.S., Usman, M.A., Oloruntoba, M.M., 2020. Adsorptive desulphurization of diesel using activated sewage sludge: kinetics, equilibrium and thermodynamics studies. Appl. Petrochem. Res. 10, 1–12. https://doi.org/10.1007/s13203-019-00239-2

Bruker Axs, INC., 2005. Bruker Advanced X-ray solutions, 3. Bruker Axs, INC., Karlsruhe, West Germany.

Bu, J., Loh, G., Gwie, C.G., Dewiyanti, S., Tasrif, M., Borgna, A., 2011. Desulphurization of diesel fuels by selective adsorption on activated carbons: Competitive adsorption of polycyclic aromatic

sulphur heterocycles and polycyclic aromatic hydrocarbons. Chem. Eng. J. 166, 207–217. https://doi.org/10.1016/j.cej.2010.10.063

Burgaz, E., Erciyes, A., Andac, M., Andac, O., 2019. Synthesis and characterization of nano-sized metal organic framework-5 (MOF-5) by using consecutive combination of ultrasound and microwave irradiation methods. Inorganica Chim. Acta 485, 118–124. https://doi.org/10.1016/j.ica.2018.10.014

Crandall, B.S., Zhang, J., Stavila, V., Allendorf, M.D., Li, Z., 2019. Desulphurization of Liquid Hydrocarbon Fuels with Microporous and Mesoporous Materials: Metal-Organic Frameworks, Zeolites, and Mesoporous Silicas. Ind. Eng. Chem. Res. 58, 19322–19352. https://doi.org/10.1021/acs.iecr.9b03183

Dai, W., Tian, N., Liu, C., Yu, L., Liu, Q., Ma, N., Zhao, Y., 2017. (Zn, Ni, Cu)-BTC Functionalized with Phosphotungstic Acid for Adsorptive Desulphurization in the Presence of Benzene and Ketone. Energy Fuels 31, 13502–13508. https://doi.org/10.1021/acs.energyfuels.7b02851

Fallah, R.N., Azizian, S., 2012. Removal of thiophenic compounds from liquid fuel by different modified activated carbon cloths. Fuel Process. Technol. 93, 45–52.

Fallah, R.N., Azizian, S., Reggers, G., Carleer, R., Schreurs, S., Ahenach, J., Meynen, V., Yperman, J., 2014. Effect of aromatics on the adsorption of thiophenic sulphur compounds from model diesel fuel by activated carbon cloth. Fuel Process. Technol. 119, 278–285. https://doi.org/10.1016/j.fuproc.2013.11.016

Gao, S., Sui, Y., Wei, F., Qi, J., Meng, Q., He, Y., 2018. Facile synthesis of cuboid Ni-MOF for high-performance supercapacitors. J. Mater. Sci. 53, 6807–6818. https://doi.org/10.1007/s10853-018-2005-1

Greer, H.F., Liu, Y., Greenaway, A., Wright, P.A., Zhou, W., 2016. Synthesis and formation mechanism of textured MOF-5. Cryst. Growth Des. 16, 2104–2111.

Hashemian, S., Salari, K., Salehifar, H., Atashi Yazdi, Z., 2013. Removal of azo dyes (Violet B and Violet 5R) from aqueous solution using new activated carbon developed from orange peel. J. Chem. 2013.

Hernandez, S.P., Fino, D., Russo, N., 2010. High performance sorbents for diesel oil desulphurization. Chem. Eng. Sci. 65, 603–609.

Hu, Xinjiang, Xu, J., Wu, C., Deng, J., Liao, W., Ling, Y., Yang, Y., Zhao, Yina, Zhao, Yunlin, Hu, Xi, 2017. Ethylenediamine grafted to graphene oxide@ Fe3O4 for chromium (VI) decontamination: Performance, modelling, and fractional factorial design. PloS One 12, e0187166.

Kampouraki, Z.-C., Giannakoudakis, D.A., Nair, V., Hosseini-Bandegharaei, A., Colmenares, J.C., Deliyanni, E.A., 2019. Metal Organic Frameworks as Desulphurization Adsorbents of DBT and 4,6-DMDBT from Fuels. Molecules 24, 4525. https://doi.org/10.3390/molecules24244525

Kim, J.H., Ma, X., Zhou, A., Song, C., 2006. Ultra-deep desulphurization and denitrogenation of diesel fuel by selective adsorption over three different adsorbents: A study on adsorptive selectivity and

mechanism. Front. Catal. Mol. View Ind. Catal. 111, 74–83. https://doi.org/10.1016/j.cattod.2005.10.017

Li, Y., Liu, F.-T., Zhang, H.-X., Li, X., Dong, X.-F., Wang, C.-W., 2019. DMF-treated strategy of carbon nanospheres for high-efficient and selective removal of organic dyes. Appl. Surf. Sci. 484, 144–151.

Li, Y.-X., Jiang, W.-J., Tan, P., Liu, X.-Q., Zhang, D.-Y., Sun, L.-B., 2015. What Matters to the Adsorptive Desulphurization Performance of Metal-Organic Frameworks? J. Phys. Chem. C 119, 21969–21977. https://doi.org/10.1021/acs.jpcc.5b07546

Liang, X., Zhang, Y., Qu, Y., Han, Y., Wang, X., Cheng, A., Duan, A., Zhao, L., 2018. Synthesis of HKUST-1 and zeolite beta composites for deep desulphurization of model gasoline. RSC Adv. 8, 13750–13754. https://doi.org/10.1039/C8RA01490F

Liu, B.S., Xu, D.F., Chu, J.X., Liu, W., Au, C.T., 2007. Deep Desulphurization by the Adsorption Process of Fluidized Catalytic Cracking (FCC) Diesel over Mesoporous Al−MCM-41 Materials. Energy Fuels 21, 250–255. https://doi.org/10.1021/ef060249n

Matloob, A.M., El-Hafiz, D.R.A., Saad, L., Mikhail, S., Guirguis, D., 2019. Metal organic framework-graphene nano-composites for high adsorption removal of DBT as hazard material in liquid fuel. J. Hazard. Mater. 373, 447–458. https://doi.org/10.1016/j.jhazmat.2019.03.098

Mguni, L.L., Yao, Y., Liu, X., Yuan, Z., Hildebrandt, D., 2019. Ultra-deep desulphurization of both model and commercial diesel fuels by adsorption method. J. Environ. Chem. Eng. 7, 102957. https://doi.org/10.1016/j.jece.2019.102957

Moreira, A.M., Brandão, H.L., Hackbarth, F.V., Maass, D., Ulson de Souza, A.A., Guelli U. de Souza, S.M.A., 2017. Adsorptive desulphurization of heavy naphthenic oil: Equilibrium and kinetic studies. Chem. Eng. Sci. 172, 23–31. https://doi.org/10.1016/j.ces.2017.06.010

Olajire, A.A., Abidemi, J.J., Lateef, A., Benson, N.U., 2017. Adsorptive desulphurization of model oil by Ag nanoparticles-modified activated carbon prepared from brewer's spent grains. J. Environ. Chem. Eng. 5, 147–159. https://doi.org/10.1016/j.jece.2016.11.033

Prajapati, Y.N., Verma, N., 2017. Adsorptive desulphurization of diesel oil using nickel nanoparticle-doped activated carbon beads with/without carbon nanofibers: Effects of adsorbate size and adsorbent texture. Fuel 189, 186–194.

Roy, S., Moharir, A.S., 2019. Modeling the Generic Breakthrough Curve for Adsorption Process. ArXiv190700195 Phys.

Saleh, T.A., Al-Hammadi, S.A., Tanimu, A., Alhooshani, K., 2018. Ultra-deep adsorptive desulphurization of fuels on cobalt and molybdenum nanoparticles loaded on activated carbon derived from waste rubber. J. Colloid Interface Sci. 513, 779–787. https://doi.org/10.1016/j.jcis.2017.11.076

Saleh, T.A., Danmaliki, G.I., 2016. Influence of acidic and basic treatments of activated carbon derived from waste rubber tires on adsorptive desulphurization of thiophenes. J. Taiwan Inst. Chem. Eng. 60, 460–468.

Sarda, K.K., Bhandari, A., Pant, K.K., Jain, S., 2012. Deep desulphurization of diesel fuel by selective adsorption over Ni/Al2O3 and Ni/ZSM-5 extrudates. Fuel 93, 86–91.

Shi, R.-H., Zhang, Z.-R., Fan, H.-L., Zhen, T., Shangguan, J., Mi, J., 2017. Cu-based metal–organic framework/activated carbon composites for sulphur compounds removal. Appl. Surf. Sci. 394, 394–402. https://doi.org/10.1016/j.apsusc.2016.10.071

Sumathi, S., Bhatia, S., Lee, K.T., Mohamed, A.R., 2009. Optimization of microporous palm shell activated carbon production for flue gas desulphurization: Experimental and statistical studies. Bioresour. Technol. 100, 1614–1621.

Tan, P., Jiang, Y., Sun, L.-B., Liu, X.-Q., AlBahily, K., Ravon, U., Vinu, A., 2018. Design and fabrication of nanoporous adsorbents for the removal of aromatic sulphur compounds. J. Mater. Chem. A 6, 23978–24012. https://doi.org/10.1039/C8TA09184F

Tirmizi, S.A., Badshah, A., Ammad, H.M., Jawad, M., Abbas, S.M., Rana, U.A., Khan, S.U.-D., 2018. Synthesis of highly stable MOF-5@ MWCNTs nanocomposite with improved hydrophobic properties. Arab. J. Chem. 11, 26–33.

Ullah, L., Zhao, G., Hedin, N., Ding, X., Zhang, S., Yao, X., Nie, Y., Zhang, Y., 2019. Highly efficient adsorption of benzothiophene from model fuel on a metal-organic framework modified with dodeca-tungstophosphoric acid. Chem. Eng. J. 362, 30–40. https://doi.org/10.1016/j.cej.2018.12.141

Vikrant, K., Kim, K.-H., 2019. Nanomaterials for the adsorptive treatment of Hg (II) ions from water. Chem. Eng. J. 358, 264–282.

Wang, J., Zhang, Q., Yang, H., Qiao, C., 2020. Adsorptive Desulphurization of Organic Sulphur from Model Fuels by Active Carbon Supported Mn (II): Equilibrium, Kinetics, and Thermodynamics. Int. J. Chem. Eng. 2020, 2813946. https://doi.org/10.1155/2020/2813946

Wiβmann, G., Schaate, A., Lilienthal, S., Bremer, I., Schneider, A.M., Behrens, P., 2012. Modulated synthesis of Zr-fumarate MOF. Microporous Mesoporous Mater. 152, 64–70.

Wright, A.A., Institute of Marine Engineers, 2000. Exhaust Emissions from Combustion Machinery, MEP Series (Marine Engineering Practice Series).: Part 20. Institute of Marine Engineers.

Xiao, J., Song, C., Ma, X., Li, Z., 2012. Effects of Aromatics, Diesel Additives, Nitrogen Compounds, and Moisture on Adsorptive Desulphurization of Diesel Fuel over Activated Carbon. Ind. Eng. Chem. Res. 51, 3436–3443. https://doi.org/10.1021/ie202440t

Yu, C., Qiu, J.S., Sun, Y.F., Li, X.H., Chen, G., Zhao, Z.B., 2008. Adsorption removal of thiophene and dibenzothiophene from oils with activated carbon as adsorbent: effect of surface chemistry. J. Porous Mater. 15, 151–157.

Yu, M., Li, Z., Ji, Q., Wang, S., Su, D., Lin, Y.S., 2009. Effect of thermal oxidation of activated carbon surface on its adsorption towards dibenzothiophene. Chem. Eng. J. 148, 242–247.

Yuan, S., Feng, L., Wang, K., Pang, J., Bosch, M., Lollar, C., Sun, Y., Qin, J., Yang, X., Zhang, P., 2018. Stable metal–organic frameworks: design, synthesis, and applications. Adv. Mater. 30, 1704303.

Zahn, G., Zerner, P., Lippke, J., Kempf, F.L., Lilienthal, S., Schröder, C.A., Schneider, A.M., Behrens, P., 2014. Insight into the mechanism of modulated syntheses: *in situ* synchrotron diffraction studies on the formation of Zr-fumarate MOF. CrystEngComm 16, 9198–9207. https://doi.org/10.1039/C4CE01095G

Zhao, Z., Zuhra, Z., Qin, L., Zhou, Y., Zhang, L., Tang, F., Mu, C., 2018. Confinement of microporous MOF-74(Ni) within mesoporous γ-Al2O3 beads for excellent ultra-deep and selective adsorptive desulphurization performance. Fuel Process. Technol. 176, 276–282. https://doi.org/10.1016/j.fuproc.2018.03.037

Zhu, L., Jia, X., Bian, H., Huo, T., Duan, Z., Xiang, Y., Xia, D., 2018. Structure and adsorptive desulphurization performance of the composite material MOF-5@ AC. New J. Chem. 42, 3840–3850.

10. CONCLUSION

The ultimate goal of the thesis was to develop highly active and cost-effective carbon materials for ADS. This was to be achieved by identifying promising adsorbents and adsorbent improvement strategies that would enhance their activity using literature search and experimental work. To develop a systematic approach to identify strategies to improve adsorbent activity ML was used to determine features with high influence on adsorption activity. Thereafter, experimental work was used to evaluate adsorbent characteristics, activity and kinetics. The adsorbents evaluated include TiO_2, SiO_2, MS 13X, MS 5A, AC, AC, NiO, AC loaded with Lewis acids (metal oxides), MOF-5, Ni-BDC, and AC@Ni-BDC composite.

10.1 Conclusion remarks

Based on the observations made during the study, AC is a promising adsorbent and support for adsorptive desulphurization. The functional groups on AC are important and it has been demonstrated that they can be improved by adding metal oxides, making composites with MOFs and hydrothermal treatment with acetic acid and DMF. These results are consistent with the ML results that showed that adsorbent properties in this order metal ion > metal properties > surface area and pore volume had the greatest effect on ADS activity. The results also showed that modulated synthesis of MOF improved activity, which was attributed to improved crystallinity and an increase in the number of low coordination sites. These results should provide guidelines and new ideas for adsorbent preparation and improvement for adsorptive desulphurization.

Detailed conclusions drawn for each aspect of the investigation are provided below:

10.1.1 Literature review and ML

From the literature review, AC is the most promising adsorbent based on the figure of merit (FoM) while MOFs, TMU11, is the most promising based on activity. Thermodynamic analysis showed that solvent adsorption was desirable to enhance the activity for an entropy-driven process. The increase in activity with solvent adsorption suggests that solvent adsorption may be necessary to bring adsorbate in intimate contact with the adsorbent.

There is no consensus on the parameters that have the most influence on adsorption activity. The findings from the ML exploration suggest that: the adsorbent properties (metal ion, metal properties, surface area, and pore volume) need the most attention in order to improve adsorbent activity. These observations informed the adsorbents used in experimental work and modification strategies used in the following sections.

10.1.2 ACs, molecular sieves, SiO_2, TiO_2, Al_2O_3 as adsorbents and the effect of metal oxides loading on these adsorbents.

The experimental data for the adsorption of DBT fitted the pseudo-second-order kinetic equation closely, which suggests chemical adsorption activity between DBT and the adsorbents AC, T103, T104 and MS 13X. MS 5A showed poor activity, which could be due to the crystal structure of the molecular sieve. MS 13X showed fair activity with model diesel, but poor stability. The sulphur adsorption order for conventional diesel from South Africa decreases in the order: 4-MDBT>> 4,6-DMDBT~ 4 E,6-MDBT~ 2,4,6-TMDBT~1,4,6-TMDBT. This activity order was attributed to an increase in steric hindrance with the increase in molecular weight. A comparison of AC activity of model diesel versus conventional diesel showed that AC had activity eight times higher than conventional diesel at ambient conditions (25 $^{\circ}$C). This is due to poor selectivity, therefore selectivity has to be improved and the use of conventional diesel should be standard practice, for successful use of adsorbents.

The follow-up work investigated the effect of adding Lewis acid on the supports. AC-based adsorbents showed higher activity compared to alumina-based adsorbents. The poor activity of alumina was attributed to the poor structure, limited surface area and strong acidic nature of alumina. NiO showed the highest activity of the four Lewis acids used, namely CoO, NiO, CuO and ZnO. The high activity of NiO was attributed to it having the lowest acidity, based on the ionic-covalent parameter (ICP). Finally, it was observed that the challenge with the regeneration of the adsorbents used to treat real diesel is due to the competitive desorption of hydrocarbons and sulphur compounds.

The effect of support on the activity of NiO, the most active Lewis acid, was investigated. NiO was loaded on different supports, i.e. activated carbon (AC), alumina (Al_2O_3), silica (SiO_2) and titania (TiO_2), and this caused a slight increase in desulphurization activity. NiO loading was also observed to decrease activity/ selectivity of high molecular (Mr) weight sulphur compounds for AC and Al_2O_3, while it had a positive effect on SiO_2 but no effect on TiO_2. The positive effect was a result of synergy between NiO and SiO_2 since pure NiO was seen to favour the adsorption of low Mr weight sulphur molecules. Another positive result was that the addition of NiO on SiO_2 reduced the hydrocarbon adsorbed by the system, and hence improved its overall selectivity. Finally, when conventional diesel was used, the addition of NiO on these supports led to an increase in activity at higher temperatures. The higher activity was attributed to poor adsorption of polyaromatic hydrocarbon at higher temperatures and increased involvement of chemical bonds.

10.1.3 Modulated synthesized Ni-based MOFs and the composites of x%AC@Ni-MOF

Modulated synthesis is another strategy that can be used to improve adsorbent activity. The modulator that was used in this work was formic acid, which had four efficacy controls, i.e. crystallite size, crystallite size, morphology and accelerating Ni-BDC formation. Novel results were observed, the activity of the adsorbent increased with crystallinity for thiophene, while it decreased with crystallinity for DBT and 4,6 DMDBT. The increase in activity with crystallinity was attributed to an increase in the number of acid sites, and it is believed that this is due to more adsorption sites and low coordination sites. The overall adsorption capacity and partition coefficient (PC) for this adsorbent were 4.14 mg/g and 0.053 mg/g/ppm, respectively.

A novel composite material was, thereafter, hydrothermal synthesized using the two materials i.e AC and Ni-BDC. The quantities of both AC and the modulator were seen to influence: the nucleation of Ni-BDC; crystallite size; crystallinity. The TH-removing capacity of the composite was much higher than when using AC as the adsorbent, which remedies the disadvantage of AC, i.e. poor adsorptive selectivity of TH. The adsorption activity for the other two compounds (i.e. DBT and 4,6 DMDBT) also improved. This was attributed to improved pore structure and the introduction of Ni-BDC, which has a higher affinity for sulphur compounds, but a small pore window for sulphur compounds with high molecular weight, i.e DBT and 4,6 DMDBT. New stronger acid sites were observed, which suggests that the formation of these sites could be paramount in the improved activity of the composite. Composites are expected to lower the adsorbent cost while at the same time utilizing the general high activity of MOFs. However, a detailed cost benefict analysis of composite is required. Finally, hydrothermal treatment of AC in the presence of DMF was observed to improve the adsorbate activity of the high molecular sulphur compounds, which was attributed to improved surface chemistry.

9.2 Perspectives

This research study has provided a number of possible new insights that may be used to improve the design of adsorptive desulphurization adsorbents. The development of adsorbents that can form weak bonds with solvents is required to improve adsorbent activity. Working at slightly higher temperatures is paramount for a system when polyaromatic compounds are strongly involved in competitive adsorption with sulphur compounds. Designing materials with high crystallinity and many low coordination sites may be important to improve activity. Finally, hydrothermal treatment is a potential method to improve the surface properties of materials, e.g.

AC. Hydrothermal treatment offers an opportunity to treat adsorbents at temperatures above their boiling point.

Carbon-based adsorbents have shown potential in ADS. However, there is still work to be done to achieve deep desulphurization. One of the major challenges being competitive adsorption between polyaromatic compounds and sulphur compounds. Therefore, it is up to future researchers and scientists to develop adsorbents that not only remove sulphur selectively but also maintain the quality of the fuel. Future work, therefore, should include investigations to change sulphur compounds properties in the liquid fuel by e.g. oxidation to make it easier to separate/adsorb from the less polar polyaromatic compounds. Investigate the potential to modifying carbonous materials using hydrothermal treatment as the opportunity it offers was discussed earlier. Finally, the full potential of ADS to achieve deep desulphurization lies in the use of experimental work and computational work.

APPENDIX A: Insight into adsorptive desulphurization by zeolites: a machine learning exploration

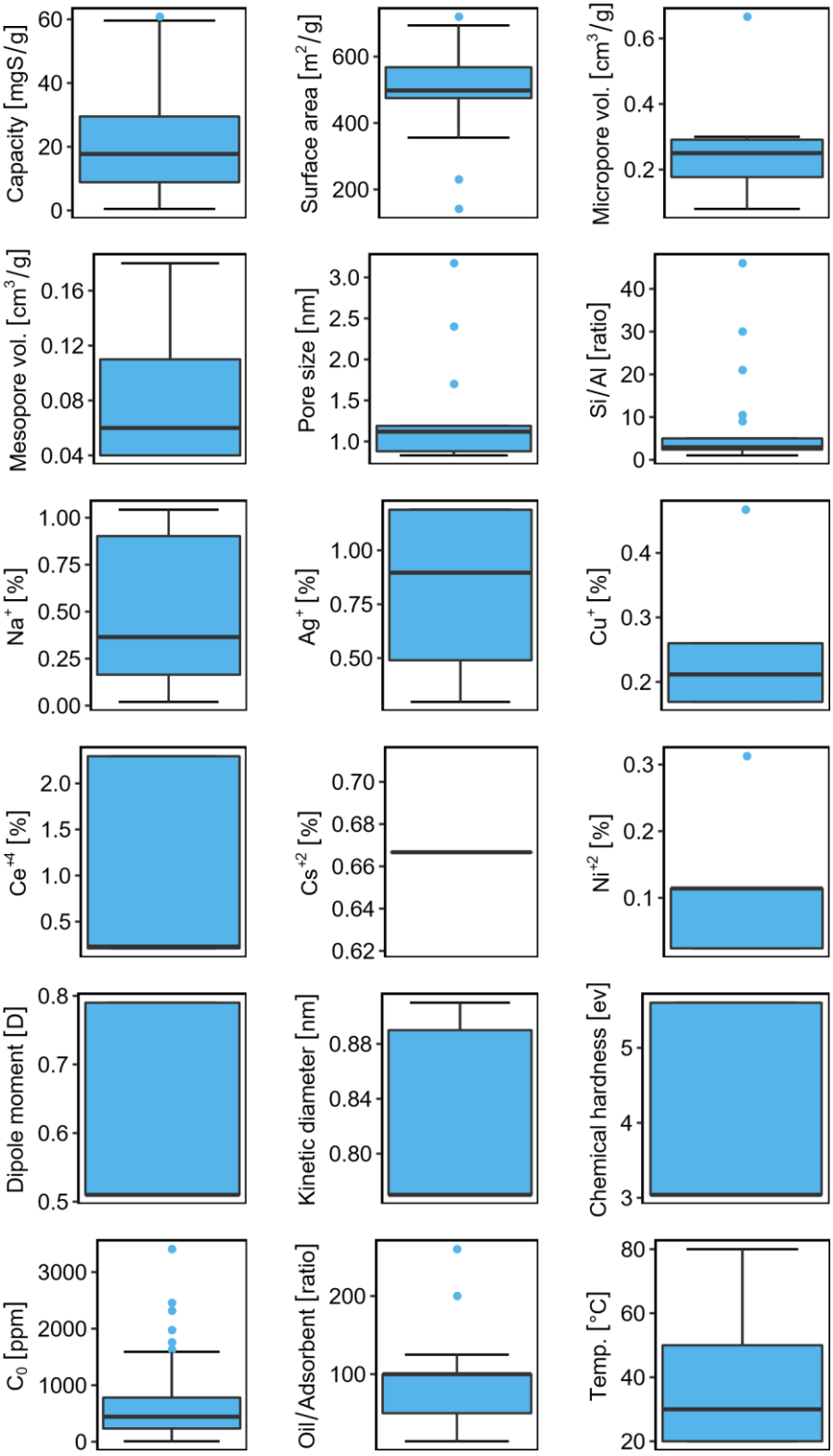

Figure A1: Analysis of the continuous variables in the zeolite properties and process parameters in the dataset.

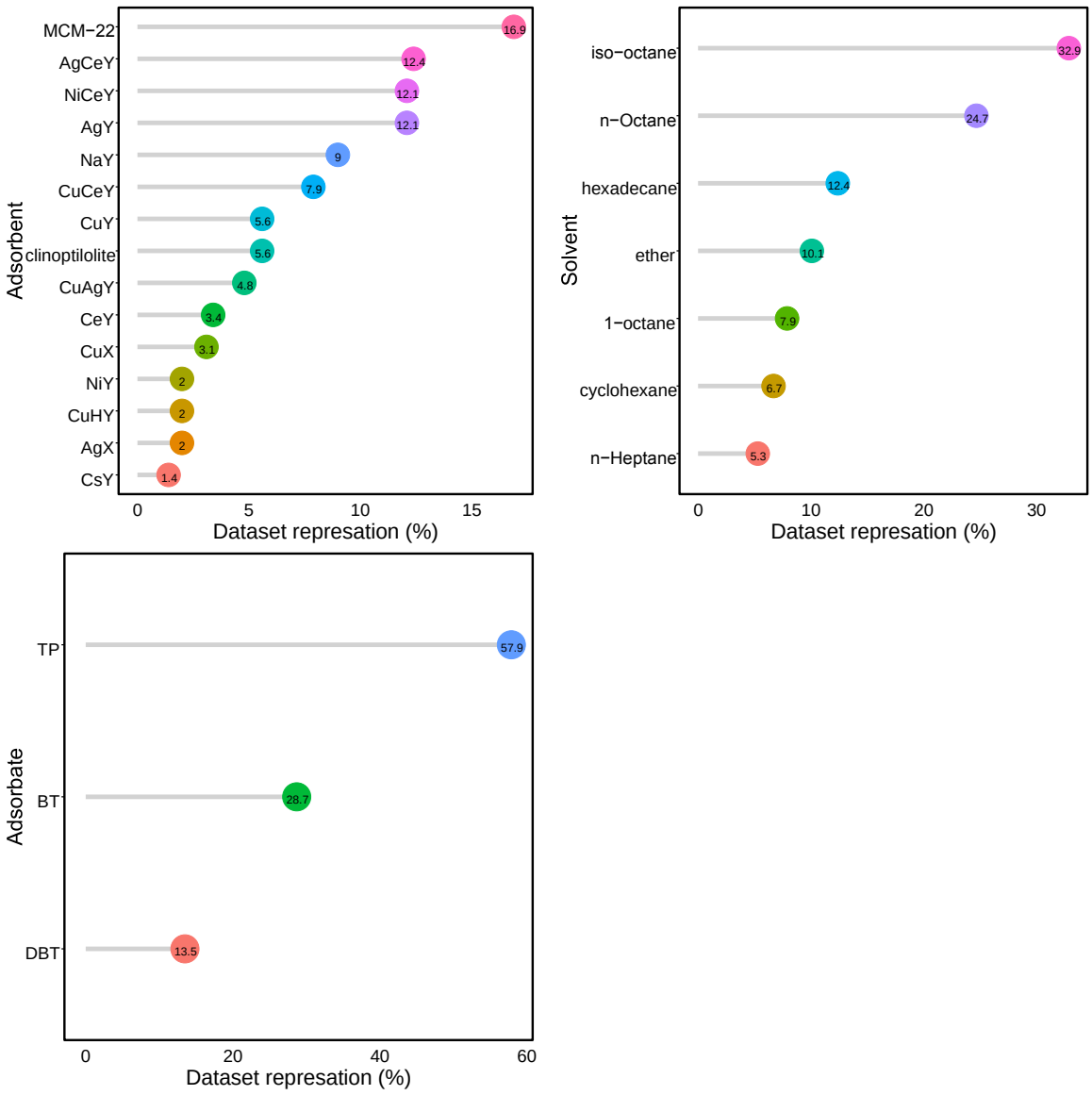

Figure A2: Analysis of distirbution on categorical variables in the adsorption desulphurization dataset.

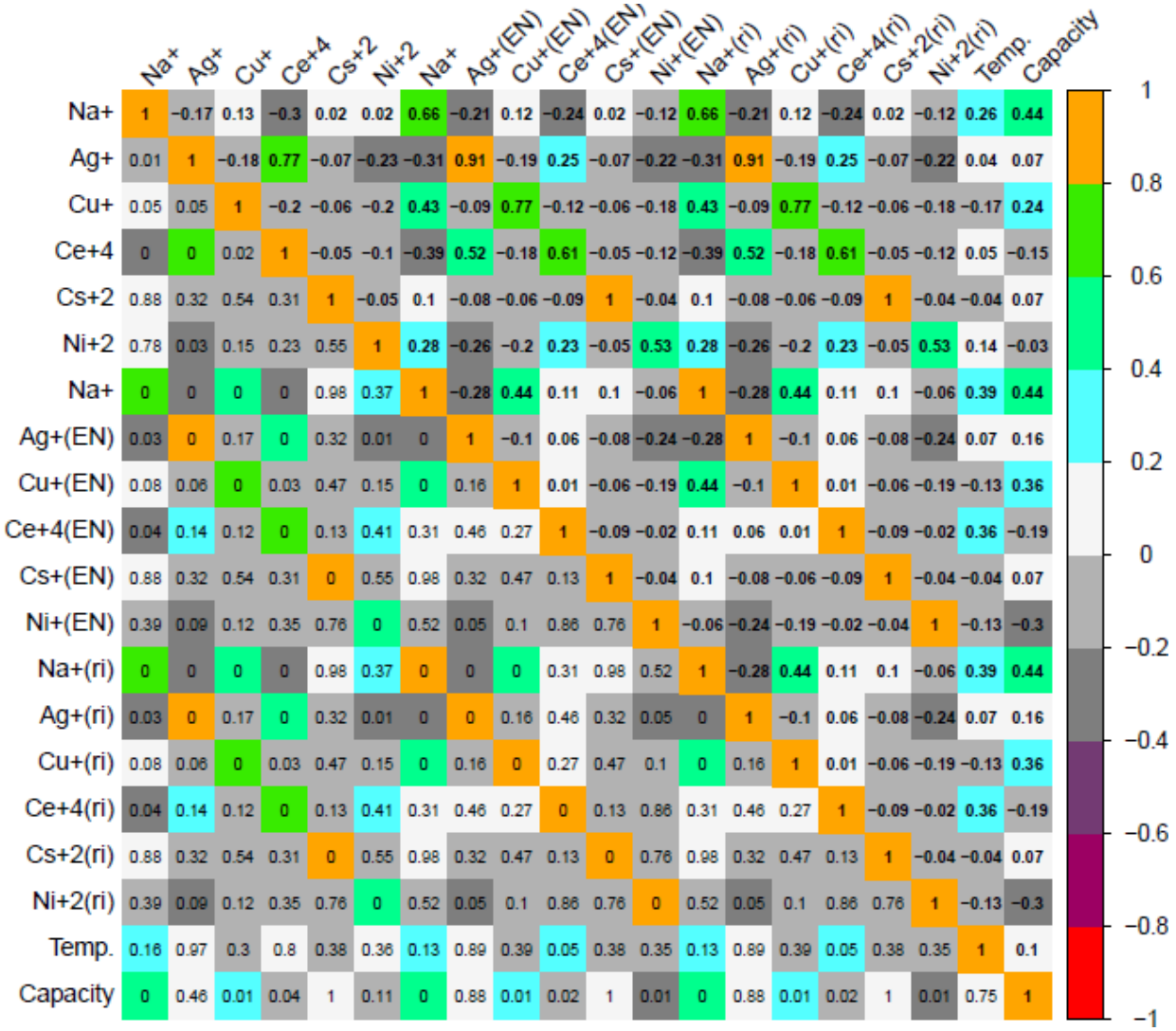

Figure A3: Correlations between metal ion properties including adsorption capacity properties. Metal property variables: ri = Ionic radius and EN = electronegativity.

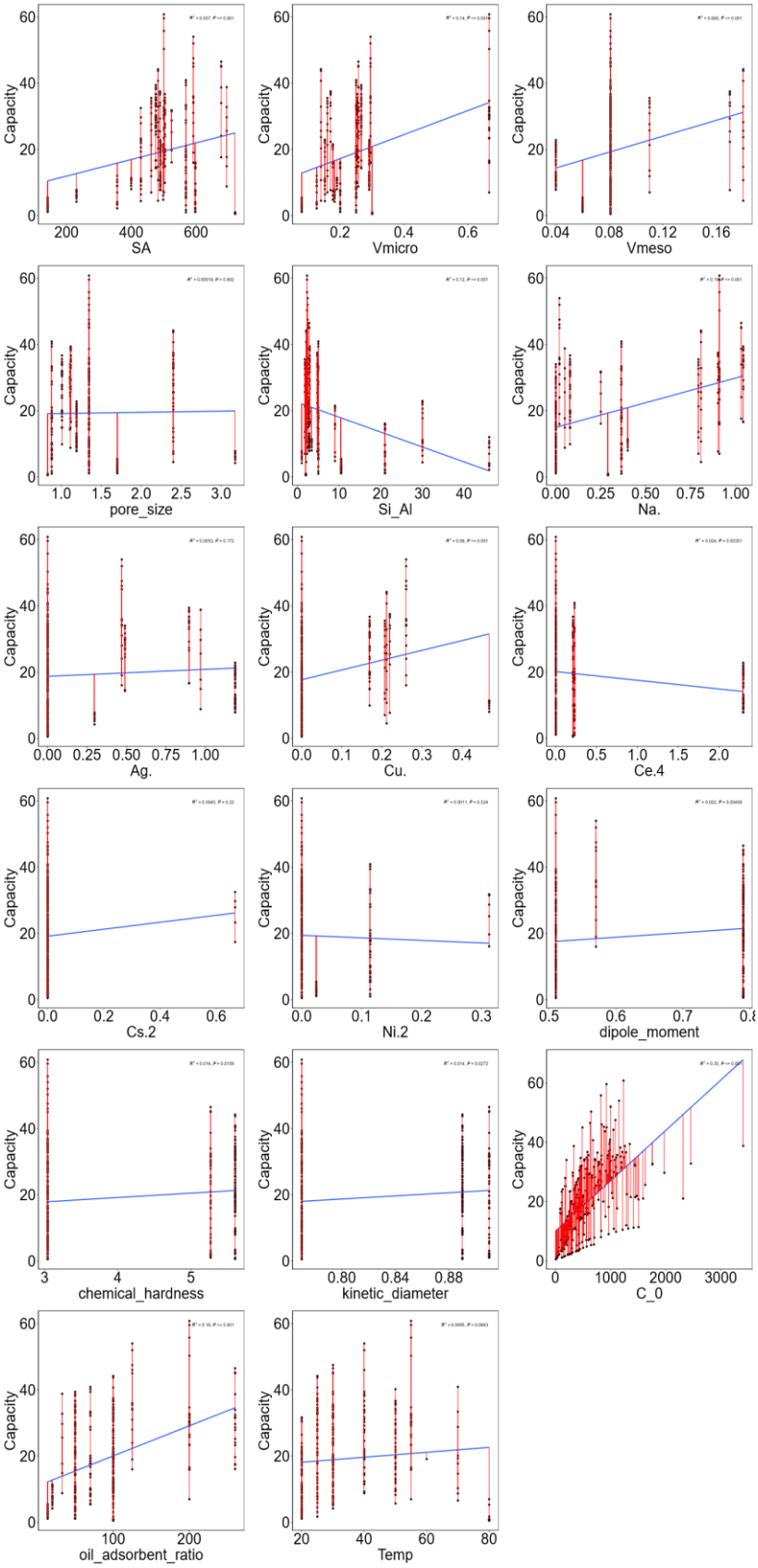

Figure A4: Regression plots of select independent variables (excluding metal ion electronegativity and ionic radius) and the dependent variable (Adsorptive capacity) with thier R^2 and p-values provided.
Residual from the fitted line (blue) are indicated in red to highlight their distrubutions.

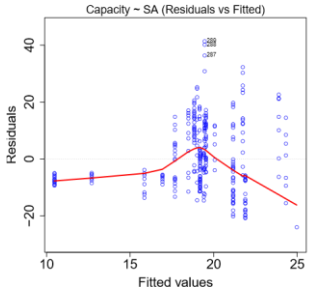
Capacity ~ SA (Residuals vs Fitted)
Residuals
Fitted values

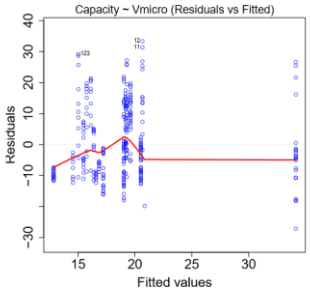
Capacity ~ Vmicro (Residuals vs Fitted)
Residuals
Fitted values

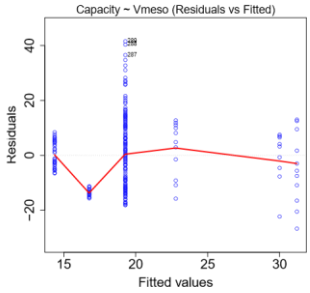
Capacity ~ Vmeso (Residuals vs Fitted)
Residuals
Fitted values

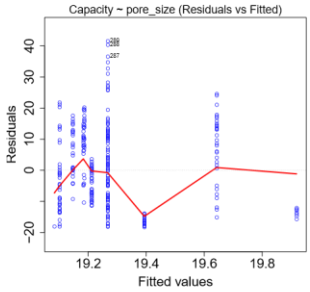
Capacity ~ pore_size (Residuals vs Fitted)
Residuals
Fitted values

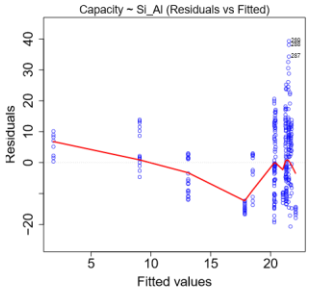
Capacity ~ Si_Al (Residuals vs Fitted)
Residuals
Fitted values

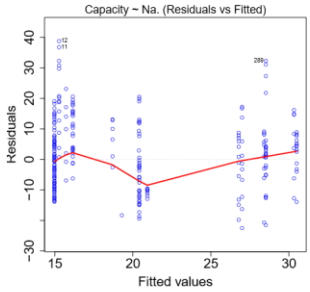
Capacity ~ Na. (Residuals vs Fitted)
Residuals
Fitted values

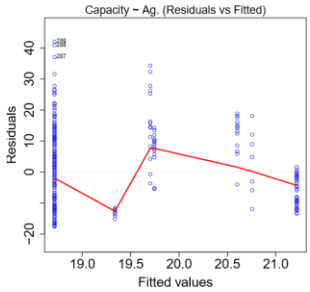
Capacity ~ Ag. (Residuals vs Fitted)
Residuals
Fitted values

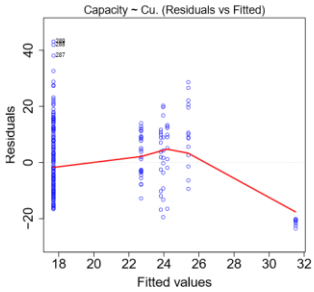
Capacity ~ Cu. (Residuals vs Fitted)
Residuals
Fitted values

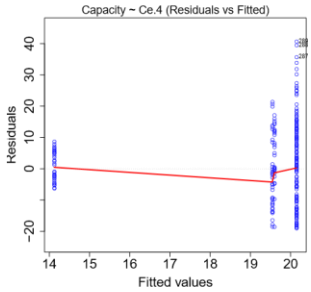
Capacity ~ Ce.4 (Residuals vs Fitted)
Residuals
Fitted values

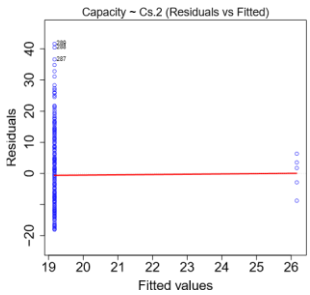
Capacity ~ Cs.2 (Residuals vs Fitted)
Residuals
Fitted values

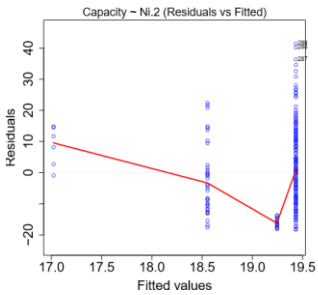
Capacity ~ Ni.2 (Residuals vs Fitted)
Residuals
Fitted values

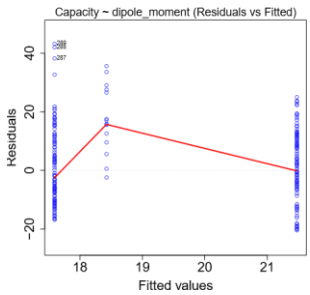
Capacity ~ dipole_moment (Residuals vs Fitted)
Residuals
Fitted values

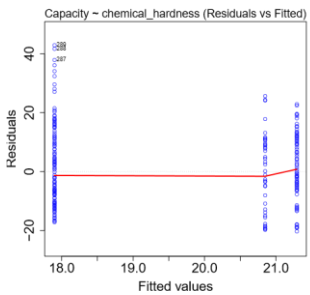
Capacity ~ chemical_hardness (Residuals vs Fitted)
Residuals
Fitted values

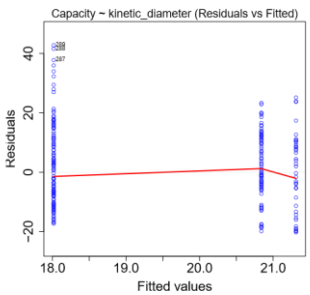
Capacity ~ kinetic_diameter (Residuals vs Fitted)
Residuals
Fitted values

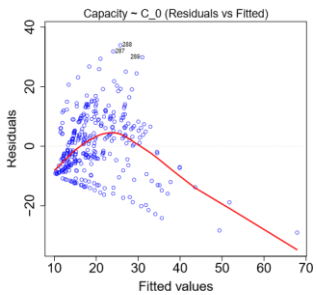
Capacity ~ C_0 (Residuals vs Fitted)
Residuals
Fitted values

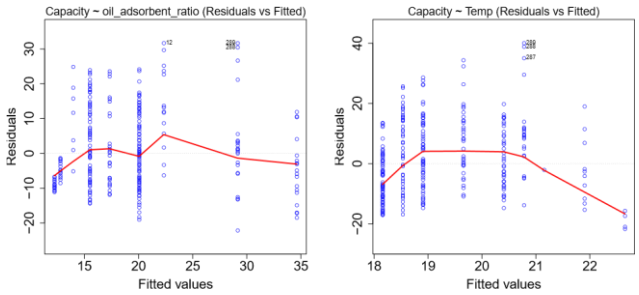

Figure A5: Residual vs fitted values plots of select independent variables in the linear model of continous variables against the dependent variable (adsorptive capacity).

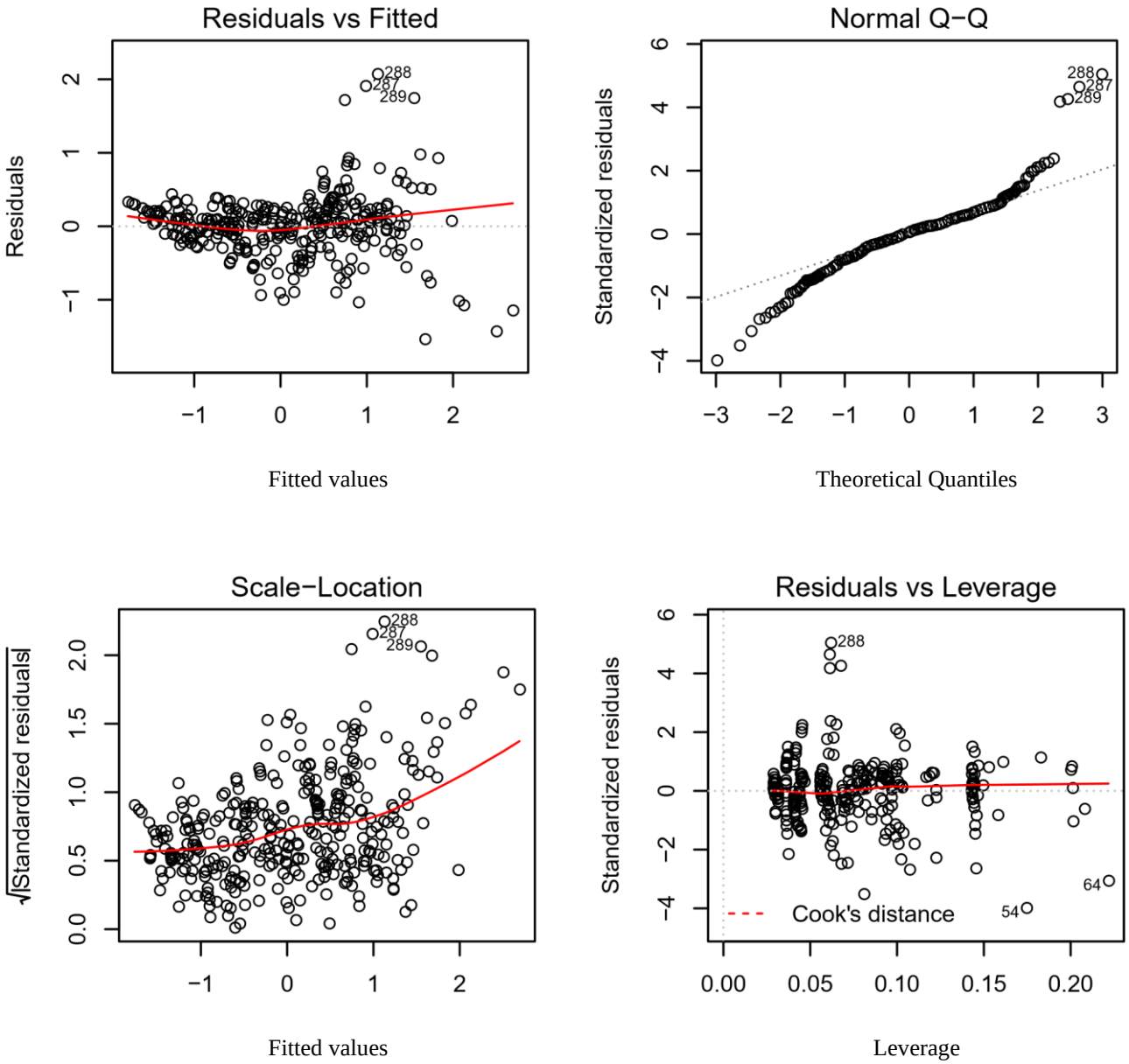

Figure A6: Diagnostic plots for the multiple linear regression analysis.

Table A1: Zeolite and adsorption capacity dataset compiled for study. Variable names: SA = Surface area; Vmicro = micropore volume; Vmeso = mesopore volume; DM = dipole moment, CH = chemical hardness and KD = kinetic diameter. Additional data columns of metal properties have been excluded for due to space constraints, the corresponding values are provided on Table A2.

	Adsorbent properties												Adsorbent conditions				Adsorption conditions				
	Adsorbent	SA	Vmicro	Vmeso	Pore size	Si/Al	Metal amount (Mn+/Al)						adsorbate	DM	CH	KD	*C*0	Solvent	Oil/Adsorbent	Temp.	Capacity
		m^2/g	cm^3/g	cm3/g	nm	ratio	Na^+	Ag^+	Cu^+	Ce+4	Cs+2	Ni+2	S	D	eV	nm	ppm		ml/g	◦C	mgS/g
1	CuAgY	591	0.295			2.43	0.02	0.4700	0.2600				TP	0.57	3.0401	0.77	291	cyclohexane	125	50	16
2	CuAgY	591	0.295			2.43	0.02	0.4700	0.2600				TP	0.57	3.0401	0.77	420	cyclohexane	125	50	24
3	CuAgY	591	0.295			2.43	0.02	0.4700	0.2600				TP	0.57	3.0401	0.77	556	cyclohexane	125	50	31
4	CuAgY	591	0.295			2.43	0.02	0.4700	0.2600				TP	0.57	3.0401	0.77	719	cyclohexane	125	50	34.3
5	CuAgY	591	0.295			2.43	0.02	0.4700	0.2600				TP	0.57	3.0401	0.77	833	cyclohexane	125	50	35.5
6	CuAgY	591	0.295			2.43	0.02	0.4700	0.2600				TP	0.57	3.0401	0.77	970	cyclohexane	125	50	36
7	CuAgY	591	0.295			2.43	0.02	0.4700	0.2600				TP	0.57	3.0401	0.77	321	cyclohexane	125	40	19
8	CuAgY	591	0.295			2.43	0.02	0.4700	0.2600				TP	0.57	3.0401	0.77	461	cyclohexane	125	40	28
9	CuAgY	591	0.295			2.43	0.02	0.4700	0.2600				TP	0.57	3.0401	0.77	587	cyclohexane	125	40	34
10	CuAgY	591	0.295			2.43	0.02	0.4700	0.2600				TP	0.57	3.0401	0.77	839	cyclohexane	125	40	46
11	CuAgY	591	0.295			2.43	0.02	0.4700	0.2600				TP	0.57	3.0401	0.77	1002	cyclohexane	125	40	52
12	CuAgY	591	0.295			2.43	0.02	0.4700	0.2600				TP	0.57	3.0401	0.77	1154	cyclohexane	125	40	54
13	CuAgY	591	0.295			2.43	0.02	0.4700	0.2600				TP	0.57	3.0401	0.77	369	cyclohexane	125	30	19
14	CuAgY	591	0.295			2.43	0.02	0.4700	0.2600				TP	0.57	3.0401	0.77	525	cyclohexane	125	30	28
15	CuAgY	591	0.295			2.43	0.02	0.4700	0.2600				TP	0.57	3.0401	0.77	716	cyclohexane	125	30	34
16	CuAgY	591	0.295			2.43	0.02	0.4700	0.2600				TP	0.57	3.0401	0.77	930	cyclohexane	125	30	45
17	CuAgY	591	0.295			2.43	0.02	0.4700	0.2600				TP	0.57	3.0401	0.77	1088	cyclohexane	125	30	47.5
18	CuCeY	503	0.254		1.01	4.86	0.08		0.1690	0.2100			BT	0.79	5.6020	0.89	265	1-octane	100	20	17.1
19	CuCeY	503	0.254		1.01	4.86	0.08		0.1690	0.2100			BT	0.79	5.6020	0.89	273	1-octane	100	30	18.2
20	CuCeY	503	0.254		1.01	4.86	0.08		0.1690	0.2100			BT	0.79	5.6020	0.89	283	1-octane	100	40	19.6
21	CuCeY	503	0.254		1.01	4.86	0.08		0.1690	0.2100			BT	0.79	5.6020	0.89	285	1-octane	100	50	19.9
22	CuCeY	503	0.254		1.01	4.86	0.08		0.1690	0.2100			BT	0.79	5.6020	0.89	280	1-octane	100	60	19.1
23	CuCeY	503	0.254		1.01	4.86	0.08		0.1690	0.2100			BT	0.79	5.6020	0.89	141	1-octane	100	20	9.9
24	CuCeY	503	0.254		1.01	4.86	0.08		0.1690	0.2100			BT	0.79	5.6020	0.89	273	1-octane	100	20	19.1
25	CuCeY	503	0.254		1.01	4.86	0.08		0.1690	0.2100			BT	0.79	5.6020	0.89	341	1-octane	100	20	23.9
26	CuCeY	503	0.254		1.01	4.86	0.08		0.1690	0.2100			BT	0.79	5.6020	0.89	380	1-octane	100	20	26.5
27	CuCeY	503	0.254		1.01	4.86	0.08		0.1690	0.2100			BT	0.79	5.6020	0.89	436	1-octane	100	20	30.4
28	CuCeY	503	0.254		1.01	4.86	0.08		0.1690	0.2100			BT	0.79	5.6020	0.89	446	1-octane	100	20	30.9
29	CuCeY	503	0.254		1.01	4.86	0.08		0.1690	0.2100			BT	0.79	5.6020	0.89	460	1-octane	100	20	31.7
30	CuCeY	503	0.254		1.01	4.86	0.08		0.1690	0.2100			BT	0.79	5.6020	0.89	461	1-octane	100	20	31.5
31	CuCeY	503	0.254		1.01	4.86	0.08		0.1690	0.2100			BT	0.79	5.6020	0.89	218	1-octane	100	30	15
32	CuCeY	503	0.254		1.01	4.86	0.08		0.1690	0.2100			BT	0.79	5.6020	0.89	282	1-octane	100	30	19.4
33	CuCeY	503	0.254		1.01	4.86	0.08		0.1690	0.2100			BT	0.79	5.6020	0.89	350	1-octane	100	30	23.9
34	CuCeY	503	0.254		1.01	4.86	0.08		0.1690	0.2100			BT	0.79	5.6020	0.89	408	1-octane	100	30	27.2
35	CuCeY	503	0.254		1.01	4.86	0.08		0.1690	0.2100			BT	0.79	5.6020	0.89	480	1-octane	100	30	32.1
36	CuCeY	503	0.254		1.01	4.86	0.08		0.1690	0.2100			BT	0.79	5.6020	0.89	528	1-octane	100	30	34.2
37	CuCeY	503	0.254		1.01	4.86	0.08		0.1690	0.2100			BT	0.79	5.6020	0.89	567	1-octane	100	30	34.8
38	CuCeY	503	0.254		1.01	4.86	0.08		0.1690	0.2100			BT	0.79	5.6020	0.89	597	1-octane	100	30	35.6
39	CuCeY	503	0.254		1.01	4.86	0.08		0.1690	0.2100			BT	0.79	5.6020	0.89	214	1-octane	100	40	14.8
40	CuCeY	503	0.254		1.01	4.86	0.08		0.1690	0.2100			BT	0.79	5.6020	0.89	289	1-octane	100	40	20.1
41	CuCeY	503	0.254		1.01	4.86	0.08		0.1690	0.2100			BT	0.79	5.6020	0.89	357	1-octane	100	40	24.6

Table A1 (Continued): Zeolite and adsorption capacity dataset compiled for study.

42	CuCeY	503	0.254		1.01	4.86	0.08		0.1690	0.2100			BT	0.79	5.6020	0.89	413	1-octane	100	40	27.8
43	CuCeY	503	0.254		1.01	4.86	0.08		0.1690	0.2100			BT	0.79	5.6020	0.89	470	1-octane	100	40	31
44	CuCeY	503	0.254		1.01	4.86	0.08		0.1690	0.2100			BT	0.79	5.6020	0.89	525	1-octane	100	40	33.8
45	CuCeY	503	0.254		1.01	4.86	0.08		0.1690	0.2100			BT	0.79	5.6020	0.89	581	1-octane	100	40	36.7
46	NiCeY	568	0.25		0.88	5	0.37			0.2290		0.114	DBT	0.79	5.2670	0.91	600	n-Octane	100	25	7
47	NiCeY	568	0.25		0.88	5	0.37			0.2290		0.114	DBT	0.79	5.2670	0.91	26	n-Octane	100	25	1.7
48	NiCeY	568	0.25		0.88	5	0.37			0.2290		0.114	DBT	0.79	5.2670	0.91	58	n-Octane	100	25	3.1
49	NiCeY	568	0.25		0.88	5	0.37			0.2290		0.114	DBT	0.79	5.2670	0.91	124	n-Octane	100	25	5.9
50	NiCeY	568	0.25		0.88	5	0.37			0.2290		0.114	DBT	0.79	5.2670	0.91	211	n-Octane	100	25	8
51	NiCeY	568	0.25		0.88	5	0.37			0.2290		0.114	DBT	0.79	5.2670	0.91	298	n-Octane	100	25	10
52	NiCeY	568	0.25		0.88	5	0.37			0.2290		0.114	DBT	0.79	5.2670	0.91	519	n-Octane	100	25	12.8
53	NiCeY	568	0.25		0.88	5	0.37			0.2290		0.114	DBT	0.79	5.2670	0.91	966	n-Octane	100	25	18.2
54	NiCeY	568	0.25		0.88	5	0.37			0.2290		0.114	DBT	0.79	5.2670	0.91	2316	n-Octane	100	25	21
55	NiCeY	568	0.25		0.88	5	0.37			0.2290		0.114	DBT	0.79	5.2670	0.91	309	n-Octane	100	80	7
56	NiCeY	568	0.25		0.88	5	0.37			0.2290		0.114	DBT	0.79	5.2670	0.91	209	n-Octane	100	80	5.3
57	NiCeY	568	0.25		0.88	5	0.37			0.2290		0.114	DBT	0.79	5.2670	0.91	39	n-Octane	100	80	1.7
58	NiCeY	568	0.25		0.88	5	0.37			0.2290		0.114	DBT	0.79	5.2670	0.91	15	n-Octane	100	80	1
59	AgY	694				2.40	0.05	0.9700					TP	0.51	3.0401	0.77	517	n-Heptane	33	25	8.8
60	AgY	694				2.40	0.05	0.9700					TP	0.51	3.0401	0.77	908	n-Heptane	33	25	14.9
61	AgY	694				2.40	0.05	0.9700					TP	0.51	3.0401	0.77	1120	n-Heptane	33	25	17.7
62	AgY	694				2.40	0.05	0.9700					TP	0.51	3.0401	0.77	1631	n-Heptane	33	25	25.6
63	AgY	694				2.40	0.05	0.9700					TP	0.51	3.0401	0.77	2456	n-Heptane	33	25	32.8
64	AgY	694				2.40	0.05	0.9700					TP	0.51	3.0401	0.77	3405	n-Heptane	33	25	38.8
65	AgY	694				2.40	0.05	0.9700					TP	0.51	3.0401	0.77	1975	n-Heptane	33	25	29.7
66	clinoptilolite	141.4	0.08	0.06	1.70	10.47						0.024	TP	0.51	3.0401	0.77	311	iso-octane	14	20	2.9
67	clinoptilolite	141.4	0.08	0.06	1.70	10.47						0.024	TP	0.51	3.0401	0.77	389	iso-octane	14	20	3.5
68	clinoptilolite	141.4	0.08	0.06	1.70	10.47						0.024	TP	0.51	3.0401	0.77	444	iso-octane	14	20	4
69	clinoptilolite	141.4	0.08	0.06	1.70	10.47						0.024	TP	0.51	3.0401	0.77	503	iso-octane	14	20	4.4
70	clinoptilolite	141.4	0.08	0.06	1.70	10.47						0.024	TP	0.51	3.0401	0.77	568	iso-octane	14	20	4.8
71	clinoptilolite	141.4	0.08	0.06	1.70	10.47						0.024	TP	0.51	3.0401	0.77	646	iso-octane	14	20	5.3
72	clinoptilolite	141.4	0.08	0.06	1.70	10.47						0.024	TP	0.51	3.0401	0.77	699	iso-octane	14	20	5.5
73	clinoptilolite	141.4	0.08	0.06	1.70	10.47						0.024	BT	0.79	5.6020	0.89	221	iso-octane	14	20	2.1
74	clinoptilolite	141.4	0.08	0.06	1.70	10.47						0.024	BT	0.79	5.6020	0.89	252	iso-octane	14	20	2.4

Table A1 (Continued): Zeolite and adsorption capacity dataset compiled for study.

	Adsorbent properties												Adsorbent conditions				Adsorption conditions				
	Adsorbent	SA	Vmicro	Vmeso	Pore size	Si/Al	Metal amount (Mn+/Al)						adsorbate	DM	CH	KD	C0	Solvent	Oil/Adsorbent	Temp.	Capacity
		m^2/g	cm^3/g	cm3/g	nm	ratio	Na^+	Ag^+	Cu^+	Ce+4	Cs+2	Ni+2	S	D	eV	nm	ppm		ml/g	◦C	mgS/g
75	clinoptilolite	141.4	0.08	0.06	1.70	10.47						0.024	BT	0.79	5.6020	0.89	287	iso-octane	14	20	2.6
76	clinoptilolite	141.4	0.08	0.06	1.70	10.47						0.024	BT	0.79	5.6020	0.89	373	iso-octane	14	20	3.2
77	clinoptilolite	141.4	0.08	0.06	1.70	10.47						0.024	BT	0.79	5.6020	0.89	414	iso-octane	14	20	3.4
78	clinoptilolite	141.4	0.08	0.06	1.70	10.47						0.024	BT	0.79	5.6020	0.89	426	iso-octane	14	20	3.4
79	clinoptilolite	141.4	0.08	0.06	1.70	10.47						0.024	DBT	0.79	5.2670	0.91	118	iso-octane	14	20	1.1
80	clinoptilolite	141.4	0.08	0.06	1.70	10.47						0.024	DBT	0.79	5.2670	0.91	152	iso-octane	14	20	1.4
81	clinoptilolite	141.4	0.08	0.06	1.70	10.47						0.024	DBT	0.79	5.2670	0.91	174	iso-octane	14	20	1.6
82	clinoptilolite	141.4	0.08	0.06	1.70	10.47						0.024	DBT	0.79	5.2670	0.91	239	iso-octane	14	20	2.1
83	clinoptilolite	141.4	0.08	0.06	1.70	10.47						0.024	DBT	0.79	5.2670	0.91	277	iso-octane	14	20	2.3
84	clinoptilolite	141.4	0.08	0.06	1.70	10.47						0.024	DBT	0.79	5.2670	0.91	290	iso-octane	14	20	2.4
85	clinoptilolite	141.4	0.08	0.06	1.70	10.47						0.024	DBT	0.79	5.2670	0.91	293	iso-octane	14	20	2.4
86	CeY	720	0.3		0.83	2	0.29			0.2100			TP	0.51	3.0401	0.77	8	n-Heptane	100	80	0.5
87	CeY	720	0.3		0.83	2	0.29			0.2100			TP	0.51	3.0401	0.77	9	n-Heptane	100	80	0.6
88	CeY	720	0.3		0.83	2	0.29			0.2100			TP	0.51	3.0401	0.77	10	n-Heptane	100	80	0.6
89	CeY	720	0.3		0.83	2	0.29			0.2100			TP	0.51	3.0401	0.77	10	n-Heptane	100	80	0.6
90	CeY	720	0.3		0.83	2	0.29			0.2100			TP	0.51	3.0401	0.77	12	n-Heptane	100	80	0.7
91	CeY	720	0.3		0.83	2	0.29			0.2100			TP	0.51	3.0401	0.77	12	n-Heptane	100	80	0.7
92	CeY	720	0.3		0.83	2	0.29			0.2100			BT	0.79	5.6020	0.89	9	n-Heptane	100	80	0.6
93	CeY	720	0.3		0.83	2	0.29			0.2100			BT	0.79	5.6020	0.89	10	n-Heptane	100	80	0.6
94	CeY	720	0.3		0.83	2	0.29			0.2100			BT	0.79	5.6020	0.89	11	n-Heptane	100	80	0.7
95	CeY	720	0.3		0.83	2	0.29			0.2100			BT	0.79	5.6020	0.89	12	n-Heptane	100	80	0.8
96	CeY	720	0.3		0.83	2	0.29			0.2100			BT	0.79	5.6020	0.89	14	n-Heptane	100	80	0.9
97	CeY	720	0.3		0.83	2	0.29			0.2100			BT	0.79	5.6020	0.89	16	n-Heptane	100	80	1
98	CuY	488	0.17	0.17		4.76	0.90		0.2195				TP	0.51	3.0401	0.77	112	n-Octane	100	25	7.7
99	CuY	488	0.17	0.17		4.76	0.90		0.2195				TP	0.51	3.0401	0.77	390	n-Octane	100	25	22.3
100	CuY	488	0.17	0.17		4.76	0.90		0.2195				TP	0.51	3.0401	0.77	563	n-Octane	100	25	29.3
101	CuY	488	0.17	0.17		4.76	0.90		0.2195				TP	0.51	3.0401	0.77	830	n-Octane	100	25	34.1
102	CuY	488	0.17	0.17		4.76	0.90		0.2195				TP	0.51	3.0401	0.77	969	n-Octane	100	25	37
103	CuY	482	0.14	0.18	2.40	2.10	0.81		0.2115				TP	0.51	3.0401	0.77	66	n-Octane	100	25	4.5
104	CuY	482	0.14	0.18	2.40	2.10	0.81		0.2115				TP	0.51	3.0401	0.77	208	n-Octane	100	25	10.7
105	CuY	482	0.14	0.18	2.40	2.10	0.81		0.2115				TP	0.51	3.0401	0.77	442	n-Octane	100	25	20.3
106	CuY	482	0.14	0.18	2.40	2.10	0.81		0.2115				TP	0.51	3.0401	0.77	556	n-Octane	100	25	23.7
107	CuY	482	0.14	0.18	2.40	2.10	0.81		0.2115				TP	0.51	3.0401	0.77	719	n-Octane	100	25	28.2
108	CuY	482	0.14	0.18	2.40	2.10	0.81		0.2115				TP	0.51	3.0401	0.77	989	n-Octane	100	25	32.9
109	CuX	461	0.16	0.11	2.40	1.78	0.79		0.2069				TP	0.51	3.0401	0.77	99	n-Octane	100	25	7
110	CuX	461	0.16	0.11	2.40	1.78	0.79		0.2069				TP	0.51	3.0401	0.77	187	n-Octane	100	25	11.9
111	CuX	461	0.16	0.11	2.40	1.78	0.79		0.2069				TP	0.51	3.0401	0.77	383	n-Octane	100	25	21.3
112	CuX	461	0.16	0.11	2.40	1.78	0.79		0.2069				TP	0.51	3.0401	0.77	579	n-Octane	100	25	27.6
113	CuX	461	0.16	0.11	2.40	1.78	0.79		0.2069				TP	0.51	3.0401	0.77	795	n-Octane	100	25	32.7
114	CuX	461	0.16	0.11	2.40	1.78	0.79		0.2069				TP	0.51	3.0401	0.77	947	n-Octane	100	25	35.5
115	CuY	488	0.17	0.17		4.76	0.90		0.2195				BT	0.79	5.6020	0.89	365	n-Octane	100	25	25.4
116	CuY	488	0.17	0.17		4.76	0.90		0.2195				BT	0.79	5.6020	0.89	580	n-Octane	100	25	33.2
117	CuY	488	0.17	0.17		4.76	0.90		0.2195				BT	0.79	5.6020	0.89	762	n-Octane	100	25	36.5
118	CuY	488	0.17	0.17		4.76	0.90		0.2195				BT	0.79	5.6020	0.89	991	n-Octane	100	25	37.5
119	CuY	482	0.14	0.18	2.40	2.10	0.81		0.2115				BT	0.79	5.6020	0.89	211	n-Octane	100	25	14.7
120	CuY	482	0.14	0.18	2.40	2.10	0.81		0.2115				BT	0.79	5.6020	0.89	368	n-Octane	100	25	25.6
121	CuY	482	0.14	0.18	2.40	2.10	0.81		0.2115				BT	0.79	5.6020	0.89	683	n-Octane	100	25	40.7
122	CuY	482	0.14	0.18	2.40	2.10	0.81		0.2115				BT	0.79	5.6020	0.89	898	n-Octane	100	25	43.7
123	CuY	482	0.14	0.18	2.40	2.10	0.81		0.2115				BT	0.79	5.6020	0.89	1051	n-Octane	100	25	44.2
124	CuX	461	0.16	0.11	2.40	1.78	0.79		0.2069				BT	0.79	5.6020	0.89	196	n-Octane	100	25	13.6

Table A1 (Continued): Zeolite and adsorption capacity dataset compiled for study.

125	CuX	461	0.16	0.11	2.40	1.78	0.79		0.2069				BT	0.79	5.6020	0.89	382	n-Octane	100	25	25.7
126	CuX	461	0.16	0.11	2.40	1.78	0.79		0.2069				BT	0.79	5.6020	0.89	585	n-Octane	100	25	30.9
127	CuX	461	0.16	0.11	2.40	1.78	0.79		0.2069				BT	0.79	5.6020	0.89	722	n-Octane	100	25	33.8
128	CuX	461	0.16	0.11	2.40	1.78	0.79		0.2069				BT	0.79	5.6020	0.89	941	n-Octane	100	25	34.6
129	AgY	475	0.266		1.11	1.91		0.4900					TP	0.51	3.0401	0.77	404	ether	50	30	14.3
130	AgY	475	0.266		1.11	1.91		0.4900					TP	0.51	3.0401	0.77	713	ether	50	30	24.5
131	AgY	475	0.266		1.11	1.91		0.4900					TP	0.51	3.0401	0.77	805	ether	50	30	25.4
132	AgY	475	0.266		1.11	1.91		0.4900					TP	0.51	3.0401	0.77	957	ether	50	30	28.8
133	AgY	475	0.266		1.11	1.91		0.4900					TP	0.51	3.0401	0.77	1012	ether	50	30	28.1
134	AgY	475	0.266		1.11	1.91		0.4900					TP	0.51	3.0401	0.77	1100	ether	50	30	28.8
135	AgY	475	0.266		1.11	1.91		0.4900					TP	0.51	3.0401	0.77	413	ether	50	50	14.6
136	AgY	475	0.266		1.11	1.91		0.4900					TP	0.51	3.0401	0.77	736	ether	50	50	25.4
137	AgY	475	0.266		1.11	1.91		0.4900					TP	0.51	3.0401	0.77	837	ether	50	50	26.8
138	AgY	475	0.266		1.11	1.91		0.4900					TP	0.51	3.0401	0.77	980	ether	50	50	29.8
139	AgY	475	0.266		1.11	1.91		0.4900					TP	0.51	3.0401	0.77	1056	ether	50	50	29.9
140	AgY	475	0.266		1.11	1.91		0.4900					TP	0.51	3.0401	0.77	1115	ether	50	50	29.5
141	AgY	475	0.266		1.11	1.91		0.4900					TP	0.51	3.0401	0.77	405	ether	50	40	14.3
142	AgY	475	0.266		1.11	1.91		0.4900					TP	0.51	3.0401	0.77	777	ether	50	40	27.2
143	AgY	475	0.266		1.11	1.91		0.4900					TP	0.51	3.0401	0.77	919	ether	50	40	30.3
144	AgY	475	0.266		1.11	1.91		0.4900					TP	0.51	3.0401	0.77	1078	ether	50	40	34
145	AgY	475	0.266		1.11	1.91		0.4900					TP	0.51	3.0401	0.77	1095	ether	50	40	31.7
146	AgY	475	0.266		1.11	1.91		0.4900					TP	0.51	3.0401	0.77	1200	ether	50	40	33.2
147	NiY	524				2.88	0.25					0.313	DBT	0.79	5.2670	0.91	698	hexadecane	260	30	31.7
148	NiY	524				2.88	0.25					0.313	DBT	0.79	5.2670	0.91	581	hexadecane	260	30	31.5
149	NiY	524				2.88	0.25					0.313	DBT	0.79	5.2670	0.91	451	hexadecane	260	30	31.8
150	NiY	524				2.88	0.25					0.313	DBT	0.79	5.2670	0.91	316	hexadecane	260	30	28.7
151	NiY	524				2.88	0.25					0.313	DBT	0.79	5.2670	0.91	177	hexadecane	260	30	25.2
152	NiY	524				2.88	0.25					0.313	DBT	0.79	5.2670	0.91	115	hexadecane	260	30	19.7
153	NiY	524				2.88	0.25					0.313	DBT	0.79	5.2670	0.91	87	hexadecane	260	30	16.1
154	CsY	429				2.88	0.36				0.6667		DBT	0.79	5.2670	0.91	844	hexadecane	260	30	32.5
155	CsY	429				2.88	0.36				0.6667		DBT	0.79	5.2670	0.91	315	hexadecane	260	30	29.7
156	CsY	429				2.88	0.36				0.6667		DBT	0.79	5.2670	0.91	178	hexadecane	260	30	27.9
157	CsY	429				2.88	0.36				0.6667		DBT	0.79	5.2670	0.91	116	hexadecane	260	30	23.3
158	CsY	429				2.88	0.36				0.6667		DBT	0.79	5.2670	0.91	89	hexadecane	260	30	17.4

Table A1 (Continued): Zeolite and adsorption capacity dataset compiled for study.

	Adsorbent properties												Adsorbent conditions				Adsorption conditions				
	Adsorbent	SA	Vmicro	Vmeso	Pore size	Si/Al	Metal amount (Mn+/Al)						adsorbate	DM	CH	KD	*C*0	Solvent	Oil/Adsorbent	Temp.	Capacity
		m^2/g	cm^3/g	cm3/g	nm	ratio	Na^+	Ag^+	Cu^+	Ce+4	Cs+2	Ni+2	S	D	eV	nm	ppm		ml/g	◦C	mgS/g
159	NaY	677				2.81	1.03						DBT	0.79	5.2670	0.91	880	hexadecane	260	30	45.2
160	NaY	677				2.81	1.03						DBT	0.79	5.2670	0.91	629	hexadecane	260	30	46.5
161	NaY	677				2.81	1.03						DBT	0.79	5.2670	0.91	490	hexadecane	260	30	45
162	NaY	677				2.81	1.03						DBT	0.79	5.2670	0.91	334	hexadecane	260	30	38.7
163	NaY	677				2.81	1.03						DBT	0.79	5.2670	0.91	201	hexadecane	260	30	34
164	NaY	677				2.81	1.03						DBT	0.79	5.2670	0.91	131	hexadecane	260	30	24.1
165	NaY	677				2.81	1.03						DBT	0.79	5.2670	0.91	93	hexadecane	260	30	17.6
166	MCM-22	597	0.2002			21							TP	0.51	3.0401	0.77	34	iso-octane	50	30	1.1
167	MCM-22	597	0.2002			21							TP	0.51	3.0401	0.77	58	iso-octane	50	30	2
168	MCM-22	597	0.2002			21							TP	0.51	3.0401	0.77	117	iso-octane	50	30	3.9
169	MCM-22	597	0.2002			21							TP	0.51	3.0401	0.77	188	iso-octane	50	30	6.2
170	MCM-22	597	0.2002			21							TP	0.51	3.0401	0.77	215	iso-octane	50	30	7.1
171	MCM-22	597	0.2002			21							TP	0.51	3.0401	0.77	231	iso-octane	50	30	7.6
172	MCM-22	597	0.2002			21							TP	0.51	3.0401	0.77	289	iso-octane	50	30	9.7
173	MCM-22	597	0.2002			21							TP	0.51	3.0401	0.77	456	iso-octane	50	30	14.8
174	MCM-22	597	0.2002			21							TP	0.51	3.0401	0.77	538	iso-octane	50	30	15.7
175	MCM-22	597	0.2002			21							TP	0.51	3.0401	0.77	510	iso-octane	50	30	14.4
176	MCM-22	597	0.2002			21							TP	0.51	3.0401	0.77	613	iso-octane	50	30	16.1
177	MCM-22	498	0.177			9							TP	0.51	3.0401	0.77	1590	iso-octane	50	30	21
178	MCM-22	498	0.177			9							TP	0.51	3.0401	0.77	1506	iso-octane	50	30	20.7
179	MCM-22	498	0.177			9							TP	0.51	3.0401	0.77	1449	iso-octane	50	30	21.5
180	MCM-22	498	0.177			9							TP	0.51	3.0401	0.77	1367	iso-octane	50	30	21.5
181	MCM-22	498	0.177			9							TP	0.51	3.0401	0.77	1039	iso-octane	50	30	21.2
182	MCM-22	498	0.177			9							TP	0.51	3.0401	0.77	869	iso-octane	50	30	20
183	MCM-22	498	0.177			9							TP	0.51	3.0401	0.77	598	iso-octane	50	30	16.1
184	MCM-22	498	0.177			9							TP	0.51	3.0401	0.77	576	iso-octane	50	30	15.6
185	MCM-22	498	0.177			9							TP	0.51	3.0401	0.77	482	iso-octane	50	30	14.6
186	MCM-22	498	0.177			9							TP	0.51	3.0401	0.77	235	iso-octane	50	30	7.4
187	MCM-22	498	0.177			9							TP	0.51	3.0401	0.77	187	iso-octane	50	30	6.1
188	MCM-22	498	0.177			9							TP	0.51	3.0401	0.77	144	iso-octane	50	30	4.8
189	MCM-22	429	0.1524			30							TP	0.51	3.0401	0.77	1476	iso-octane	50	30	21.9
190	MCM-22	429	0.1524			30							TP	0.51	3.0401	0.77	1293	iso-octane	50	30	22.5
191	MCM-22	429	0.1524			30							TP	0.51	3.0401	0.77	1025	iso-octane	50	30	22.9
192	MCM-22	429	0.1524			30							TP	0.51	3.0401	0.77	780	iso-octane	50	30	20.6
193	MCM-22	429	0.1524			30							TP	0.51	3.0401	0.77	689	iso-octane	50	30	19.3
194	MCM-22	429	0.1524			30							TP	0.51	3.0401	0.77	701	iso-octane	50	30	17.7
195	MCM-22	429	0.1524			30							TP	0.51	3.0401	0.77	378	iso-octane	50	30	10.5
196	MCM-22	429	0.1524			30							TP	0.51	3.0401	0.77	356	iso-octane	50	30	11.2
197	MCM-22	429	0.1524			30							TP	0.51	3.0401	0.77	341	iso-octane	50	30	10.8
198	MCM-22	429	0.1524			30							TP	0.51	3.0401	0.77	305	iso-octane	50	30	10.2
199	MCM-22	429	0.1524			30							TP	0.51	3.0401	0.77	294	iso-octane	50	30	9.1
200	MCM-22	429	0.1524			30							TP	0.51	3.0401	0.77	240	iso-octane	50	30	8
201	MCM-22	429	0.1524			30							TP	0.51	3.0401	0.77	205	iso-octane	50	30	6.4
202	MCM-22	429	0.1524			30							TP	0.51	3.0401	0.77	135	iso-octane	50	30	4.4
203	MCM-22	356	0.1268			46							TP	0.51	3.0401	0.77	1286	iso-octane	50	30	12
204	MCM-22	356	0.1268			46							TP	0.51	3.0401	0.77	1059	iso-octane	50	30	10.8
205	MCM-22	356	0.1268			46							TP	0.51	3.0401	0.77	830	iso-octane	50	30	10.1
206	MCM-22	356	0.1268			46							TP	0.51	3.0401	0.77	513	iso-octane	50	30	9
207	MCM-22	356	0.1268			46							TP	0.51	3.0401	0.77	421	iso-octane	50	30	8.9

Table A1 (Continued): Zeolite and adsorption capacity dataset compiled for study.

208	MCM-22	356	0.1268			46						TP	0.51	3.0401	0.77	315	iso-octane	50	30	7
209	MCM-22	356	0.1268			46						TP	0.51	3.0401	0.77	161	iso-octane	50	30	4
210	MCM-22	356	0.1268			46						TP	0.51	3.0401	0.77	150	iso-octane	50	30	4.1
211	MCM-22	356	0.1268			46						TP	0.51	3.0401	0.77	125	iso-octane	50	30	3.3
212	MCM-22	356	0.1268			46						TP	0.51	3.0401	0.77	110	iso-octane	50	30	3.4
213	MCM-22	356	0.1268			46						TP	0.51	3.0401	0.77	72	iso-octane	50	30	2.2
214	AgY	475	0.266		1.12	2.93	1.04	0.8964				TP	0.51	3.0401	0.77	1245	ether	50	30	34.9
215	AgY	475	0.266		1.12	2.93	1.04	0.8964				TP	0.51	3.0401	0.77	1181	ether	50	30	35.2
216	AgY	475	0.266		1.12	2.93	1.04	0.8964				TP	0.51	3.0401	0.77	1099	ether	50	30	34.8
217	AgY	475	0.266		1.12	2.93	1.04	0.8964				TP	0.51	3.0401	0.77	985	ether	50	30	33
218	AgY	475	0.266		1.12	2.93	1.04	0.8964				TP	0.51	3.0401	0.77	767	ether	50	30	26.5
219	AgY	475	0.266		1.12	2.93	1.04	0.8964				TP	0.51	3.0401	0.77	469	ether	50	30	16.7
220	AgY	475	0.266		1.12	2.93	1.04	0.8964				TP	0.51	3.0401	0.77	1348	ether	50	40	39.4
221	AgY	475	0.266		1.12	2.93	1.04	0.8964				TP	0.51	3.0401	0.77	1260	ether	50	40	38.7
222	AgY	475	0.266		1.12	2.93	1.04	0.8964				TP	0.51	3.0401	0.77	1178	ether	50	40	38.2
223	AgY	475	0.266		1.12	2.93	1.04	0.8964				TP	0.51	3.0401	0.77	1038	ether	50	40	35.2
224	AgY	475	0.266		1.12	2.93	1.04	0.8964				TP	0.51	3.0401	0.77	829	ether	50	40	29.2
225	AgY	475	0.266		1.12	2.93	1.04	0.8964				TP	0.51	3.0401	0.77	468	ether	50	40	16.6
226	AgY	475	0.266		1.12	2.93	1.04	0.8964				TP	0.51	3.0401	0.77	1282	ether	50	50	36.6
227	AgY	475	0.266		1.12	2.93	1.04	0.8964				TP	0.51	3.0401	0.77	1216	ether	50	50	36.7
228	AgY	475	0.266		1.12	2.93	1.04	0.8964				TP	0.51	3.0401	0.77	1120	ether	50	50	35.7
229	AgY	475	0.266		1.12	2.93	1.04	0.8964				TP	0.51	3.0401	0.77	1003	ether	50	50	33.7
230	AgY	475	0.266		1.12	2.93	1.04	0.8964				TP	0.51	3.0401	0.77	785	ether	50	50	27.3
231	AgY	475	0.266		1.12	2.93	1.04	0.8964				TP	0.51	3.0401	0.77	468	ether	50	50	16.6
232	AgCeY	489	0.291	0.04	1.19	2.78		1.1885		2.2949		TP	0.51	3.0401	0.77	126	n-Octane	100	20	7.8
233	AgCeY	489	0.291	0.04	1.19	2.78		1.1885		2.2949		TP	0.51	3.0401	0.77	179	n-Octane	100	20	10.2
234	AgCeY	489	0.291	0.04	1.19	2.78		1.1885		2.2949		TP	0.51	3.0401	0.77	214	n-Octane	100	20	10.5
235	AgCeY	489	0.291	0.04	1.19	2.78		1.1885		2.2949		TP	0.51	3.0401	0.77	250	n-Octane	100	20	10.6
236	AgCeY	489	0.291	0.04	1.19	2.78		1.1885		2.2949		TP	0.51	3.0401	0.77	286	n-Octane	100	20	10.7
237	AgCeY	489	0.291	0.04	1.19	2.78		1.1885		2.2949		TP	0.51	3.0401	0.77	127	n-Octane	100	30	8
238	AgCeY	489	0.291	0.04	1.19	2.78		1.1885		2.2949		TP	0.51	3.0401	0.77	183	n-Octane	100	30	10.8
239	AgCeY	489	0.291	0.04	1.19	2.78		1.1885		2.2949		TP	0.51	3.0401	0.77	221	n-Octane	100	30	11.2
240	AgCeY	489	0.291	0.04	1.19	2.78		1.1885		2.2949		TP	0.51	3.0401	0.77	257	n-Octane	100	30	11.6
241	AgCeY	489	0.291	0.04	1.19	2.78		1.1885		2.2949		TP	0.51	3.0401	0.77	296	n-Octane	100	30	12.1
242	AgCeY	489	0.291	0.04	1.19	2.78		1.1885		2.2949		TP	0.51	3.0401	0.77	133	n-Octane	100	40	8.8

Table A1 (Continued): Zeolite and adsorption capacity dataset compiled for study.

	Adsorbent properties												Adsorbent conditions				Adsorption conditions				
	Adsorbent	**SA**	**Vmicro**	**Vmeso**	**Pore size**	**Si/Al**	**Metal amount (Mn+/Al)**						**adsorbate**	**DM**	**CH**	**KD**	*C*0	**Solvent**	**Oil/Adsorbent**	**Temp.**	**Capacity**
		m^2/g	cm^3/g	**cm3/g**	**nm**	**ratio**	**Na^+**	**Ag^+**	**Cu^+**	**Ce+4**	**Cs+2**	**Ni+2**	**S**	**D**	**eV**	**nm**	**ppm**		ml/g	◦C	**mgS/g**
243	AgCeY	489	0.291	0.04	1.19	2.78		1.1885		2.2949			TP	0.51	3.0401	0.77	188	n-Octane	100	40	11.5
244	AgCeY	489	0.291	0.04	1.19	2.78		1.1885		2.2949			TP	0.51	3.0401	0.77	222	n-Octane	100	40	11.6
245	AgCeY	489	0.291	0.04	1.19	2.78		1.1885		2.2949			TP	0.51	3.0401	0.77	263	n-Octane	100	40	12.3
246	AgCeY	489	0.291	0.04	1.19	2.78		1.1885		2.2949			TP	0.51	3.0401	0.77	299	n-Octane	100	40	12.4
247	AgCeY	489	0.291	0.04	1.19	2.78		1.1885		2.2949			TP	0.51	3.0401	0.77	139	n-Octane	100	50	9.6
248	AgCeY	489	0.291	0.04	1.19	2.78		1.1885		2.2949			TP	0.51	3.0401	0.77	190	n-Octane	100	50	11.8
249	AgCeY	489	0.291	0.04	1.19	2.78		1.1885		2.2949			TP	0.51	3.0401	0.77	228	n-Octane	100	50	12.4
250	AgCeY	489	0.291	0.04	1.19	2.78		1.1885		2.2949			TP	0.51	3.0401	0.77	267	n-Octane	100	50	13
251	AgCeY	489	0.291	0.04	1.19	2.78		1.1885		2.2949			TP	0.51	3.0401	0.77	305	n-Octane	100	50	13.2
252	AgCeY	489	0.291	0.04	1.19	2.78		1.1885		2.2949			BT	0.79	5.6020	0.89	132	n-Octane	100	20	8.8
253	AgCeY	489	0.291	0.04	1.19	2.78		1.1885		2.2949			BT	0.79	5.6020	0.89	249	n-Octane	100	20	15.3
254	AgCeY	489	0.291	0.04	1.19	2.78		1.1885		2.2949			BT	0.79	5.6020	0.89	336	n-Octane	100	20	17.7
255	AgCeY	489	0.291	0.04	1.19	2.78		1.1885		2.2949			BT	0.79	5.6020	0.89	409	n-Octane	100	20	18.3
256	AgCeY	489	0.291	0.04	1.19	2.78		1.1885		2.2949			BT	0.79	5.6020	0.89	482	n-Octane	100	20	18.9
257	AgCeY	489	0.291	0.04	1.19	2.78		1.1885		2.2949			BT	0.79	5.6020	0.89	555	n-Octane	100	20	19.4
258	AgCeY	489	0.291	0.04	1.19	2.78		1.1885		2.2949			BT	0.79	5.6020	0.89	134	n-Octane	100	30	9
259	AgCeY	489	0.291	0.04	1.19	2.78		1.1885		2.2949			BT	0.79	5.6020	0.89	252	n-Octane	100	30	15.8
260	AgCeY	489	0.291	0.04	1.19	2.78		1.1885		2.2949			BT	0.79	5.6020	0.89	342	n-Octane	100	30	18.3
261	AgCeY	489	0.291	0.04	1.19	2.78		1.1885		2.2949			BT	0.79	5.6020	0.89	419	n-Octane	100	30	19.4
262	AgCeY	489	0.291	0.04	1.19	2.78		1.1885		2.2949			BT	0.79	5.6020	0.89	492	n-Octane	100	30	20
263	AgCeY	489	0.291	0.04	1.19	2.78		1.1885		2.2949			BT	0.79	5.6020	0.89	564	n-Octane	100	30	20.5
264	AgCeY	489	0.291	0.04	1.19	2.78		1.1885		2.2949			BT	0.79	5.6020	0.89	136	n-Octane	100	40	9.3
265	AgCeY	489	0.291	0.04	1.19	2.78		1.1885		2.2949			BT	0.79	5.6020	0.89	257	n-Octane	100	40	16.5
266	AgCeY	489	0.291	0.04	1.19	2.78		1.1885		2.2949			BT	0.79	5.6020	0.89	348	n-Octane	100	40	19.2
267	AgCeY	489	0.291	0.04	1.19	2.78		1.1885		2.2949			BT	0.79	5.6020	0.89	429	n-Octane	100	40	20.8
268	AgCeY	489	0.291	0.04	1.19	2.78		1.1885		2.2949			BT	0.79	5.6020	0.89	501	n-Octane	100	40	21.4
269	AgCeY	489	0.291	0.04	1.19	2.78		1.1885		2.2949			BT	0.79	5.6020	0.89	576	n-Octane	100	40	22.1
270	AgCeY	489	0.291	0.04	1.19	2.78		1.1885		2.2949			BT	0.79	5.6020	0.89	136	n-Octane	100	50	9.4
271	AgCeY	489	0.291	0.04	1.19	2.78		1.1885		2.2949			BT	0.79	5.6020	0.89	261	n-Octane	100	50	16.8
272	AgCeY	489	0.291	0.04	1.19	2.78		1.1885		2.2949			BT	0.79	5.6020	0.89	354	n-Octane	100	50	19.8
273	AgCeY	489	0.291	0.04	1.19	2.78		1.1885		2.2949			BT	0.79	5.6020	0.89	432	n-Octane	100	50	21.3
274	AgCeY	489	0.291	0.04	1.19	2.78		1.1885		2.2949			BT	0.79	5.6020	0.89	507	n-Octane	100	50	22
275	AgCeY	489	0.291	0.04	1.19	2.78		1.1885		2.2949			BT	0.79	5.6020	0.89	581	n-Octane	100	50	22.8
276	AgX	230.16	0.1826		3.17	1.03		0.2970					TP	0.51	3.0401	0.77	302	iso-octane	20	30	4.2
277	AgX	230.16	0.1826		3.17	1.03		0.2970					TP	0.51	3.0401	0.77	384	iso-octane	20	30	5.2
278	AgX	230.16	0.1826		3.17	1.03		0.2970					TP	0.51	3.0401	0.77	435	iso-octane	20	30	5.8
279	AgX	230.16	0.1826		3.17	1.03		0.2970					TP	0.51	3.0401	0.77	486	iso-octane	20	30	6.3
280	AgX	230.16	0.1826		3.17	1.03		0.2970					TP	0.51	3.0401	0.77	560	iso-octane	20	30	7
281	AgX	230.16	0.1826		3.17	1.03		0.2970					TP	0.51	3.0401	0.77	623	iso-octane	20	30	7.4
282	AgX	230.16	0.1826		3.17	1.03		0.2970					TP	0.51	3.0401	0.77	706	iso-octane	20	30	7.8
283	NaY	500	0.666			2.29	0.91						TP	0.51	3.0401	0.77	129	hexadecane	200	55	7
284	NaY	500	0.666			2.29	0.91						TP	0.51	3.0401	0.77	249	hexadecane	200	55	16.6
285	NaY	500	0.666			2.29	0.91						TP	0.51	3.0401	0.77	457	hexadecane	200	55	34.7
286	NaY	500	0.666			2.29	0.91						TP	0.51	3.0401	0.77	648	hexadecane	200	55	50.3
287	NaY	500	0.666			2.29	0.91						TP	0.51	3.0401	0.77	826	hexadecane	200	55	55.8
288	NaY	500	0.666			2.29	0.91						TP	0.51	3.0401	0.77	927	hexadecane	200	55	59.6
289	NaY	500	0.666			2.29	0.91						TP	0.51	3.0401	0.77	1235	hexadecane	200	55	60.8
290	NaY	500	0.666			2.29	0.91						BT	0.79	5.6020	0.89	113	hexadecane	200	55	16.1
291	NaY	500	0.666			2.29	0.91						BT	0.79	5.6020	0.89	271	hexadecane	200	55	23.5

Table A1 (Continued): Zeolite and adsorption capacity dataset compiled for study.

292	NaY	500	0.666			2.29	0.91					BT	0.79	5.6020	0.89	451	hexadecane	200	55	26.5
293	NaY	500	0.666			2.29	0.91					BT	0.79	5.6020	0.89	623	hexadecane	200	55	29.5
294	NaY	500	0.666			2.29	0.91					BT	0.79	5.6020	0.89	818	hexadecane	200	55	30.3
295	NaY	500	0.666			2.29	0.91					BT	0.79	5.6020	0.89	994	hexadecane	200	55	30.6
296	NaY	500	0.666			2.29	0.91					BT	0.79	5.6020	0.89	1199	hexadecane	200	55	31.5
297	NaY	500	0.666			2.29	0.91					BT	0.79	5.6020	0.89	1440	hexadecane	200	55	32.5
298	NaY	500	0.666			2.29	0.91					BT	0.79	5.6020	0.89	1759	hexadecane	200	55	32.8
299	NaY	500	0.666			2.29	0.91					DBT	0.79	5.2670	0.91	111	hexadecane	200	55	15.9
300	NaY	500	0.666			2.29	0.91					DBT	0.79	5.2670	0.91	258	hexadecane	200	55	23.3
301	NaY	500	0.666			2.29	0.91					DBT	0.79	5.2670	0.91	444	hexadecane	200	55	25.8
302	NaY	500	0.666			2.29	0.91					DBT	0.79	5.2670	0.91	614	hexadecane	200	55	29.1
303	NaY	500	0.666			2.29	0.91					DBT	0.79	5.2670	0.91	812	hexadecane	200	55	30
304	NaY	500	0.666			2.29	0.91					DBT	0.79	5.2670	0.91	1000	hexadecane	200	55	30.5
305	NaY	500	0.666			2.29	0.91					DBT	0.79	5.2670	0.91	1197	hexadecane	200	55	31.4
306	NaY	500	0.666			2.29	0.91					DBT	0.79	5.2670	0.91	1444	hexadecane	200	55	32.1
307	NaY	500	0.666			2.29	0.91					DBT	0.79	5.2670	0.91	1758	hexadecane	200	55	32.5
308	MCM-22	597	0.2002			21						TP	0.51	3.0401	0.77	38	iso-octane	50	30	1.3
309	MCM-22	597	0.2002			21						TP	0.51	3.0401	0.77	67	iso-octane	50	30	2.3
310	MCM-22	597	0.2002			21						TP	0.51	3.0401	0.77	100	iso-octane	50	30	3.4
311	MCM-22	597	0.2002			21						TP	0.51	3.0401	0.77	121	iso-octane	50	30	4.1
312	MCM-22	597	0.2002			21						TP	0.51	3.0401	0.77	192	iso-octane	50	30	6.4
313	MCM-22	597	0.2002			21						TP	0.51	3.0401	0.77	215	iso-octane	50	30	7.2
314	MCM-22	597	0.2002			21						TP	0.51	3.0401	0.77	231	iso-octane	50	30	7.7
315	MCM-22	597	0.2002			21						TP	0.51	3.0401	0.77	284	iso-octane	50	30	9.6
316	MCM-22	597	0.2002			21						TP	0.51	3.0401	0.77	443	iso-octane	50	30	14.6
317	MCM-22	597	0.2002			21						TP	0.51	3.0401	0.77	509	iso-octane	50	30	15.6
318	MCM-22	597	0.2002			21						TP	0.51	3.0401	0.77	475	iso-octane	50	30	14.2
319	MCM-22	597	0.2002			21						TP	0.51	3.0401	0.77	560	iso-octane	50	30	15.8
320	NiCeY	568	0.25		0.88	5	0.37			0.2290		0.114	TP	0.51	3.0401	0.77	160	iso-octane	70	30	5.4
321	NiCeY	568	0.25		0.88	5	0.37			0.2290		0.114	TP	0.51	3.0401	0.77	299	iso-octane	70	30	9.7
322	NiCeY	568	0.25		0.88	5	0.37			0.2290		0.114	TP	0.51	3.0401	0.77	441	iso-octane	70	30	13.6
323	NiCeY	568	0.25		0.88	5	0.37			0.2290		0.114	TP	0.51	3.0401	0.77	564	iso-octane	70	30	16.7
324	NiCeY	568	0.25		0.88	5	0.37			0.2290		0.114	TP	0.51	3.0401	0.77	674	iso-octane	70	30	18.6
325	NiCeY	568	0.25		0.88	5	0.37			0.2290		0.114	TP	0.51	3.0401	0.77	163	iso-octane	70	50	5.7
326	NiCeY	568	0.25		0.88	5	0.37			0.2290		0.114	TP	0.51	3.0401	0.77	303	iso-octane	70	50	10.1

Table A1 (Continued): Zeolite and adsorption capacity dataset compiled for study.

	Adsorbent properties												Adsorbent conditions				Adsorption conditions				
	Adsorbent	**SA**	**Vmicro**	**Vmeso**	**Pore size**	**Si/Al**	**Metal amount (Mn+/Al)**						**adsorbate**	**DM**	**CH**	**KD**	*C*0	**Solvent**	**Oil/Adsorbent**	**Temp.**	**Capacity**
		m^2/g	cm^3/g	**cm3/g**	**nm**	**ratio**	**Na^+**	**Ag^+**	**Cu^+**	**Ce**+4	**Cs**+2	**Ni**+2	**S**	**D**	**eV**	**nm**	**ppm**		ml/g	◦C	**mgS/g**
327	NiCeY	568	0.25		0.88	5	0.37			0.2290		0.114	TP	0.51	3.0401	0.77	447	iso-octane	70	50	14.4
328	NiCeY	568	0.25		0.88	5	0.37			0.2290		0.114	TP	0.51	3.0401	0.77	577	iso-octane	70	50	17.7
329	NiCeY	568	0.25		0.88	5	0.37			0.2290		0.114	TP	0.51	3.0401	0.77	683	iso-octane	70	50	19.4
330	NiCeY	568	0.25		0.88	5	0.37			0.2290		0.114	TP	0.51	3.0401	0.77	179	iso-octane	70	70	6.6
331	NiCeY	568	0.25		0.88	5	0.37			0.2290		0.114	TP	0.51	3.0401	0.77	293	iso-octane	70	70	10.3
332	NiCeY	568	0.25		0.88	5	0.37			0.2290		0.114	TP	0.51	3.0401	0.77	435	iso-octane	70	70	14.7
333	NiCeY	568	0.25		0.88	5	0.37			0.2290		0.114	TP	0.51	3.0401	0.77	559	iso-octane	70	70	17.8
334	NiCeY	568	0.25		0.88	5	0.37			0.2290		0.114	TP	0.51	3.0401	0.77	689	iso-octane	70	70	20.1
335	NiCeY	568	0.25		0.88	5	0.37			0.2290		0.114	BT	0.79	5.6020	0.89	180	iso-octane	70	30	7.9
336	NiCeY	568	0.25		0.88	5	0.37			0.2290		0.114	BT	0.79	5.6020	0.89	408	iso-octane	70	30	17.5
337	NiCeY	568	0.25		0.88	5	0.37			0.2290		0.114	BT	0.79	5.6020	0.89	660	iso-octane	70	30	28
338	NiCeY	568	0.25		0.88	5	0.37			0.2290		0.114	BT	0.79	5.6020	0.89	780	iso-octane	70	30	32.2
339	NiCeY	568	0.25		0.88	5	0.37			0.2290		0.114	BT	0.79	5.6020	0.89	979	iso-octane	70	30	39.4
340	NiCeY	568	0.25		0.88	5	0.37			0.2290		0.114	BT	0.79	5.6020	0.89	187	iso-octane	70	50	8.3
341	NiCeY	568	0.25		0.88	5	0.37			0.2290		0.114	BT	0.79	5.6020	0.89	411	iso-octane	70	50	17.9
342	NiCeY	568	0.25		0.88	5	0.37			0.2290		0.114	BT	0.79	5.6020	0.89	654	iso-octane	70	50	28
343	NiCeY	568	0.25		0.88	5	0.37			0.2290		0.114	BT	0.79	5.6020	0.89	785	iso-octane	70	50	32.9
344	NiCeY	568	0.25		0.88	5	0.37			0.2290		0.114	BT	0.79	5.6020	0.89	987	iso-octane	70	50	40.2
345	NiCeY	568	0.25		0.88	5	0.37			0.2290		0.114	BT	0.79	5.6020	0.89	192	iso-octane	70	70	8.7
346	NiCeY	568	0.25		0.88	5	0.37			0.2290		0.114	BT	0.79	5.6020	0.89	429	iso-octane	70	70	19.3
347	NiCeY	568	0.25		0.88	5	0.37			0.2290		0.114	BT	0.79	5.6020	0.89	663	iso-octane	70	70	28.8
348	NiCeY	568	0.25		0.88	5	0.37			0.2290		0.114	BT	0.79	5.6020	0.89	789	iso-octane	70	70	33.4
349	NiCeY	568	0.25		0.88	5	0.37			0.2290		0.114	BT	0.79	5.6020	0.89	993	iso-octane	70	70	40.9
350	CuHY	399.29	0.19			3.40	0.40		0.4670				TP	0.51	3.0401	0.77	826	cyclohexane	20	30	8
351	CuHY	399.29	0.19			3.40	0.40		0.4670				TP	0.51	3.0401	0.77	966	cyclohexane	20	30	9
352	CuHY	399.29	0.19			3.40	0.40		0.4670				TP	0.51	3.0401	0.77	1100	cyclohexane	20	30	9.8
353	CuHY	399.29	0.19			3.40	0.40		0.4670				TP	0.51	3.0401	0.77	1219	cyclohexane	20	30	10.5
354	CuHY	399.29	0.19			3.40	0.40		0.4670				TP	0.51	3.0401	0.77	1321	cyclohexane	20	30	10.9
355	CuHY	399.29	0.19			3.40	0.40		0.4670				TP	0.51	3.0401	0.77	1418	cyclohexane	20	30	11.2
356	CuHY	399.29	0.19			3.40	0.40		0.4670				TP	0.51	3.0401	0.77	1508	cyclohexane	20	30	11.4

Table A2: Metal ion properties included in the dataset provided in Table A1.

	Metal	Electronegativity (eV)	Ionic radius (Å)
1	Na^{+}	26.20	1.02
2	Ag^{+}	14.60	1.15
3	Cu^{+}	14.00	0.77
4	$Ce^{+}4$	3.04	0.87
5	$Cs^{+}2$	0.67	1.67
6	$Ni^{+}2$	27.20	0.70

Table A3: Corresponding references for database entries provided in Table A1.

Entry number	Reference
1-17	Lu Y, Wang R, Nan Y, Liu F, Yang X. Removal of sulphur from model gasoline by CuAgY zeolite: equilibrium, thermodynamics and kinetics. RSC Advances 2017;7:51528–37.
18-45	Song H, Chang Y, Wan X, Dai M, Song H, Jin Z. Equilibrium, kinetic, and thermodynamic studies on adsorptive desulphurization onto CuICeIVY zeolite. Industrial & Engineering Chemistry Research 2014;53:5701–8.
46-58	Wang J, Xu F, Xie W, Mei Z, Zhang Q, Cai J, et al. The enhanced adsorption of dibenzothiophene onto cerium/nickel-exchanged zeolite Y. Journal of Hazardous Materials 2009;163:538–43.
59-65	Lin L, Zhang Y, Zhang H, Lu F. Adsorption and solvent desorption behavior of ion-exchanged modified Y zeolites for sulphur removal and for fuel cell applications. Journal of Colloid and Interface Science 2011;360:753–9.
66-85	Mahmoudi R, Falamaki C. Ni2+-ion-exchanged dealuminated clinoptilolite: A superior adsorbent for deep desulphurization. Fuel 2016;173:277–84.
86-97	Xue M, Chitrakar R, Sakane K, Hirotsu T, Ooi K, Yoshimura Y, et al. Selective adsorption of thiophene and 1-benzothiophene on metal-ion-exchanged zeolites in organic medium. Journal of Colloid and Interface Science 2005;285:487–92.
98-128	Cui W, Wang J, Xu Y, Cao Z, Zeng Y. Stability Improvement of FAU Zeolites Ion-Exchanged with Copper–Ammonia Solution for the Removal of Thiophene and Benzothiophene from Model Fuel. Journal of Chemical & Engineering Data 2019;64:5439–47.
129-146	Song H, Wan X, Sun X. Preparation of Agy zeolites using microwave irradiation and study on their adsorptive desulphurization performance. The Canadian Journal of Chemical Engineering 2013;91:915–23.
147-165	Thomas JK, Gunda K, Rehbein P, Ng FT. Flow calorimetry and adsorption study of dibenzothiophene, quinoline and naphthalene over modified Y zeolites. Applied Catalysis B: Environmental 2010;94:225–33.
166-213	Delitala C, Cadoni E, Delpiano D, Meloni D, Alba M, Becerro A, et al. Liquid-phase thiophene adsorption on MCM-22 zeolites. Acidity, adsorption behaviour and nature of the adsorbed products. Microporous and Mesoporous Materials 2009;118:11–20.
214-231	Song H, Jiang B-L, Song H-L, Jin Z-S, Sun X-L. Preparation of AgY zeolite and study on its adsorption equilibrium and kinetics. Research on Chemical Intermediates

2015;41:3837–54.

232-275 Song H, Yang G, Song H, Cui X, Li F, Yuan D. Kinetic and thermodynamic studies on adsorption of thiophene and benzothiophene onto AgCeY Zeolite. Journal of the Taiwan Institute of Chemical Engineers 2016;63:125–32.

276-282 Bakhtiari G, Abdouss M, Bazmi M, Royaee S. Optimization of sulphur adsorption over Ag-zeolite nanoadsorbent by experimental design method. International Journal of Environmental Science and Technology 2016;13:803–12.

283-307 Ng FT, Rahman A, Ohasi T, Jiang M. A study of the adsorption of thiophenic sulphur compounds using flow calorimetry. Applied Catalysis B: Environmental 2005;56:127–36.

308-319 Delitala C, Cadoni E, Delpiano D, Meloni D, Melis S, Ferino I. Liquid-phase thiophene adsorption on MCM-22 zeolite and activated carbon. Microporous and Mesoporous Materials 2008;110:197–215.

320-349 Fei L, Rui J, Wang R, Lu Y, Yang X. Equilibrium and kinetic studies on the adsorption of thiophene and benzothiophene onto NiCeY zeolites. RSC Advances 2017;7:23011–20.

350-356 Guo X, Bao L, Chang L, Bao W, Liao J. Influence of modifications on the deep desulphurization behavior of NaY and Na13X zeolites in gasoline. Environmental Science and Pollution Research 2019;26:13138–46.

Table A4: Missingness of variables in the dataset. Variable names: C_0 = Initial concentration; "x Metal" = corresponding electro-negativity for the metal and "R Metal" = ionic radius.

Variables	Missingness (%)
Adsorbents	0.00
SA	0.00
Vmicro	7.30
Vmeso	73.31
pore_size	40.45
si/Al ratio	0.00
Na+	41.85
Ag+	68.82
Cu+	76.69
Ce+4	64.33
Cs+2	98.6
Ni+2	80.34
adsorbate	0.00
dipole_moment	0.00
chemical_hardness	0.00
C	0.00
solvent	0.00
oil/adsorbate ratio	0.00
Temperature	0.00
Capacity	0.00

Table A5: Kolmogorov-Smirnov test results for raw vs imputed dataset.

Variable	Statistic	p-value
Micropore volume (Raw vs imputed)	0.0434	9.04×10^{-1}
Mesopore volume (Raw vs imputed)	0.494	2.22×10^{-16}
Pore size (Raw vs imputed)	0.291	3.20×10^{-10}

Table A6: Pairwise regression statistics arranged by p-value of continous variables in the dataset against adsorptive capacity.

Variable		R^2	t-statistic	p-value
1	Conc. [initial]	0.34547	186.84369	0.00000
2	Na+(EN)	0.19788	87.32804	0.00000
3	Na+(ri)	0.19788	87.32804	0.00000
4	Na+	0.19014	83.11055	0.00000
5	Oil/Adsorbent	0.18392	79.78260	0.00000
6	Micropore vol.	0.13519	55.33889	0.00000
7	Cu+(EN)	0.12661	51.31811	0.00000
8	Cu+(ri)	0.12661	51.31811	0.00000
9	Si/Al ratio	0.11966	48.11855	0.00000
10	Mesopore vol.	0.06926	26.34310	0.00000
11	Cu+	0.05967	22.46228	0.00000
12	Surface area	0.05693	21.37123	0.00001
13	Ni+(EN)	0.05443	20.37768	0.00001
14	Ni+2(ri)	0.05443	20.37768	0.00001
15	Ce+4(EN)	0.03460	12.68613	0.00042
16	Ce+4(ri)	0.03460	12.68613	0.00042
17	Ag+(EN)	0.02691	9.78912	0.00190
18	Ag+(ri)	0.02691	9.78912	0.00190
19	Ce+4	0.02381	8.63453	0.00351
20	Dipole moment	0.02250	8.14827	0.00456
21	Chemical hardness	0.01630	5.86601	0.01594
22	Kinetic diameter	0.01370	4.91832	0.02721
23	Temp.	0.00949	3.39250	0.06633
24	Ag+	0.00526	1.87213	0.17210
25	Cs+2	0.00426	1.51292	0.21951
26	Cs+2(ri)	0.00426	1.51292	0.21951
27	Cs+(EN)	0.00426	1.51292	0.21951
28	Ni+2	0.00115	0.40731	0.52375
29	Pore size	0.00018	0.06315	0.80173

Table A7: Results of the assessment of linear models of variables individually fitted against the response variable adsorptive capacity using the Global Validation of Linear Models Assumptions (gvlma) package (ver 1.0.0.3). P-values (<0.05) indicate violations of linear model assumptions.

Variable	Global Stat	Skewness	Kurtosis	Link Function	Heteroscedasticity
Surface area	3.9×10^{-11}	3.8×10^{-3}	9.5×10^{-1}	3.4×10^{-11}	1.3×10^{-1}
Micropore vol.	4.5×10^{-7}	1.9×10^{-4}	8.8×10^{-2}	3.5×10^{-3}	1.8×10^{-3}
Mesopore vol.	5.2×10^{-4}	2.7×10^{-4}	9.4×10^{-1}	5.6×10^{-2}	8.3×10^{-2}
Pore size	4.4×10^{-5}	9.4×10^{-5}	2.8×10^{-1}	2.5×10^{-2}	4.9×10^{-2}
Si/Al	2.1×10^{-5}	4.9×10^{-3}	5.0×10^{-1}	1.9×10^{-4}	3.3×10^{-2}
Na+	1.5×10^{-11}	1.5×10^{-4}	7.4×10^{-1}	9.6×10^{-4}	2.3×10^{-8}
Ag+	6.8×10^{-12}	2.0×10^{-5}	3.3×10^{-1}	1.9×10^{-9}	8.5×10^{-2}
Cu+	9.7×10^{-9}	1.0×10^{-4}	8.4×10^{-1}	2.1×10^{-7}	3.2×10^{-1}
Ce3+	7.1×10^{-4}	3.5×10^{-3}	2.4×10^{-1}	2.4×10^{-2}	3.9×10^{-2}
Cs+	2.3×10^{-4}	4.3×10^{-5}	3.5×10^{-1}	10.0×10^{-1}	4.3×10^{-2}
Ni+	2.0×10^{-6}	1.0×10^{-4}	2.5×10^{-1}	5.5×10^{-4}	5.9×10^{-2}
Na+	9.7×10^{-2}	2.4×10^{-1}	9.8×10^{-1}	10.0×10^{-1}	1.1×10^{-2}
Ag+(EN)	2.2×10^{-4}	5.8×10^{-6}	5.0×10^{-1}	1	3.7×10^{-1}
Cu+(EN)	7.7×10^{-6}	1.5×10^{-7}	2.5×10^{-1}	1	7.4×10^{-1}
Ce+3(EN)	6.5×10^{-3}	2.2×10^{-3}	1.6×10^{-1}	10.0×10^{-1}	8.4×10^{-2}
Cs+(EN)	2.3×10^{-4}	4.3×10^{-5}	3.5×10^{-1}	10.0×10^{-1}	4.3×10^{-2}
Ni^+(EN)	1.9×10^{-3}	3.9×10^{-5}	6.7×10^{-1}	10.0×10^{-1}	9.6×10^{-1}
Na+(ri)	9.7×10^{-2}	2.4×10^{-1}	9.8×10^{-1}	10.0×10^{-1}	1.1×10^{-2}
Ag+(ri)	2.2×10^{-4}	5.8×10^{-6}	5.0×10^{-1}	1	3.7×10^{-1}
Cu+(ri)	7.7×10^{-6}	1.5×10^{-7}	2.5×10^{-1}	1	7.4×10^{-1}
Ce3+(ri)	6.5×10^{-3}	2.2×10^{-3}	1.6×10^{-1}	1	8.4×10^{-2}
Cs+(ri)	2.3×10^{-4}	4.3×10^{-5}	3.5×10^{-1}	1	4.3×10^{-2}
Ni+(ri)	1.9×10^{-3}	3.9×10^{-5}	6.7×10^{-1}	1	9.6×10^{-1}
Dipole moment	2.7×10^{-11}	2.8×10^{-5}	8.5×10^{-1}	6.3×10^{-8}	3.5×10^{-3}
Chemical hardness	1.9×10^{-5}	2.1×10^{-5}	9.7×10^{-1}	3.6×10^{-1}	4.2×10^{-3}
Kinetic diameter	1.7×10^{-5}	3.2×10^{-5}	9.3×10^{-1}	1.8×10^{-1}	4.0×10^{-3}
Conc. [initial]	7.8×10^{-14}	8.0×10^{-3}	1.9×10^{-1}	2.0×10^{-13}	2.9×10^{-2}
Ce	8.9×10^{-12}	1.1×10^{-3}	5.9×10^{-2}	3.1×10^{-10}	5.2×10^{-2}
Oil/Adsorbent	2.7×10^{-6}	6.1×10^{-5}	1.7×10^{-1}	1.5×10^{-2}	6.9×10^{-3}
Temp.	0	7.2×10^{-4}	3.0×10^{-1}	0	5.8×10^{-3}

Table A8: Shapiro-Wilk test for normality on residuals of the pairwise regression model of variables in the dataset against adsorption capacity.

	Fullname	statistic	p-value
1	Ag+	0.9525960	0.0000000
2	Conc. [initial]	0.9889341	0.0084293
3	Ce+4	0.9671824	0.0000003
4	Chemical hardness	0.9682925	0.0000005
5	Cs+2	0.9593263	0.0000000
6	Cu+	0.9714412	0.0000018
7	Dipole moment	0.9705517	0.0000013
8	Kinetic diameter	0.9683836	0.0000005
9	Na+	0.9781658	0.0000319
10	Ni+2	0.9600803	0.0000000
11	Oil/Adsorbent	0.9664498	0.0000003
12	Pore size	0.9591489	0.0000000
13	Ag+(ri)	0.9499243	0.0000000
14	Ce+4(ri)	0.9695565	0.0000009
15	Cs+2(ri)	0.9593263	0.0000000
16	Cu+(ri)	0.9610617	0.0000000
17	Na+(ri)	0.9893910	0.0110106
18	Ni+2(ri)	0.9672801	0.0000004
19	Surface area	0.9788497	0.0000438
20	Si/Al ratio	0.9778985	0.0000283
21	Temp.	0.9735103	0.0000042
22	Mesopore vol.	0.9723222	0.0000026
23	Micropore vol.	0.9655698	0.0000002
24	Ag+(EN)	0.9499243	0.0000000
25	Ce+4(EN)	0.9695565	0.0000009
26	Cs+(EN)	0.9593263	0.0000000
27	Cu+(EN)	0.9610617	0.0000000
28	Na+(EN)	0.9893910	0.0110106
29	Ni+(EN)	0.9672801	0.0000004

Table A9: Summary statistics of the multiple linear model fit for the selected features according to stepAIC.

	Predictor	Co-efficient estimate	std. error	t-statistic	p-value
1	Ce+4	6464633.70	3175130.52	2.04	4.25×10^{-2}
2	(Intercept)	2182199.21	1071797.08	2.04	4.25×10^{-2}
3	AgX	500467.75	245800.44	2.04	4.25×10^{-2}
4	Chemical hardness	243399.08	119542.16	2.04	4.25×10^{-2}
5	CeY	212741.96	104488.55	2.04	4.25×10^{-2}
6	Kinetic diameter	210183.79	103229.50	2.04	4.25×10^{-2}
7	Cu+(EN)	106326.05	52222.03	2.04	4.25×10^{-2}
8	Ni+(EN)	36935.71	18140.67	2.04	4.25×10^{-2}
9	CuHY	9131.65	4491.26	2.03	4.28×10^{-2}
10	Ag+	2317.75	1141.36	2.03	4.31×10^{-2}
11	Na+	543.16	266.52	2.04	4.23×10^{-2}
12	Cs+2	112.47	55.19	2.04	4.24×10^{-2}
13	Micropore vol.	49.26	24.44	2.02	4.46×10^{-2}
14	Mesopore vol.	27.69	13.63	2.03	4.30×10^{-2}
15	Si/Al ratio	1.18	0.59	2.01	4.52×10^{-2}
16	Conc. [initial]	0.60	0.03	19.43	0.00
17	Oil/Adsorbent	−1.09	0.38	−2.84	4.84×10^{-3}
18	Surface area	−12.40	6.22	−1.99	4.71×10^{-2}
19	Na+(EN)	−751.01	369.95	−2.03	4.32×10^{-2}
20	Cu+	−1833.90	901.41	−2.03	4.27×10^{-2}
21	Ni+2	−16277.13	7994.45	−2.04	4.25×10^{-2}
22	Ag+(EN)	−27747.77	13629.80	−2.04	4.26×10^{-2}
23	Pore size	−114508.23	56239.27	−2.04	4.25×10^{-2}
24	Dipole moment	−445657.01	218879.01	−2.04	4.25×10^{-2}
25	Ce+4(EN)	−1038344.07	509984.56	−2.04	4.25×10^{-2}
26	AgCeY	−17795068.63	8740128.76	−2.04	4.25×10^{-2}

Table A10: Parameters used in generating the RF model as implimented in the sklearn.ensemble.RandomForestClassifier Python module (ver. 0.24.1). Only parameters relevant to the model generation are provied.

Parameter variable	Value	Description
bootstrap	True	Subsampling of dataset when building trees.
criterion	mse	Measure of quality of the tree splits
max depth	20	Maximum depth for expanding nodes are expanded unless min samples split samples is reached.
max features	18	Number of features to identify best split.
max leaf nodes	None	Maximum number for leaf node growth.
max samples	None	Maximum number of samples bootstapped to train each estimator.
min impurity _decrease	0.0	Minimum impurity value for splitting nodes.
min samples leaf	1	Minimum number of samples required after spliting a node.
min samples split	2	Minimum number of samples required to split a node
n estimators	8	The number of trees (estimators) in the random forests model.
random state	1000	Controls randomness subsampling samples and features during

Table A11: Model metrics of the RF model.

R^2	MAE	MSE	RMSE	MAPE
0.929868	2.395139	14.06329	8.713183	0.159007

Abbreviations: MAE = mean absolute error; RMSE = mean squared error and MAPE = mean absolute percentage error.

Table A12: Variable importance for the RF predictive model. Metal property variables: ri = Ionic radius and EN = electronegativity.

Feature		Importance (%)
1	Conc. [initial]	41.887
2	Oil/Adsorbent	11.227
3	Temp.	8.896
4	Surface area	5.553
5	Si/Al ratio	5.040
6	iso-octane	3.079
7	Chemical hardness	2.796
8	Pore size	2.015
9	hexadecane	1.967
10	Na+	1.732
11	Micropore vol.	1.587
12	AgY	1.319
13	Cu+	1.305
14	BT	1.291
15	ether	1.058
16	Ce+4	0.877
17	Kinetic diameter	0.864
18	CeY	0.851
19	TP	0.778
20	Dipole moment	0.721
21	Cu+(EN)	0.566
22	Ag+(EN)	0.481
23	Ni+2	0.420
24	Mesopore vol.	0.379
25	1-octane	0.372
26	cyclohexane	0.353
27	Ag+(ri)	0.351
28	Cu+(ri)	0.323
29	Ce+4(ri)	0.263
30	n-Octane	0.236
31	Na+(EN)	0.210
32	MCM-22	0.176
33	Na+(ri)	0.156
34	n-octane	0.154
35	AgCeY	0.107
36	CuAgY	0.103
37	clinoptilolite	0.102
38	CuY	0.088
39	Ag+	0.083
40	NiY	0.058
41	NiCeY	0.050
42	CuCeY	0.034
43	CuX	0.034
44	DBT	0.011
45	Ni+2(ri)	0.010

46	Cs+(EN)	0.010
47	Ni+(EN)	0.006
48	NaY	0.006
49	CsY	0.006
50	Cs+2	0.004
51	Ce+4(EN)	0.004
52	n-heptane	0.003
53	Cs+2(ri)	0.001
54	AgX	0.000
55	CuHY	0.000
56	n-Heptane	0.000

APPENDIX B: Modulated synthesized Ni based MOF with improved adsorptive desulphurization activity

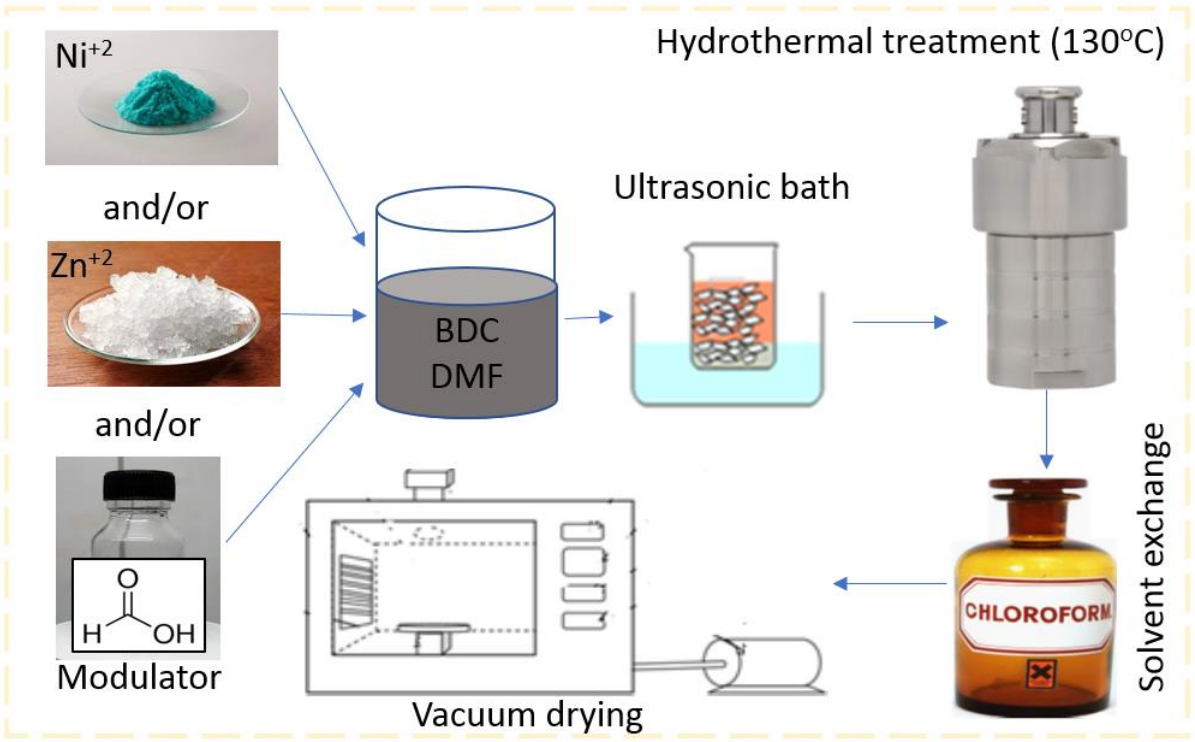

Figure B1: Schematic diagram for adsorbent synthesis.

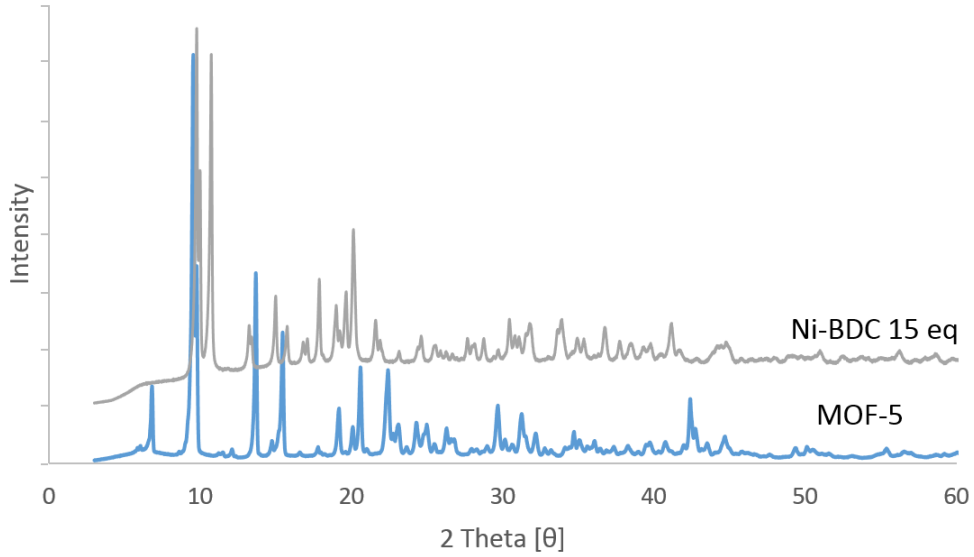

Figure B2: XRD spetrum for MOF-5 and Ni-BDC 15 eq

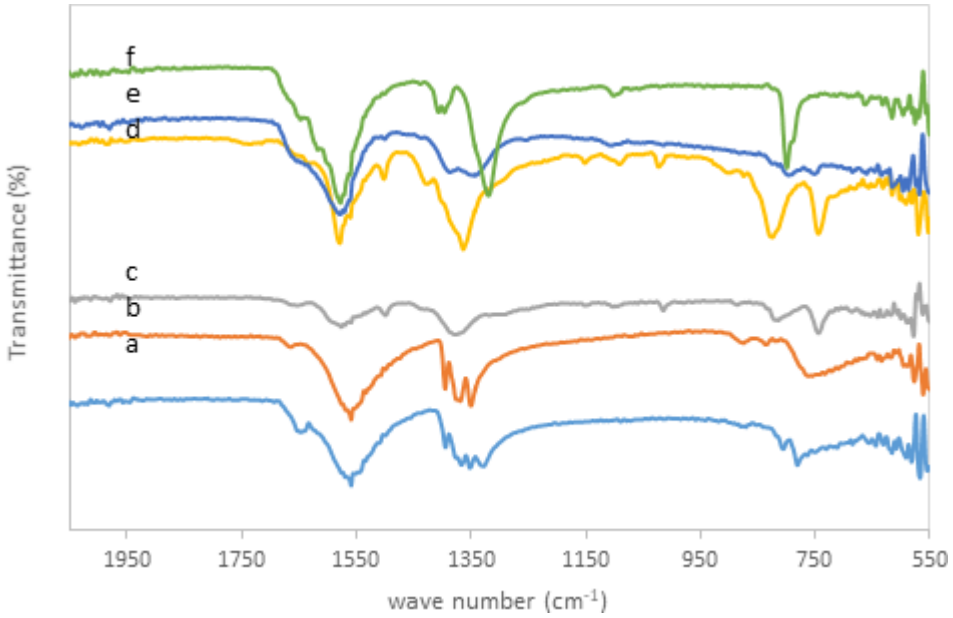

Figure B3: XRD spectrum for: a) MOF-5; b) (25Ni/Zn)-BDC; c) (50Ni/Zn)-BDC; d) (75Ni/Zn)-BDC; e) Ni-BDC and f) Ni-BDC 10eq

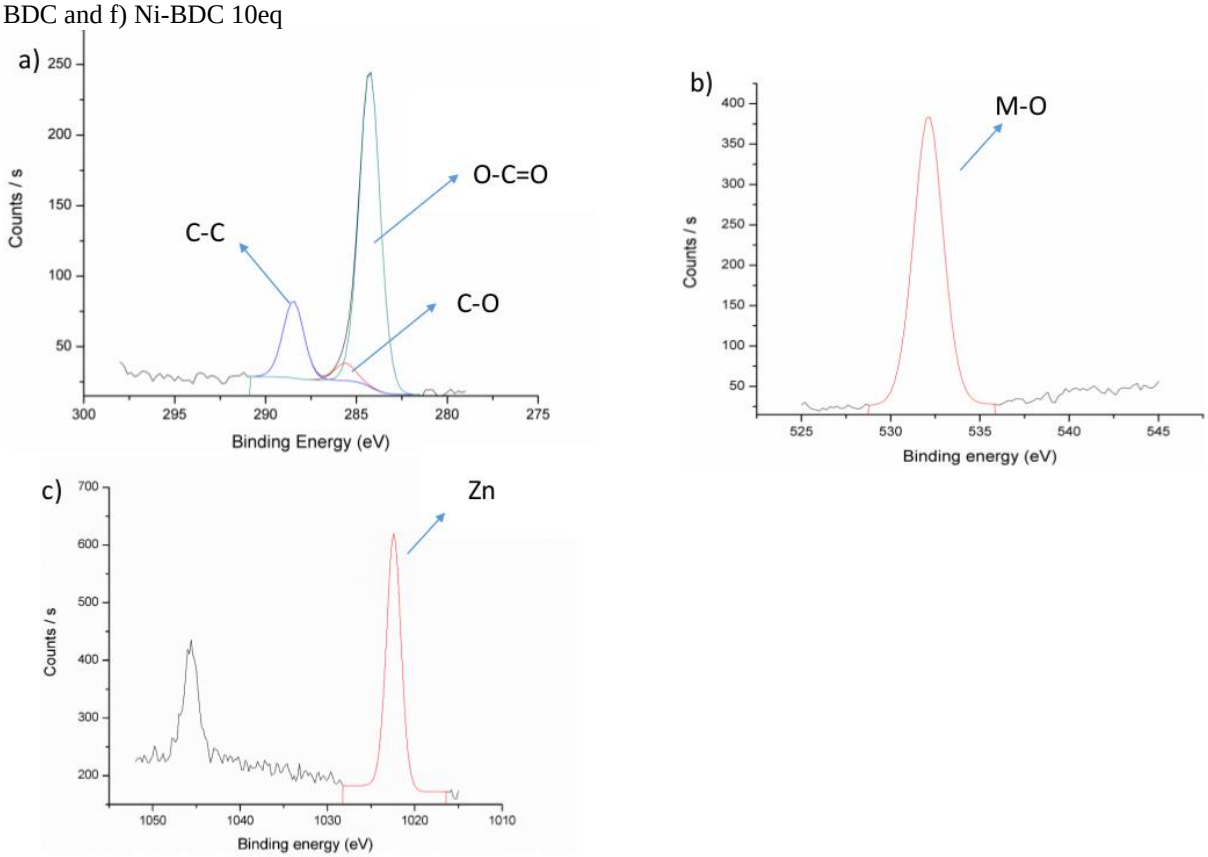

Figure B4: MOF-5 XPS spectrum(a) C 1s (b) O 1s and (c) Zn 2p.

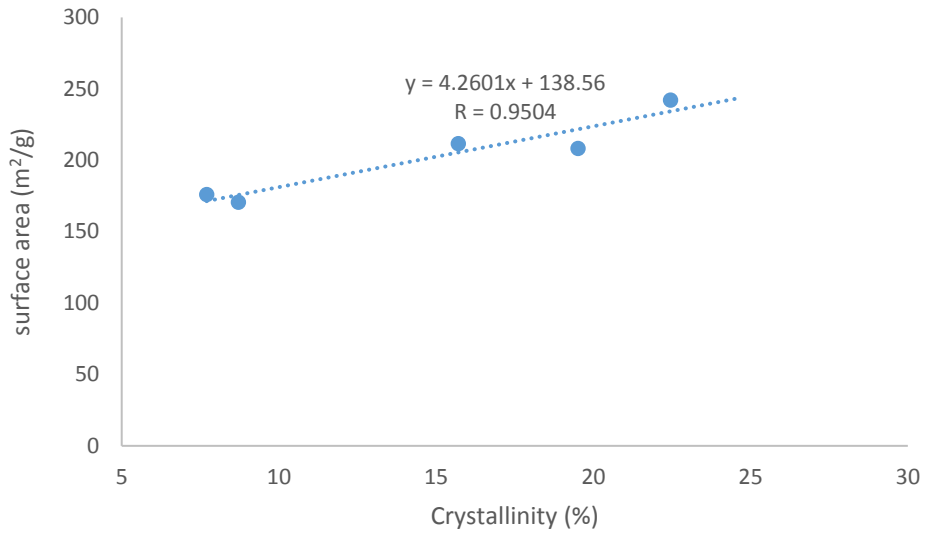

Figure B5: Modulated Ni-BDC correlation crystallinity (%) versus surface area.

Table B1: Mole ratios among Zn, Ni and the modulator formic acid used for the synthesis of the adsorbents.

Absorbent	molar ratio	
	Ni/(Ni+Zn)*100	eq[a]=(Formic acid)/(Ni+Zn)
MOF-5	0	0
MOF-5 10eq	0	10
MOF-5 100eq	0	100
MOF-5 (25Ni/Zn)	25	0
(25Ni/Zn)-BDC 10eq	25	10
(25Ni/Zn)-BDC 100eq	25	100
(50Ni/Zn)-BDC	50	0
(50Ni/Zn)-BDC 10eq	50	10
(50Ni/Zn)-BDC 100eq	50	100
(75Ni/Zn)-BDC	75	0
(75Ni/Zn)-BDC 10eq	75	10
(75Ni/Zn)-BDC 100eq	75	100
Ni-BDC	100	0
Ni-BDC 10eq	100	10
Ni-BDC 25eq	100	25
Ni-BDC 50eq	100	50
Ni-BDC 75eq	100	75
Ni-BDC 100eq	100	100

[a] eq refers to the equivalent amount (eq) of formic acid

Table B2: Effect of formic acid modulator on crystallite size and crystallinity

Ni-BDC	Crystallite size	crystallinity
0	-	-
2.5	-	1.47
5	-	3.93
10	38.17	7.70
15	46.52	25.69
25	56.06	22.45
50	57.82	19.51
75	65.44	12.70
100	53.25	10.36

APPENDIX C: Modulated synthesis of a novel nickel based metal organic framework composite material for the adsorptive desulphurization of liquid fuels

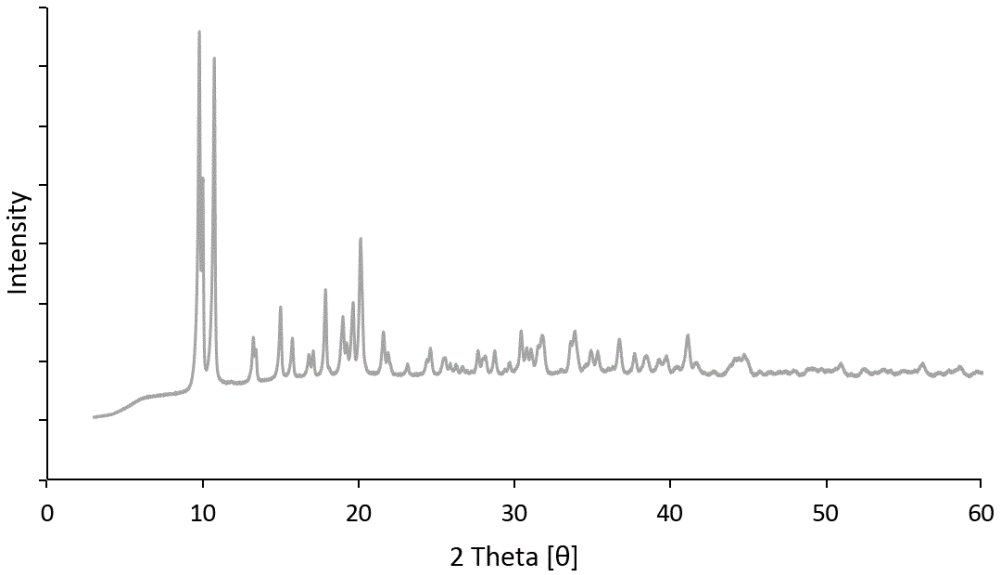

Figure C1: XRD pattern for Ni-BDC 50eq

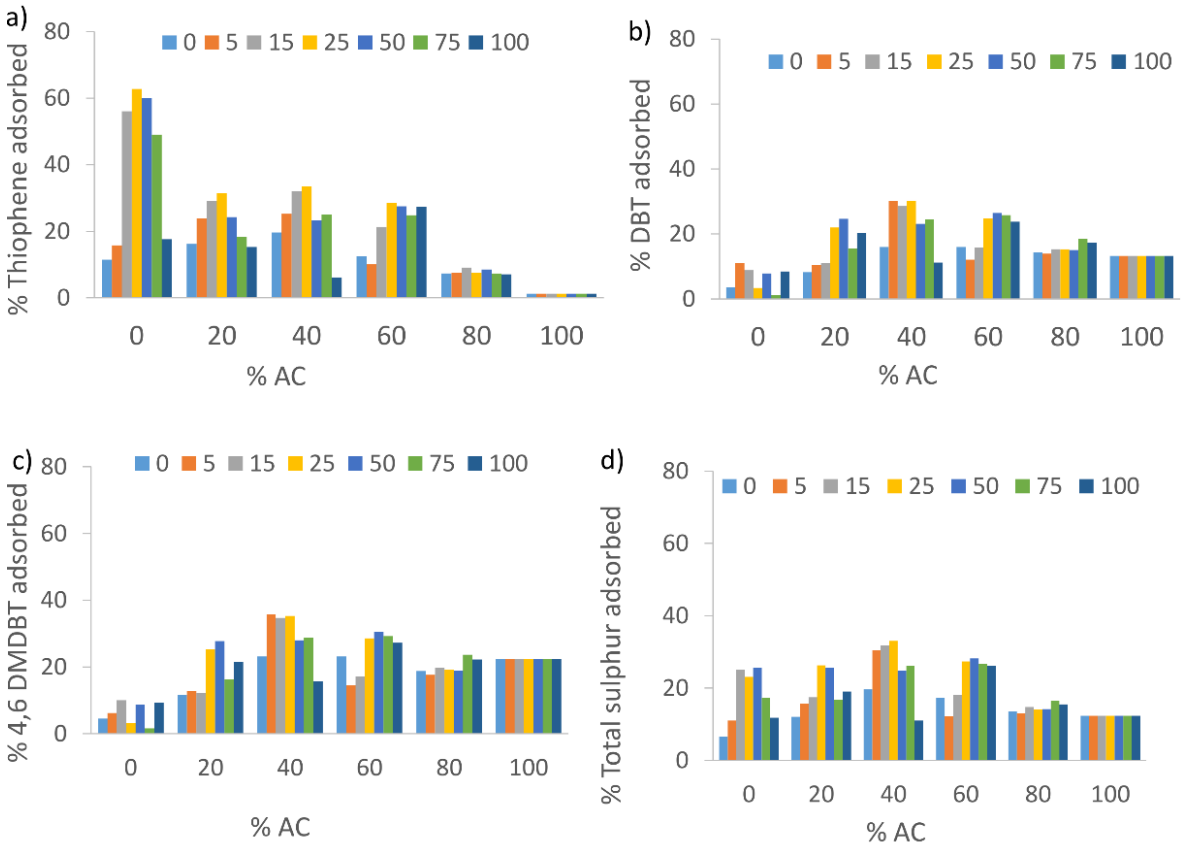

Figure C2: Effect of AC content and formic acid on the activity of x% AC@Ni-BDC y eq composite: a) thiophene; b) DBT; c) 4,6 DMDBT; d) overall sulphur activity. Operating condition: dosage - 200mg/10ml; stirring speed - 1300 rpm; temperature - 25°C and 180 min. Where: x = 0, 20, 40, 60, 80,100; y = 0, 5, 15, 25, 50, 75, 100.

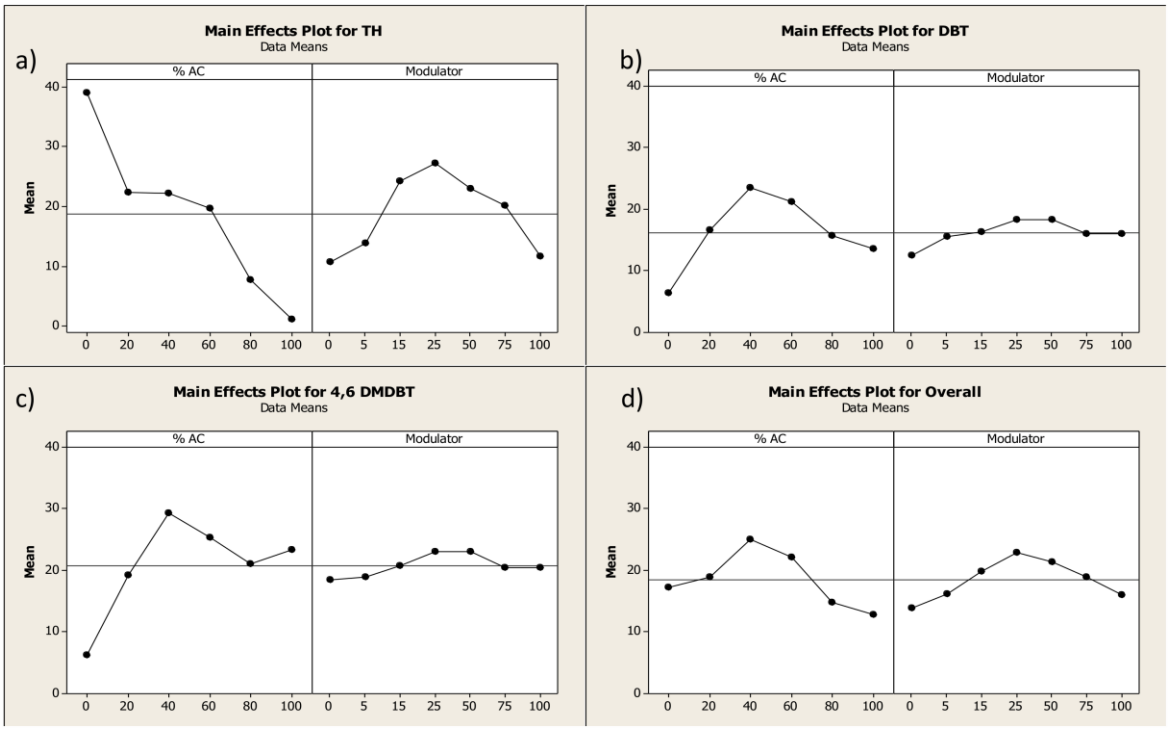

Figure C3: Main effects for the adsorption of: a) thiophene; b) DBT; c) 4,6DMDBT; d) overall adsorption.

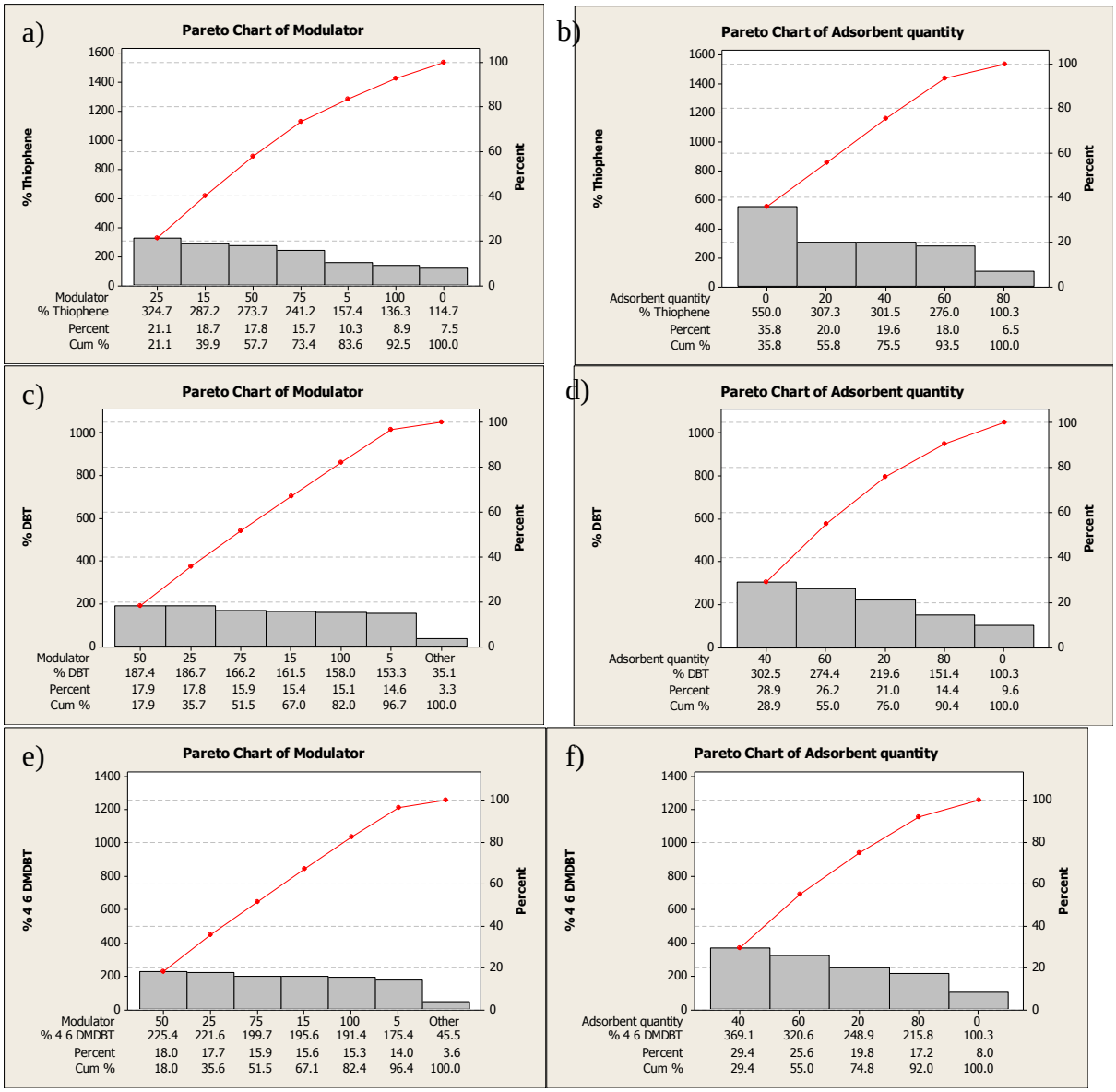

Figure C4: Pareto charts for modulator and adsorbent quantity

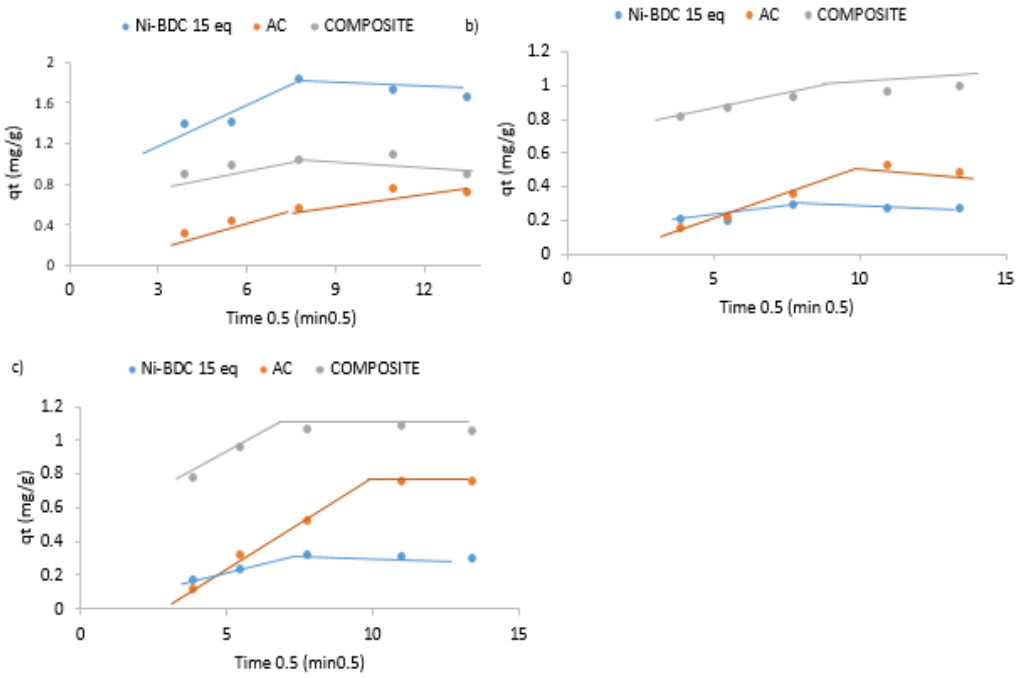

Figure C5: Intraparticle diffusion model for different sulphur compounds: a) Thiophene b) DBT and c) 4,6 DMDBT

Table C1: Two-factor design for AC@Ni-BDC composites

Factor	**Level**						
a) Two-factorial design for modulator and AC loading on the AC@Ni-BDC composite							
Modulator equivalent	0	5	15	25	50	75	100
AC loading (%)	0	20	40	60	80	100	/
b) Two-factorial design for quantity of modulator and concentration of acid for AC treatment							
Modulator equivalent	0	5	15	25	50	75	100
Acid concentration (xxH[a])	10	30	50	65	/	/	/

Table C2: Kinetic adsorption parameters for the AC, Ni-BDC 15eq and 40%AC@Ni-BDC 25eq composites

		1st order		**2nd order kinetics**		
Adsorbent	**Adsorbate**	**k_1**	**R^2**	**K_2**	**h**	**R^2**
Ni-BDC 15eq	TH	0.0490	0.7718	0.3689	1.0650	0.9954
	DBT	0.0390	0.7264	0.7169	0.0560	0.9937
	4,6 DMDBT	0.0420	0.9520	0.3770	0.0390	0.9931
AC	TH	0.0216	0.9646	0.0284	0.0269	0.9862
	DBT	0.0186	0.9951	0.0151	0.0109	0.9727
	4,6 DMDBT	0.0200	0.9895	0.0070	0.0012	0.8640
40%AC@Ni-BDC 15eq	TH	0.0410	0.8567	0.2144	0.2694	0.9990
	DBT	0.0552	0.9071	0.2707	0.2681	0.9990
	4,6 DMDBT	0.0605	0.9869	0.1410	0.1876	0.9960

Table C3: Correlation between crystallite size and adsorption activity

		Correlation (crystallite size vs activity) R^2		
Adsorbent	**Acidity**	**Thiophene**	**DBT**	**4,6DMDBT**
	0	0.5966	0.5634	0.6349
	10	0.0217	0.2147	0.2379
40%AC-xxH@Ni-BDC	30	0.0882	0.0270	0.1410
	50	0.0650	0.4003	0.3767
	65	0.2690	0.3976	0.4780
	Carbon %			
	0	0.0045	0.8401	0.8355
	20	0.0116	0.6930	0.6718
x%AC@Ni-BDC	40	0.5966	0.5634	0.6349
	60	0.0786	0.4096	0.4498
	80	0.0586	0.0038	0.0193

Table C4: Correlation between crystallinity and adsorption activity

		Correlation Crystallinity vs activity R^2		
Adsorbent	**Acidity**	**Thiophene**	**DBT**	**4,6DMDBT**
	0	0.9559	0.9566	0.9587
	10	0.1056	0.2033	0.2290
40%AC-Xh@Ni-BDC	30	0.5652	0.5817	0.2470
	50	0.0464	0.5197	0.5760
	65	0.7992	0.5781	0.5353
	Carbon %			
	0	0.9171	0.0493	0.0397
	20	0.6191	0.0044	0.0014
x%AC@Ni-BDC	40	0.9559	0.9566	0.9587
	60	0.1274	0.095	0.1084
	80	0.0043	0.2749	0.3564

Table C5: Sulphur adsorption capacity and partition coefficient for tested adsorbates and others reported in literature

Adsorbent	Initial Concentration (Final Concentration), ppm					Adsorption capacity, (mg-S/g-adsorbent)					Partition Coefficient (mg/g/ppm× 10^2)					Ref.
	TH	BT	DBT	4,6DMDBT	Total	TH	BT	DBT	4,6DMDBT	Total	TH	BT	DBT	4,6DMDBT	Total	
AC	150(132)	/	153(126)	151(120)	454(378)	0.78	/	1.04	1.61	3.43	0.591		0.825	1.341	2.758	
Ni-BDC 25eq	150(68)	/	153(139)	151(136)	454(343)	3.09	/	0.5	0.55	4.14	4.544		0.360	0.404	5.308	Current work
40%AC@Ni-BDC 25eq	150(100)	/	153(105)	151(95)	454(300)	2.01	/	1.88	2.25	6.14	2.008		1.792	2.364	6.164	
MOF-5@HMSS	500	/	/	/	500	1.4	/	/	/	1.4	/	/	/	/	/	(Jia et al, 2016)
MOF-5@AC	✓	✓	✓	/	100(51.4)	✓	✓	✓	/	3.83	✓	✓	✓	/	7.451	(Zhu et al, 2018)
	✓	✓	✓	/	300(179.7)	✓	✓	✓	/	9.48	✓	✓	✓	/	5.268	
	✓	✓	✓	/	400(256.0)	✓	✓	✓	/	11.34	✓	✓	✓	/	4.43	

A tick (✓) indicates that a sulphur compound is present, although the quantity is unknown, and only the total sulphur concentration is given.